Structural and Mechanical Elements Important for Kinesin Force Generation in Cells

by

Breane Budaitis

A dissertation submitted in partial fulfillment
of the requirements for the degree of
Doctor of Philosophy
(Cellular and Molecular Biology)
in the University of Michigan
2020

Doctoral Committee:

Professor Kristen J. Verhey, Chair
Associate Professor Ajit P. Joglekar
Associate Professor Ann Miller
Professor David Sept
Professor Lois Wesiman

Breane G. Budaitis

budaitis@umich.edu

ORCID iD: 0000-0003-1212-3705

Dedication

To my family

Acknowledgements

I would like to thank everyone who has been a part of my journey in graduate school, for your constant support and encouragement.

First, I would like to thank my PhD mentor, Kristen Verhey. My time and growth in graduate school would be very different if I had a different PhD mentor. Your unwavering support and confidence that I can do anything has helped me become a more confident scientist and to strive for any goal. You have taught me how to be a good scientist, and just as importantly how to be a good mentor. You have changed the way I approach and think about science and academia and I am forever thankful.

My thesis committee: Ajit Joglekar, Ann Miller, David Sept, and Lois Weisman. Your feedback has been instrumental for my growth in graduate school. Thank you for your support, encouragement, and advice, especially as I started my search for a postdoctoral position.

The Verhey lab. I am thankful to work in such a collaborative, welcoming community and lucky to call you my friends. Thank you to Martin Engelke, who helped me to get started in the lab. Thank you to Lynne Blasius, Kristin Schimert, Yang Yue, and Allison Boss. Sometimes days are not science days; thank you for being dramatic with me and thank you for all the laughs and life advice. I would also like to thank former and current lab members: Daisuke Takao, Jeremy Welsh, Andy Poulos, Nnaemeka Unaegbu, and Sarah Kearns for the all fun times.

I would especially like to thank everyone who has collaborated and helped me drive my projects in graduate school forward. Thank you to Matt Lang and Nikki Reinemann for inviting us to visit Vanderbilt and teaching us about optical trapping experiments. Thank you especially to Shashank Jariwala, David Sept, Guido Scarabelli, and Barry Grant for discussions and important work to better understand our experimental results. You have broadened the way I think about science and you have all been critical for the work included in this thesis.

Thank you to the cytoskeletal community and Michigan: The Ohi, Cianfrocco, Sept, and DeSantis labs. Your constant ideas, enthusiasm, and discussions have helped us turn to new directions when we reached a roadblock in a project. I will miss all the fun times we have going to conferences. Thank you also to the Tsai, Duncan, and Fingar labs for your feedback and support in Thursday group meetings.

I would like to thank Bob Fuller and the Cellular and Molecular Biology Program for supporting me throughout my time as a graduate student. I would also like to thank the Cell and Developmental Biology Department for providing a warm, welcoming community at Michigan. Thank you to the CDB and CMB administrative staff for providing generous help and support.

I also would like to thank all the friends I have made in Michigan. Thank you for all the crazy adventures, collective commiseration, and good friendship. Thank you for reminding me to take a break and to live my best life.

Thank you to my family for your constant support and encouragement. Thank you to my sister for the movie nights and DeLish pizza. A special thank you to my parents, who have unconditionally supported me in whatever I strive to do. Thank you for talking to me at all hours of the day and for coming up to visit me throughout my time at UM.

Thank you to the funding sources, Rackham Predoctoral Fellowship, NSF Graduate Research Fellowships Program 1256260, NIH Cellular and Molecular Biology Training Grant T32-GM007315, Rackham Graduate Student Research Grant, and Endowment for the Development of Graduate Education Award, for support throughout my graduate career.

Table of Contents

List of Figures

Abstract

Eukaryotic cells contain a cytoskeleton that forms the structural framework for fundamental cellular processes including cell division, cell motility, intracellular trafficking, and cilia function. The functional output of the microtubule cytoskeleton depends on a family of molecular motor proteins called kinesins. Genetic analysis has indicated that the human genome encodes for over 45 kinesin motor proteins belonging to 19 different families. All kinesins share a highly-conserved catalytic motor domain that converts the chemical energy of ATP hydrolysis into the mechanical outputs of force generation and directed "stepping" along microtubule tracks. How individual kinesins have adapted this basic enzymatic output for their specific functional roles in cells is an outstanding question in the field.

Previous work has largely focused on characterizing kinesin motility (e.g. velocity, run length) under single-motor, unloaded conditions using *in vitro* assays. However, in the crowded cellular environment, kinesins work in teams to transport membrane-bound cargos along a complex network of microtubules. Therefore, although we have a better understanding of the functional diversity of the kinesin motor domain under single molecule conditions, how divergent motility properties lead to emergent mechanisms of transport in cells is not clear. To bridge this gap, I adapted artificial cargo transport assays in cells to correlate how changes in a motor's single molecule properties impact their ability to collectively drive transport under physiological conditions.

Recent theoretical, biophysical, and computational studies predict that a motor's behavior under force is a critical parameter that dictates transport in cells. Generation of force by kinesin motors involves ATP-induced docking of the neck linker (NL) along the motor's core; however, the contributions of the proposed substeps of NL docking are unclear. Furthermore, whether sequence changes that modulate NL docking is a strategy to tune the functional output of a motor in cells has not been addressed.

In this dissertation, I first present work that uses a combination of techniques (computational, biophysical, and cellular) to address how NL docking impacts the functional output of kinesin-1 motors. Surprisingly, I find that motors with weakened NL docking are faster and more processive but at a cost to their force production. Furthermore, motors with weakened NL docking are crippled in their ability to drive transport of high-load cargo in cells, providing the first evidence that a power-stroke mechanism of force generation is critical for multi-motor driven transport under physiological conditions (Chapter 2). I further extend these results to other kinesin family members (Chapter 3).

Although biophysical studies have led to a better understanding of how family-specific sequence divergence within the kinesin superfamily tunes motility, how single residue changes implicated in disease impacts the functional output of a motor can be difficult to predict. We find that a majority of disease-associated mutations cluster in elements of the motor domain important for microtubule binding, force generation, and nucleotide binding/hydrolysis. We characterized the effect of two mutations predicted to impair NL docking in the kinesin-3 motor KIF1A under different load regimes to provide insight into how these mutations manifest in disease (Chapter 4). Collectively this work confirms the proposed role of the NL as a mechanical element important for force generation by kinesin motors and drives our understanding of how kinesins adapted this feature for their functional roles in the cell.

Chapter 1: Introduction

1.1 Introduction: the cytoskeleton builds the framework of a cell

Eukaryotic cells are highly complex. Their cellular contents can undergo dramatic reorganization and their overall structural organization can change to drive their movement. For instance, during cell division, chromosomes dynamically align and are pulled to opposite sides of the cell, ensuring proper inheritance of genetic material by each daughter cell. In highly polarized cells such as neurons, proteins and vesicles in the cell body move hundreds of microns to axon terminals within minutes (Craciun, Brown, & Friedman, 2005; Smith & Simmons, 2001). Finally, at the site of injury in a tissue, cells surrounding a wound undergo dramatic movement and constriction to promote closure of the wound (Rothenberg & Fernandez-Gonzalez, 2019). Although diffusion is responsible for many biochemical processes within a cell, it is unlikely that this type of motion could drive such dynamic, coordinated movements on a short time scale (Craciun et al., 2005; Fulton, 1982; Kristensson & Olsson, 1973)

Instead, to facilitate this complex set of cellular behaviors, eukaryotic cells evolved a dynamic network of cytoskeletal filaments that build the foundational framework of the cell. Specifically, actin and microtubules are polarized cytoskeletal filaments that are built from smaller subunits. Their disassembly and assembly into filaments is dependent on the ATP- or GTPase activity of their individual subunits (Erickson & O'Brien, 1992; R. Li & Gundersen, 2008). In cells, the slow-growing ends of microtubules (minus-ends) are typically anchored at the centrosome near the nucleus of the cell and their fast-growing ends (plus-ends) extend outwards in a radial array to span a large portion of the cell. Similarly, the pointed ends of actin (minus-ends) are oriented towards the center of the cell while the barbed ends (plus-ends) are directed outwards toward the cell periphery (Fletcher & Mullins, 2010).

The functional output of cytoskeletal filaments depends on their inherent dynamics and also on three major classes of molecular motors: microtubule-based kinesin and dynein motors and actin-based myosin motors. Specifically, motor proteins

convert the chemical energy of ATP hydrolysis into mechanical outputs of force generation and directed movement along cytoskeletal tracks (Schliwa & Woehlke, 2003; Vale, 2003). How the collective function of molecular motors drives such distinct, dynamic processes such as cell division, neuronal transport, and cell migration has been a longstanding question in cell biology and will provide fundamental insight into how disruption of cellular organization can manifest in disease (Hirokawa, Niwa, & Tanaka, 2010; Yu & Feng, 2010). This chapter will review what is known about how sequence conservation and divergence of the kinesin motor domain tunes its mechanical output as single motors, and how distinct single-molecule motility properties can manifest in functionally distinct outputs by groups of motors in a physiological context.

1.2 Molecular motors: diverse strategies for cellular organization

Although the dynamic nature of chromosomes and organelles has been noted as early as the late 1700s, technological advances in microscopy and fluorescent protein design in the 1980s led to a revolution of single-molecule techniques to study fundamental mechanisms of movement by cytoskeletal motor proteins (Allen et al., 1982; Ashkin et al., 1986; Axelrod, 1981; Brady, Lasek, & Allen, 1982; Kozminski et al., 1993). All three classes of motors have a globular motor domain that has ATPase activity and filament binding capabilities. Two catalytic motor domains are typically oligomerized through a coiled-coil element and a tail domain located at the end of the molecule specifies cargo binding (Schliwa & Woehlke, 2003; Vale, 2003). Changes in how motor proteins couple the energy of ATP hydrolysis to mechanical output and “stepping” along cytoskeletal filaments, allows motors to orchestrate a striking number of fundamental tasks in the cell, including intracellular transport, cytoskeletal organization, cell division, cilia function, and cell motility.

Kinesin and myosin motors each comprise two large superfamilies of motor proteins that typically walk to plus-ends of microtubules (Hirokawa et al., 2009; Verhey & Hammond, 2009) or actin filaments, respectively (Hartman & Spudich, 2012; Syamaladevi, Spudich, & Sowdhamini, 2012). The catalytic core of kinesin and myosin motors are composed of a similar set of structural elements (G-protein Ras-like fold), suggesting that they share a common ancestor and therefore similarities in how

nucleotide binding and hydrolysis are coupled to their mechanical output (Kull & Endow, 2013; Kull, Sablin et al., 1996; Kull, Vale, & Fletterick, 1998). Initially, the core motor domain of kinesin or myosin was predicted to impart the same mechanical output for all motors within each superfamily. Instead, the tail domain was thought to be the critical determinant for their distinct functions in cells. However, careful biophysical characterization of different kinesin and myosin motors suggest that subtle sequence divergence within each protein superfamily imparts distinct motility properties to a given motor (Hirokawa et al., 2009; Verhey & Hammond, 2009; Woolner & Bement, 2009).

Dynein (dynein heavy chain) is a member of the AAA+ superfamily, with a characteristic hexameric ring complex that is important for ATP hydrolysis and microtubule-based movement (Snider, Thibault, & Houry, 2008; Vale & Milligan, 2000). Unlike kinesin or myosin motors, where gene duplication events and sequence divergence resulted in a large number of motor proteins with distinct motility properties, there is only one dynein isoform that is responsible for microtubule minus end-directed transport in the cytoplasm of the cell [cytoplasmic dynein 1, (Paschal, Shpetner, & Vallee, 1987; Paschal & Vallee, 1987; Pazour, Dickert, & Witman, 1999; Porter et al., 1999)]. Instead, recent single-molecule work found that a number of proteins associate with dynein and can modulate its mechanical output to suit different functional requirements in the cell (Reck-Peterson et al., 2018).

Although prokaryotic organisms have tubulin- and actin-related proteins, new functional pressures faced by eukaryotic organisms led to the evolution of a “toolbox” of cytoskeletal motor proteins. Specifically, genomic analysis across a diverse number of eukaryotic organisms including fungi, parasites, plants and animals has revealed dramatic differences in their cytoskeletal motors and the cellular tasks they orchestrate (Vale, 2003). For instance, plants lack genes encoding for the dynein motor and instead have an expanded group of kinesin motors responsible for microtubule minus-end directed transport (Nebenfuhr & Dixit, 2018). Additionally, in *Saccharomyces cerevisiae*, the typical canonical transport kinesin-1 is lost and instead many transport events are driven along actin filaments by myosin motors (Bertrand et al., 1998; Catlett et al., 2000; Reck-Peterson et al., 2000). How diversification of the cytoskeletal “toolbox” leads to

distinct strategies to modulate the functional output of the cytoskeletal network across the eukaryotic kingdom is an exciting and open question in cell biology.

1.3 The kinesin superfamily: design principles of a motor protein

Shortly after the purification and characterization of conventional kinesin (kinesin-1) from squid axoplasm (Svoboda & Block, 1994; Vale & Fletterick, 1997; Vale, Reese, & Sheetz, 1985; Vale et al., 1985), many additional kinesin motors across the eukaryotic kingdom, including fungi, plants, and animals were identified. Genetic analysis now indicates that the human genome encodes for over 45 kinesin proteins belonging to 19 different families (Hirokawa et al., 2009; Lawrence et al., 2004; Miki, Okada, & Hirokawa, 2005; Verhey & Hammond, 2009).

All kinesins have a highly typical architectural structure. They have a conserved core motor domain (~40-60% sequence identity) with signature sequences for binding nucleotide and microtubules. Kinesins are grouped according the position of the motor domain in the protein: the motor domain is located at the amino-terminal end in N-kinesins, the carboxy-terminal end in C-kinesins, and in the middle of the protein for M-kinesins (Hirokawa et al., 2009). Following the core motor domain is a short, flexible element called the neck linker [NL, (Hariharan & Hancock, 2009; Kozielski et al., 1997)] and a coiled-coil sequence responsible for dimerizing the two motor domains. The coiled-coil stalk contains stretches of uncoiled hinges that enable the motor to fold into an autoinhibited conformation, preventing the motor domain from interacting with the microtubule track and futile consumption of ATP (Cai et al., 2007; Coy, Wagenbach, & Howard, 1999; Friedman & Vale, 1999; Verhey & Hammond, 2009). Finally, a divergent globular tail domain is responsible for facilitating interaction with a variety of cargoes including membrane-bound organelles and vesicles, mRNA, protein complexes, or microtubules. Different adaptor proteins associate with kinesins, providing additional mechanisms to regulate motor activity and cargo specificity in cells (Akhmanova & Hammer, 2010; Hirokawa & Noda, 2008; Kamal & Goldstein, 2002; Verhey & Hammond, 2009).

Since the discovery of the first kinesin motor, the molecular mechanism responsible for its ability to move along microtubules has been of great interest. The first hints towards a mechanism of transport came from classical biochemical experiments

that found that (1) kinesin-1 motors co-sediment with microtubules in the presence of a non-hydrolyzable ATP analog (AMPPNP) and (2) purified kinesin motors drive fast, long-range transport of latex beads in an ATP-dependent manner (Block, Goldstein, & Schnapp, 1990; Howard, Hudspeth, & Vale, 1989; Svoboda & Block, 1994; Svoboda et al., 1993; Vale et al., 1985).

Soon after, electron paramagnetic resonance (EPR) spectroscopy and fluorescence resonance energy transfer (FRET) studies found that the NL undergoes considerable conformational changes (Rice et al., 1999; Rosenfeld, Jefferson, & King, 2001). In addition, structural studies reveal that the NL is docked along the motor domain when in the ATP-bound state (Kozielski et al., 1997; Kull et al., 1996; Sack et al., 1997). Collectively, this led to the prediction that the NL serves as a mechanical element important for processive stepping and force generation. Indeed, deletion or mutation of the NL severely compromised directed, plus-end movement of kinesin-1 motors (Case et al., 1997; Case et al., 2000).

Substantial work since these seminal observations have led to a detailed mechanism of how kinesin-1 motors step along microtubules. Specifically, the NL undergoes a transformation from being flexible in both the ADP-bound and nucleotide-free states to being docked along the core motor domain in the ATP-bound state (Asenjo, Weinberg, & Sosa, 2006; Gigant et al., 2013; Rice et al., 1999; Rosenfeld et al., 2001; Shang et al., 2014; Sindelar et al., 2002; Sindelar & Downing, 2010; Skiniotis et al., 2003; Wade & Kozielski, 2000). Thus, in a dimeric kinesin motor, NL docking of the leading motor domain positions the lagging motor domain forward along the microtubule track, thereby specifying direction of motility (Figure 1.1). Moreover, high-resolution tracking of kinesin-1 motors demonstrate that they step in a foot-over-foot manner, taking one 8 nm step per hydrolysis of one molecule of ATP (Asbury, Fehr, & Block, 2003; Coy et al., 1999; Schnitzer & Block, 1997; Svoboda & Block, 1994; Yildiz et al., 2004).

Strikingly, under single-molecule conditions, kinesin-1 motors can take over a hundred steps along the microtubule track before dissociating, which suggests that the activity of each motor domain is somehow coupled to one another. Indeed, studies where the orientation of the NL was carefully manipulated using an optical trap indicate

that the docked versus undocked state of the NL is responsible for coordinating the ATPase cycles of the two motor domains. Tight coupling between the ATPase activity of the motor and force generation ensures that one domain always remains bound to the microtubule as the other steps forward (Case et al., 2000; Clancy et al., 2011; Dogan et al., 2015; Hahlen et al., 2006; Isojima et al., 2016; Liu et al., 2017; Tomishige & Vale, 2000; Yildiz et al., 2008). Collectively, this work explains the mechanochemical model for kinesin motility, where the motor's biochemical activities are tightly coupled to its mechanical movement (Figure 1.1).

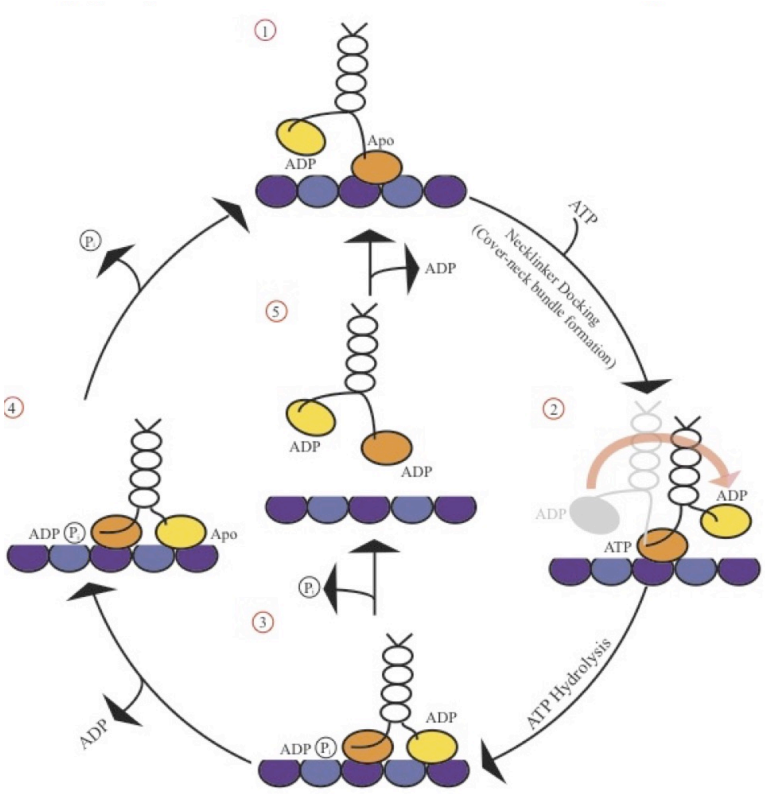

Figure 1.1. Kinesin mechanochemical cycle.

The nucleotide state of each motor domain (yellow and orange) is tightly coupled to the motor's affinity to the microtubule (light purple α-tubulin, dark purple β-tubulin). **(1)** Microtubule binding causes the release of ADP and strong microtubule binding (apo, orange). **(2)** ATP binding and causes conformational changes across the motor domain resulting in cover-neck bundle formation and neck linker docking along the motor domain (orange). Neck linker docking causes forward stepping of the lagging head to the next binding site along the microtubule (yellow) **(3)** ATP is hydrolyzed in the now lagging head (orange) to ADP and P_i. **(4)** The now leading head (yellow), binds to the microtubule, releases ADP, and binds tightly to the microtubule. The lagging head (orange) eventually releases P_i and detaches from the microtubule track. The motor is then poised for the next hydrolysis cycle. Continued coordination of alternating ATPase cycles of each motor domain results in processive stepping along the microtubule.

1.4 Design principles of a kinesin motor

Given the high sequence and structural conservation of the kinesin motor domain, the biological significance for why organisms require a large number of kinesins is an important question in cell biology. Indeed, knock out or known down of specific motors across the kinesin superfamily in a variety of model organisms suggest that motors serve unique, specialized roles in fundamental mechanisms of a cell and play important roles at the multicellular level during development (Hirokawa et al., 2009). One possibility is that the divergent tail domain is important for defining the specificity of a motor in a biological context. Strikingly, studies where the catalytic core of a kinesin was replaced by one from a different kinesin motor, found that the chimeric motor was not functionally equivalent (Kim, Fonseca, & Stumpff, 2014; Ravindran et al., 2017). Thus, in addition to the functional specificity imparted by the tail domain, the catalytic core and NL are also important for specifying the mechanical output of a motor to best suit its function in cells.

Although much of what we know about kinesin mechanochemistry is based on biophysical and biochemical studies of kinesin-1 (velocity, run length, landing rate, force generation, sensitivity to detaching from the microtubule track under force), in the past 10 years the motility properties of other kinesin families have been characterized to provide insight into their functional diversity in cells. Many kinesin motors are processive, meaning they can take many steps along the microtubule track before detaching [kinesin-1 (Howard et al., 1989); kinesin-2 (Muthukrishnan et al., 2009); kinesin-3 (Soppina & Verhey, 2014); kinesin-5 (Valentine et al., 2006); kinesin-7 (Yardimci et al., 2008); kinesin-8 (Varga et al., 2006)]. Processive motors typically serve important roles driving intracellular transport or movement of microtubules during cell division (Hirokawa et al., 2009). Surprisingly, there are a number of kinesin motors that are non-processive, taking only a few steps before detaching from the microtubule, or immotile and are unable to step [kinesin-4; (He et al., 2014; Yue et al., 2018); kinesin-10 (Cochran et al., 2009); kinesin-14 (Furuta et al., 2013; Jonsson et al., 2015)]. Kinesin motors can also influence microtubule dynamics [kinesin-4 (Yue et al., 2018); kinesin-5 (Chen et al., 2019; Chen & Hancock, 2015); kinesin-8 (Locke et al., 2017); kinesin-13

(Helenius et al., 2006; Hunter et al., 2003)]. How the highly conserved motor domain imparts striking diversity in the mechanical output of a kinesin motor is not clear.

Much like how the engine of a car is built to reach high speeds in a matter of seconds or to generate enough power to pull large loads, how the kinesin motor domain is built is thought to tune its mechanical output to best meet its functional needs in cells. Almost 10 years after the discovery of conventional kinesin, the first structure of the kinesin motor domain was solved by x-ray crystallography (Kozielski, et al., 1997; Kull et al., 1996; Sack et al., 1997). Since then, over 100 kinesin structures across a number of different kinesin families have been deposited on the Protein Data Bank, revealing that the topology of the kinesin motor domain is highly conserved. Specifically, the kinesin motor domain consists of eight central beta-sheets (β1-β8, purple) surrounded by six alpha helices (α1- α6, yellow) that are connected by flexible loop regions [(Cao et al., 2014), cyan, Figure 1.2]. Notably, there are many family-specific sequence variations within the flexible loop elements. At the N- and C-terminus of the motor domain are short mechanical elements called the coverstrand (CS) and neck liker [NL, (Hariharan & Hancock, 2009; Hwang, Lang, & Karplus, 2008; Khalil et al., 2008; Nitta, Okada, & Hirokawa, 2008)].

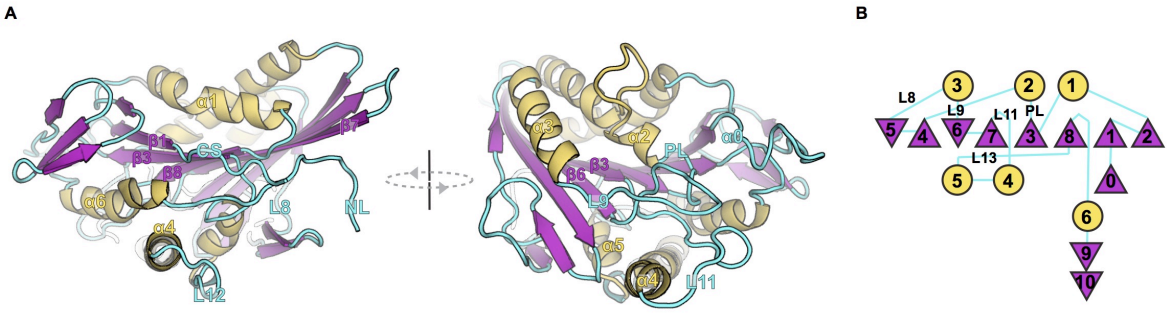

Figure 1.2. Conserved topology of the kinesin motor domain

(**A**) Cartoon ribbon representation of the kinesin-1 (*Rn*KIF5C) motor domain in ATP-bound state (PDB 4HNA). Secondary structure elements are indicated: α-helix (yellow), β-sheet (purple), loop (cyan). Left image shows the neck linker (NL) docked along the motor domain; Right image shows the motor domain rotated 90° to show the nucleotide-binding pocket.
(**B**) Diagram of secondary structure topology of the kinesin motor domain. β-sheets are depicted as triangles, α-helixes as circles, and loops as lines. Secondary elements are colored as in (A).

Structural elements of the kinesin motor domain can be grouped according to their functional roles in motility, such as microtubule binding, nucleotide binding/hydrolysis, and stepping/force generation. Thus, sequence divergence within these elements or sequence changes in other regions of the motor domain that influence the coupling between these functional elements may have a substantial impact on whether a motor functions as a transporter, cytoskeletal tether, and/or regulator of microtubule dynamics in cells. Below I will review what is known about how sequence divergence of the kinesin motor domain modulates its functional output.

1.4.1 The Nucleotide-binding pocket is highly conserved across the kinesin superfamily

Surprisingly, the first structures of the kinesin motor domain revealed that the nucleotide-binding pocket is highly similar to the nucleotide-binding pocket of myosin motors and G-proteins [P-Loop containing proteins with a Walker fold; (Kull et al., 1998; Walker et al., 1982)]. There are four motifs that make up the nucleotide-binding pocket: P-Loop, Switch1, Switch2, and N4-α0 (Figure 1.3). These elements are important for ATPase activity and for communication with microtubule binding and force generating elements. For instance, kinetic and structural studies reveal that the P-Loop (GXXXXGKT/S, Loop4) and N4-α0 are critical for tight nucleotide binding, making important interactions with α- and β-phosphates and the purine base of the nucleotide, respectively (Kull et al., 1996; Sablin et al., 1996; Sack et al., 1997).

Switch1 (NXXSSR, β6-Loop9) and Switch2 (DXXGXE, β7-Loop11-α4) of the nucleotide-binding pocket undergo considerable conformational changes throughout the ATPase cycle of the motor domain and serve a critical role in coupling microtubule binding and force generation to the nucleotide state of the motor domain. Specifically, collision of the ADP-bound motor domain with the microtubule results in elongation of Loop11-α4 in Switch2 allowing the motor to strongly bind to the microtubule. The conformational change in Loop11-α4 is relayed to the nucleotide-binding pocket and ADP is exchanged for ATP. Thus, the conformation of Switch2 plays a critical role in stimulating ATPase activity of the motor domain in the presence of microtubules (Atherton et al., 2014; Gigant et al., 2013; Shang et al., 2014).

In addition, the conformation of Switch1 and 2 (open or closed) is tightly coupled to elements important for generating force. Specifically, closure of Switch1 and 2 when ATP binds results in extension of α6 to position the NL into the docking pocket for force generation [Figure 1.5, (Atherton et al., 2014; Gigant et al., 2013; Shang et al., 2014)]. Recent kinetic studies suggest that docking of the NL locks the motor domain in a hydrolysis competent state (nucleotide-binding pocket is closed). Thus, in addition to playing a role in force generation, NL docking regulates ATPase activity of the motor domain (Cao et al., 2014; Geeves & Holmes, 1999; Hahlen et al., 2006; Parke et al., 2010). Once ATP is hydrolyzed and phosphate is released, Loop11-α4 of Switch2 shortens and the motor domain detaches from the microtubule (Atherton et al., 2014; Gigant et al., 2013; Shang et al., 2014). Collectively, for a motor to step processively, Switch2 must stimulate ADP release upon binding to the microtubule, and closure of Switch1 and 2 after ATP binding must drive stepping and ATP hydrolysis. Tight coupling of these two steps would enable one motor domain to remain attached the microtubule as the next head steps forward (Muretta et al., 2015; Muretta et al., 2018).

Sequence alignment of the elements important for nucleotide binding show considerable conservation, highlighting a common mechanochemical strategy for ATPase activity across the kinesin superfamily (Figure 1.3). Single amino acid residue changes in elements of the nucleotide-binding pocket of processive, transport kinesins abolishes their ATPase activity or decouples communication between the nucleotide-binding pocket with elements important for microtubule binding and force generation (Auerbach & Johnson, 2005; Brendza et al., 1999; Cao et al., 2017; Jennings et al., 2017; Song & Endow, 1998; Yun et al., 2001).

Kinesin motors that do not step processively have subtle sequence changes in elements important for nucleotide binding and hydrolysis or sequence changes that decouple microtubule binding with nucleotide binding and hydrolysis. For example, kinesin-10 NOD, kinesin-6 MKLP2, and kinesin-13 motor MCAK have 2 amino acid residue changes in N4-α0 that are predicted to destabilize nucleotide binding to cause slow catalytic activity (Atherton et al., 2017; Cochran et al., 2009). Strikingly, non-motile kinesin-4 motor KIF7 fails to release ADP when it binds to a microtubule (Yue et al., 2018), consistent with structural studies that find Loop11 of Switch2 is elongated and

adopts a strong microtubule binding conformation independent of the nucleotide status of the motor domain (Jiang et al., 2019). Decoupling microtubule binding from nucleotide binding results in a motor that binds strongly to a microtubule independent of the nucleotide state of the motor, potentially allowing this motor to serve as a cytoskeletal tether rather than a canonical transport motor.

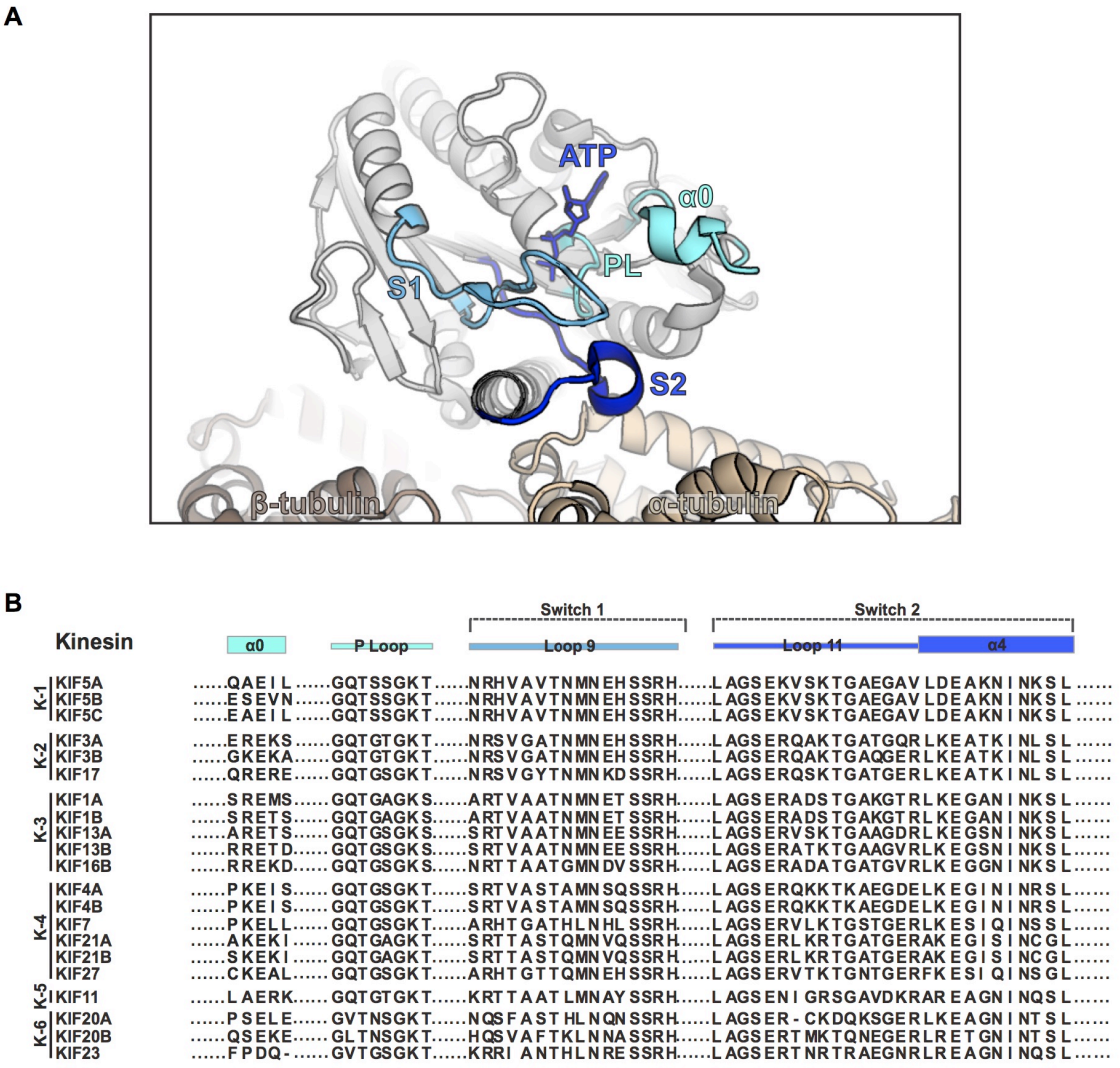

Figure 1.3. Nucleotide-binding pocket of the kinesin motor domain

(**A**) The kinesin-1 motor domain in the ATP-bound, post-power stroke state is shown as a cartoon ribbon representation (PDB 4HNA). Secondary structure elements of the nucleotide-binding pocket are colored: α0 (cyan), PL (P-Loop, cyan), Switch1 (S1, blue), Switch2 (S2, dark blue). (**B**) Sequence alignment of secondary elements that make up the nucleotide-binding pocket of human kinesin-1, -2, -3, -4, -5, and -6 families. Secondary elements colored as in (A).

In addition, sequence changes or point mutations in elements outside the nucleotide-binding pocket can also impact nucleotide binding and hydrolysis. Specifically, kinesin-5 motors contain a unique sequence insertion in Loop-5, which is located above the nucleotide-binding pocket. Loop5 is predicted to regulate ATP binding and closure of Swich1 and 2, interfering with coupling between NL docking and ATPase activity (Cochran et al., 2005; Sindelar & Downing, 2010; Yun et al., 2001). Loose coupling between closure of the nucleotide binding pocket and force generation creates a situation where the motor domain remains bound to the microtubule track for some time after it generates a power stroke. This may be favorable for motors to resist detachment from the microtubule track under high forces, consistent with Eg5's role in sliding microtubules during cell division (Muretta et al., 2015; Muretta et al., 2018).

1.4.2 Microtubule-binding footprint

As a dimer in solution, the kinesin motor domain is bound to ADP and has a low affinity for the microtubule. However, collision of the motor domain with the microtubule results in the release of ADP and the motor domain consequently adopts a strong microtubule-binding state. When bound to the microtubule, α4 of the kinesin motor domain sits at the intradimer cleft of an αβ-tubulin dimer and Loop2, Loop7, Loop8, Loop11, Loop12, α5, and the N-terminus of α6 of the kinesin motor domain make important electrostatic interactions with α- and β-tubulin (Figure 1.4). Previous work comparing the sequence of elements that make up the microtubule binding interface across eleven kinesin family members identified a conserved set of positively charged residues (R161, K166, K237, R278, K281, and R284; residue number with respect to kinesin-1 KIF5C) that are predicted to be critical for binding to negatively charged residues of α- and β-tubulin. However, there are also family-specific differences in the electrostatic properties of the microtubule-binding interface and family-specific sequence insertions that change the way the motor domain binds to a microtubule. Collectively, this suggests that different kinesins have tuned their ability to interact with microtubules to best meet their functional needs in the cell [Figure 1.4; (Grant et al., 2011)].

For processive kinesins, sequence changes in elements important for binding to the microtubule can impact the ability for the motor to associate with the microtubule to start a processive run (landing rate) and also the distance a motor travels along the microtubule before it detaches (processivity, run length). For instance, kinesin-3 motor KIF1A is known for its high landing rate and superprocessivity. Sequence alignment of the motor domain reveals a family-specific insertion of positively charged lysine residues in Loop12 (K-loop) of the motor domain (Figure 1.4). Structural and biophysical studies reveal that the K-loop tethers the motor domain to negatively-charged glutamate

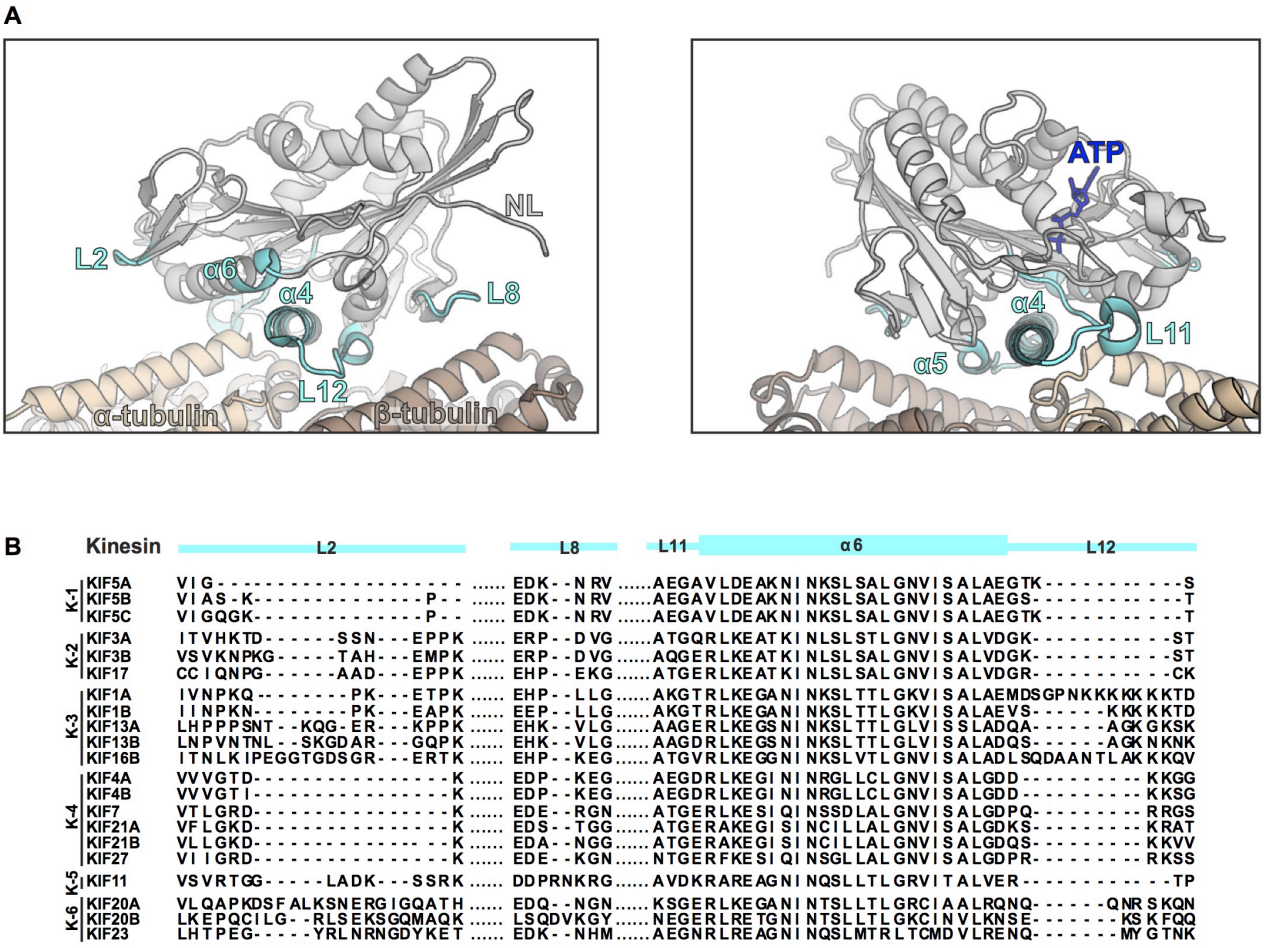

Figure 1.4 Sequence alignment of microtubule-binding elements of the kinesin motor domain

(**A**) The kinesin-1 motor domain in the ATP-bound, post-power stroke state is shown as a cartoon ribbon representation (PDB 4HNA). Left image shows the neck linker docking pocket, right image is a 90° rotation to view the nucleotide-binding pocket. Secondary structure elements important for microtubule binding are colored in cyan. (**B**) Sequence alignment of secondary elements important for microtubule binding of human kinesin-1, -2, -3, -4, -5, and -6 families. Secondary elements colored as in (A).

residues in the C-terminal tail of tubulin (E-Hook), enhancing the motor's initial interaction with the microtubule (Kikkawa, Okada, & Hirokawa, 2000; Okada & Hirokawa, 1999, 2000; Soppina & Verhey, 2014). Furthermore, recent molecular dynamics simulations that compared KIF1A and KIF5C (kinesin-1) binding to tubulin find that KIF1A has a unique set of positively-charged residues within Loop8, Loop11, and α6 that make important interactions with negatively-charged residues in α- and β-tubulin throughout the ATPase cycle. Mutation of these residues in biophysical experiments has attributed these residues to be important for endowing KIF1A motors with superprocessivity (Nitta et al., 2004; Scarabelli et al., 2015; Soppina & Verhey, 2014; Uchimura et al. , 2010). A high landing rate and superprocessivity would assure that vesicles containing only a few KIF1A motors will associate with the microtubule to begin transport and once associated will ensure that cargoes will reach their destination. This may be critical in neurons, where cargoes are transported long distances over a short period of time (Hall & Hedgecock, 1991; Okada et al., 1995; Otsuka et al., 1991).

Unlike processive kinesin motors that couple tight and weak microtubule binding to the nucleotide state of the motor domain, there are kinesins whose affinity to the microtubule is not tightly coupled to the nucleotide state of the motor domain and are non-processive or non-motile (Atherton et al., 2017; Cochran et al., 2009; Yue et al., 2018). These "non-canonical" motors tend to have sequence changes within nucleotide-binding elements that decouple nucleotide and microtubule binding (1.4.1) as well as striking differences in elements important for binding to the microtubule. For instance, kinesin-6 motor MKLP2 has a sequence insertion of positively charged residues in Loop12 as well as a net increase in positively charged residues that make up the microtubule-binding interface that collectively are predicted to allow for strong binding to the microtubule independent of the nucleotide state of the motor domain. Furthermore, large sequence insertions in Loops 2 and 8 alter the way the motor domain interacts with the microtubule and may be important to specify the motor's preference for a subset of microtubules within the spindle (Atherton et al., 2017). Furthermore, recent structural studies of a non-motile kinesin-4 motor KIF7 find that the net negative charge of the microtubule-binding interface of the motor domain changes the way the motor domain interacts with the microtubule to specify motor binding to GTP tubulin at the tips

of microtubules (Jiang et al., 2019). However live imaging experiments characterizing the motor's localization along microtubules in cells combined with mutational analysis is needed to confirm this prediction. Collectively, striking differences in how MKLP2 and KIF7 interact with the microtubule may reflect an important requirement for motors to serve as cytoskeletal tethers in specific cellular compartments (midbody or cilia) for proper signaling or cell division.

Finally, kinesin motors can alter microtubule dynamics. Electron micrographs suggest that microtubule plus-ends undergoing growth or catastrophe consist of curved bundles of protofilaments (McIntosh et al., 2018; Pyles & Hastie, 1993; Rice, 2018). Thus, growth requires tubulin at the plus-end to undergo a curved to straight transition, a conformation compatible for incorporation into the lattice by lateral contacts with neighboring tubulin. However, if tubulin at the plus-end is stabilized in a curved conformation, tubulin is unable make lateral contacts with neighboring tubulin and eventually the plus end depolymerizes (Arellano-Santoyo et al., 2017; Benoit, Asenjo, & Sosa, 2018; Wang et al., 2016). Thus, a motor's preference to bind (1) curved versus straight tubulin, and (2) tubulin polymers at the ends of microtubules versus tubulin incorporated into the lattice is predicted to determine whether a motor can impact microtubule dynamics (Chen et al., 2019). Indeed, a sequence insertion in Loop2 of kinesin-13 motor MCAK is important for the motor's ability to bind tubulin curls at microtubule plus ends and promote depolymerization (Asenjo et al., 2013; Friel & Howard, 2011; Ogawa et al., 2004; Shipley et al., 2004).

A number of recent biophysical studies have found that Loop11 of the kinesin motor domain, which sits at the interface of α- and β-tubulin (Figure 1.4), confers unique abilities for processive kinesins to recognize and/or change the conformation of tubulin at microtubule plus-ends. Specifically, kinesin-8 motor Kip3 walks processively and accumulates at the plus-ends of microtubules (Locke et al., 2017; Wang et al., 2016). At the microtubule plus-end, Loop11 specifies binding of Kip3 to curved tubulin to promote disassembly (Arellano-Santoyo et al., 2017). In contrast, α4-Loop11 of kinesin-5 motor Eg5 encourages straightening of curved tubulin to promote assembly at microtubule plus-ends (Chen et al., 2019; Chen & Hancock, 2015). This is consistent with α4-Loop11 of kinesin-1 motor KIF5C imparting preference for the motor to bind GTP-like

tubulin in the microtubule lattice (straight tubulin) (Shima et al., 2018). Notably, binding of KIF5C to a GDP-compacted lattice can drive lattice expansion by driving straightening of tubulin dimers (Peet, Burroughs, & Cross, 2018; Shima et al., 2018). Collectively, these results suggest subtle sequence changes in Loop11 not only specify a motor's preference to a specific population of tubulin but can also confer structural changes to tubulin and alter microtubule dynamics. We are just starting to understand the nuances of how kinesin motors bind to microtubules and/or free tubulin. Additional biophysical and structural studies are needed to assess whether this is a conserved strategy to shed light on functional differences across members of the kinesin superfamily.

1.4.3 Elements important for stepping and force generation have subtle sequence changes that are predicted to impact kinesin motility

Although the roles of the NL for specifying stepping directionality and processivity are better understood (1.3), the role of the NL in force generation has been controversial. Optical trapping studies find that single kinesin-1 motors can step against 5-7 pN of force (Svoboda & Block, 1994). However, how conformational changes in a short, flexible element are responsible for robust force production was unclear (Astumian & Derenyi, 1999; Block, 2007; Kikkawa et al., 2001; Mather & Fox, 2006). Recent studies combining single-molecule assays and molecular dynamics simulations have provided insight into how ATP-dependent NL docking drives stepping against load by kinesin-1 motors. Specifically, NL docking involves distinct interactions of the two β-strands that comprise the NL, β9 and β10 (Figure 1.5A). The first half of the NL, β9, pairs with another β-strand, the coverstrand (CS or β0), located at the opposite end of the core motor domain. The zippering of β9 of the NL with β0 of the CS forms a 2-stranded β-sheet, termed the cover-neck bundle (CNB), to provide the power-stroke for force generation [Figure 1.5A, (Budaitis et al., 2019; Hwang et al., 2008; Khalil et al., 2008)]. After CNB formation, the C-terminal segment of the NL (β10) docks along the surface of the core motor domain. In particular, an asparagine residue between β9 and β10 begins the process of docking β10 of the NL onto β7 of the motor core (Figure 1.5A). This asparagine residue (N334) serves as a latch (the N-latch) to hold the docked

NL along the core motor domain and coordinate stepping under load (Budaitis et al., 2019; Hwang et al., 2008).

1.4.3.1 Conservation of the cover-neck bundle

Although CNB formation has been observed structurally for other kinesin motors (Atherton et al., 2014; Atherton et al., 2017; Gigant et al., 2013; Hesse et al., 2013; Ren et al., 2018), a mechanical role in force generation has only been tested for kinesin-1 (Budaitis et al., 2019; Hesse et al., 2013; Khalil et al., 2008). For kinesin-1, zippering of the CS and β9 of the NL to form the CNB is initiated by C-terminal residue (CTR) I9 of the CS and N-terminal residue (NTR) I327 of β9. Indeed, the CTR and NTR of all kinesins are hydrophobic residues that have a high propensity to form a β-sheet (Kim & Berg, 1993). However, the remaining residues of the CS are highly variable in length and sequence (Figure 1.5B).

Notably, point mutations to weaken CNB of kinesin-1 increased the speed and processivity of single motors but at the cost to generating a strong power stroke and transporting continuously under load (Budaitis et al., 2019; Khalil et al., 2008). Thus, it is tempting to predict that differences in CNB formation in other processive kinesins may be a strategy to fine-tune motility. It is interesting that kinesin-3 motors have the shortest coverstrand (4-6 residues compared to 9-10 residues for kinesin-1, Figure 1.5B) and are predicted to have weak, dynamic CNB formation (Ren et al., 2018). It is possible that kinesin-3 motors evolved to have a short coverstrand for fast processive, transport of presynaptic vesicles over long distances in neurons, where high force production may not be required (Hall & Hedgecock, 1991; Okada et al., 1995; Otsuka et al., 1991). Future work characterizing the behavior of kinesin-3 motors with sequence changes to lengthen CNB formation under load will be important to test this possibility.

Unlike kinesin-1 motors that slow and stall under load [stall force 5-7 pN; (Svoboda & Block, 1994)] the kinesin-5 motor Eg5 has a tendency to abruptly detach from the microtubule track [detachment force 1.5 pN – 4.6 pN, (Korneev, Lakamper, & Schmidt, 2007; Lakamper et al., 2010; Muretta et al., 2018; Valentine et al., 2006)]. Particularly, Eg5 has a proline residue in β9 of the NL that is predicted to shorten CNB formation and therefore the motor is predicted to have a reduced power stroke and a

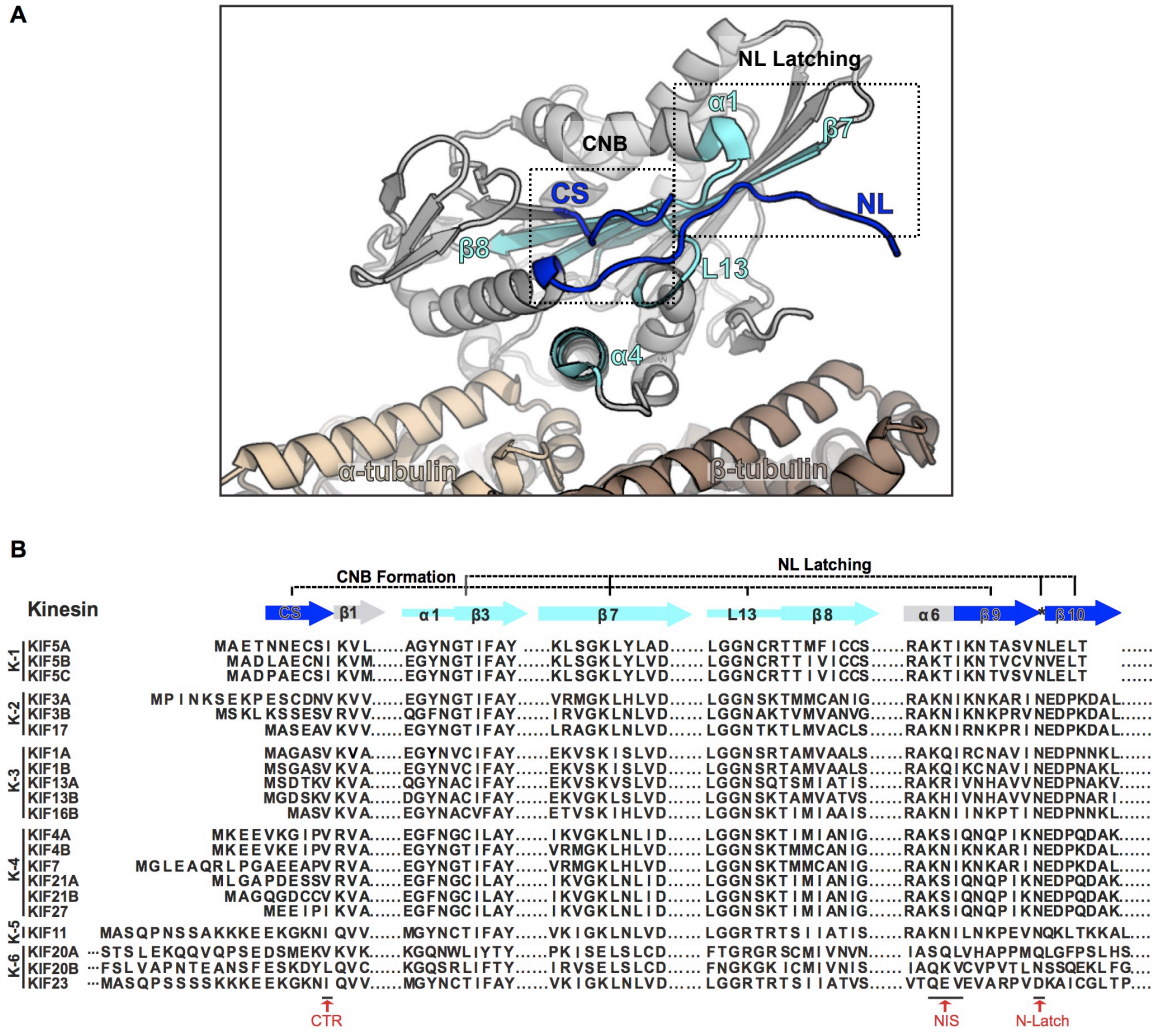

Figure 1.5 Sequence Alignment of Elements Important for Stepping and Force Generation

(**A**) The kinesin-1 motor domain in the ATP-bound, post-power stroke state is shown as a cartoon ribbon representation (PDB 4HNA). Secondary structure elements are colored: coverstrand (CS, blue), α1-β3 (cyan), β7 (cyan), Loop13 (L13, cyan), β8 (cyan), neck linker (NL, β9-β10, blue). (**B**) Sequence alignment of elements important for stepping and force generation from human kinesin-1, -2, -3, -4, -5, and -6 families. Secondary elements colored as in (A).

sensitivity to detaching from the microtubule under load. However, increased electrostatic interactions between β9 of the NL and Loop13 of the docking pocket are predicted to help lock β9 along the motor domain to compensate for poor CNB formation and enable the motor to step under moderate forces (Hesse et al., 2013). A number of other kinesin motors (kinesin-2, -3, -4) have a proline residue in of β9 of the NL (Figure 1.5B), although its impact on the force output of these motors is not clear.

Unlike many kinesins that processively step along microtubules, many non-processive or immotile kinesins have large N-terminal extensions (>40 residues long).

These N-terminal extensions are predicted to form a globular structure and bind to cytoskeletal elements or signaling components [kinesin-3 KIF14, (Arora et al., 2014; S. Rice, 2014); kinesin-5 Cut7 (Edamatsu, 2016), BimC (Stock, Chu, & Hackney, 2003); kinesin 6 MKLP2 (Atherton et al., 2017), KIF20B (Das et al., 2018), MKLP1 (Guan et al., 2017); kinesin-10 NOD (Cochran et al., 2009)]. It is possible that these motors are unable to form a typical CNB to generate a power stroke and therefore step like kinesin-1 motors. Unfortunately, the impact of large N-terminal extensions on motility properties to these motors is not clear as many structural, biochemical, and biophysical studies remove this region. Therefore, studies of non-truncated motors are required to understand the effects of N-terminal extensions on the ATPase activity and stepping behavior of these motors to better understand how this sequence divergence is functionally advantageous.

1.4.3.2 Conservation of neck linker latching

For kinesin-1, an asparagine residue between β9 and β10 begins the process of docking β10 of the NL onto β7 of the motor core (Figure 1.5). This asparagine residue (N334) serves as a latch (the N-latch) to hold the docked NL along the core motor domain and coordinate stepping under load (Budaitis et al., 2019; Hwang et al., 2008). The asparagine residue involved in N-latch formation is highly conserved across processive kinesins, suggesting that N-latch formation may be a conserved feature for kinesin force generation (Figure 1.5B). However, whether N-latch formation and docking of β10 along the core motor domain play important roles beyond kinesin-1 remains to be investigated.

A number of kinesin motors lack the N-latch and/or have an extended NL (>20 residues [orphan kinesin PAKRP2 (Gicking et al., 2019); kinesin-6 MKLP2 (Atherton et al., 2017), KIF20B (Das et al., 2018), MKLP1 (Guan et al., 2017); kinesin-4 KIF7 and KIF27 (Yue et al., 2018), kinesin-10 NOD (Cochran et al., 2009)]. Extension of the NL is predicted to prevent coordination of the two motor domains in a dimeric motor and compromise processivity. Although single-molecule studies where extension of the NL in transport kinesin-1, -2, and -3 families disrupts stepping (Kutys, Fricks, & Hancock, 2010; Shastry & Hancock, 2010, 2011), kinesins with an extended NL display a surprising diversity in their motility properties. For example, PAKRP2 in plants has an

extended NL but is surprisingly highly processive as single motors. High-resolution tracking of PAKRP2 motility reveals that its ability to sidestep paired with the slow ATP hydrolysis rate of the motor head results in tight mechanochemical coupling required for processive motility (Gicking et al., 2019). In addition, kinesin-6 motor MKLP1 that plays an important role in organization of the central spindle during cytokinesis (White & Glotzer, 2012), has an extended NL [75 residues, (Guan et al., 2017)]. It predicted that the extended NL allows the motor to bind to microtubules in a two-head bound state, important for its cross-linking and bundling activity. In addition, the NL contains a binding site for a Rho-GTPase. Binding of MgcRacGAP (Rho-GTPase) is predicted to "zip" up the NL and allow for slow, plus-end motility (Glotzer, 2005; Nishimura & Yonemura, 2006). Thus, depending on the functional demands of the cell, MKLP1 may uniquely serve as a microtubule tethering element, a microtubule organizer, or a transport motor.

Finally, kinesin-4 motor KIF7 that plays an important role in hedgehog signaling has an extended NL and is immotile (Yue et al., 2018). NL swapping studies suggest that the inability for KIF7 to move along microtubules is not due to reduced mechanochemical coupling between motor domains but instead a result of properties of the catalytic core, consistent with recent structural studies (Jiang et al., 2019; Yue et al., 2018). Why KIF7 has a long NL and whether it serves an important role for binding to the microtubule in a two-headed bound state or serves as an important region for binding to signaling elements is not clear.

Collectively, kinesins have unexpected strategies to achieve processive motility and this highlights the importance of not assuming a motor's motility properties solely based on sequence comparison to the kinesin-1 motor domain.

1.5 Limitations of *in vitro,* single-molecule assays

Development of a number of *in vitro* motility assays [microtubule gliding assays, single-molecule total internal reflection fluorescence (TIRF) microscopy assays, and bead/optical trap transport assays; (Block et al., 1990; Funatsu et al., 1995; Howard et al., 1989; Sheetz & Spudich, 1983; Svoboda & Block, 1994; Vale, Schnapp, et al., 1985)] led to remarkable insights into the mechanism of how kinesin-1 motors move along microtubules. Building off of our understanding of the mechanochemical cycle of

kinesin-1 motors, there has been extensive characterization of the motility properties of other kinesin families (velocity, run length, landing rate, force generation, sensitivity to detaching under load). Although *in vitro* motility assays allow for high spatial and temporal tracking of motors, revolutionizing our understanding of diversity in the functional output of kinesin motors, this simplified approach does not always reflect the physiological environment of the cell that kinesins were evolved to function under. Therefore, how different single-molecule motility properties adapt a motor for its specialized functions in cells is not well understood.

1.5.1 Single-molecule total internal reflection fluorescence (TIRF) microscopy assays

In standard single-molecule TIRF assays, the motility of single motors is tracked along taxol-stabilized microtubules. However, in cells, the microtubule network is dynamic, dense, decorated by a number of different microtubule-associated proteins (MAPs), and often carries posttranslational modifications (Amos & Schlieper, 2005; Magiera & Janke, 2014; Yu, Garnham, & Roll-Mecak, 2015). Therefore, how kinesin motors respond to this complexity or have adopted different strategies to overcome this complexity to carry out their functions in cells is difficult to predict. To address this, a number of groups have built complexity into *in vitro* assays to more closely resemble the environment of the cell. For instance, characterization of kinesin motility along dynamic microtubules, posttranslationally-modified microtubules, microtubules decorated by MAPs and other road blocks, or transport across microtubule intersections have provided substantial insights into the behavior of kinesin motors in cells. Specifically, kinesin-1 motors are likely to pause at roadblocks or microtubule intersections while kinesin-2 and -3 motors can sidestep or detach from and reattach to the microtubule track and continue to drive transport. In addition, kinesin motors have different preferences for posttranslational modifications or MAPs, which may dictate the tracks of microtubules they can drive transport along in cells. This is predicted to play a critical role dictating transport and organization in neurons (Bergman et al., 2018; Hoeprich et al., 2017; Kaul, Soppina, & Verhey, 2014; Lessard et al., 2019; Ross et al., 2008; Schneider et al., 2015).

Single-molecule TIRF assays are used to characterize a motor's unloaded motility properties. However, in cells, motors may be tasked with driving transport of cargoes that require high force production. Standard optical trapping studies show that single kinesin-1 motors can continuously step against high forces [5-7 pN (Svoboda & Block, 1994)], while kinesin-2 motor KIF3AB tends to detach from the microtubule track when subjected to low forces [1 pN, (Andreasson et al., 2015)]. Therefore, although both motors are fast and processive under unloaded conditions, their ability to drive transport against high load is strikingly different and suggests they have different functional requirements for their tasks in cells. Surprisingly, highly related kinesin-2 motors, KIF3AB and KIF17, exhibit very different behaviors under load (Andreasson et al., 2015; Milic et al., 2017). Thus, despite high sequence conservation between motors within a family, subtle sequence changes can lead to dramatic differences in their motility and suggests that the behavior of a family of motors cannot be assumed based on biophysical properties of one motor [consistent with the diverse motility properties of the kinesin-4 family, (Yue et al., 2018)].

1.5.2 Optical trap and bead assays

For optical trap assays, a recent study demonstrates the importance of considering assay geometry, bead size, and tether length when characterizing the behavior of kinesin motors under load. Specifically, in a standard optical trap assays, single kinesin motors are likely to detach from the microtubule due to interactions between the bead and the microtubule. This effect is more dramatic the larger the bead size (Pyrpassopoulos, Shuman, & Ostap, 2020; Spudich, 2011). Thus, differences in the size of a bead used to measure the force output of single kinesin motors may lead to different conclusions about the motor's maximum force generation or sensitivity to detachment under load.

Changing the geometry of the assay, such that motors only experience forces parallel to the microtubule (three bead optical trap assay), kinesin-1 is found to stall at higher force and for longer periods of time (Pyrpassopoulos et al., 2020). In cells, kinesin motors may be required to withstand different components of horizontal and vertical force depending on their microtubule-based task (intracellular transport versus microtubule sliding). Therefore, careful characterization of the load-bearing capacity

(vertical versus horizontal force components) of kinesin motors from different families may reveal novel behaviors that adapt them to serve specific tasks in cells.

Lastly, in bead assays the manner that motors are attached to a bead is different from how motors are associated with endogenous cargo in cells. Specifically, motors are statically immobilized on the surface of a bead in *in vitro* assays. However in cells, motors on the surface of a vesicle can diffuse through a lipid membrane as they drive transport. In a multi-motor situation, theoretical studies predict that the cooperative behavior of a group of motors is related to whether motors are tightly (static bead attachment) or loosely coupled [lipid membrane, (Grover et al., 2016)]. Furthermore, *in vitro* studies demonstrate that loosely coupled kinesin-1 motors are able to drive gliding of microtubules at faster speeds than tightly coupled kinesin-1 motors (Grover et al., 2016). Efforts characterizing motor transport of lipid-coated beads, lipid droplets, and purified cargoes from cells have provided a better understanding of this (Barak et al., 2013; Bartsch et al., 2013; Hendricks, Goldman, & Holzbaur, 2014).

1.5.3 Methods of preparing protein for single-molecule assays

Motors used for *in vitro* assays are mass-produced and purified from mammalian cells, insect cells, or bacteria. Therefore, motors are made and their motility is characterized under conditions that may be very different than the physiological context they normally function under. A number of studies have found that kinesin motors behave similar in cells and *in vitro* [single molecule velocity and run lengths, (Cai et al., 2009; Courty et al., 2006)]. However, a recent study identified a cell cycle-dependent posttranslational modification of the kinesin-5 motor Eg5 that changes its force output and cooperative behavior to slide microtubules during cell division (Muretta et al., 2018). Thus, whether a motor's motility measured from *in vitro* assays represents the full scope of its activity in cells is unclear. A number of other kinesin motors are predicted to be posttranslationally modified and how this impacts their motility properties is not well understood (Bickel et al., 2017; DeBerg et al., 2013; Guse, Mishima, & Glotzer, 2005; Hornbeck et al., 2015; Liu et al., 2014).

Overall, although *in vitro,* single molecule studies have led to greater understanding of the movement of motors along cytoskeletal filaments, one must be

careful directly assuming a motor's function in cells based solely off of its single-molecule motility properties.

1.6 How does a motor's single-molecule motility properties lead to emergent mechanisms of transport in cells?

Characterization of the motility of single motors using *in* vitro assays has led to a number of properties we use to define the function of a motor, including velocity, run length, landing rate, force generation, and sensitivity to detachment under load. However, how these properties collectively contribute to distinct mechanisms of transport in cells is unclear. Early electron microscopy studies revealed that vesicles in a cell are tethered to a microtubule by many cargo-microtubule cross bridges. These unknown cross-bridges were predicted to be cytoskeletal motors (Ashkin et al., 1990; Hirokawa et al., 1989; Miller & Lasek, 1985), suggesting that motors work in teams to drive transport. More recent work carefully characterized populations of motors on membrane-bound cargoes in cells and find that they have between 1-7 associated kinesin, myosin, and/or dynein motors. For example, lipid droplets in *Drosophila* embryos have 1-2 kinesin-1 motors (Shubeita et al., 2008), endosomes in *Dictyostelium* have 4-8 dynein motors and one kinesin motor (Soppina et al., 2009), neuronal vesicles in mice have 1-5 dynein motors and 1-4 kinesin-1 or -2 motors (Hendricks et al., 2010), and early endosomes in *Ustilago maydis* have 1 dynein motor and 4-5 kinesin-3 motors (Schuster et al., 2011). Diversity in the number and classes of motors associated with a cargo has motivated groups to address how teams of motors coordinate their activities and how is this is functionally advantageous in cells.

As expected, increasing the number of motors associated with a cargo permits transport over longer distances compared to transport driven by single motors. Specifically, if one motor disengages from the track as a result of a MAP, microtubule crossing, or roadblock in the crowded cellular environment, other cargo-associated motors can replace this motor and continue to drive transport (Beeg et al., 2008; Coy et al., 1999; Klumpp & Lipowsky, 2005; Kunwar et al., 2008; Lakadamyali, 2014; Mallik et al., 2005; Seitz & Surrey, 2006). However, a number of studies characterizing transport driven by groups of motors that are artificially linked by protein or DNA scaffolds or by

teams of motors coupled through a lipid membrane in cells have revealed surprising emergent transport behaviors by teams of motors.

1.6.1 A motor's processivity as a single motor does not always predict its ability to drive transport as a team in cells.

All kinesin motors form stable dimers or dimerize at the surface of a cargo (Hirokawa et al., 2009; Huo et al., 2012; Soppina et al., 2014; Tomishige, Klopfenstein, & Vale, 2002) leading to the assumption that the dimerization of two motor domains to form a motor capable of stepping processively is a critical parameter to drive transport at a low copy number in cells. Indeed, kinesin-1, -2, and -3 families that drive transport of membrane-bound vesicles, protein complexes, or mRNA in cells are processive motors. Notably, kinesin-3 motor KIF1A is a highly processive motor with a high-microtubule-landing rate (Soppina & Verhey, 2014). In neurons, KIF1A motors are tasked with transporting presynaptic vesicles to axons terminals, hundreds of microns away from the cell body, within a matter of minutes (Hall & Hedgecock, 1991; Okada et al., 1995; Otsuka et al., 1991). Therefore, a high microtubule-landing rate will guarantee that vesicles containing only a few motors will engage with the track to begin transport. Its enhanced processivity will ensure that cargoes will reach their destination once engaged with the track.

However, a number of dimeric kinesin motors are non-processive under single-molecule conditions, taking only one or a few steps before detaching from the microtubule track. Therefore, how these motors contribute to intracellular transport and whether they can drive directed movement of cargo in cells is unclear. Furuta et al. found that as single motors, minus-end directed kinesin-14 Ncd is nonprocessive. However, Ncd motors linked as a team using an artificial DNA-scaffold were able to generate force and move longer distances along microtubules (Furuta et al., 2008; Furuta et al., 2013). Thus, despite uncoordinated foot-over-foot stepping as single motors, as a team, multiple Ncd motors can bind to the microtubule to keep cargo tethered to the cytoskeletal track as motors stochastically step forward (Hackney, 1996; Leibler & Huse, 1993). Moreover, there are a number of other cytoskeletal motors that are non-processive, including myosin-2 and flagellar dynein motors, which are also required to work as teams to drive cytoskeletal-based movement.

There are a number of myosin motors that function as a monomer in cells. Surprisingly, teams of monomeric myosin motors can drive cargo transport at similar speeds as dimeric myosin motors in cells (Sivaramakrishnan & Spudich, 2009). Theoretical studies predict that monomeric motors can act as “rowers,” where collective transient interactions with the cytoskeletal track can generate forward directed movement (Hackney, 1996; Leibler & Huse, 1993). Recent work extends this model to kinesins, where teams of monomeric kinesin motors can drive transport of peroxisomes in cells (Schimert et al., 2019).

Why has the cell evolved a strategy for non-processive dimers or monomeric motors to drive movement in cells? Although non-processive motors may seem like a disadvantage, it is possible that grouping non-processive motors together may provide sensitive regulation of transport. Controlling the number of motors associated with a cargo may impact the speeds and distances a cargo is transported or sensitize a cargo to switch direction of transport by modulating the force opposing motors must compete against.

1.6.2 A motor’s sensitivity to slowing down and stalling versus abruptly detaching from the microtubule track is an important parameter dictating transport in cells.

Biophysical and computational studies predict that a motor’s response to load is a key parameter that underlies emergent mechanisms of microtubule-based transport in cells (Arpăg et al, 2014; Norris et al., 2014; Ohashi et al., 2019). This is consistent with previous theoretical studies that predict that a motor’s sensitivity to slowing down versus detaching under force is an important determinant for whether motors are able to productively cooperate (Driver et al., 2011; Jamison, Driver, & Diehl, 2012; Uppulury et al., 2012). Below I will discuss three scenarios where differences in the composition of teams of motors on a cargo can lead to differences in transport as a result of their behaviors under force.

1.6.2.1 Teams of motors with the same mechanical output

Numerous groups have found that the motility of single kinesin-1 motors is largely insensitive to load, and at high forces it slows and eventually stalls while

remaining bound to the microtubule track (Budaitis et al., 2019; Khalil et al., 2008; Svoboda & Block, 1994). In a multi-motor scenario where two kinesin motors are attached to a bead, optical trapping studies find that motors do not generate additive forces if they are transporting against loads lower than their stall force. However their forces can be additive when subjected to loads higher than their stall force (Bieling et al., 2008; Hunt, Gittes, & Howard, 1994; Jamison et al., 2010; Vershinin et al., 2007). Therefore, in cells, kinesin-1 motors are predicted to work independently of each other when driving low-load transport. Indeed, varying the number of kinesin-1 motors at the surface of peroxisomes does not affect transport to the cell periphery (Efremov et al., 2014). This suggests that kinesin-1 motors may have evolved to work at limiting concentrations, to drive robust transport in cells.

Unlike kinesin-1, kinesin-3 family member KIF1A has a tendency to detach from the microtubule track when subjected to low loads (Arpağ et al., 2014; Norris et al., 2014; Tomishige et al., 2002). Teams of KIF1A motors drive fast, long-range transport of presynaptic vesicles in neurons (Hall & Hedgecock, 1991; Okada et al., 1995; Otsuka et al., 1991). As presynaptic vesicles are small membrane-bound organelles (diameter ~ 50 nm), it is likely that teams of KIF1A motors do not have to collectively generate large forces to drive transport (Efremov et al., 2014). Furthermore, as a team of motors drive transport, individual motors experience assistive (pulling) and resistive (pushing) forces as neighboring motors step (Nelson, Trybus, & Warshaw, 2014). Under this low-load transport regime, it may be advantageous for KIF1A motors to abruptly detach. Specifically, if motors experiencing higher forces at the leading edge were to slow or stall, the overall speed of transport may be compromised. Instead, additional cargo-associated KIF1A motors can continue to drive transport, replacing a recently detached motor without a cost to speed. An increased detachment frequency of individual motors may also help navigate obstacles, allowing for fast, continuous transport. Collectively, this mechanism of transport may be critical in highly polarized cells like neurons, when KIF1A motors are required to drive transport over hundreds of microns on the time scale of a few minutes (Hall & Hedgecock, 1991; Okada et al., 1995; Otsuka et al., 1991).

Conversely, myosin Va motors slow and stall under low force [stall force 1 pN, (Purcell, Sweeney, & Spudich, 2005; Uemura et al., 2004)]. Thus, myosin Va motors will

slow and remain bound to actin filaments even under minimal loads creating a situation where actin-bound motors can share load. Efremov et al. found that increasing the concentration of myosin Va motors at the surface of a peroxisome leads to higher force production and faster transport speeds as a result of coopertivity between motors (Efremov et al., 2014). Thus, myosin Va motors are likely required to work as a team in cells, where regulation of the number of associated myosin Va motors on a cargo can lead to large differences in transport speed and force production, a strategy that would allow tight regulation of cargo distribution in cells.

1.6.2.2 Teams of motors with the same directionality but different mechanical output

In cells, teams of kinesin motors with different mechanical outputs often drive transport of membrane-bound cargoes. As teams driving transport, individual kinesin motors experience assistive (pulling) and resistive (pushing) forces as neighboring motors step. In gliding assays of mixed populations of kinesin motors, kinesins display different sensitivities to detaching under load [least sensitive Kinesin-1 > 7 > 5 > 2 > 3; (Arpăg et al., 2014)]. Therefore, kinesins that resist detachment from the microtubule track can dominate transport driven by mixed populations of motors (Arpăg et al., 2014; Norris et al., 2014; Ohashi et al., 2019) and lead to distinct mechanisms of transport in cells.

Teams of kinesin-1 and -3 motors drive the transport of vesicles in neurons, however the transport speed of vesicles is most comparable to the speed of kinesin-1 motors. Knock out of kinesin-1 in neurons results in an increase in transport speeds of vesicles, consistent with the prediction that the sensitivity for kinesin-3 motors to detach from the microtubule track results in kinesin-1 motors dominating transport of vesicles that contain both kinesin-1 and -3 motors (Arpăg et al., 2014; Encalada et al., 2011; Norris et al., 2014). Why cells use a strategy of two plus-end directed kinesins with different motility characteristics to drive transport is not clear. One possibility is that different kinesin motors have different preferences for microtubules with posttranslational modifications or associated MAPs, and therefore tunes the types of tracks a cargo is transported along to ensure specific subcellular localizations in neurons. Indeed, kinesin-1, -2, and -3 motors have different abilities to walk along

microtubules decorated with tau and MAP2 (Chaudhary et al., 2019; Dixit et al., 2008; Monroy et al., 2018) and different preferences and/or motility properties when walking along acetylated or polyglutamylated microtubules (Cai et al., 2009; Kaul et al., 2014; Lessard et al., 2019; Monroy et al., 2018). Collectively this may highlight a combination of strategies that the cell utilizes to tightly control transport and subcellular localization of contents.

In addition, heterodimeric kinesin-2 motor KIF3AB and homodimeric kinesin-2 motor KIF17 motor transport IFT particles in cilia. Despite high sequence conservation, they behave differently under single molecule conditions. KIF3AB motors are slow and sensitive to detaching from the microtubule track under low loads [detachment force 1 pN, (Andreasson et al., 2015)], while KIF17 motors are fast and less likely to detach from the microtubule track [stall force 6 pN, (Milic et al., 2017)]. Whether these motors cooperate and how their cooperativity is important to drive IFT transport has been an interest of many groups (Evans et al., 2007; Milic et al., 2017; Ou et al., 2005; Pan et al., 2006; Prevo et al., 2015; Snow et al., 2004). In worms, once IFT trains are localized in the cilium, KIF3AB motors drive slow IFT transport along doublet microtubules. However, once IFT trains reach singlet microtubules, KIF17 motors are predicted to dominate to drive fast transport while the few remaining associated KIF3AB motors are likely to detach from the microtubule track and contribute little to transport (Evans et al., 2007; Milic et al., 2017; Ou et al., 2005; Pan et al., 2006; Prevo et al., 2015; Snow et al., 2004). The functional advantage for this mechanism of transport and why this is not a conserved mechanism of IFT transport in other organisms is not clear.

1.6.2.3 Teams of motors with different directionalities

Live-cell imaging experiments reveals that many intracellular transport events exhibit dynamic back-and-forth movements along microtubules, where cargo localization is specified by the overall net directionality (Ally et al., 2009; Gross, 2003; Welte, 2004). Indeed, many membrane-bound cargo in cells have associated dynein and kinesin motors (Hendricks et al., 2010; Schuster et al., 2011; Shubeita et al., 2008; Soppina et al., 2009), however what dictates net directionality of transport has been controversial.

One possibility is that both minus-end and plus-end cargo-associated motors are active, such that they are engaged in a tug-of-war. In this scenario, the direction of movement is dictated by a motor's ability to remain bound to the microtubule track and to generate high force. Kinesin-1 and fully active dynein (dynein-dynactin-BicD2, DDB) have equivalent force outputs (Belyy et al., 2016) and therefore the number of active kinesin-1 or DDB motors engaged in transport are expected to determine the direction of transport (Ohashi et al., 2019). Conversely, kinesin-2 motors are sensitive to even small opposing loads [1 pN, (Andreasson et al., 2015; Arpăg et al., 2014)], thus many kinesin-2 motors are required to match the force output of one DDB (Andreasson et al., 2015; Arpăg et al., 2014; Ohashi et al., 2019). Furthermore, recent work has identified proteins that bind to dynein and modulates its behavior under force. For instance, Lis1 binds to dynein and enhances its ability to remain attached to the microtubule track under load (McKenney et al., 2010). Overall, different combinations of dynein and kinesin motors that differ in their force generation or sensitivity to detaching from the microtubule track are predicted to finely tune directionality and distribution of cellular contents.

Another instance where the balance of forces between opposing cytoskeletal motors is important is in the spindle during cell division. A number of plus-end and minus-end microtubule-based motors play an important role in establishing and maintaining spindle architecture to ensure proper segregation of chromosomes (Dynein, Kinesin-4, -5, -6, -7, -8, -10, -12, -13, and -14 families; Titus and Wadsworth, 2012). Inhibiting the activity of Eg5 leads to collapse of the bipolar spindle (Kapoor et al., 2000), highlighting its important contribution to balance forces in the spindle. Although single Eg5 motors are sensitive to slowing down and detaching under moderate forces, as a team, the ability for Eg5 motors to slow in response to load leads to a situation where motors share load (Kunwar et al., 2008; Mallik et al., 2005). This load-sharing behavior is predicted to allow ensembles of Eg5 motors to serve as a breaking force during separation of centrosomes or to resist opposing forces generated by dynein motors in the spindle during cell division. Furthermore, a cell cycle-specific posttranslational modification of α2 in the Eg5 motor domain has allosteric effects on elements important for coupling ATPase activity and force generation, resulting in

motors that are more likely to stall, leading to even better opposition to force (Muretta et al., 2018).

Although many multi-motor *in vitro* experiments can recapitulate bidirectional motion in cells (Blehm et al., 2013; Hendricks et al., 2010; Kapitein et al., 2010; Soppina et al., 2009), knockout or inhibition of kinesin or dynein motors found that impairing transport in one direction also impaired transport in the opposite direction. Therefore, another possible way to control net directionality of transport is by regulating the activities or abilities of cargo-associated motors to engage with the cytoskeleton and drive transport (Barkus et al., 2008; Brady et al., 1982; Encalada et al., 2011; Goldberg, 1982; Martin et al., 1999; Waterman-Storer et al., 1997). Indeed, there are many cargo-adaptor proteins and motor-binding proteins that can specifically impact the activity of kinesin and dynein motors (Blasius et al., 2007; Egan, Tan, & Reck-Peterson, 2012; Hammond et al., 2009; Xu et al., 2012; Yamada, Hanada, & Chishti, 2007). It is likely that the cell has evolved to use both strategies to fine-tune transport.

Collectively a quantitative understanding of both a motor's single-molecule motility properties and their collective behavior in cells is critical to better understand how different kinesin motors across the kinesin superfamily are functionally distinct from one another.

1.7 References

Akhmanova, A., & Hammer, J. A., 3rd. (2010). Linking molecular motors to membrane cargo. *Curr Opin Cell Biol, 22*(4), 479-487. doi:10.1016/j.ceb.2010.04.008

Allen, R. D., Metuzals, J., Tasaki, I., Brady, S. T., & Gilbert, S. P. (1982). Fast axonal transport in squid giant axon. *Science, 218*(4577), 1127-1129. doi:10.1126/science.6183744

Ally, S., Larson, A. G., Barlan, K., Rice, S. E., & Gelfand, V. I. (2009). Opposite-polarity motors activate one another to trigger cargo transport in live cells. *J Cell Biol, 187*(7), 1071-1082. doi:10.1083/jcb.200908075

Amos, L. A., & Schlieper, D. (2005). Microtubules and maps. *Adv Protein Chem, 71*, 257-298. doi:10.1016/S0065-3233(04)71007-4

Andreasson, J. O., Shastry, S., Hancock, W. O., & Block, S. M. (2015). The Mechanochemical Cycle of Mammalian Kinesin-2 KIF3A/B under Load. *Curr Biol, 25*(9), 1166-1175. doi:10.1016/j.cub.2015.03.013

Arellano-Santoyo, H., Geyer, E. A., Stokasimov, E., Chen, G. Y., Su, X., Hancock, W., Rice, L. M., Pellman, D. (2017). A Tubulin Binding Switch Underlies Kip3/Kinesin-8 Depolymerase Activity. *Dev Cell, 42*(1), 37-51 e38. doi:10.1016/j.devcel.2017.06.011

Arora, K., Talje, L., Asenjo, A. B., Andersen, P., Atchia, K., Joshi, M., Sosa, H., Allingham, J. S., Kwok, B. H. (2014). KIF14 binds tightly to microtubules and adopts a rigor-like conformation. *J Mol Biol, 426*(17), 2997-3015. doi:10.1016/j.jmb.2014.05.030

Arpăg, G., Shastry, S., Hancock, W. O., & Tuzel, E. (2014). Transport by populations of fast and slow kinesins uncovers novel family-dependent motor characteristics important for in vivo function. *Biophys J, 107*(8), 1896-1904. doi:10.1016/j.bpj.2014.09.009

Asbury, C. L., Fehr, A. N., & Block, S. M. (2003). Kinesin moves by an asymmetric hand-over-hand mechanism. *Science, 302*(5653), 2130-2134. doi:10.1126/science.1092985

Asenjo, A. B., Chatterjee, C., Tan, D., DePaoli, V., Rice, W. J., Diaz-Avalos, R., Silvestry, M., Sosa, H. (2013). Structural model for tubulin recognition and deformation by kinesin-13 microtubule depolymerases. *Cell Rep, 3*(3), 759-768. doi:10.1016/j.celrep.2013.01.030

Asenjo, A. B., Weinberg, Y., & Sosa, H. (2006). Nucleotide binding and hydrolysis induces a disorder-order transition in the kinesin neck-linker region. *Nat Struct Mol Biol, 13*(7), 648-654. doi:10.1038/nsmb1109

Ashkin, A., Dziedzic, J. M., Bjorkholm, J. E., & Chu, S. (1986). Observation of a single-beam gradient force optical trap for dielectric particles. *Opt Lett, 11*(5), 288. doi:10.1364/ol.11.000288

Ashkin, A., Schutze, K., Dziedzic, J. M., Euteneuer, U., & Schliwa, M. (1990). Force generation of organelle transport measured in vivo by an infrared laser trap. *Nature, 348*(6299), 346-348. doi:10.1038/348346a0

Astumian, R. D., & Derenyi, I. (1999). A chemically reversible Brownian motor: application to kinesin and Ncd. *Biophys J, 77*(2), 993-1002. doi:10.1016/S0006-3495(99)76950-X

Atherton, J., Farabella, I., Yu, I. M., Rosenfeld, S. S., Houdusse, A., Topf, M., & Moores, C. A. (2014). Conserved mechanisms of microtubule-stimulated ADP release, ATP binding, and force generation in transport kinesins. *Elife, 3*, e03680. doi:10.7554/eLife.03680

Atherton, J., Yu, I. M., Cook, A., Muretta, J. M., Joseph, A., Major, J., Sourigues, Y., Clause, J., Topf, M., Rosenfeld, S. S., Houdusse, A., Moores, C. A. (2017). The divergent mitotic kinesin MKLP2 exhibits atypical structure and mechanochemistry. *Elife, 6*. doi:10.7554/eLife.27793

Auerbach, S. D., & Johnson, K. A. (2005). Kinetic effects of kinesin switch I and switch II mutations. *J Biol Chem, 280*(44), 37061-37068. doi:10.1074/jbc.M502985200

Axelrod, D. (1981). Cell-substrate contacts illuminated by total internal reflection fluorescence. *J Cell Biol, 89*(1), 141-145. doi:10.1083/jcb.89.1.141

Barak, P., Rai, A., Rai, P., & Mallik, R. (2013). Quantitative optical trapping on single organelles in cell extract. *Nat Methods, 10*(1), 68-70. doi:10.1038/nmeth.2287

Barkus, R. V., Klyachko, O., Horiuchi, D., Dickson, B. J., & Saxton, W. M. (2008). Identification of an axonal kinesin-3 motor for fast anterograde vesicle transport that facilitates retrograde transport of neuropeptides. *Mol Biol Cell, 19*(1), 274-283. doi:10.1091/mbc.e07-03-0261

Bartsch, T. F., Longoria, R. A., Florin, E. L., & Shubeita, G. T. (2013). Lipid droplets purified from Drosophila embryos as an endogenous handle for precise motor transport measurements. *Biophys J, 105*(5), 1182-1191. doi:10.1016/j.bpj.2013.07.026

Beeg, J., Klumpp, S., Dimova, R., Gracia, R. S., Unger, E., & Lipowsky, R. (2008). Transport of beads by several kinesin motors. *Biophys J, 94*(2), 532-541. doi:10.1529/biophysj.106.097881

Belyy, V., Schlager, M. A., Foster, H., Reimer, A. E., Carter, A. P., & Yildiz, A. (2016). The mammalian dynein-dynactin complex is a strong opponent to kinesin in a tug-of-war competition. *Nat Cell Biol, 18*(9), 1018-1024. doi:10.1038/ncb3393

Benoit, M., Asenjo, A. B., & Sosa, H. (2018). Cryo-EM reveals the structural basis of microtubule depolymerization by kinesin-13s. *Nat Commun, 9*(1), 1662. doi:10.1038/s41467-018-04044-8

Bergman, J. P., Bovyn, M. J., Doval, F. F., Sharma, A., Gudheti, M. V., Gross, S. P., Allard, J. F., Vershinin, M. D. (2018). Cargo navigation across 3D microtubule intersections. *Proc Natl Acad Sci U S A, 115*(3), 537-542. doi:10.1073/pnas.1707936115

Bertrand, E., Chartrand, P., Schaefer, M., Shenoy, S. M., Singer, R. H., & Long, R. M. (1998). Localization of ASH1 mRNA particles in living yeast. *Mol Cell, 2*(4), 437-445. doi:10.1016/s1097-2765(00)80143-4

Bickel, K. G., Mann, B. J., Waitzman, J. S., Poor, T. A., Rice, S. E., & Wadsworth, P. (2017). Src family kinase phosphorylation of the motor domain of the human kinesin-5, Eg5. *Cytoskeleton (Hoboken), 74*(9), 317-330. doi:10.1002/cm.21380

Bieling, P., Telley, I. A., Piehler, J., & Surrey, T. (2008). Processive kinesins require loose mechanical coupling for efficient collective motility. *EMBO Rep, 9*(11), 1121-1127. doi:10.1038/embor.2008.169

Blasius, T. L., Cai, D., Jih, G. T., Toret, C. P., & Verhey, K. J. (2007). Two binding partners cooperate to activate the molecular motor Kinesin-1. *J Cell Biol, 176*(1), 11-17. doi:10.1083/jcb.200605099

Blehm, B. H., Schroer, T. A., Trybus, K. M., Chemla, Y. R., & Selvin, P. R. (2013). In vivo optical trapping indicates kinesin's stall force is reduced by dynein during intracellular transport. *Proc Natl Acad Sci U S A, 110*(9), 3381-3386. doi:10.1073/pnas.1219961110

Block, S. M. (2007). Kinesin motor mechanics: binding, stepping, tracking, gating, and limping. *Biophys J, 92*(9), 2986-2995. doi:10.1529/biophysj.106.100677

Block, S. M., Goldstein, L. S., & Schnapp, B. J. (1990). Bead movement by single kinesin molecules studied with optical tweezers. *Nature, 348*(6299), 348-352. doi:10.1038/348348a0

Brady, S. T., Lasek, R. J., & Allen, R. D. (1982). Fast axonal transport in extruded axoplasm from squid giant axon. *Science, 218*(4577), 1129-1131. doi:10.1126/science.6183745

Brendza, K. M., Rose, D. J., Gilbert, S. P., & Saxton, W. M. (1999). Lethal kinesin mutations reveal amino acids important for ATPase activation and structural coupling. *J Biol Chem, 274*(44), 31506-31514. doi:10.1074/jbc.274.44.31506

Budaitis, B. G., Jariwala, S., Reinemann, D. N., Schimert, K. I., Scarabelli, G., Grant, B. J., Sept, D., Lang, M. J., Verhey, K. J. (2019). Neck linker docking is critical for Kinesin-1 force generation in cells but at a cost to motor speed and processivity. *Elife, 8*. doi:10.7554/eLife.44146

Cai, D., Hoppe, A. D., Swanson, J. A., & Verhey, K. J. (2007). Kinesin-1 structural organization and conformational changes revealed by FRET stoichiometry in live cells. *J Cell Biol, 176*(1), 51-63. doi:10.1083/jcb.200605097

Cai, D., McEwen, D. P., Martens, J. R., Meyhofer, E., & Verhey, K. J. (2009). Single molecule imaging reveals differences in microtubule track selection between Kinesin motors. *PLoS Biol, 7*(10), e1000216. doi:10.1371/journal.pbio.1000216

Cao, L., Cantos-Fernandes, S., & Gigant, B. (2017). The structural switch of nucleotide-free kinesin. *Sci Rep, 7*, 42558. doi:10.1038/srep42558

Cao, L., Wang, W., Jiang, Q., Wang, C., Knossow, M., & Gigant, B. (2014). The structure of apo-kinesin bound to tubulin links the nucleotide cycle to movement. *Nat Commun, 5*, 5364. doi:10.1038/ncomms6364

Case, R. B., Pierce, D. W., Hom-Booher, N., Hart, C. L., & Vale, R. D. (1997). The directional preference of kinesin motors is specified by an element outside of the motor catalytic domain. *Cell, 90*(5), 959-966. doi:10.1016/s0092-8674(00)80360-8

Case, R. B., Rice, S., Hart, C. L., Ly, B., & Vale, R. D. (2000). Role of the kinesin neck linker and catalytic core in microtubule-based motility. *Curr Biol, 10*(3), 157-160. doi:10.1016/s0960-9822(00)00316-x

Catlett, N. L., Duex, J. E., Tang, F., & Weisman, L. S. (2000). Two distinct regions in a yeast myosin-V tail domain are required for the movement of different cargoes. *J Cell Biol, 150*(3), 513-526. doi:10.1083/jcb.150.3.513

Chaudhary, A. R., Lu, H., Krementsova, E. B., Bookwalter, C. S., Trybus, K. M., & Hendricks, A. G. (2019). MAP7 regulates organelle transport by recruiting

kinesin-1 to microtubules. *J Biol Chem, 294*(26), 10160-10171. doi:10.1074/jbc.RA119.008052

Chen, G. Y., Cleary, J. M., Asenjo, A. B., Chen, Y., Mascaro, J. A., Arginteanu, D. F. J., . . . Hancock, W. O. (2019). Kinesin-5 Promotes Microtubule Nucleation and Assembly by Stabilizing a Lattice-Competent Conformation of Tubulin. *Curr Biol, 29*(14), 2259-2269 e2254. doi:10.1016/j.cub.2019.05.075

Chen, Y., & Hancock, W. O. (2015). Kinesin-5 is a microtubule polymerase. *Nat Commun, 6*, 8160. doi:10.1038/ncomms9160

Clancy, B. E., Behnke-Parks, W. M., Andreasson, J. O., Rosenfeld, S. S., & Block, S. M. (2011). A universal pathway for kinesin stepping. *Nat Struct Mol Biol, 18*(9), 1020-1027. doi:10.1038/nsmb.2104

Cochran, J. C., Gatial, J. E., 3rd, Kapoor, T. M., & Gilbert, S. P. (2005). Monastrol inhibition of the mitotic kinesin Eg5. *J Biol Chem, 280*(13), 12658-12667. doi:10.1074/jbc.M413140200

Cochran, J. C., Sindelar, C. V., Mulko, N. K., Collins, K. A., Kong, S. E., Hawley, R. S., & Kull, F. J. (2009). ATPase cycle of the nonmotile kinesin NOD allows microtubule end tracking and drives chromosome movement. *Cell, 136*(1), 110-122. doi:10.1016/j.cell.2008.11.048

Courty, S., Luccardini, C., Bellaiche, Y., Cappello, G., & Dahan, M. (2006). Tracking individual kinesin motors in living cells using single quantum-dot imaging. *Nano Lett, 6*(7), 1491-1495. doi:10.1021/nl060921t

Coy, D. L., Wagenbach, M., & Howard, J. (1999). Kinesin takes one 8-nm step for each ATP that it hydrolyzes. *J Biol Chem, 274*(6), 3667-3671. doi:10.1074/jbc.274.6.3667

Craciun, G., Brown, A., & Friedman, A. (2005). A dynamical system model of neurofilament transport in axons. *J Theor Biol, 237*(3), 316-322. doi:10.1016/j.jtbi.2005.04.018

Das, A., Cesario, J., Hinman, A. M., Jang, J. K., & McKim, K. S. (2018). Kinesin 6 Regulation in Drosophila Female Meiosis by the Non-conserved N- and C-Terminal Domains. *G3 (Bethesda), 8*(5), 1555-1569. doi:10.1534/g3.117.300571

DeBerg, H. A., Blehm, B. H., Sheung, J., Thompson, A. R., Bookwalter, C. S., Torabi, S. F., Schroer, T. A., Berger, C. L., Lu, Y., Trybus, K. M., Selvin, P. R. (2013). Motor domain phosphorylation modulates kinesin-1 transport. *J Biol Chem, 288*(45), 32612-32621. doi:10.1074/jbc.M113.515510

Dixit, R., Ross, J. L., Goldman, Y. E., & Holzbaur, E. L. (2008). Differential regulation of dynein and kinesin motor proteins by tau. *Science, 319*(5866), 1086-1089. doi:10.1126/science.1152993

Dogan, M. Y., Can, S., Cleary, F. B., Purde, V., & Yildiz, A. (2015). Kinesin's front head is gated by the backward orientation of its neck linker. *Cell Rep, 10*(12), 1967-1973. doi:10.1016/j.celrep.2015.02.061

Driver, J. W., Jamison, D. K., Uppulury, K., Rogers, A. R., Kolomeisky, A. B., & Diehl, M. R. (2011). Productive cooperation among processive motors depends inversely on their mechanochemical efficiency. *Biophys J, 101*(2), 386-395. doi:10.1016/j.bpj.2011.05.067

Edamatsu, M. (2016). Molecular properties of the N-terminal extension of the fission yeast kinesin-5, Cut7. *Genet Mol Res, 15*(1). doi:10.4238/gmr.15017799

Efremov, A. K., Radhakrishnan, A., Tsao, D. S., Bookwalter, C. S., Trybus, K. M., & Diehl, M. R. (2014). Delineating cooperative responses of processive motors in living cells. *Proc Natl Acad Sci U S A, 111*(3), E334-343. doi:10.1073/pnas.1313569111

Egan, M. J., Tan, K., & Reck-Peterson, S. L. (2012). Lis1 is an initiation factor for dynein-driven organelle transport. *J Cell Biol, 197*(7), 971-982. doi:10.1083/jcb.201112101

Encalada, S. E., Szpankowski, L., Xia, C. H., & Goldstein, L. S. (2011). Stable kinesin and dynein assemblies drive the axonal transport of mammalian prion protein vesicles. *Cell, 144*(4), 551-565. doi:10.1016/j.cell.2011.01.021

Erickson, H. P., & O'Brien, E. T. (1992). Microtubule dynamic instability and GTP hydrolysis. *Annu Rev Biophys Biomol Struct, 21*, 145-166. doi:10.1146/annurev.bb.21.060192.001045

Evans, B. A., Shields, A. R., Carroll, R. L., Washburn, S., Falvo, M. R., & Superfine, R. (2007). Magnetically actuated nanorod arrays as biomimetic cilia. *Nano Lett, 7*(5), 1428-1434. doi:10.1021/nl070190c

Fletcher, D. A., & Mullins, R. D. (2010). Cell mechanics and the cytoskeleton. *Nature, 463*(7280), 485-492. doi:10.1038/nature08908

Friedman, D. S., & Vale, R. D. (1999). Single-molecule analysis of kinesin motility reveals regulation by the cargo-binding tail domain. *Nat Cell Biol, 1*(5), 293-297. doi:10.1038/13008

Friel, C. T., & Howard, J. (2011). The kinesin-13 MCAK has an unconventional ATPase cycle adapted for microtubule depolymerization. *EMBO J, 30*(19), 3928-3939. doi:10.1038/emboj.2011.290

Fulton, A. B. (1982). How crowded is the cytoplasm? *Cell, 30*(2), 345-347. doi:10.1016/0092-8674(82)90231-8

Funatsu, T., Harada, Y., Tokunaga, M., Saito, K., & Yanagida, T. (1995). Imaging of single fluorescent molecules and individual ATP turnovers by single myosin molecules in aqueous solution. *Nature, 374*(6522), 555-559. doi:10.1038/374555a0

Furuta, K., Edamatsu, M., Maeda, Y., & Toyoshima, Y. Y. (2008). Diffusion and directed movement: in vitro motile properties of fission yeast kinesin-14 Pkl1. *J Biol Chem, 283*(52), 36465-36473. doi:10.1074/jbc.M803730200

Furuta, K., Furuta, A., Toyoshima, Y. Y., Amino, M., Oiwa, K., & Kojima, H. (2013). Measuring collective transport by defined numbers of processive and nonprocessive kinesin motors. *Proc Natl Acad Sci U S A, 110*(2), 501-506. doi:10.1073/pnas.1201390110

Geeves, M. A., & Holmes, K. C. (1999). Structural mechanism of muscle contraction. *Annu Rev Biochem, 68*, 687-728. doi:10.1146/annurev.biochem.68.1.687

Gicking, A. M., Wang, P., Liu, C., Mickolajczyk, K. J., Guo, L., Hancock, W. O., & Qiu, W. (2019). The Orphan Kinesin PAKRP2 Achieves Processive Motility via a Noncanonical Stepping Mechanism. *Biophys J, 116*(7), 1270-1281. doi:10.1016/j.bpj.2019.02.019

Gigant, B., Wang, W., Dreier, B., Jiang, Q., Pecqueur, L., Pluckthun, A., Wang, C., Knossow, M. (2013). Structure of a kinesin-tubulin complex and implications for kinesin motility. *Nat Struct Mol Biol, 20*(8), 1001-1007. doi:10.1038/nsmb.2624

Glotzer, M. (2005). The molecular requirements for cytokinesis. *Science, 307*(5716), 1735-1739. doi:10.1126/science.1096896

Goldberg, D. J. (1982). Microinjection into an identified axon to study the mechanism of fast axonal transport. *Proc Natl Acad Sci U S A, 79*(15), 4818-4822. doi:10.1073/pnas.79.15.4818

Grant, B. J., Gheorghe, D. M., Zheng, W., Alonso, M., Huber, G., Dlugosz, M., McCammon, J. A., Cross, R. A. (2011). Electrostatically biased binding of kinesin to microtubules. *PLoS Biol, 9*(11), e1001207. doi:10.1371/journal.pbio.1001207

Gross, S. P. (2003). Dynactin: coordinating motors with opposite inclinations. *Curr Biol, 13*(8), R320-322.

Grover, R., Fischer, J., Schwarz, F. W., Walter, W. J., Schwille, P., & Diez, S. (2016). Transport efficiency of membrane-anchored kinesin-1 motors depends on motor density and diffusivity. *Proc Natl Acad Sci U S A, 113*(46), E7185-E7193. doi:10.1073/pnas.1611398113

Guan, R., Zhang, L., Su, Q. P., Mickolajczyk, K. J., Chen, G. Y., Hancock, W. O., Sun, Y., Zhao, Y., Chen, Z. (2017). Crystal structure of Zen4 in the apo state reveals a missing conformation of kinesin. *Nat Commun, 8*, 14951. doi:10.1038/ncomms14951

Hackney, D. D. (1996). The kinetic cycles of myosin, kinesin, and dynein. *Annu Rev Physiol, 58*, 731-750. doi:10.1146/annurev.ph.58.030196.003503

Hahlen, K., Ebbing, B., Reinders, J., Mergler, J., Sickmann, A., & Woehlke, G. (2006). Feedback of the kinesin-1 neck-linker position on the catalytic site. *J Biol Chem, 281*(27), 18868-18877. doi:10.1074/jbc.M508019200

Hall, D. H., & Hedgecock, E. M. (1991). Kinesin-related gene unc-104 is required for axonal transport of synaptic vesicles in C. elegans. *Cell, 65*(5), 837-847. doi:10.1016/0092-8674(91)90391-b

Hammond, J. W., Cai, D., Blasius, T. L., Li, Z., Jiang, Y., Jih, G. T., Meyhofer, E., Verhey, K. J. (2009). Mammalian Kinesin-3 motors are dimeric in vivo and move

by processive motility upon release of autoinhibition. *PLoS Biol, 7*(3), e72. doi:10.1371/journal.pbio.1000072

Hariharan, V., & Hancock, W. O. (2009). Insights into the Mechanical Properties of the Kinesin Neck Linker Domain from Sequence Analysis and Molecular Dynamics Simulations. *Cell Mol Bioeng, 2*(2), 177-189. doi:10.1007/s12195-009-0059-5

Hartman, M. A., & Spudich, J. A. (2012). The myosin superfamily at a glance. *J Cell Sci, 125*(Pt 7), 1627-1632. doi:10.1242/jcs.094300

He, M., Subramanian, R., Bangs, F., Omelchenko, T., Liem, K. F., Jr., Kapoor, T. M., & Anderson, K. V. (2014). The kinesin-4 protein Kif7 regulates mammalian Hedgehog signalling by organizing the cilium tip compartment. *Nat Cell Biol, 16*(7), 663-672. doi:10.1038/ncb2988

Helenius, J., Brouhard, G., Kalaidzidis, Y., Diez, S., & Howard, J. (2006). The depolymerizing kinesin MCAK uses lattice diffusion to rapidly target microtubule ends. *Nature, 441*(7089), 115-119. doi:10.1038/nature04736

Hendricks, A. G., Goldman, Y. E., & Holzbaur, E. L. (2014). Reconstituting the motility of isolated intracellular cargoes. *Methods Enzymol, 540*, 249-262. doi:10.1016/B978-0-12-397924-7.00014-5

Hendricks, A. G., Perlson, E., Ross, J. L., Schroeder, H. W., 3rd, Tokito, M., & Holzbaur, E. L. (2010). Motor coordination via a tug-of-war mechanism drives bidirectional vesicle transport. *Curr Biol, 20*(8), 697-702. doi:10.1016/j.cub.2010.02.058

Hesse, W. R., Steiner, M., Wohlever, M. L., Kamm, R. D., Hwang, W., & Lang, M. J. (2013). Modular aspects of kinesin force generation machinery. *Biophys J, 104*(9), 1969-1978. doi:10.1016/j.bpj.2013.03.051

Hirokawa, N., Niwa, S., & Tanaka, Y. (2010). Molecular motors in neurons: transport mechanisms and roles in brain function, development, and disease. *Neuron, 68*(4), 610-638. doi:10.1016/j.neuron.2010.09.039

Hirokawa, N., & Noda, Y. (2008). Intracellular transport and kinesin superfamily proteins, KIFs: structure, function, and dynamics. *Physiol Rev, 88*(3), 1089-1118. doi:10.1152/physrev.00023.2007

Hirokawa, N., Noda, Y., Tanaka, Y., & Niwa, S. (2009). Kinesin superfamily motor proteins and intracellular transport. *Nat Rev Mol Cell Biol, 10*(10), 682-696. doi:10.1038/nrm2774

Hirokawa, N., Pfister, K. K., Yorifuji, H., Wagner, M. C., Brady, S. T., & Bloom, G. S. (1989). Submolecular domains of bovine brain kinesin identified by electron microscopy and monoclonal antibody decoration. *Cell, 56*(5), 867-878. doi:10.1016/0092-8674(89)90691-0

Hoeprich, G. J., Mickolajczyk, K. J., Nelson, S. R., Hancock, W. O., & Berger, C. L. (2017). The axonal transport motor kinesin-2 navigates microtubule obstacles via protofilament switching. *Traffic, 18*(5), 304-314. doi:10.1111/tra.12478

Hornbeck, P. V., Zhang, B., Murray, B., Kornhauser, J. M., Latham, V., & Skrzypek, E. (2015). PhosphoSitePlus, 2014: mutations, PTMs and recalibrations. *Nucleic Acids Res, 43*(Database issue), D512-520. doi:10.1093/nar/gku1267

Howard, J., Hudspeth, A. J., & Vale, R. D. (1989). Movement of microtubules by single kinesin molecules. *Nature, 342*(6246), 154-158. doi:10.1038/342154a0

Hunt, A. J., Gittes, F., & Howard, J. (1994). The force exerted by a single kinesin molecule against a viscous load. *Biophys J, 67*(2), 766-781. doi:10.1016/S0006-3495(94)80537-5

Hunter, A. W., Caplow, M., Coy, D. L., Hancock, W. O., Diez, S., Wordeman, L., & Howard, J. (2003). The kinesin-related protein MCAK is a microtubule depolymerase that forms an ATP-hydrolyzing complex at microtubule ends. *Mol Cell, 11*(2), 445-457. doi:10.1016/s1097-2765(03)00049-2

Huo, L., Yue, Y., Ren, J., Yu, J., Liu, J., Yu, Y., Ye, Y., Xu, T., Shang, M., Feng, W. (2012). The CC1-FHA tandem as a central hub for controlling the dimerization and activation of kinesin-3 KIF1A. *Structure, 20*(9), 1550-1561. doi:10.1016/j.str.2012.07.002

Hwang, W., Lang, M. J., & Karplus, M. (2008). Force generation in kinesin hinges on cover-neck bundle formation. *Structure, 16*(1), 62-71. doi:10.1016/j.str.2007.11.008

Isojima, H., Iino, R., Niitani, Y., Noji, H., & Tomishige, M. (2016). Direct observation of intermediate states during the stepping motion of kinesin-1. *Nat Chem Biol, 12*(4), 290-297. doi:10.1038/nchembio.2028

Jamison, D. K., Driver, J. W., & Diehl, M. R. (2012). Cooperative responses of multiple kinesins to variable and constant loads. *J Biol Chem, 287*(5), 3357-3365. doi:10.1074/jbc.M111.296582

Jamison, D. K., Driver, J. W., Rogers, A. R., Constantinou, P. E., & Diehl, M. R. (2010). Two kinesins transport cargo primarily via the action of one motor: implications for intracellular transport. *Biophys J, 99*(9), 2967-2977. doi:10.1016/j.bpj.2010.08.025

Jennings, S., Chenevert, M., Liu, L., Mottamal, M., Wojcik, E. J., & Huckaba, T. M. (2017). Characterization of kinesin switch I mutations that cause hereditary spastic paraplegia. *PLoS One, 12*(7), e0180353. doi:10.1371/journal.pone.0180353

Jiang, S., Mani, N., Wilson-Kubalek, E. M., Ku, P. I., Milligan, R. A., & Subramanian, R. (2019). Interplay between the Kinesin and Tubulin Mechanochemical Cycles Underlies Microtubule Tip Tracking by the Non-motile Ciliary Kinesin Kif7. *Dev Cell, 49*(5), 711-730 e718. doi:10.1016/j.devcel.2019.04.001

Jonsson, E., Yamada, M., Vale, R. D., & Goshima, G. (2015). Clustering of a kinesin-14 motor enables processive retrograde microtubule-based transport in plants. *Nat Plants, 1*(7). doi:10.1038/NPLANTS.2015.87

Kamal, A., & Goldstein, L. S. (2002). Principles of cargo attachment to cytoplasmic motor proteins. *Curr Opin Cell Biol, 14*(1), 63-68. doi:10.1016/s0955-0674(01)00295-2

Kapitein, L. C., Schlager, M. A., van der Zwan, W. A., Wulf, P. S., Keijzer, N., & Hoogenraad, C. C. (2010). Probing intracellular motor protein activity using an inducible cargo trafficking assay. *Biophys J, 99*(7), 2143-2152. doi:10.1016/j.bpj.2010.07.055

Kapoor, T. M., Mayer, T. U., Coughlin, M. L., & Mitchison, T. J. (2000). Probing spindle assembly mechanisms with monastrol, a small molecule inhibitor of the mitotic kinesin, Eg5. *J Cell Biol, 150*(5), 975-988. doi:10.1083/jcb.150.5.975

Kaul, N., Soppina, V., & Verhey, K. J. (2014). Effects of alpha-tubulin K40 acetylation and detyrosination on kinesin-1 motility in a purified system. *Biophys J, 106*(12), 2636-2643. doi:10.1016/j.bpj.2014.05.008

Khalil, A. S., Appleyard, D. C., Labno, A. K., Georges, A., Karplus, M., Belcher, A. M., . . . Lang, M. J. (2008). Kinesin's cover-neck bundle folds forward to generate force. *Proc Natl Acad Sci U S A, 105*(49), 19247-19252. doi:10.1073/pnas.0805147105

Kikkawa, M., Okada, Y., & Hirokawa, N. (2000). 15 A resolution model of the monomeric kinesin motor, KIF1A. *Cell, 100*(2), 241-252. doi:10.1016/s0092-8674(00)81562-7

Kikkawa, M., Sablin, E. P., Okada, Y., Yajima, H., Fletterick, R. J., & Hirokawa, N. (2001). Switch-based mechanism of kinesin motors. *Nature, 411*(6836), 439-445. doi:10.1038/35078000

Kim, C. A., & Berg, J. M. (1993). Thermodynamic beta-sheet propensities measured using a zinc-finger host peptide. *Nature, 362*(6417), 267-270. doi:10.1038/362267a0

Kim, H., Fonseca, C., & Stumpff, J. (2014). A unique kinesin-8 surface loop provides specificity for chromosome alignment. *Mol Biol Cell, 25*(21), 3319-3329. doi:10.1091/mbc.E14-06-1132

Klumpp, S., & Lipowsky, R. (2005). Active diffusion of motor particles. *Phys Rev Lett, 95*(26), 268102. doi:10.1103/PhysRevLett.95.268102

Korneev, M. J., Lakamper, S., & Schmidt, C. F. (2007). Load-dependent release limits the processive stepping of the tetrameric Eg5 motor. *Eur Biophys J, 36*(6), 675-681. doi:10.1007/s00249-007-0134-6

Kozielski, F., Sack, S., Marx, A., Thormahlen, M., Schonbrunn, E., Biou, V., Thompson, A., Mandelkow, E. M., Mandelkow, E. (1997). The crystal structure of dimeric kinesin and implications for microtubule-dependent motility. *Cell, 91*(7), 985-994. doi:10.1016/s0092-8674(00)80489-4

Kozielski, F., Schonbrunn, E., Sack, S., Muller, J., Brady, S. T., & Mandelkow, E. (1997). Crystallization and preliminary X-ray analysis of the single-headed and double-headed motor protein kinesin. *J Struct Biol, 119*(1), 28-34. doi:10.1006/jsbi.1997.3872

Kozminski, K. G., Johnson, K. A., Forscher, P., & Rosenbaum, J. L. (1993). A motility in the eukaryotic flagellum unrelated to flagellar beating. *Proc Natl Acad Sci U S A, 90*(12), 5519-5523. doi:10.1073/pnas.90.12.5519

Kristensson, K., & Olsson, Y. (1973). Diffusion pathways and retrograde axonal transport of protein tracers in peripheral nerves. *Prog Neurobiol, 1*(2), 87-109.

Kull, F. J., & Endow, S. A. (2013). Force generation by kinesin and myosin cytoskeletal motor proteins. *J Cell Sci, 126*(Pt 1), 9-19. doi:10.1242/jcs.103911

Kull, F. J., Sablin, E. P., Lau, R., Fletterick, R. J., & Vale, R. D. (1996). Crystal structure of the kinesin motor domain reveals a structural similarity to myosin. *Nature, 380*(6574), 550-555. doi:10.1038/380550a0

Kull, F. J., Vale, R. D., & Fletterick, R. J. (1998). The case for a common ancestor: kinesin and myosin motor proteins and G proteins. *J Muscle Res Cell Motil, 19*(8), 877-886. doi:10.1023/a:1005489907021

Kunwar, A., Vershinin, M., Xu, J., & Gross, S. P. (2008). Stepping, strain gating, and an unexpected force-velocity curve for multiple-motor-based transport. *Curr Biol, 18*(16), 1173-1183. doi:10.1016/j.cub.2008.07.027

Kutys, M. L., Fricks, J., & Hancock, W. O. (2010). Monte Carlo analysis of neck linker extension in kinesin molecular motors. *PLoS Comput Biol, 6*(11), e1000980. doi:10.1371/journal.pcbi.1000980

Lakadamyali, M. (2014). Navigating the cell: how motors overcome roadblocks and traffic jams to efficiently transport cargo. *Phys Chem Chem Phys, 16*(13), 5907-5916. doi:10.1039/c3cp55271c

Lakamper, S., Thiede, C., Duselder, A., Reiter, S., Korneev, M. J., Kapitein, L. C., Peterman, E. J., Schmidt, C. F. (2010). The effect of monastrol on the processive motility of a dimeric kinesin-5 head/kinesin-1 stalk chimera. *J Mol Biol, 399*(1), 1-8. doi:10.1016/j.jmb.2010.03.009

Lawrence, C. J., Dawe, R. K., Christie, K. R., Cleveland, D. W., Dawson, S. C., Endow, S. A., Goldstein, L. S. B., Goodson, H. V., Hirokawa, N., Howard, J., Malmberg, R. L., McIntosh, R. J., Miki, H., Mitchison, T. J., Okada, Y., Reddy, A. S. N., Saxton, W. M., Schliwa, M., Scholey, J. M., Vale, R. D., Walczak, C. E.,

Wordeman, L. (2004). A standardized kinesin nomenclature. *J Cell Biol, 167*(1), 19-22. doi:10.1083/jcb.200408113

Leibler, S., & Huse, D. A. (1993). Porters versus rowers: a unified stochastic model of motor proteins. *J Cell Biol, 121*(6), 1357-1368. doi:10.1083/jcb.121.6.1357

Lessard, D. V., Zinder, O. J., Hotta, T., Verhey, K. J., Ohi, R., & Berger, C. L. (2019). Polyglutamylation of tubulin's C-terminal tail controls pausing and motility of kinesin-3 family member KIF1A. *J Biol Chem, 294*(16), 6353-6363. doi:10.1074/jbc.RA118.005765

Li, R., & Gundersen, G. G. (2008). Beyond polymer polarity: how the cytoskeleton builds a polarized cell. *Nat Rev Mol Cell Biol, 9*(11), 860-873. doi:10.1038/nrm2522

Liu, D., Liu, X., Shang, Z., & Sindelar, C. V. (2017). Structural basis of cooperativity in kinesin revealed by 3D reconstruction of a two-head-bound state on microtubules. *Elife, 6*. doi:10.7554/eLife.24490

Liu, Z., Wang, Y., Gao, T., Pan, Z., Cheng, H., Yang, Q., Cheng, Z., Guo, A., Ren, J., Xue, Y. (2014). CPLM: a database of protein lysine modifications. *Nucleic Acids Res, 42*(Database issue), D531-536. doi:10.1093/nar/gkt1093

Locke, J., Joseph, A. P., Pena, A., Mockel, M. M., Mayer, T. U., Topf, M., & Moores, C. A. (2017). Structural basis of human kinesin-8 function and inhibition. *Proc Natl Acad Sci U S A, 114*(45), E9539-E9548. doi:10.1073/pnas.1712169114

Magiera, M. M., & Janke, C. (2014). Post-translational modifications of tubulin. *Curr Biol, 24*(9), R351-354. doi:10.1016/j.cub.2014.03.032

Mallik, R., Petrov, D., Lex, S. A., King, S. J., & Gross, S. P. (2005). Building complexity: an in vitro study of cytoplasmic dynein with in vivo implications. *Curr Biol, 15*(23), 2075-2085. doi:10.1016/j.cub.2005.10.039

Martin, M., Iyadurai, S. J., Gassman, A., Gindhart, J. G., Jr., Hays, T. S., & Saxton, W. M. (1999). Cytoplasmic dynein, the dynactin complex, and kinesin are interdependent and essential for fast axonal transport. *Mol Biol Cell, 10*(11), 3717-3728. doi:10.1091/mbc.10.11.3717

Mather, W. H., & Fox, R. F. (2006). Kinesin's biased stepping mechanism: amplification of neck linker zippering. *Biophys J, 91*(7), 2416-2426. doi:10.1529/biophysj.106.087049

McIntosh, J. R., O'Toole, E., Morgan, G., Austin, J., Ulyanov, E., Ataullakhanov, F., & Gudimchuk, N. (2018). Microtubules grow by the addition of bent guanosine triphosphate tubulin to the tips of curved protofilaments. *J Cell Biol, 217*(8), 2691-2708. doi:10.1083/jcb.201802138

McKenney, R. J., Vershinin, M., Kunwar, A., Vallee, R. B., & Gross, S. P. (2010). LIS1 and NudE induce a persistent dynein force-producing state. *Cell, 141*(2), 304-314. doi:10.1016/j.cell.2010.02.035

Miki, H., Okada, Y., & Hirokawa, N. (2005). Analysis of the kinesin superfamily: insights into structure and function. *Trends Cell Biol, 15*(9), 467-476. doi:10.1016/j.tcb.2005.07.006

Milic, B., Andreasson, J. O. L., Hogan, D. W., & Block, S. M. (2017). Intraflagellar transport velocity is governed by the number of active KIF17 and KIF3AB motors and their motility properties under load. *Proc Natl Acad Sci U S A, 114*(33), E6830-E6838. doi:10.1073/pnas.1708157114

Miller, R. H., & Lasek, R. J. (1985). Cross-bridges mediate anterograde and retrograde vesicle transport along microtubules in squid axoplasm. *J Cell Biol, 101*(6), 2181-2193. doi:10.1083/jcb.101.6.2181

Monroy, B. Y., Sawyer, D. L., Ackermann, B. E., Borden, M. M., Tan, T. C., & Ori-McKenney, K. M. (2018). Competition between microtubule-associated proteins directs motor transport. *Nat Commun, 9*(1), 1487. doi:10.1038/s41467-018-03909-2

Muretta, J. M., Jun, Y., Gross, S. P., Major, J., Thomas, D. D., & Rosenfeld, S. S. (2015). The structural kinetics of switch-1 and the neck linker explain the functions of kinesin-1 and Eg5. *Proc Natl Acad Sci U S A, 112*(48), E6606-6613. doi:10.1073/pnas.1512305112

Muretta, J. M., Reddy, B. J. N., Scarabelli, G., Thompson, A. F., Jariwala, S., Major, J., Venere, M., Rich, J. N., Willard, B., Thomas, D. D., Stumpff, J., Grant, B. J., Gross, S. P., Rosenfeld, S. S. (2018). A posttranslational modification of the mitotic kinesin Eg5 that enhances its mechanochemical coupling and alters its mitotic function. *Proc Natl Acad Sci U S A, 115*(8), E1779-E1788. doi:10.1073/pnas.1718290115

Muthukrishnan, G., Zhang, Y., Shastry, S., & Hancock, W. O. (2009). The processivity of kinesin-2 motors suggests diminished front-head gating. *Curr Biol, 19*(5), 442-447. doi:10.1016/j.cub.2009.01.058

Nebenfuhr, A., & Dixit, R. (2018). Kinesins and Myosins: Molecular Motors that Coordinate Cellular Functions in Plants. *Annual Review of Plant Biology, Vol 69, 69*, 329-361. doi:10.1146/annurev-arplant-042817-040024

Nishimura, Y., & Yonemura, S. (2006). Centralspindlin regulates ECT2 and RhoA accumulation at the equatorial cortex during cytokinesis. *J Cell Sci, 119*(Pt 1), 104-114. doi:10.1242/jcs.02737

Nitta, R., Kikkawa, M., Okada, Y., & Hirokawa, N. (2004). KIF1A alternately uses two loops to bind microtubules. *Science, 305*(5684), 678-683. doi:10.1126/science.1096621

Nitta, R., Okada, Y., & Hirokawa, N. (2008). Structural model for strain-dependent microtubule activation of Mg-ADP release from kinesin. *Nat Struct Mol Biol, 15*(10), 1067-1075. doi:10.1038/nsmb.1487

Norris, S. R., Nunez, M. F., & Verhey, K. J. (2015). Influence of fluorescent tag on the motility properties of kinesin-1 in single-molecule assays. *Biophys J, 108*(5), 1133-1143. doi:10.1016/j.bpj.2015.01.031

Norris, S. R., Soppina, V., Dizaji, A. S., Schimert, K. I., Sept, D., Cai, D., Sivaramakrishnan, S., Verhey, K. J. (2014). A method for multiprotein assembly in cells reveals independent action of kinesins in complex. *J Cell Biol, 207*(3), 393-406. doi:10.1083/jcb.201407086

Ogawa, T., Nitta, R., Okada, Y., & Hirokawa, N. (2004). A common mechanism for microtubule destabilizers-M type kinesins stabilize curling of the protofilament using the class-specific neck and loops. *Cell, 116*(4), 591-602. doi:10.1016/s0092-8674(04)00129-1

Ohashi, K. G., Han, L., Mentley, B., Wang, J., Fricks, J., & Hancock, W. O. (2019). Load-dependent detachment kinetics plays a key role in bidirectional cargo transport by kinesin and dynein. *Traffic, 20*(4), 284-294. doi:10.1111/tra.12639

Okada, Y., & Hirokawa, N. (1999). A processive single-headed motor: kinesin superfamily protein KIF1A. *Science, 283*(5405), 1152-1157. doi:10.1126/science.283.5405.1152

Okada, Y., & Hirokawa, N. (2000). Mechanism of the single-headed processivity: diffusional anchoring between the K-loop of kinesin and the C terminus of tubulin. *Proc Natl Acad Sci U S A, 97*(2), 640-645. doi:10.1073/pnas.97.2.640

Okada, Y., Yamazaki, H., Sekine-Aizawa, Y., & Hirokawa, N. (1995). The neuron-specific kinesin superfamily protein KIF1A is a unique monomeric motor for anterograde axonal transport of synaptic vesicle precursors. *Cell, 81*(5), 769-780. doi:10.1016/0092-8674(95)90538-3

Otsuka, A. J., Jeyaprakash, A., Garcia-Anoveros, J., Tang, L. Z., Fisk, G., Hartshorne, T., Franco, R., Born, T. (1991). The C. elegans unc-104 gene encodes a putative kinesin heavy chain-like protein. *Neuron, 6*(1), 113-122. doi:10.1016/0896-6273(91)90126-k

Ou, G., Blacque, O. E., Snow, J. J., Leroux, M. R., & Scholey, J. M. (2005). Functional coordination of intraflagellar transport motors. *Nature, 436*(7050), 583-587. doi:10.1038/nature03818

Pan, X., Ou, G., Civelekoglu-Scholey, G., Blacque, O. E., Endres, N. F., Tao, L., Mogilner, A., Leroux, M. R., Vale, R. D., Scholey, J. M. (2006). Mechanism of transport of IFT particles in C. elegans cilia by the concerted action of kinesin-II and OSM-3 motors. *J Cell Biol, 174*(7), 1035-1045. doi:10.1083/jcb.200606003

Parke, C. L., Wojcik, E. J., Kim, S., & Worthylake, D. K. (2010). ATP hydrolysis in Eg5 kinesin involves a catalytic two-water mechanism. *J Biol Chem, 285*(8), 5859-5867. doi:10.1074/jbc.M109.071233

Paschal, B. M., Shpetner, H. S., & Vallee, R. B. (1987). MAP 1C is a microtubule-activated ATPase which translocates microtubules in vitro and has dynein-like properties. *J Cell Biol, 105*(3), 1273-1282. doi:10.1083/jcb.105.3.1273

Paschal, B. M., & Vallee, R. B. (1987). Retrograde transport by the microtubule-associated protein MAP 1C. *Nature, 330*(6144), 181-183. doi:10.1038/330181a0

Pazour, G. J., Dickert, B. L., & Witman, G. B. (1999). The DHC1b (DHC2) isoform of cytoplasmic dynein is required for flagellar assembly. *J Cell Biol, 144*(3), 473-481. doi:10.1083/jcb.144.3.473

Peet, D. R., Burroughs, N. J., & Cross, R. A. (2018). Kinesin expands and stabilizes the GDP-microtubule lattice. *Nat Nanotechnol, 13*(5), 386-391. doi:10.1038/s41565-018-0084-4

Porter, M. E., Bower, R., Knott, J. A., Byrd, P., & Dentler, W. (1999). Cytoplasmic dynein heavy chain 1b is required for flagellar assembly in Chlamydomonas. *Mol Biol Cell, 10*(3), 693-712. doi:10.1091/mbc.10.3.693

Prevo, B., Mangeol, P., Oswald, F., Scholey, J. M., & Peterman, E. J. (2015). Functional differentiation of cooperating kinesin-2 motors orchestrates cargo import and transport in C. elegans cilia. *Nat Cell Biol, 17*(12), 1536-1545. doi:10.1038/ncb3263

Purcell, T. J., Sweeney, H. L., & Spudich, J. A. (2005). A force-dependent state controls the coordination of processive myosin V. *Proc Natl Acad Sci U S A, 102*(39), 13873-13878. doi:10.1073/pnas.0506441102

Pyles, E. A., & Hastie, S. B. (1993). Effect of the B ring and the C-7 substituent on the kinetics of colchicinoid-tubulin associations. *Biochemistry, 32*(9), 2329-2336. doi:10.1021/bi00060a026

Pyrpassopoulos, S., Shuman, H., & Ostap, E. M. (2020). Modulation of Kinesin's Load-Bearing Capacity by Force Geometry and the Microtubule Track. *Biophys J, 118*(1), 243-253. doi:10.1016/j.bpj.2019.10.045

Ravindran, M. S., Engelke, M. F., Verhey, K. J., & Tsai, B. (2017). Exploiting the kinesin-1 molecular motor to generate a virus membrane penetration site. *Nat Commun, 8*, 15496. doi:10.1038/ncomms15496

Reck-Peterson, S. L., Provance, D. W., Jr., Mooseker, M. S., & Mercer, J. A. (2000). Class V myosins. *Biochim Biophys Acta, 1496*(1), 36-51. doi:10.1016/s0167-4889(00)00007-0

Reck-Peterson, S. L., Redwine, W. B., Vale, R. D., & Carter, A. P. (2018). The cytoplasmic dynein transport machinery and its many cargoes. *Nat Rev Mol Cell Biol, 19*(6), 382-398. doi:10.1038/s41580-018-0004-3

Ren, J., Zhang, Y., Wang, S., Huo, L., Lou, J., & Feng, W. (2018). Structural Delineation of the Neck Linker of Kinesin-3 for Processive Movement. *J Mol Biol, 430*(14), 2030-2041. doi:10.1016/j.jmb.2018.05.010

Rice, L. M. (2018). A new look for the growing microtubule end? *J Cell Biol, 217*(8), 2609-2611. doi:10.1083/jcb.201807036

Rice, S. (2014). Structure of kif14: an engaging molecular motor. *J Mol Biol, 426*(17), 2993-2996. doi:10.1016/j.jmb.2014.06.008

Rice, S., Lin, A. W., Safer, D., Hart, C. L., Naber, N., Carragher, B. O., Cain, S. M., Pechatnikova, E., Wilson-Kubalek, E. M., Whittaker, M., Pate, E., Cooke, R., Taylor, E. W., Milligan, R. A., Vale, R. D. (1999). A structural change in the kinesin motor protein that drives motility. *Nature, 402*(6763), 778-784. doi:10.1038/45483

Rosenfeld, S. S., Jefferson, G. M., & King, P. H. (2001). ATP reorients the neck linker of kinesin in two sequential steps. *J Biol Chem, 276*(43), 40167-40174. doi:10.1074/jbc.M103899200

Ross, J. L., Shuman, H., Holzbaur, E. L., & Goldman, Y. E. (2008). Kinesin and dynein-dynactin at intersecting microtubules: motor density affects dynein function. *Biophys J, 94*(8), 3115-3125. doi:10.1529/biophysj.107.120014

Rothenberg, K. E., & Fernandez-Gonzalez, R. (2019). Forceful closure: cytoskeletal networks in embryonic wound repair. *Mol Biol Cell, 30*(12), 1353-1358. doi:10.1091/mbc.E18-04-0248

Sablin, E. P., Kull, F. J., Cooke, R., Vale, R. D., & Fletterick, R. J. (1996). Crystal structure of the motor domain of the kinesin-related motor ncd. *Nature, 380*(6574), 555-559. doi:10.1038/380555a0

Sack, S., Muller, J., Marx, A., Thormahlen, M., Mandelkow, E. M., Brady, S. T., & Mandelkow, E. (1997). X-ray structure of motor and neck domains from rat brain kinesin. *Biochemistry, 36*(51), 16155-16165. doi:10.1021/bi9722498

Scarabelli, G., Soppina, V., Yao, X. Q., Atherton, J., Moores, C. A., Verhey, K. J., & Grant, B. J. (2015). Mapping the Processivity Determinants of the Kinesin-3 Motor Domain. *Biophys J, 109*(8), 1537-1540. doi:10.1016/j.bpj.2015.08.027

Schimert, K. I., Budaitis, B. G., Reinemann, D. N., Lang, M. J., & Verhey, K. J. (2019). Intracellular cargo transport by single-headed kinesin motors. *Proc Natl Acad Sci U S A, 116*(13), 6152-6161. doi:10.1073/pnas.1817924116

Schliwa, M., & Woehlke, G. (2003). Molecular motors. *Nature, 422*(6933), 759-765. doi:10.1038/nature01601

Schneider, R., Korten, T., Walter, W. J., & Diez, S. (2015). Kinesin-1 motors can circumvent permanent roadblocks by side-shifting to neighboring protofilaments. *Biophys J, 108*(9), 2249-2257. doi:10.1016/j.bpj.2015.03.048

Schnitzer, M. J., & Block, S. M. (1997). Kinesin hydrolyses one ATP per 8-nm step. *Nature, 388*(6640), 386-390. doi:10.1038/41111

Schuster, M., Kilaru, S., Fink, G., Collemare, J., Roger, Y., & Steinberg, G. (2011). Kinesin-3 and dynein cooperate in long-range retrograde endosome motility along a nonuniform microtubule array. *Mol Biol Cell, 22*(19), 3645-3657. doi:10.1091/mbc.E11-03-0217

Seitz, A., & Surrey, T. (2006). Processive movement of single kinesins on crowded microtubules visualized using quantum dots. *EMBO J, 25*(2), 267-277. doi:10.1038/sj.emboj.7600937

Shang, Z., Zhou, K., Xu, C., Csencsits, R., Cochran, J. C., & Sindelar, C. V. (2014). High-resolution structures of kinesin on microtubules provide a basis for nucleotide-gated force-generation. *Elife, 3*, e04686. doi:10.7554/eLife.04686

Shastry, S., & Hancock, W. O. (2010). Neck linker length determines the degree of processivity in kinesin-1 and kinesin-2 motors. *Curr Biol, 20*(10), 939-943. doi:10.1016/j.cub.2010.03.065

Shastry, S., & Hancock, W. O. (2011). Interhead tension determines processivity across diverse N-terminal kinesins. *Proc Natl Acad Sci U S A, 108*(39), 16253-16258. doi:10.1073/pnas.1102628108

Sheetz, M. P., & Spudich, J. A. (1983). Movement of myosin-coated fluorescent beads on actin cables in vitro. *Nature, 303*(5912), 31-35. doi:10.1038/303031a0

Shima, T., Morikawa, M., Kaneshiro, J., Kambara, T., Kamimura, S., Yagi, T., . . . Hirokawa, N. (2018). Kinesin-binding-triggered conformation switching of

microtubules contributes to polarized transport. *J Cell Biol, 217*(12), 4164-4183. doi:10.1083/jcb.201711178

Shipley, K., Hekmat-Nejad, M., Turner, J., Moores, C., Anderson, R., Milligan, R., Sakowicz, R., Fletterick, R. (2004). Structure of a kinesin microtubule depolymerization machine. *EMBO J, 23*(7), 1422-1432. doi:10.1038/sj.emboj.7600165

Shubeita, G. T., Tran, S. L., Xu, J., Vershinin, M., Cermelli, S., Cotton, S. L., Welte, M. A., Gross, S. P. (2008). Consequences of motor copy number on the intracellular transport of kinesin-1-driven lipid droplets. *Cell, 135*(6), 1098-1107. doi:10.1016/j.cell.2008.10.021

Sindelar, C. V., Budny, M. J., Rice, S., Naber, N., Fletterick, R., & Cooke, R. (2002). Two conformations in the human kinesin power stroke defined by X-ray crystallography and EPR spectroscopy. *Nat Struct Biol, 9*(11), 844-848. doi:10.1038/nsb852

Sindelar, C. V., & Downing, K. H. (2010). An atomic-level mechanism for activation of the kinesin molecular motors. *Proc Natl Acad Sci U S A, 107*(9), 4111-4116. doi:10.1073/pnas.0911208107

Sivaramakrishnan, S., & Spudich, J. A. (2009). Coupled myosin VI motors facilitate unidirectional movement on an F-actin network. *J Cell Biol, 187*(1), 53-60. doi:10.1083/jcb.200906133

Skiniotis, G., Surrey, T., Altmann, S., Gross, H., Song, Y. H., Mandelkow, E., & Hoenger, A. (2003). Nucleotide-induced conformations in the neck region of dimeric kinesin. *EMBO J, 22*(7), 1518-1528. doi:10.1093/emboj/cdg164

Smith, D. A., & Simmons, R. M. (2001). Models of motor-assisted transport of intracellular particles. *Biophys J, 80*(1), 45-68. doi:10.1016/S0006-3495(01)75994-2

Snider, J., Thibault, G., & Houry, W. A. (2008). The AAA+ superfamily of functionally diverse proteins. *Genome Biol, 9*(4), 216. doi:10.1186/gb-2008-9-4-216

Snow, J. J., Ou, G., Gunnarson, A. L., Walker, M. R., Zhou, H. M., Brust-Mascher, I., & Scholey, J. M. (2004). Two anterograde intraflagellar transport motors cooperate

to build sensory cilia on C. elegans neurons. *Nat Cell Biol, 6*(11), 1109-1113. doi:10.1038/ncb1186

Song, H., & Endow, S. A. (1998). Decoupling of nucleotide- and microtubule-binding sites in a kinesin mutant. *Nature, 396*(6711), 587-590. doi:10.1038/25153

Soppina, V., Norris, S. R., Dizaji, A. S., Kortus, M., Veatch, S., Peckham, M., & Verhey, K. J. (2014). Dimerization of mammalian kinesin-3 motors results in superprocessive motion. *Proc Natl Acad Sci U S A, 111*(15), 5562-5567. doi:10.1073/pnas.1400759111

Soppina, V., Rai, A. K., Ramaiya, A. J., Barak, P., & Mallik, R. (2009). Tug-of-war between dissimilar teams of microtubule motors regulates transport and fission of endosomes. *Proc Natl Acad Sci U S A, 106*(46), 19381-19386. doi:10.1073/pnas.0906524106

Soppina, V., & Verhey, K. J. (2014). The family-specific K-loop influences the microtubule on-rate but not the superprocessivity of kinesin-3 motors. *Mol Biol Cell, 25*(14), 2161-2170. doi:10.1091/mbc.E14-01-0696

Spudich, J. A. (2011). Molecular motors: forty years of interdisciplinary research. *Mol Biol Cell, 22*(21), 3936-3939. doi:10.1091/mbc.E11-05-0447

Stock, M. F., Chu, J., & Hackney, D. D. (2003). The kinesin family member BimC contains a second microtubule binding region attached to the N terminus of the motor domain. *J Biol Chem, 278*(52), 52315-52322. doi:10.1074/jbc.M309419200

Svoboda, K., & Block, S. M. (1994). Force and velocity measured for single kinesin molecules. *Cell, 77*(5), 773-784. doi:10.1016/0092-8674(94)90060-4

Svoboda, K., Schmidt, C. F., Schnapp, B. J., & Block, S. M. (1993). Direct observation of kinesin stepping by optical trapping interferometry. *Nature, 365*(6448), 721-727. doi:10.1038/365721a0

Syamaladevi, D. P., Spudich, J. A., & Sowdhamini, R. (2012). Structural and functional insights on the Myosin superfamily. *Bioinform Biol Insights, 6*, 11-21. doi:10.4137/BBI.S8451

Tomishige, M., Klopfenstein, D. R., & Vale, R. D. (2002). Conversion of Unc104/KIF1A kinesin into a processive motor after dimerization. *Science, 297*(5590), 2263-2267. doi:10.1126/science.1073386

Tomishige, M., & Vale, R. D. (2000). Controlling kinesin by reversible disulfide cross-linking. Identifying the motility-producing conformational change. *J Cell Biol, 151*(5), 1081-1092. doi:10.1083/jcb.151.5.1081

Uchimura, S., Oguchi, Y., Hachikubo, Y., Ishiwata, S., & Muto, E. (2010). Key residues on microtubule responsible for activation of kinesin ATPase. *EMBO J, 29*(7), 1167-1175. doi:10.1038/emboj.2010.25

Uemura, S., Higuchi, H., Olivares, A. O., De La Cruz, E. M., & Ishiwata, S. (2004). Mechanochemical coupling of two substeps in a single myosin V motor. *Nat Struct Mol Biol, 11*(9), 877-883. doi:10.1038/nsmb806

Uppulury, K., Efremov, A. K., Driver, J. W., Jamison, D. K., Diehl, M. R., & Kolomeisky, A. B. (2012). How the interplay between mechanical and nonmechanical interactions affects multiple kinesin dynamics. *J Phys Chem B, 116*(30), 8846-8855. doi:10.1021/jp304018b

Vale, R. D. (2003). The molecular motor toolbox for intracellular transport. *Cell, 112*(4), 467-480. doi:10.1016/s0092-8674(03)00111-9

Vale, R. D., & Fletterick, R. J. (1997). The design plan of kinesin motors. *Annu Rev Cell Dev Biol, 13*, 745-777. doi:10.1146/annurev.cellbio.13.1.745

Vale, R. D., & Milligan, R. A. (2000). The way things move: looking under the hood of molecular motor proteins. *Science, 288*(5463), 88-95. doi:10.1126/science.288.5463.88

Vale, R. D., Reese, T. S., & Sheetz, M. P. (1985). Identification of a novel force-generating protein, kinesin, involved in microtubule-based motility. *Cell, 42*(1), 39-50. doi:10.1016/s0092-8674(85)80099-4

Vale, R. D., Schnapp, B. J., Reese, T. S., & Sheetz, M. P. (1985). Organelle, bead, and microtubule translocations promoted by soluble factors from the squid giant axon. *Cell, 40*(3), 559-569. doi:10.1016/0092-8674(85)90204-1

Valentine, M. T., Fordyce, P. M., Krzysiak, T. C., Gilbert, S. P., & Block, S. M. (2006). Individual dimers of the mitotic kinesin motor Eg5 step processively and support substantial loads in vitro. *Nat Cell Biol, 8*(5), 470-476. doi:10.1038/ncb1394

Varga, V., Helenius, J., Tanaka, K., Hyman, A. A., Tanaka, T. U., & Howard, J. (2006). Yeast kinesin-8 depolymerizes microtubules in a length-dependent manner. *Nat Cell Biol, 8*(9), 957-962. doi:10.1038/ncb1462

Verhey, K. J., & Hammond, J. W. (2009). Traffic control: regulation of kinesin motors. *Nat Rev Mol Cell Biol, 10*(11), 765-777. doi:10.1038/nrm2782

Vershinin, M., Carter, B. C., Razafsky, D. S., King, S. J., & Gross, S. P. (2007). Multiple-motor based transport and its regulation by Tau. *Proc Natl Acad Sci U S A, 104*(1), 87-92. doi:10.1073/pnas.0607919104

Wade, R. H., & Kozielski, F. (2000). Structural links to kinesin directionality and movement. *Nat Struct Biol, 7*(6), 456-460. doi:10.1038/75850

Walker, J. E., Saraste, M., Runswick, M. J., & Gay, N. J. (1982). Distantly related sequences in the alpha- and beta-subunits of ATP synthase, myosin, kinases and other ATP-requiring enzymes and a common nucleotide binding fold. *EMBO J, 1*(8), 945-951.

Wang, J., Wang, Y., Liu, X., Xu, Y., & Ma, Q. (2016). Microtubule Polymerization Functions in Hypersensitive Response and Accumulation of H2O2 in Wheat Induced by the Stripe Rust. *Biomed Res Int, 2016*, 7830768. doi:10.1155/2016/7830768

Waterman-Storer, C. M., Karki, S. B., Kuznetsov, S. A., Tabb, J. S., Weiss, D. G., Langford, G. M., & Holzbaur, E. L. (1997). The interaction between cytoplasmic dynein and dynactin is required for fast axonal transport. *Proc Natl Acad Sci U S A, 94*(22), 12180-12185. doi:10.1073/pnas.94.22.12180

Welte, M. A. (2004). Bidirectional transport along microtubules. *Curr Biol, 14*(13), R525-537. doi:10.1016/j.cub.2004.06.045

Woolner, S., & Bement, W. M. (2009). Unconventional myosins acting unconventionally. *Trends Cell Biol, 19*(6), 245-252. doi:10.1016/j.tcb.2009.03.003

Xu, J., Reddy, B. J., Anand, P., Shu, Z., Cermelli, S., Mattson, M. K., Tripathy, S. K., Hoss, M. T., James, N. S., King, S. J., Huang, L., Bardwell, L., Gross, S. P. (2012). Casein kinase 2 reverses tail-independent inactivation of kinesin-1. *Nat Commun, 3*, 754. doi:10.1038/ncomms1760

Yamada, K. H., Hanada, T., & Chishti, A. H. (2007). The effector domain of human Dlg tumor suppressor acts as a switch that relieves autoinhibition of kinesin-3 motor GAKIN/KIF13B. *Biochemistry, 46*(35), 10039-10045. doi:10.1021/bi701169w

Yardimci, H., van Duffelen, M., Mao, Y., Rosenfeld, S. S., & Selvin, P. R. (2008). The mitotic kinesin CENP-E is a processive transport motor. *Proc Natl Acad Sci U S A, 105*(16), 6016-6021. doi:10.1073/pnas.0711314105

Yildiz, A., Tomishige, M., Gennerich, A., & Vale, R. D. (2008). Intramolecular strain coordinates kinesin stepping behavior along microtubules. *Cell, 134*(6), 1030-1041. doi:10.1016/j.cell.2008.07.018

Yildiz, A., Tomishige, M., Vale, R. D., & Selvin, P. R. (2004). Kinesin walks hand-over-hand. *Science, 303*(5658), 676-678. doi:10.1126/science.1093753

Yu, I., Garnham, C. P., & Roll-Mecak, A. (2015). Writing and Reading the Tubulin Code. *J Biol Chem, 290*(28), 17163-17172. doi:10.1074/jbc.R115.637447

Yu, Y., & Feng, Y. M. (2010). The role of kinesin family proteins in tumorigenesis and progression: potential biomarkers and molecular targets for cancer therapy. *Cancer, 116*(22), 5150-5160. doi:10.1002/cncr.25461

Yue, Y., Blasius, T. L., Zhang, S., Jariwala, S., Walker, B., Grant, B. J., Cochran, J. C., Verhey, K. J. (2018). Altered chemomechanical coupling causes impaired motility of the kinesin-4 motors KIF27 and KIF7. *J Cell Biol, 217*(4), 1319-1334. doi:10.1083/jcb.201708179

Yun, M., Zhang, X., Park, C. G., Park, H. W., & Endow, S. A. (2001). A structural pathway for activation of the kinesin motor ATPase. *EMBO J, 20*(11), 2611-2618. doi:10.1093/emboj/20.11.2611

Zhao, Y. C., Kull, F. J., & Cochran, J. C. (2010). Modulation of the kinesin ATPase cycle by neck linker docking and microtubule binding. *J Biol Chem, 285*(33), 25213-25220. doi:10.1074/jbc.M110.123067

Chapter 2: Neck Linker Docking is Critical for Kinesin-1 Force Generation in Cells but at a Cost to Motor Speed and Processivity

Portions of this chapter have been adapted from the following publication

Budaitis, B.G., Jariwala, S., Reinemann, D.N.*, Schimert, K.I.*, Scarabelli, G., Grant, B.J., Sept, D., Lang, M.J., Verhey, K.J. (2019). Neck linker docking is critical for kinesin-1 force generation in cells but at a cost to motor speed and processivity. Elife 8:e44146.*

**Authors contributed equally, listed alphabetically*

Author contributions:

B.G.B performed all assays except optical trapping assays and molecular dynamics simulations. D.N.R performed optical trapping assays, S.J. performed molecular dynamics, and K.I.S developed the inducible cargo dispersion assays. B.G.B, D.N.R, and S.J. analyzed data. B.G.B and K.J.V wrote the text and composed figures with input from all authors.

2.1 Introduction

Kinesin motor proteins are responsible for orchestrating fundamental microtubule-based processes including cell division, intracellular trafficking, cytoskeletal organization, and cilia function (Hirokawa et al., 2009; Verhey & Hammond, 2009). All kinesins contain a highly conserved motor domain with signature sequences for nucleotide and microtubule binding. How nucleotide dependent conformational changes in the catalytic site result in a mechanical output that drives cargo transport has been a fundamental question in the field.

The two motor domains in most dimeric kinesin motors are linked via a flexible 12–18 amino acid sequence called the neck linker [NL, (Hariharan & Hancock, 2009; Kozielski et al., 1997)]. The NL has been suggested to serve as a structural element critical for both directed motility and force generation of kinesin motors.

For kinesin-1, the founding member of the kinesin superfamily, structural and spectroscopic studies have shown that conformational changes in the NL are coupled to the nucleotide state of the motor domain. Specifically, the NL undergoes a transformation from being flexible in both the ADP-bound and nucleotide-free states to being docked along the core motor domain in the ATP-bound state (Asenjo et al., 2006; Gigant et al., 2013; Rice et al., 1999; Rosenfeld et al., 2001; Shang et al., 2014; Sindelar et al., 2002; Sindelar & Downing, 2010; Skiniotis et al., 2003). NL docking of the leading motor domain positions the lagging motor domain forward along the microtubule track, thereby specifying direction of motility. NL docking also coordinates the alternating ATPase cycles of the two motor domains to ensure processive stepping (Case et al., 2000; Clancy et al., 2011; Dogan et al., 2015; Hahlen et al., 2006; Isojima et al., 2016; Liu et al., 2017; Tomishige & Vale, 2000; Yildiz et al., 2008). Recent work has extended the model that nucleotide-dependent conformational change in the NL drive processive stepping to other members of the kinesin superfamily (Atherton et al., 2014; Atherton et al., 2017; Cao et al., 2014; Muthukrishnan et al., 2009; Nitta et al., 2008; Ren et al., 2018; Shastry & Hancock, 2010, 2011).

The role of the NL in force generation has been more difficult to discern (Block, 2007). ATP induced NL docking involves distinct interactions of the two β-strands that comprise the NL, β9 and β10 (Figure 2.1C,D). The first half of the NL, β9, pairs with another β-strand, the coverstrand (CS or β0), located at the opposite end of the core motor domain. The zippering of β9 of the NL with β0 of the CS forms a 2-stranded β-sheet, termed the cover-neck bundle (CNB), to provide the power stroke for force generation by kinesin-1 (Hwang et al., 2008; Khalil et al., 2008). Support for the CNB as a mechanical element comes from optical trap assays where point mutations in the CS designed to hinder β-strand formation, or deletion of the entire CS, in the fly kinesin-1 motor significantly reduced the motor's ability to withstand load (Khalil et al., 2008). CNB formation may be a critical element for force generation across the kinesin superfamily as recent work has shown that the coverstrand (CS or β0) and NL (β9) of members of the kinesin-5 and kinesin-6 families engage in CNB formation in response to ATP binding (Atherton et al., 2017; Hesse et al., 2013).

After CNB formation, the C-terminal segment of the NL (β10) is predicted to dock along the surface of the core motor domain. In particular, an asparagine residue between β9 and β10 begins the process of docking β10 of the NL onto β7 of the motor core. This asparagine residue (N334) is predicted to serve as a latch (the N-latch) to hold the docked NL along the core motor domain (Hwang et al., 2008) but its role in force generation has not been directly tested. The N-latch residue is conserved in most kinesins, particularly motors known to processively step along microtubules (Figure 2.1C), suggesting that N-latch formation may also be a conserved feature of kinesin force generation.

Whether CNB and/or N-latch formation are critical for multiple kinesin motors to drive transport of membrane-bound cargo under physiological conditions is not known. To address this, we combined molecular dynamics simulations, *in vitro* single-molecule assays, and cell-based transport assays to delineate how NL docking influences kinesin-1 motors cooperating in teams to transport membrane-bound cargoes in cells. We found that mutations that disrupt CNB formation and/or N-latch formation severely reduced the ability of single kinesin-1 motors to successfully transport against load in an optical trap. Strikingly, single mutant motors traveled faster and for longer distances under unloaded conditions as compared to wild type (WT) motors. These results indicate that mutations to the CS and N-latch of kinesin-1 can enhance processivity and velocity but at a cost to force production. Mutant motors with impaired CNB formation or N-latch formation are able to cooperate to transport low-load cargo in cells. However, the mutant motors are unable to effectively cooperate to transport high-load cargo in cells. Overall, these findings suggest that CNB and N-latch formation are required for transport of high-load cargoes in cells, even when kinesin-1 motors work collectively as a team

2.2 Materials and Methods

Plasmids: A truncated, constitutively active kinesin-1 [rat KIF5C(1-560)] was used (Cai et al., 2007). Point mutations to impair CNB and/or N-latch formation were generated using QuickChange site-directed mutagenesis and all plasmids were verified by DNA sequencing. Motors were tagged with three tandem monomeric Citrine fluorescent proteins (3xmCit) for single molecule imaging assays (Cai et al., 2007), a FLAG-tag for

optical trapping assays, and monomeric NeonGreen (mNG)-FRB for inducible cargo dispersion assays in cells (Kapitein et al., 2010). The peroxisome-targeting PEX3-mRFP-FKBP construct was a gift from Casper Hoogenraad (Utrecht University). The Golgi targeting GMAP-mRFP-FKBP construct is described in (Engelke et al., 2016; Schimert et al., 2019). KIF18A(1-452) was a gift from Claire Walczak (Indiana University, [Weaver et al., 2011]). Constructs coding for FRB (DmrA) and FKBP (DmrC) sequences were obtained from ARIAD Pharmaceuticals and are now available from Takara Bio Inc. Plasmids encoding monomeric NeonGreen were obtained from Allele Biotechnology.

Cell culture, transfection, and lysate preparation: COS-7 (African green monkey kidney fibroblasts, American Type Culture Collection, RRID: CVCL_0224) were grown at 37˚C with 5% (vol/vol) CO_2 in Dulbecco's Modified Eagle Medium (Gibco) supplemented with 10% (vol/vol) Fetal Clone III (HyClone) and 2 mM GlutaMAX (L-alanyl-L-glutamine dipeptide in 0.85% NaCl, Gibco). Cells are checked annually for mycoplasma contamination and were authenticated through mass spectrometry (the protein sequences exactly match those in the African green monkey genome). 24 hr after seeding, the cells were transfected with plasmids encoding for the expression of motor tagged with three tandem monomeric citrines or FLAG, TransIT-LT1 transfection reagent (Mirus), and Opti-MEM Reduced Serum Medium (Gibco). Cells were trypsinized and harvested 24 hr after transfection by low-speed centrifugation at 3000 x g at 4˚C for 3 min. The pellet was resuspended in cold 1X PBS, centrifuged at 3000 x g at 4˚C for 3 min, and the pellet was resuspended in 50 µL of cold lysis buffer [25 mM HEPES/KOH, 115 mM potassium acetate, 5 mM sodium acetate, 5 mM $MgCl_2$, 0.5 mM EGTA, and 1% (vol/vol) Triton X-100, pH 7.4] with 1 mM ATP, 1 mM phenylmethylsulfonyl fluoride, and 1% (vol/vol) protease inhibitor cocktail (P8340, SigmaAldrich). Lysates were clarified by centrifugation at 20,000 x g at 4˚C for 10 min and lysates were snap frozen in 5 µL aliquots in liquid nitrogen and stored at 80˚C

Optical trapping assays: Tubulin was reconstituted and polymerized into microtubules as described previously (Reinemann et al., 2018; Reinemann et al., 2017). Tubulin

(bovine brain, Cytoskeleton TL238) was reconstituted in 25 µL BRB80 buffer [80 mM PIPES (Sigma P-1851), 1 mM EGTA (Sigma E-4378), 1 mM $MgCl_2$ (Mallinckrodt H590), pH adjusted to 6.9 with KOH] supplemented with 1 mM GTP (Cytoskeleton BST06) and kept on ice. 13 µL PEM104 buffer (104 mM PIPES, 1.3 mM EGTA, 6.3 mM $MgCl_2$, pH adjusted to 6.9 with KOH), 2.2 µL 10 mM GTP, and 2.2 µL DMSO were mixed. 4.8 µL of 10 mg/mL tubulin were added to the mixture and allowed to incubate for 40 min at 37˚C. Subsequently, 2 µL of stabilization solution [STAB: 38.6 mL PEM80, 0.5 mL 100 mM GTP, 4.7 mL 65 g/L NaN_3 (Sigma S-8032), 1.2 µL 10 mM Taxol (Cytoskeleton TXD01), 5 µL DMSO (Cytoskeleton)] was added to the stock microtubule solution at room temperature.

Optical trap assays were performed as described previously (Reinemann et al., 2017; Reinemann et al., 2018). 0.44 mm anti-FLAG-coated beads were prepared by crosslinking anti-FLAG (Thermo Fisher Scientific) antibodies to carboxy polystyrene beads (Spherotech) via EDC chemistry. Lysates containing FLAG-tagged motors were diluted in assay buffer [AB: P12 buffer (12 mM PIPES (Sigma P-1851), 1 mM EGTA (Sigma E-4378), 1 mM $MgCl_2$ (Mallinckrodt H590), pH adjusted to 6.9 with KOH), 1 mM DTT (Sigma Aldrich), 20 µM Taxol (Cytoskeleton), 1 mg/mL casein (Blotting-Grade Blocker, Biorad), 1 mM ATP (Sigma Aldrich)] were incubated with gently sonicated anti-FLAG beads to allow binding for 1 hr at 4˚C on a rotator in the presence of oxygen scavenging reagents (5 mg/ mL b-D-glucose (Sigma Aldrich), 0.25 mg/mL glucose oxidase (Sigma Aldrich), and 0.03 mg/mL catalase (Sigma Aldrich).

A flow cell that holds a volume of ~15 µL was assembled using a microscope slide, etched coverslips, and double-sided tape. Before assembly, etched coverslips were incubated in a solution of 100 mL poly-l-lysine (PLL, Sigma P8920) in 30 mL ethanol for 15 min. The coverslip was then dried with a filtered air line. After flow cell assembly, microtubules were diluted 150 times from the stock in a solution of PemTax (1 mL 10 mM Taxol in 500 mL P12). The diluted microtubules were added to the flow cell and allowed to incubate to the PLL surface for 10 min. Unbound microtubules were then washed out with 20 µL PemTax. A solution of casein (Blotting-Grade Blocker, Biorad 1706404) diluted in PemTax (1:8 mixture) was then added to the flow cell and allowed to incubate for 10 min to block the remainder of the surface to prevent non-

specific binding. After the incubation, the flow cell was washed with 50 mL PemTax and 80 mL assay buffer (AB). 20 µL of the bead/motor incubation was then added to the flow cell.

Optical trapping measurements were obtained using a custom-built instrument with separate trapping and detection systems. The instrument setup and calibration procedures have been described previously (Khalil et al., 2008). Briefly, beads were trapped with a 1,064 nm laser that was coupled to an inverted microscope with a 100x/1.3 NA oil-immersion objective. Bead displacements from the trap center were recorded at 3 kHz and further antialias filtered at 1.5 kHz. To ensure that we were at the single molecule limit for the motility assay, the protein-bead ratio was adjusted so that fewer than half of the beads trapped and tested on microtubules showed binding, actually having 5–10% binding the majority of the time. A motor-coated bead was trapped in solution and subjected to position calibration and trap stiffness Labview routines. Afterward, the bead was brought close to a surface-bound microtubule to allow for binding. Bead position displacement and force generation were measured for single motor-bound beads. Detachment forces are plotted as a dot plot where each dot indicates the maximum detachment force of an event and the mean for each construct is indicated by a black horizontal line. Statistical differences between the maximum detachment force of wild type and mutant motors were calculated by using a two-tailed unpaired Student's t test.

Single-molecule motility assays: Microtubules were polymerized (purified tubulin unlabeled and HiLyte-647-labeled tubulin, Cytoskeleton Inc) in BRB80 buffer (80 mM Pipes/KOH pH 6.8, 1 mM $MgCl_2$, 1 mM EGTA) supplemented with GTP and $MgCl_2$ and incubated for 60 min at 37^{o}C. 2 µM taxol in prewarmed BRB80 was added and incubated for 60 min to stabilize microtubules. Microtubules were stored in the dark at room temperature for up to 2 weeks. Flow cells were prepared by attaching a #1.5 mm^2 coverslip (Thermo Fisher Scientific) to a glass slide (Thermo Fisher Scientific) using double-sided tape. Microtubules were diluted in fresh BRB80 buffer supplemented with 10 µM taxol, infused into flow cells, and incubated for four minutes to allow for nonspecific absorption to the glass. Flow cells were then incubated with blocking buffer

[30 mg/mL casein in P12 buffer (12 mM Pipes/KOH pH 6.8, 1 mM $MgCl_2$, 1 mM EGTA) supplemented with 10 μM taxol] for four minutes. Flow cells were then infused with motility mixture (0.5–1.0 μL of COS-7 cell lysate, 25 μL P12 buffer, 15 μL blocking buffer, 1.0 μL 100 mM ATP, 0.5 μL 100 mM DTT, 0.5 μL 20 mg/mL glucose oxidase, 0.5 μL 8 mg/mL catalase, and 0.5 μL 1 M glucose), sealed with molten paraffin wax, and imaged on an inverted Nikon Ti-E/B total internal reflection fluorescence (TIRF) microscope with a perfect focus system, a 100x/1.49 NA oil immersion TIRF objective, three 20 mW diode lasers (488 nm, 561 nm, and 640 nm) and EMCCD camera (iXon+ DU879; Andor). Image acquisition was controlled using Nikon Elements software and all assays were performed at room temperature.

Motility data were analyzed by first generating maximum intensity projections to identify microtubule tracks (width = 3 pixels) and then generating kymographs in ImageJ (National Institutes of Health). Only motility events that lasted for at least three frames were analyzed. Furthermore, events that ended as a result of a motor reaching the end of a microtubule were included; therefore, the reported run lengths for highly processive motors are likely to be an underestimation. For the Latch and CNB+Latch motors, the run lengths are reported as the distance moved between gaps in the runs. Run length and velocities were plotted as cumulative distributions in MATLAB and used for statistical analysis. The cumulative distributions of motor velocities were fit to a Gaussian cumulative distribution as previously described (Arpağ et al., 2014; Norris et al., 2014) and a one-way analysis of variance test was used to assess whether velocity distributions were significantly different between motors. The cumulative distribution of WT motor run lengths was fit to an exponential distribution as previously described (Norris et al., 2014). However, a fit to an exponential decay function was not an appropriate model to describe the cumulative distributions of the CNB, Latch, and CNB +Latch motor run lengths. Rather, the cumulative distributions of the run lengths of the mutant motors were well fit to a gamma distribution. The scale parameter was fixed (assuming a rate of 1 or 2) and the shape parameter was the only fit parameter. The expected mean run length was calculated by multiplying the shape and scale parameters. A Kuskal-Wallis one-way analysis of variance was used to assess whether run length distributions were significantly different between motors. For each motor

construct, the velocities and run lengths were binned and a histogram was generated by plotting the number of motility events for each bin. A corresponding Gaussian, exponential, or gamma distribution was overlaid on each histogram plot using rate and shape parameters derived from fitting the cumulative distributions.

Molecular dynamics simulations: Simulation models of rat kinesin-1 (*Rn*KIF5C) motor domain in complex with tubulin heterodimer were constructed for motors in the no nucleotide (apo) and ATP-bound states based on PDB 4LNU (Cao et al., 2014) and PDB 4HNA (Gigant et al., 2013), respectively. Since the motor domain in both template structures (PDBs 4LNU and 4HNA) is KIF5B, residues that differ were mutated to match the sequence of rat KIF5C (UniprotID: P56536). The tubulin dimer was left unmodified. Missing coordinates were modeled using MODELLER v9.18 (Sali and Blundell, 1993). The ATP-hydrolysis transition-state analog, ADP–AlF_4, in PDB 4HNA was converted to ATP. The resulting systems of motor domain associated with tubulin dimer contained a total of ~170,000 atoms each. Models of ADP-bound wild type and CNB+Latch mutant motor domains (not associated with the tubulin heterodimer) were prepared from PDB 2KIN (Sack et al., 1997).

Energy minimization and molecular dynamics simulations were performed with AMBER14 (Case et al., 2005) and the ff99SB AMBER force field (Hornak et al., 2006). Nucleotide parameters were obtained from (Meagher, Redman, & Carlson, 2003). Histidine protonation states were assigned based on the their pKa values calculated by PROPKA (Bas, Rogers, & Jensen, 2008). Starting structures were solvated in a cubic box of pre-equilibrated TIP3P waters molecules, extending 12 Å in each dimension from the surface of the solute. Sodium ions (Na^+) were added to neutralize the systems, followed by addition of sodium and chloride (Cl^-) ions to bring the ionic strength to 0.050 M. Energy minimization was performed in four stages, with each stage consisting of 500 steps of steepest descent followed by 4,000 steps of conjugate gradient. First, minimization of solvent was performed by keeping positions of protein and nucleotides fixed. Second, side-chains and nucleotides were relaxed keeping the backbone positions fixed. Third, protein and nucleotide atoms were relaxed while keeping the solvent atoms fixed. Fourth, a last minimization stage was performed with no restraints.

The system was gradually heated to 300K over 25 ps of simulation time in constant-volume (NVT) and periodic boundary conditions (PBC), with restraint of 20 kcal/mol/Å^2 on backbone atoms. Constant-temperature (T = 300K) and constant-pressure (p=1 bar) (NpT) equilibration was then performed in six stages. First, a 400 ps NpT equilibration was performed with restraint of 20 kcal/mol/Å^2 on backbone atoms. Further stages involved gradually reducing restraints of 20, 10, 5, and one kcal/mol/Å^2 on a carbons over five ns each. A final NpT equilibration was carried out without any restraints for five ns. Subsequent production phase molecular dynamics simulations were then performed under NpT and PBC with random velocity assignments for each run. Particle-mesh Ewald summation was adopted for treating long-range electrostatics. A 12 Å cutoff for energy minimization, and a 10 Å cutoff for molecular dynamics simulations was used to truncate non-bonded interactions. A two fs time-step was adopted for all molecular dynamics simulations. Hydrogen atoms were constrained using the SHAKE algorithm. All simulations were performed in-house on NVIDIA GPU cards with the GPU version of PMEMD (pmemd.cuda). Molecular dynamics simulations were started from equilibrated structures with four independent runs of 100 ns each. Trajectory analysis was carried out in R using the Bio3D v2.3–3 package (Skjaerven et al., 2014).

Simulation analysis: inter-residue distances: Statistically significant residue-residue distance differences between apo, ATP-bound and mutant states were identified with ensemble difference distance matrix (eDDM) analysis routine (Muretta et al., 2018). A total of 400 conformations were obtained for each state under comparison by extracting 100 equally time-spaced conformations from the last 20 ns of each simulation replicate. Distance matrices for each state were constructed from residue-residue distances, defined as the minimum distance between all heavy atoms of every residue pair in a given conformation. The distances matrices were processed by applying a smooth function to mask long distances. The significance of residue distance variation between apo and ATP-bound states, and between ATP-bound and mutant states, were evaluated with the Wilcoxon test. Residue pairs showing a p-value 1 Å were considered statistically significant residue-residue distance differences for further analysis.

Simulation analysis: principal component analysis: A set of 17 experimental structures from the RCSB protein data bank, nine in ADP-like state not associated with the microtubule and eight in ATP-like state bound to tubulin heterodimer, were selected for examining the major conformational differences of the kinesin motor domain in these two states. Principal component analysis (PCA) is a dimensionality reduction technique involving orthogonal transformation of the original data into a set of linearly uncorrelated variables termed principal components. PCA was performed on 112 equivalent, non-gap Ca atoms from each of the structures after superposition onto an invariant core comprising of structural elements β1, β2, β3, P-loop, α2, β6, β7 and α6 (Scarabelli & Grant, 2013). The trajectories from MD simulations of ADP-bound wild type and CNB+Latch mutant kinesin motor domains were projected on to the PC sub-space defined by the first two PCA eigenvectors to allow comparison of the conformational space spanned by the simulations and the experimental structures.

Inducible cargo dispersion assays: Plasmids for expression of wild type or mutant KIF5C(560) motors tagged with monomeric NeonGreen and an FRB domain were cotransfected into COS-7 cells with a plasmid for expression of PEX3-mRFP-FKBP or GMAP210p-mRFP-2xFKBP at a ratio of 6:1 and 3:1 respectively with TransITLT1 transfection reagent (Mirus). Eight hours after transfection, rapamycin (Calbiochem, Millipore Sigma) was added to final concentration of 44 nM to promote FRB and FKBP heterodimerization and recruitment of motor the peroxisome or Golgi surface. Cells were fixed with 3.7% formaldehyde (Thermo Fisher Scientific) in 1X PBS, quenched in 50 mM ammonium chloride in PBS for 5 min, permeabilized for 5 min in 0.2% Triton-X 100 in PBS for 5 min and blocked in 0.2% fish skin gelatin in PBS for 5 min. Primary and secondary antibodies were added to blocking buffer and incubated for 1 hr at room temperature. Primary antibodies: polyclonal antibody against cis-Golgi marker giantin (1:1200 PRB-114C, Covance), antibody against β-tubulin (1:2000, Developmental Studies Hybridoma Bank #E7). Secondary antibodies: goat anti-rabbit Alexa680-labeled secondary antibody (1:500, Jackson ImmunoResearch). Coverslips were mounted in ProlongGold (Invitrogen) and imaged using an inverted epifluorescence microscope (Nikon TE2000E) with a 40x/0.75 NA objective and a CoolSnapHQ camera

(Photometrics). Only cells expressing low levels of motor-mNG-FRB were imaged and included in quantification, as high expression of mutant KIF5C disrupted the microtubule network. Cargo localization before and after motor recruitment was quantified using two different methods. First, the phenotype of cargo dispersion was scored as clustered, partial dispersion, diffuse dispersion, or peripheral dispersion based on the signal localization in the PEX3 (peroxisome) or giantin (Golgi) signal. Second, a distance-based analysis using a custom ImageJ plugin was applied. Statistical differences between mean cargo intensity at each binned distance between wild type and mutant motors were calculated by using a two-tailed unpaired Student's t test.

2.3 Results

2.3.1 Molecular dynamics simulations highlight residues critical for ATP-dependent NL docking

To test whether CNB and/or N-latch formation serve as mechanical elements for kinesin-1 force generation, we sought to identify critical interactions between the CS (β0, aa 4–9), motor core (β1-α6, aa 10–326), and NL (β9-β10, aa 327–338) that we could target for mutagenesis. We performed 100 ns all-atom molecular dynamics (MD) simulations of the rat kinesin-1 (*Rn*KIF5C) motor domain in association with tubulin. Four replicate simulations were carried out for motors in the nucleotide-free (apo) state [PDB 4LNU (Cao et al., 2014)] and the ATP-bound state [PDB 4HNA (Gigant et al., 2013)], similar to previous analyses of kinesin-5 (Muretta et al., 2018). We then compared residue-residue interactions between the apo and ATP-bound states (Figure 2.1B) with analysis across replicates to predict statistically significant distance differences ($p<0.05$). In the apo state (Cao et al., 2014), the NL is flexible (Figure 2.1A top) and forms few interactions with the motor domain (Figure 2.1B) while the CS interacts with residues in α4 and in Loop13 (Figure 2.1B, red boxes marked CS-α4 and CS-L13). Specifically, the C-terminal residue (CTR) of the CS (I9) points down into a hydrophobic pocket called the docking pocket (Sindelar, 2011) where it contacts residues I266, L269, and A270 of α4 and the remaining residues of the CS contact Loop13 (Figure 2.2A,B). Collectively, these interactions sterically block the NL from accessing the docking pocket.

In the ATP-bound state (Gigant et al., 2013), the NL is docked along the core motor domain, with each half of the NL (β9 and β10) forming contacts with distinct structural elements (Figure 2.1A bottom, Figure 2.1C). For the N-terminal half of the NL, β9 forms contacts with the CS to form the cover-neck bundle (CNB) (Figure 2.1B, blue box marked NL-CS) as well as contacts with α4 and Loop13 (Figure 2.1B, blue boxes marked NL-α4 and NL-L13). These contacts are made possible by the ATP-dependent formation of an extra turn at the end of α6, the NL initiation sequence [NIS (Nitta et al., 2008)], that positions β9 for insertion between the CS and α4 [Figure 2.2C,D (Lang & Hwang, 2010; Sindelar & Downing, 2010)]. The first residue of β9 (I327) now occupies the docking pocket and forms contacts with residues I266, L269, and A270 of α4 (Figure 2.2C,D). The remaining residues of β9 interact with the CS via a series of backbone-backbone interactions to complete CNB formation (Figure 2.2C,D). For the C-terminal half of the NL, β10 docks along the core motor domain through interactions with α1 and β7 (Figure 2.1B, blue boxes marked NL-α1 and NL-β7). Specifically, the N-latch residue (N334) forms interactions with residues E76 and G77 in α1 and residues S225 and L224 in β7 and the remaining residues of β10 provide further backbone interactions with β7 to complete NL docking (Figure 2.2C,E).

Overall, the MD simulations build on previous work (Cao et al., 2014; Gigant et al., 2013; Hwang et al., 2008; Hwang, Lang, & Karplus, 2017; Khalil et al., 2008; Nitta et al., 2008) and identify several residues critical for regulating the flexible-to-docked transformation of the NL. First, the CTR of the CS (I9) occupies the docking pocket bordered by α6, α4, and L13 in the nucleotide-free state such that the NL remains undocked and flexible. Second, I327 of the NIS occupies this pocket in the ATP-bound state and begins the process of NL docking along the core motor domain. We note that the presence of an isoleucine or valine as the CTR and NIS residues is a conserved feature of most kinesin motors that undergo processive motility (Figure 2.3). This conservation suggests that the ability of these residues to occupy the docking pocket in a mutually exclusive manner may be a conserved mechanism for kinesin motility and force generation. Third, residue N334 interacts with both α1 and β7 to position the NL along the core motor domain, thereby specifying the direction of motion. As noted previously (Hwang et al., 2008; Khalil et al., 2008), an asparagine residue between β9

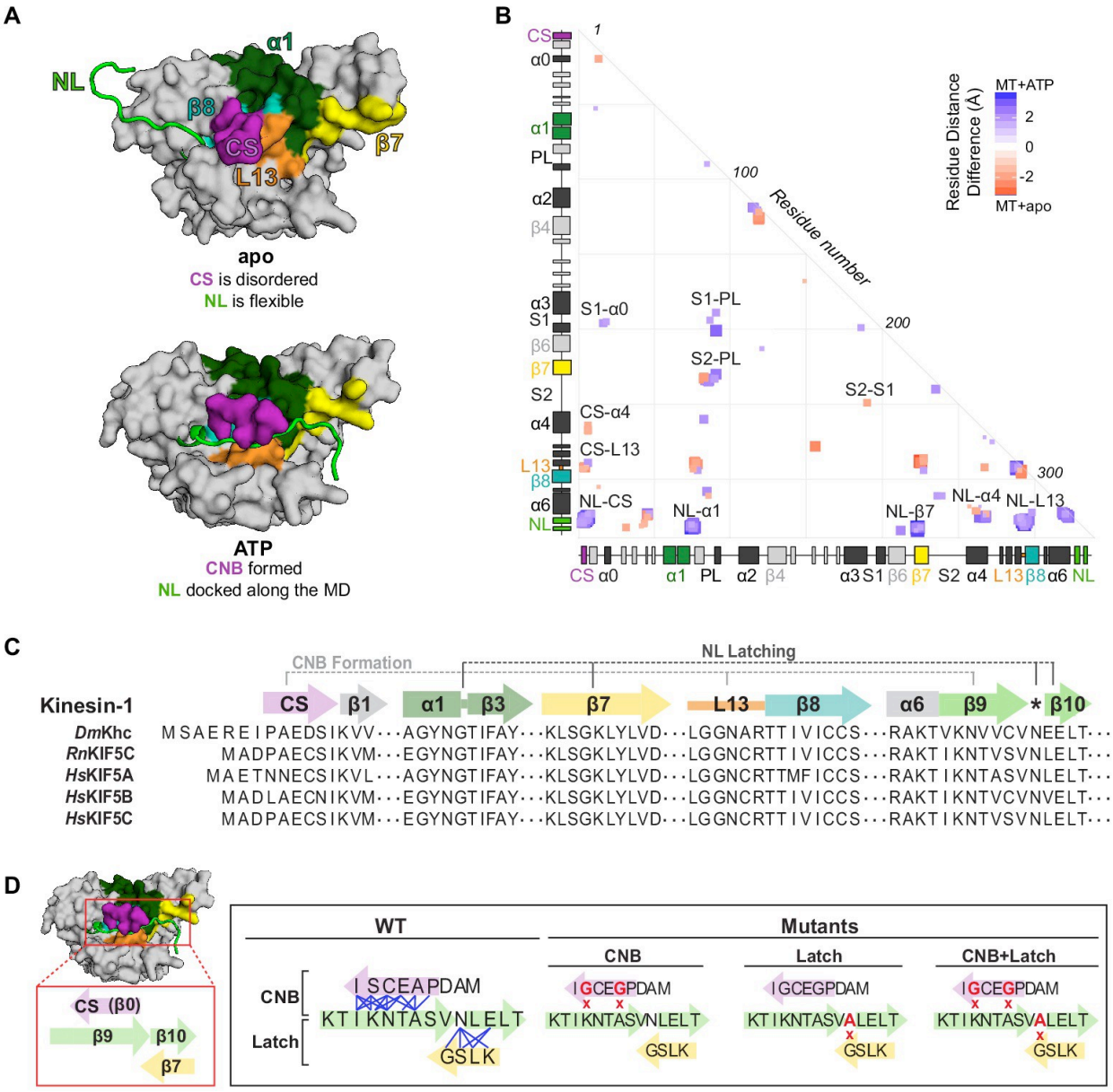

Figure 2.1 MD simulations identify key interactions between the kinesin-1 NL and motor domain.

(**A**) Surface representation of the kinesin-1 (*Rn*KIF5C) motor domain in the nucleotide-free (apo) state (top, PDB 4LNU) or ATP-bound, post-power stroke state (bottom, PDB 4HNA). The neck linker (NL, light green) is represented as a cartoon and is flexible in the apo state and docked along the motor domain in the ATP-bound state. Additional secondary structure elements are indicated: coverstrand (CS, purple), α1 (dark green), β7 (yellow), Loop13 (L13, orange), β8 (teal), neck linker (NL: β9 and β10, light green). (**B**) Differences in residue-residue distances between kinesin-1 motors in the apo versus ATP-bound states as determined from MD simulations. The secondary structure elements are laid out along the x- and y-axes with α-helices colored in black, β-strands in grey, or colored according to (A). Residue-residue interactions that are significantly closer ($p<0.05$) in the apo state (red) or ATP-bound state (blue) are indicated on the graph. The magnitude of the distance change is indicated by color intensity. Interactions between key structural elements are labeled. (**C**) Sequence alignment of the kinesin-1 motor domain across species (*Dm*, *Drosophila melanogaster; Rn*, *Rattus norvegicus; Hs*, *Homo sapiens*). For simplicity, only secondary structure elements indicated in (A) are displayed; an asterisk indicates the asparagine-latch (N-Latch). (**D**) Schematic of key structural elements involved in CNB formation and NL latching in WT and mutant motors. The first-half of the NL (β9, light green) interacts with the C-terminal end of the CS (purple) to form the cover-neck bundle (CNB). The second half of the NL (N-Latch and β10) interacts with β7 (yellow) of the core motor domain for NL docking. Residue-residue contacts for NL docking are depicted as blue lines. Point mutations generated to disrupt CNB formation, N-latch formation, or both are shown in red text.

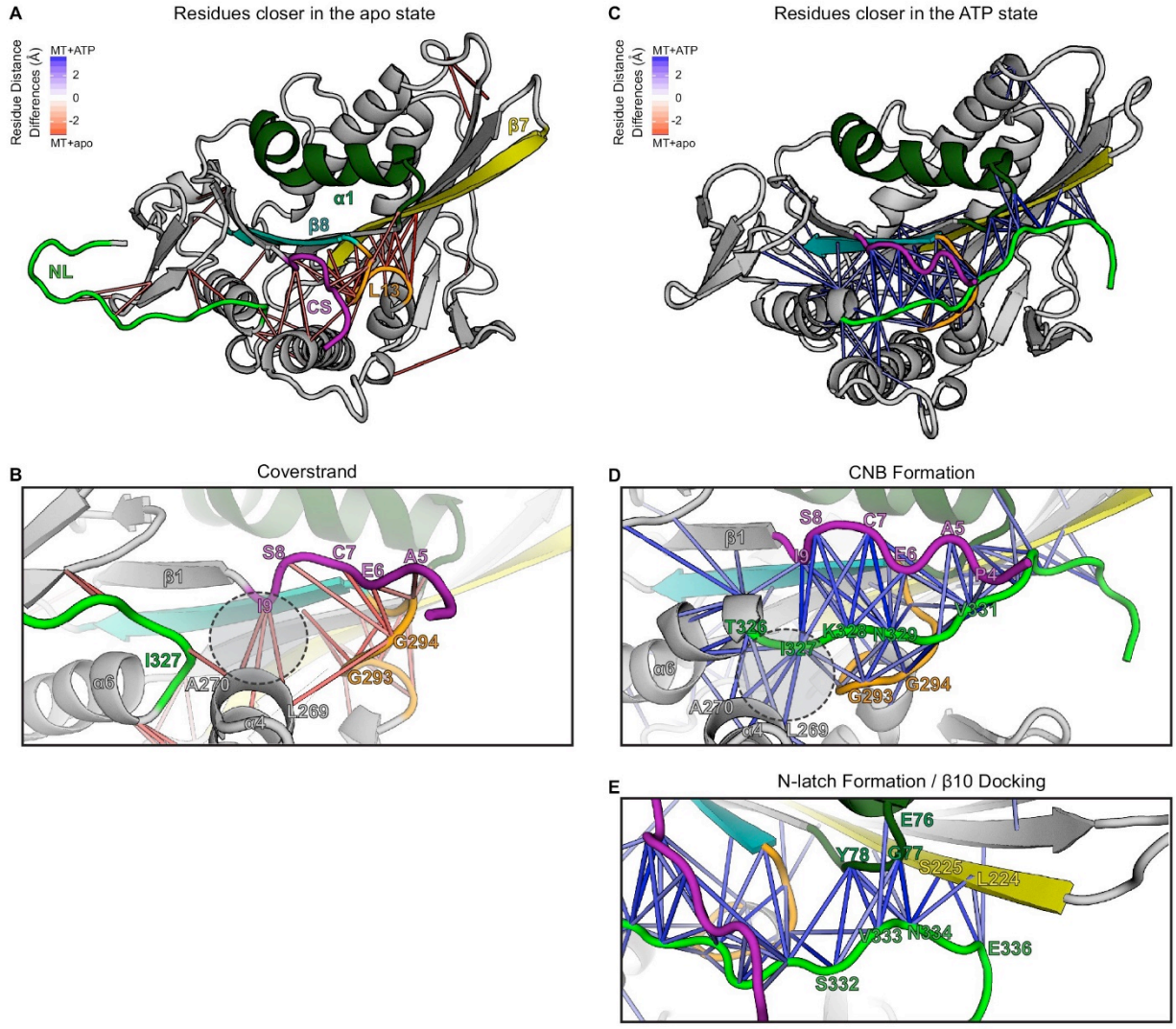

Figure 2.2 CS and NL interactions in the no nucleotide (apo) and ATP-bound, post-power stroke states of the kinesin-1 motor domain bound to tubulin.

(**A, B**) Nucleotide-free (apo) state. (**A**) Cartoon representation of the kinesin-1 motor domain (PDB 4LNU) in the nucleotide-free (apo) state. Secondary structure elements: coverstrand (CS, purple), α1 (dark green), β7 (yellow), Loop13 (orange), β8 teal, neck linker (NL: β9 and β10, light green). Red lines depict residue-residue distances that are significantly closer ($p<0.05$) in the apo state compared to the ATP-bound state across replicate MD simulations. The magnitude of the distance change is indicated by color intensity. The CS (purple) shows close interactions with Loop13 (orange) and α4 (grey). The NL (light green) is flexible and shows few interactions with other elements of the motor domain. (**B**) Enlarged view of CS interactions. The C-terminal residue of the CS [the coverstrand terminal residue (CTR), I9] lies in the docking pocket (dashed circle) and interacts with residues in α4 (I266, L269, A270), while the N-terminal residues of the CS (A5, E6, C7, S8) interact with residues in Loop13 (L292, G293, G294, N295). (**C–E**) ATP-bound state. (**C**) Cartoon representation of the kinesin-1 motor domain (PDB 4HNA) in the ATP-bound state. Secondary structure elements are colored as in (A). Blue lines depict residue-residue distances that are significantly closer ($p<0.05$) in the ATP-bound state compared to the apo state across replicate MD simulations. The magnitude of the distance change is indicated by color intensity. The CS and N-terminal half of the NL (β9) interact to form the cover-neck bundle (CNB) and the C-terminal half of the NL (N-latch and β10) interacts with the core motor domain (α1 and β7) to complete NL docking. (**D**) Enlarged view of CNB interactions. The N-terminal residue of the NL (I327) now occupies the docking pocket (dashed circle) and interacts with residues in α4 (I266, L269, A270). The CS (A5, E6, C7, S8, I9) interacts with residues in β9 of the NL (K328, N329, T330) to form the CNB. (**E**) Enlarged view of NL docking interactions. The highly conserved asparagine residue (N-latch, N334) forms critical interactions with α1 residues (G77, Y78) and β7 residues (S225, G226). Interactions between subsequent residues of β10 of the NL (E336) and β7 (L224, S225) complete NL docking.

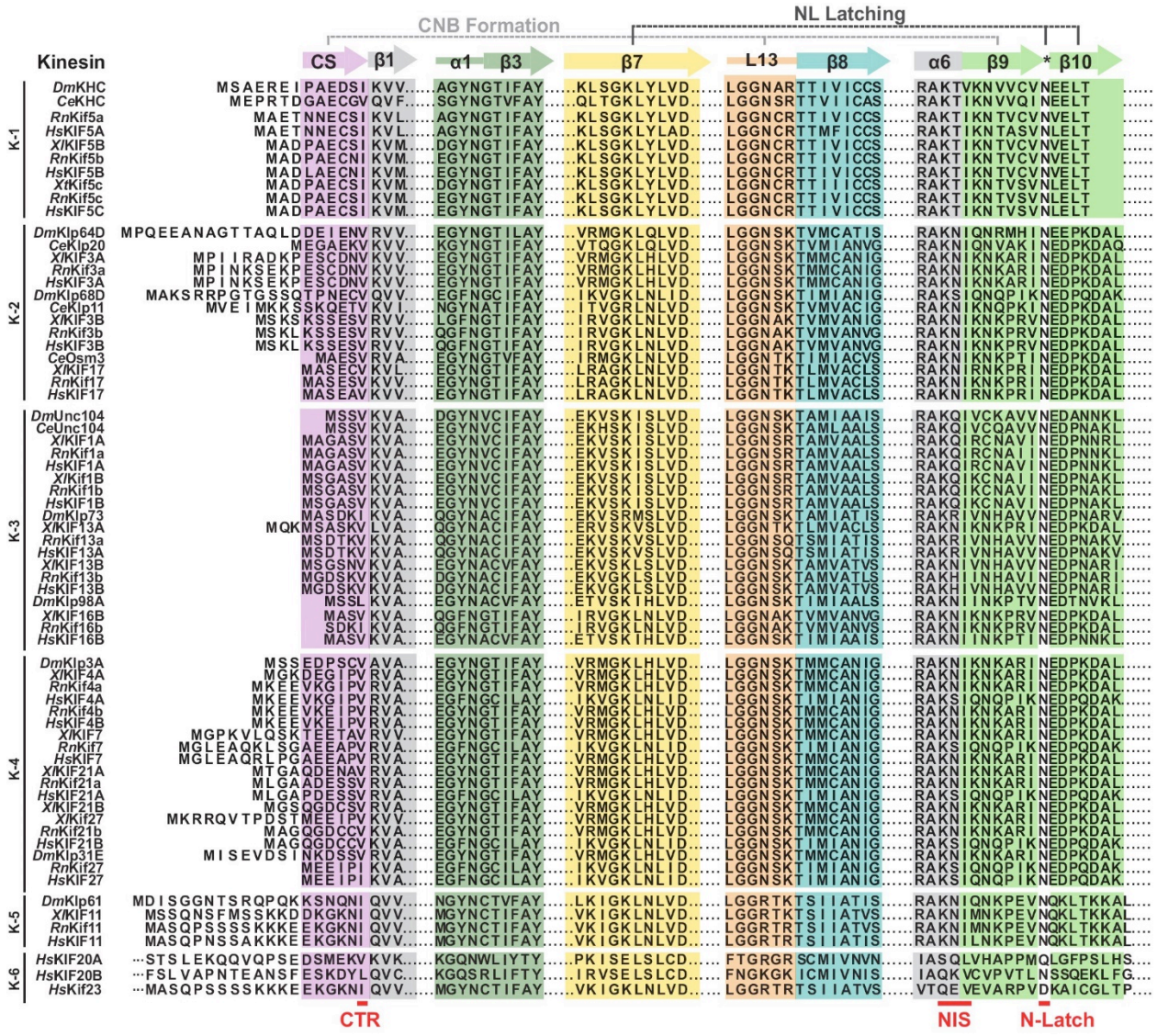

Figure 2.3 Sequence alignment of the motor domain reveals subtle sequence changes that may alter CNB formation and NL docking across the kinesin superfamily.

Sequence alignment of the motor domain from kinesin-1, –2, −3, –4, −5, and –6 families across species (*Dm*, *Drosophila melanogaster; Ce*, *Caenorhabditis elegans*, *Xl*, *Xenopus laevis; Rn*, *Rattus norvegicus; Hs*, *Homo sapiens*). For simplicity, only secondary structure elements critical for CNB and N-Latch formation in kinesin-1 are indicated: coverstrand (CS, purple), α1 (dark green), β7 (yellow), Loop13 (L13, orange), β8 (teal), neck linker (NL: β9 and β10, light green). The coverstrand terminal residue (CTR), NL initiation sequence (NIS), and asparagine-latch (N-Latch) are indicated at the bottom in red text.

and β10 is a conserved feature of many kinesin motors with an N-terminal motor domain (Figure 2.1C asterisk, Figure 2.3).

2.3.2 CNB and N-latch mutations severely cripple single kinesin-1 motor stepping under load

To delineate the importance of CNB formation and N-latch formation for force generation and transport by kinesin-1 motors, we generated mutations that would weaken the CNB, N-latch, or both. To test the role of CNB formation, CS residues A5 and S8 were mutated to glycine residues (Figure 2.1D, CNB mutant), which have a low propensity to form a β-sheet (Minor and Kim, 1993). The A5G/S8G double mutation was previously reported to impair force generation for single *Drosophila melanogaster* kinesin-1 motors in optical trap experiments (Khalil et al., 2008). Whether the analogous mutations alter the force generation and/or motility of mammalian kinesin-1 motors has not been tested. To test the role of the N-latch, residue N334 was mutated to an alanine residue (Figure 2.1D, Latch mutant). CNB mutations were also combined with the Latch mutation to assess the importance of CNB formation followed by NL docking in tandem (Figure 2.1D, CNB+Latch mutant).

To verify the effects of the mutations, we carried out MD simulations of the Latch and CNB+Latch mutant motors in the tubulin- and ATP-bound state (post-power stroke) [PDB 4HNA (Gigant et al., 2013)]. For the Latch mutant, the simulations predict that the N-latch and β10 residues make fewer interactions with α1 and β7 (Figure 2.5B–D). For the CNB+Latch mutant, the simulations predict that mutation of the CS (A5G,S8G) results in intra-CS interactions (Figure 2.4D,E) rather than interactions with β9 of the NL (Figure 2.4A,B) and that mutation of the N-latch residue (N334A) results in interactions of β10 with the CS and β8 (Figure 2.4D,F) rather than with α1 and β7 (Figure 2.4A,C). Thus, mutations of CS and N-latch residues weaken CNB formation and NL latching, respectively.

We used a custom-built optical trap apparatus with nanometer-level spatial resolution to assess the effect of the CNB and Latch mutations on kinesin-1's force output. COS-7 cell lysates containing FLAG-tagged, constitutively-active versions of WT [*Rn*KIF5C(1-560)] or mutant kinesin-1 motors were subjected to standard single-

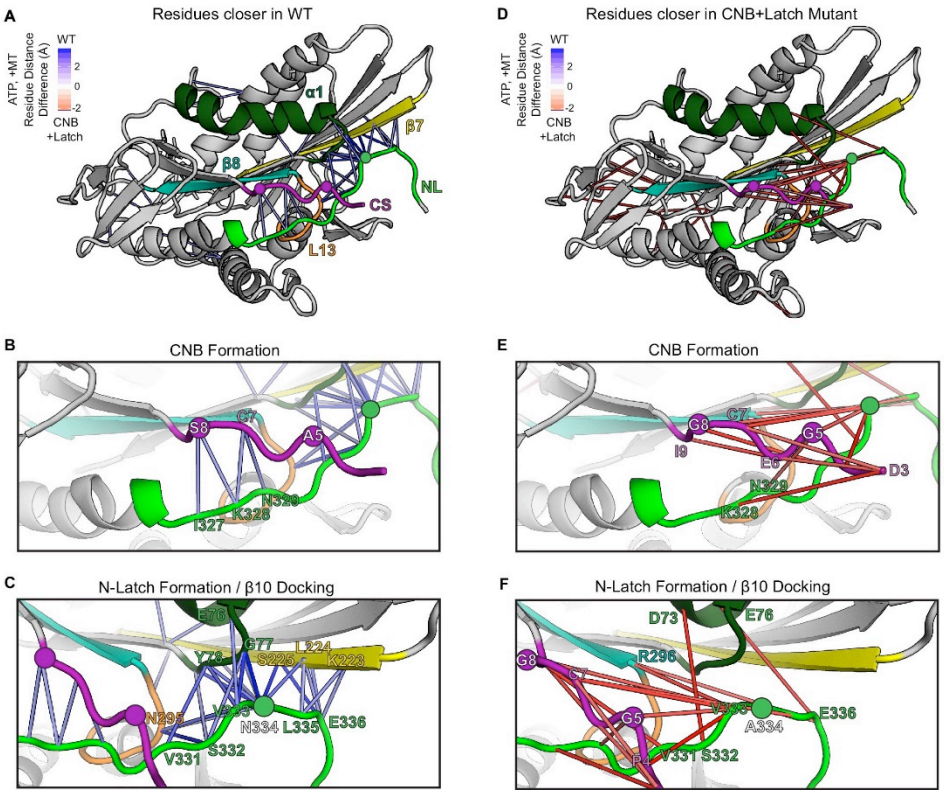

Figure 2.4 MD simulations predict that CNB+Latch mutations alter CNB formation and NL docking.

(**A–F**) The kinesin-1 motor domain in the ATP-bound, post-power stroke state is shown as a cartoon representation (PDB 4HNA). Secondary structure elements are colored: coverstrand (CS, purple), α1 (dark green), β7 (yellow), Loop13 (L13, orange), β8 (teal), neck liker (NL: β9 and β10, light green). Residues targeted for mutations are indicated as circles. (**A, D**) (**A**) Blue lines depict residue-residue distances that are significantly ($p<0.05$) closer in the WT motor as compared to the CNB+Latch mutant across replicate MD simulations. The magnitude of the distance change is indicated by color intensity. (**D**) Red lines depict residue-residue distances that are significantly ($p<0.05$) closer in the CNB+Latch mutant as compared to the WT motor across replicate MD simulations. The magnitude of the distance change is indicated by color intensity. (**B, E**) Enlarged view of CNB interactions. (**B**) Contacts between the CS (residues S8, C7) and the NL (β9 residues I327, K328, N329) are shorter in the WT motor, suggesting that CNB formation is disrupted in the CNB+Latch mutant. (**E**) The mutated CS makes intra-CS contacts rather than interactions with the NL. (**C, F**) Enlarged view of NL-β7 interactions. (**C**) The WT motor shows shorter contacts for (i) the N-latch (N334) with β7 (L224, S225) and α1 (G77, Y78) residues, (ii) the N-terminal half of the NL (β9 residues V331, S332, V333) with the core motor domain (L13 residue N295 and α1 residues E76, G77, Y78), and (iii) the C-terminal half of the NL (β10 residue E336) with the core motor domain (β7 residues L224, S225). This suggests that NL docking is disrupted in the CNB+Latch mutant. (**F**) The mutated NL makes interactions with the CS rather than β7.

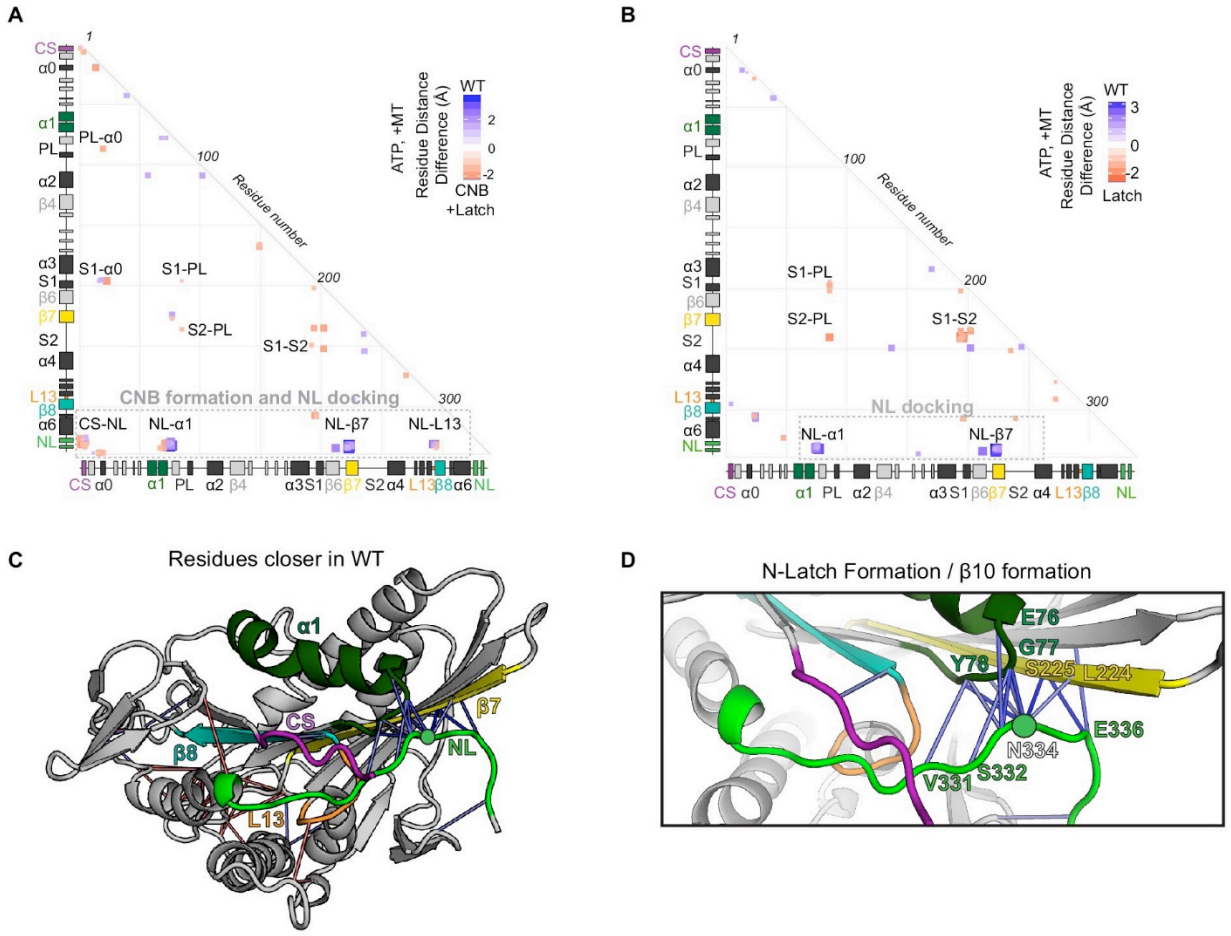

Figure 2.5 MD simulations predict that mutations of the N-Latch alter CNB formation and NL docking.

(**A, B**) Differences in residue-residue distances between (**A**) WT and CNB+Latch mutant motors or (**B**) WT and Latch mutant motors based on MD simulations of tubulin-bound motors in the ATP-bound state. The secondary structure elements are laid out along the x- and y-axes with α- helices in black, β-strands in grey, or colored according to Figure 2.4. Distances that are significantly ($p<0.05$) shorter in the apo state (red) or ATP-bound state (blue) are displayed. The magnitude of the distance change is indicated by color intensity; interactions between elements are labeled. (**C, D**) Ribbon representation of (**C**) the kinesin-1 motor domain with N-latch mutation (PDB 4HNA) associated with tubulin in the ATP-bound state and (**D**) enlarged view of NL docking interactions. Secondary structure elements responsible for NL docking are colored; coverstrand (CS, purple), α1 (dark green), β7 (yellow), Loop13 (L13, orange), β8 (teal), neck linker (NL: β9 and β10, light green). Blue lines depict residue contacts that are closer in the WT motor as compared to the Latch mutant. The magnitude of distance change is indicated by line color intensity. Contacts between the N-latch (N334) with the core motor domain (β7 residues L224, S225 and α1 residues G77, Y78) and contacts between the C-terminal half of the NL (β10 residue E336) with the core motor domain (β7 residues L224, S225) are closer in the WT, suggesting that NL docking is disrupted in the Latch mutant.

molecule trapping assays [Figure 2.6, (Reinemann et al., 2018; Reinemann et al., 2017; Svoboda & Block, 1994)]. Individual WT motors were motile in the absence of load, stalled on the microtubule when approaching the detachment force, and detached from the microtubule at an average force of 4.6 ± 0.8 pN (Figure 2.6B,C), consistent with previous studies (Khalil et al., 2008; Svoboda and Block, 1994). In contrast, the CNB mutant detached from the microtubule before stalling (Figure 2.6C) and at much lower loads than WT motors (mean detachment force 0.91 ± 0.6 pN, Figure 2.6B), overall similar to the behavior of the fly kinesin-1 with identical mutations in the CS (Khalil et al., 2008).

The Latch mutant was also sensitive to small opposing forces exerted by the trap. We found that motors with a weakened N-latch (Latch mutant) did not stall under load (Figure 2.6C) and detached from the microtubule when subjected to a mean force of 0.84 ± 0.4 pN (Figure 2.6B), similar to the CNB mutant motor. This is consistent with previous MD simulations where forced rupturing of the N-Latch led to the rapid unbinding of the entire NL from the core motor domain (Khalil et al., 2008). Thus, mutations that weaken either CNB or N-latch formation resulted in motors equally impaired in their ability to drive bead motility under load. The effects of the CNB and Latch mutations were not additive as individual CNB+Latch mutant motors displayed

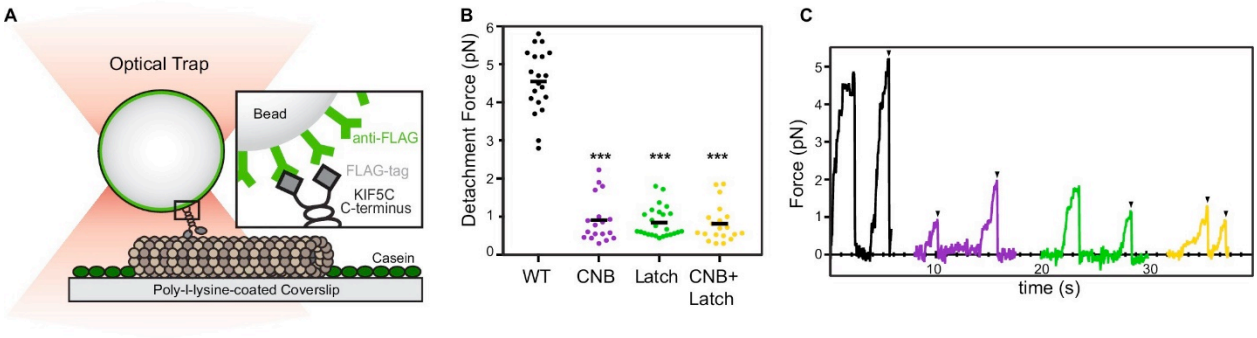

Figure 2.6 CNB and N-Latch formation are critical for force generation by single kinesin-1 motors.

(**A**) Schematic of single-molecule optical trap assay. Cell lysates containing FLAG-tagged KIF5C(1-560) motors were incubated with beads functionalized with anti-FLAG antibodies and subjected to standard optical trapping assays. (**B, C**) Force generation of WT (black), CNB (purple), Latch (green), and CNB+Latch (yellow) motors under single-molecule conditions. (**B**) Detachment forces are plotted as a dot plot where each dot indicates the maximum detachment force of an event and the mean for each construct is indicated by a black horizontal line. Maximum detachment forces include motility events where single motors reached a plateau stall before detachment and events where the motor abruptly detached from the microtubule. N ≥ 20 events for each construct; ***, $p<0.001$, compared to the WT motor. (**C**) Representative traces. Black arrowheads indicate abrupt detachment events.

behaviors similar to the CNB and Latch motors: a tendency to detach rather than stall when subjected to load (Figure 2.6C) and detachment from the microtubule at low loads (mean detachment force 0.81 ± 0.5 pN, Figure 2.6B). These results indicate that both CNB formation and N-latch formation are critical for single kinesin-1 motors to generate a strong power stroke and transport continuously under load.

2.3.3 CNB and latch mutants display enhanced unloaded motility properties

We used single-molecule motility assays to examine the behavior of the CNB and Latch mutants under unloaded conditions. Cell lysates containing kinesin-1 KIF5C(1-560) motors tagged with three tandem monomeric citrine fluorescent proteins (3xmCit) were added to flow chambers containing polymerized microtubules and their single-molecule motility was examined using total internal reflection fluorescence (TIRF) microscopy. The velocity, run length, and microtubule landing rate were determined from kymograph analysis with time displayed horizontally and distance vertically (Figure 2.7A). At least 250 motility events were quantified for each motor across three independent trials and summarized as a histogram or dot plot (Figure 2.7B–D).

Although weakening of the CNB, N-Latch, or both severely diminished the ability of the mutant motors to bear load in the optical trap assay (Figure 2.6), remarkably, all mutant motors were faster and more processive than the WT motor under unloaded conditions. CNB, Latch, and CNB+Latch motors displayed faster velocities of 0.771 ± 0.004 μm/s, 0.761 ± 0.005 μm/s, and 0.788 ± 0.005 μm/s, respectively, compared to 0.617 ± 0.005 μm/s for WT motors (Figure 2.7B). The mutant motors also displayed longer run lengths of 2.07 ± 0.057 μm, 4.27 ± 0.073 μm, and 5.332 ± 0.096 μm, respectively, as compared to 0.990 ± 0.039 μm for WT motors (Figure 2.7C).

Examination of the kymographs indicated an increase in the number of motility events for the mutant motors. We therefore quantified how often motors landed on a microtubule to start a processive run (landing rate) and measured landing rates of 0.525 ± 0.01, 1.463 ± 0.03, and 2.442 ± 0.6 events/μm•nM•s, respectively, compared with WT motor rate of 0.172 ± 0.006 events/μm•nM•s (Figure 2.7D). Examination of the kymographs also indicated that the Latch and CNB+Latch mutant motors displayed small gaps between runs (Figure 2.7E). One possibility is that the gaps indicate the reattachment of motors such that multiple runs are joined into superprocessive runs. An

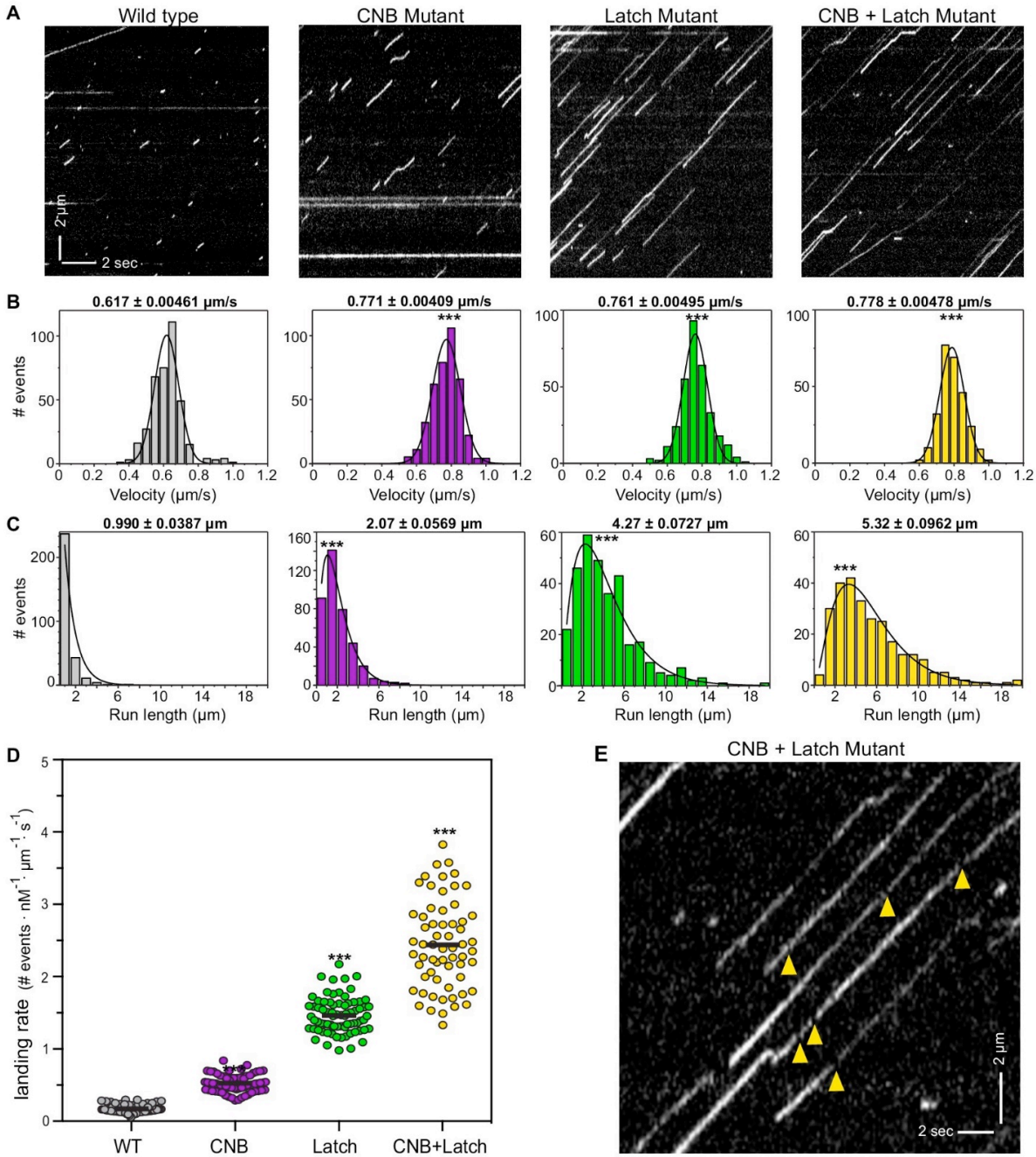

Figure 2.7 CNB and Latch mutants display enhanced motility properties under single-molecule, unloaded conditions.

(**A**) Motility properties of WT or mutant motors tagged with three tandem monomeric Citrines (3xmCit) at their C-termini were analyzed in standard single-molecule motility assays using TIRF microscopy. Representative kymographs are shown with time displayed on the x-axis (bar, 2 s) and distance displayed on the y-axis (bar, 2 µm). (**B–D**) Quantification of motility properties. From the kymographs, single-motor (**B**) velocities, (**C**) run lengths, and (**D**) landing rates were determined and the data for each population is plotted as a histogram. (**B, C**) The mean ± SEM are indicated above each graph; N ≥ 250 events across three independent experiments for each construct; ***, p<0.001 as compared to the WT motor. (**D**) Each dot indicates the landing rate along a single microtubule with the mean indicated by horizontal black line; (**E**) Magnified view of the representative kymograph of the CNB+Latch mutant shown in (A) (y-axis bar, 2 µm; x-axis bar, 2 s); yellow arrowheads indicate gaps in the runs.

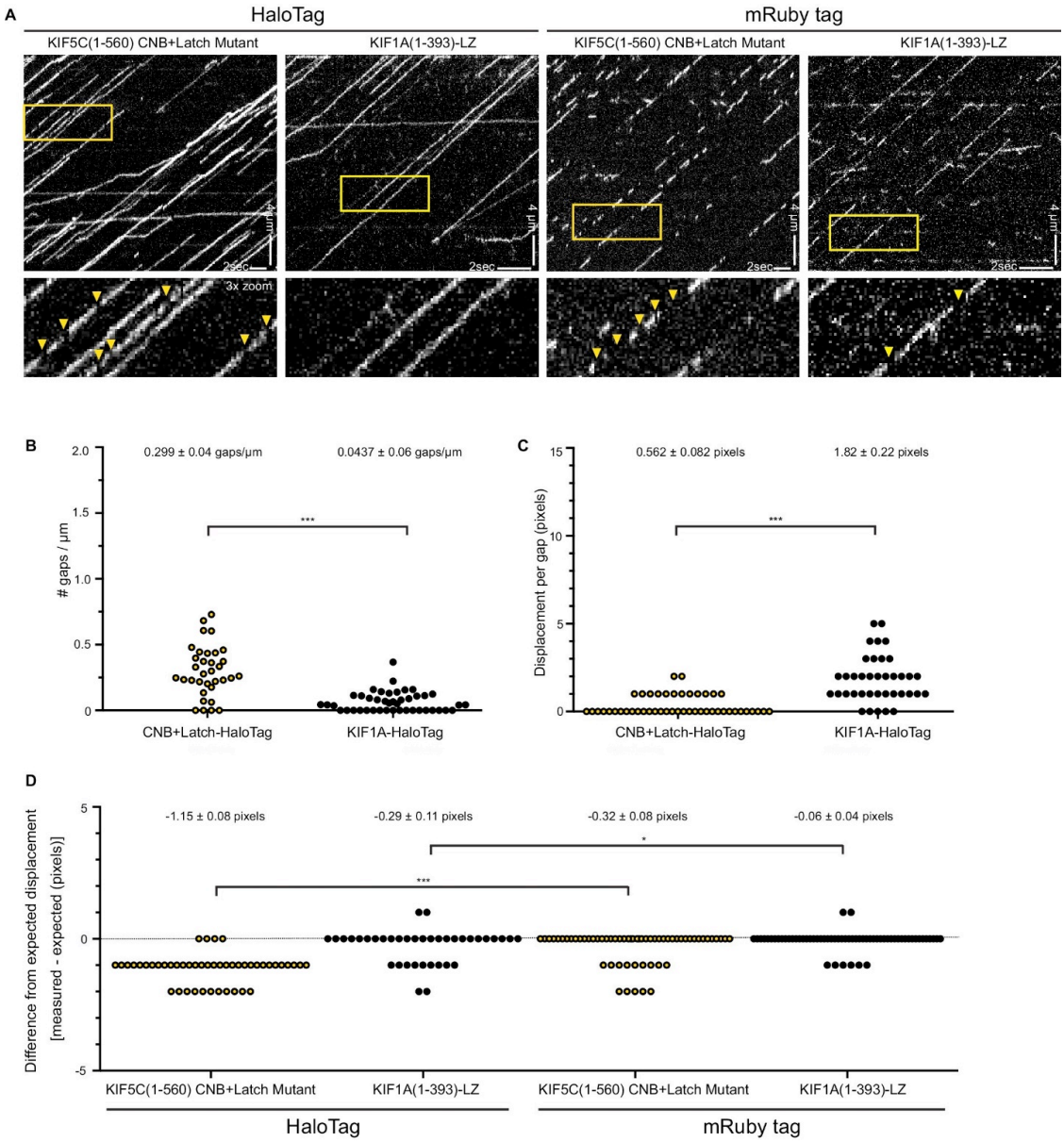

Figure 2.8 CNB+Latch mutants exhibit fast reattachment events during processive runs.

(**A**) Motility properties of kinesin-1 KIF5C(1-560) CNB+Latch mutant or the highly processive kinesin-3 motor KIF1A(1-393)-LZ. The motors were tagged with either a HaloTag and labeled with an JF649 fluorescent dye or with monomeric Ruby3 fluorescent protein. Motors were analyzed in cell lysates in standard single-molecule motility assays using TIRF microscopy. Representative kymographs are shown with time displayed on the x-axis (bar, 2 s) and distance displayed on the y-axis (bar, 4 µm). Red boxes indicate magnified region displayed in bottom panels; arrow heads indicate gaps in runs. (**B–D**) Characterization of gaps. (**B**) The number of gaps per µm of microtubule for motors labeled with HaloTag-JF649. The data for each population is plotted as a dot plot; the mean ± SEM are indicated at the top of the graph; ***, p<0.001. (**C**) The displacement during the gap for motors labeled with HaloTag-JF649. The data for each population is plotted as a dot plot; the mean ± SEM are indicated at the top of the graph; ***, p<0.001. (**D**) The difference in measured versus expected displacement during the gap for motors labeled with HaloTag-JF649 or mRuby3. The displacement during the gaps was measured from the kymographs. The expected displacement of the motor during the time frame of the same gap was calculated using the measured velocity of the motor. The difference between measured and expected displacement for each population is plotted as a dot plot; the mean ± SEM are indicated at the top of the graph; ***, p<0.001 for HaloTagged compared to mRuby-tagged versions for each motor. If the gaps in the runs are due to fluorophore blinking, the measured displacement during the gap will be the same as the expected displacement (difference = 0, dotted black line). If the gaps in the runs are due to fast reattachment of the motor to the microtubule track, the measured distance during the gap will be shorter than the expected displacement (difference <0).

alternative possibility is that the mutant motors are superprocessive with the gaps in the runs due to blinking of the fluorescent tag. To distinguish between these possibilities, we compared the single-molecule motility behavior of the CNB+Latch mutant when tagged with a fluorescent marker that does (mRuby) or does not (HaloTag with JF549 dye) exhibit blinking behavior (Figure 2.8A). As a control, we carried out the same analysis for a known superprocessive motor, the kinesin-3 motor KIF1A (Soppina et al., 2014) (Figure 2.8A). For the CNB +Latch mutant motors, the distance moved during a gap was ~1 pixel less than the distance expected for a motor undergoing constant motility (Figure 2.8D), where KIF1A motors, the distance moved during a gap was nearly identical to the distance expected for a motor undergoing constant velocity (Figure 2.8D). These data are consistent with the idea that the gaps in the kymographs are due to CNB+Latch mutant motors undergoing detachment and reattachment events rather than constant motility. However, we cannot rule out the possibility that the gaps in the kymographs are due to blinking of the fluorescent markers used to track CNB+Latch motors given that i) the distances moved during the gaps are at the limit of resolution of our microscope system and ii) the fluorescent markers may behave differently when attached to the CNB+Latch mutant motor versus the KIF1A motor. Regardless of whether the gaps in the kymographs are due to reattachment events that string together multiple runs or due to blinking behavior during superprocessive runs, the single molecule motility data highlight the differences in motor behavior under unloaded and loaded conditions. For kinesin-1 motors, mutations that result in weakened CNB and/or N-latch formation lead to a decreased detachment from the microtubule track (increased run length) under unloaded single-molecule conditions (Figure 2.7) but a more rapid detachment from the microtubule when subjected to a load (Figure 2.6).

2.3.4 MD simulations predict that modulating CNB and N-latch formation enhances microtubule binding and catalytic site closure

We hypothesized that the enhanced motility properties of the mutant motors under unloaded conditions are due to allosteric effects of mutations designed to hinder NL docking on the nucleotide and microtubule binding regions of the motor domain. We thus re-examined the MD simulations of the Latch and CNB+Latch mutant motors

associated with tubulin in the ATP-bound state [PDB 4HNA (Gigant et al., 2013)] with a focus on residue interactions outside of the CNB and NL docking regions.

The MD simulations revealed enhanced interactions between elements important for coordinating and hydrolyzing nucleotide in the CNB+Latch mutant as compared to the WT motor (Figure 2.9 A, B). Specifically, the residue-residue distances are shorter between the P-loop and α0 (Figure 2.9B, red box PL-α0; 2.10D–F). As the P-loop coordinates ATP in the nucleotide pocket and α0 gates ATP binding (Hwang et al., 2017), this result suggests that modulating NL docking influences the ability to capture and/or hold ATP in the nucleotide-binding pocket. Shorter residue-residue distances are also observed between Switch 1 and α0 (Figure 2.9, red box S1-α0; Figure2.10D–F) and between switch 1 and Switch 2 (Figure 2.9, red box S1-S2; Figure2.10D–F). Enhanced interactions between residues involved in coordinating and hydrolyzing nucleotide are also observed in the Latch mutant (Figure 2.10G–I). As closure of the switch regions is necessary for ATP hydrolysis (Cao et al., 2014; Clancy et al., 2011; Parke et al., 2010; Turner et al., 2001), these results indicate that the Latch and CNB+Latch mutations result in enhanced catalytic site closure and ATP hydrolysis that could account for the increase in velocity of the mutant motors under single-molecule, unloaded conditions.

To gain an understanding of how mutations that hinder CNB formation and/or NL docking can result in enhanced microtubule binding (landing rate) and processivity of the mutant motors, we used principle component analysis (PCA) to create a map of the conformational differences of the microtubule-binding surface of the kinesin-1 motor domain in the microtubule-free (and ADP-bound) state as compared to the microtubule-bound (and ATP-bound) state. The structures of seventeen motor domains from five different kinesins were subjected to interconformer analysis with PCA. The CS and NL regions were excluded from the analysis due to their absence from most ADP-bound structures. PCA analysis revealed that the first two dimensions account for over 80% of the variance in atomic positional displacements of the microtubule-binding surface between these states (PC1 79.66%, PC2 4.95%, Figure 2.9C). Thus, PC1 and PC2

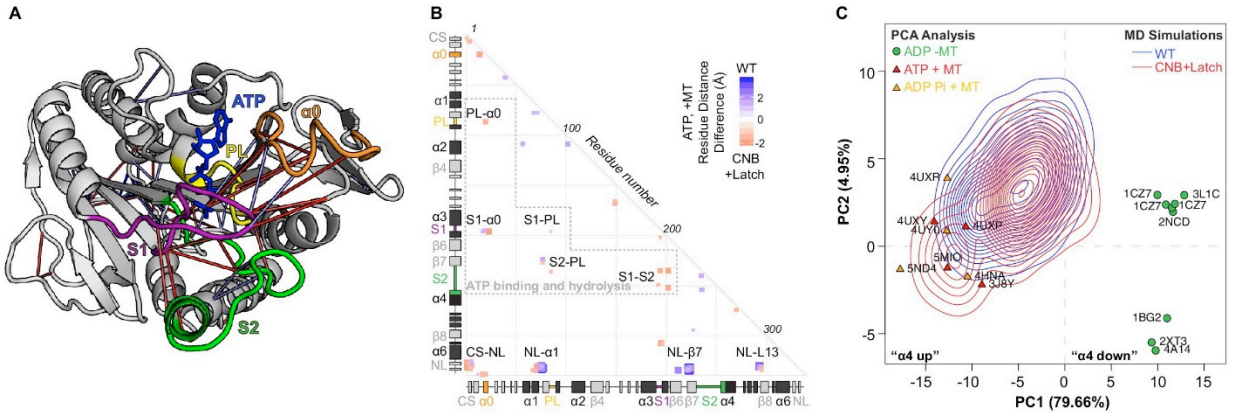

Figure 2.9 CNB+Latch mutations enhance microtubule binding and catalytic site closure.

(**A**) Ribbon representation of the kinesin-1 motor domain in the ATP-bound, post-power stroke state (PDB 4HNA). Secondary structure elements critical for nucleotide binding and hydrolysis are colored as follows: Switch 1 (S1, purple), Switch 2 (S2, green), P-loop (yellow), and α0 (orange). Red lines depict residue-residue distances that are shorter in the CNB+Latch mutant motor versus WT motor ($p<0.05$); blue lines depict residue-residue distances that are shorter in the WT motor versus CNB+Latch mutant motor ($p<0.05$). The magnitude of the distance change is indicated by line color intensity. Note that the point of view is rotated with respect to previous figures. (**B**) Differences in residue-residue distances between WT kinesin-1 and CNB+Latch mutant motors in the ATP-bound, tubulin-bound state in MD simulations. The secondary structure elements are laid out along the x- and y-axes with α- helices in black, β-strands in grey, or colored according to (A). Distances that are significantly shorter ($p<0.05$) in CNB+Latch (red) or WT (blue) motor are displayed. The magnitude of the distance changes is indicated by color intensity; interactions between structural elements are labeled. (**C**) Principle component analysis (PCA) was used to define states of the microtubule-binding surface of kinesin-1. The x-ray structures of seventeen motor domains from five different kinesin families in the ADP-bound or ATP-bound states were utilized. The position of each motor domain structure within the PCA map is indicated together with its nucleotide state (red, ATP; yellow, ADP-Pi; green, ADP), microtubule state (circle, no microtubule; triangle, bound to microtubule), and PDB code. The first two principle components (PC1 and PC2) represent over 80% of the structural variation across the microtubule-binding surface between the ADP-bound and ATP-bound states. PC1 represents the positioning of α4 as 'down' in the ADP-like state and 'up' in the ATP-like state. The ability of WT versus CNB+Latch mutant motors to sample these states was then analyzed by MD simulations starting from the 2KIN structure in the ADP-bound and microtubule-free state. The conformational space explored by each motor is projected as a topographic map (WT, blue; CNB+Latch, red) onto the PCA analysis plot.

provide a suitable conformational space to describe the structural dynamics of kinesin motor domains transitioning from an ADP-bound, microtubule-free state to an ATP-bound, microtubule-bound state. The major conformational difference between these states can be described by PC1 which involves a displacement of α4, where α4 is in a 'down' orientation in the ADP-like, microtubule-free structures and in an 'up' orientation in the ATP-like, microtubule-bound structures (Figure 2.9C), consistent with previous studies (Scarabelli & Grant, 2013).

We then used the PCA conformational space to compare how often the WT and CNB+Latch motor domains could adopt the ATP-bound, microtubule-bound state from between the ADP-bound, microtubule-free and the ATP-bound, microtubule-bound

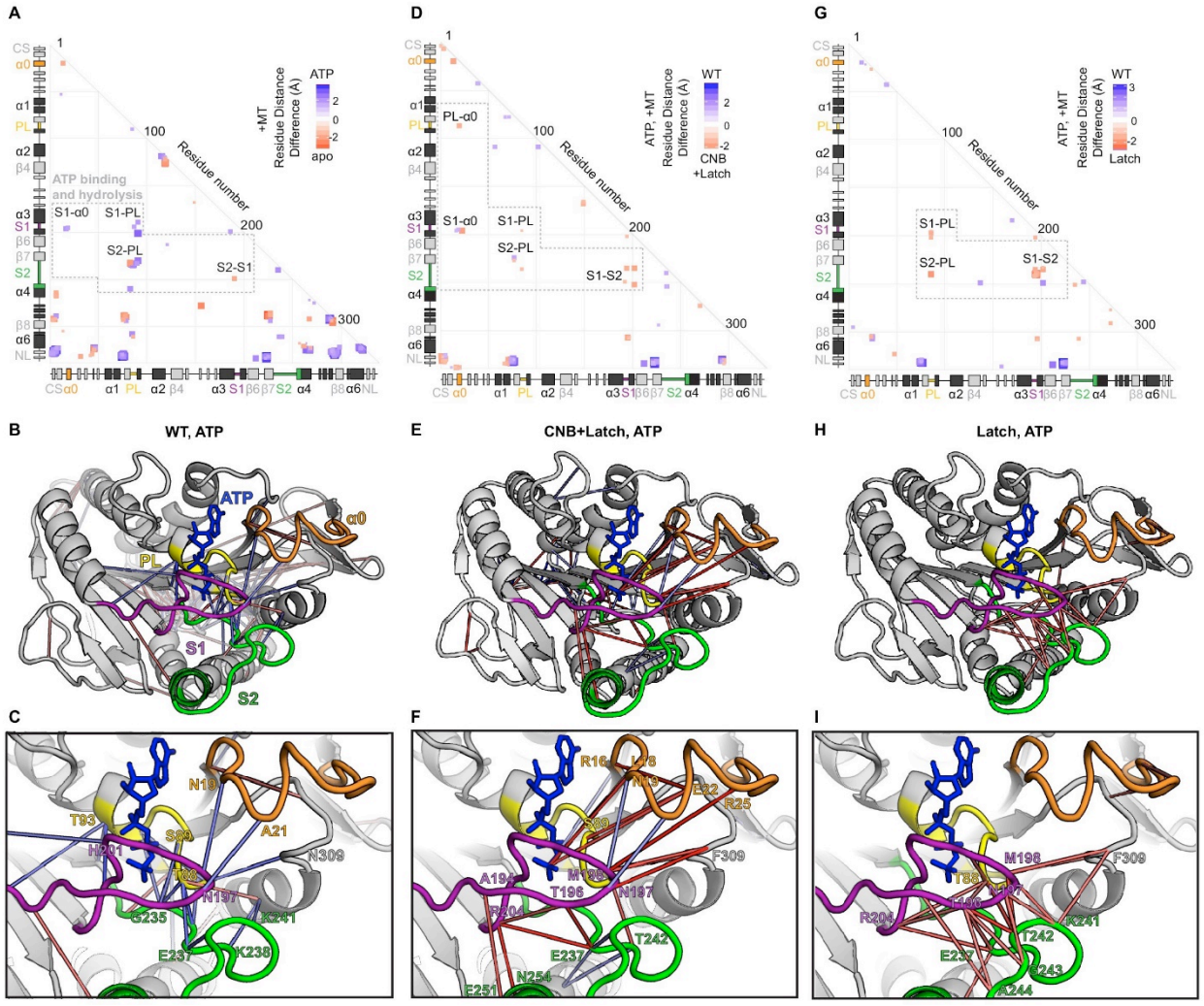

Figure 2.10 Interactions between nucleotide coordinating elements (P-Loop, Switch 1, Switch 2, and α0) in WT, CNB+Latch, and Latch mutant motors.

Differences in residue-residue distances based on MD simulations between (**A–C**) the nucleotide-free (apo) and ATP-bound states of WT kinesin-1 associated with tubulin, (**D–F**) WT and CNB+Latch mutants associated with tubulin in the ATP-bound state, and (**G–I**) WT and Latch mutants associated with tubulin in the ATP-bound state. (**A,D,G**) Summary of distance differences. The secondary structure elements are laid out along the x- and y-axes with α- helices in black, β-strands in grey, or colored according to Figure 2.9. Distances that are significantly ($p<0.05$) shorter are indicated by the color of the boxes. The magnitude of the distance change is indicated by intensity; interactions between elements are labeled. (**B,E,H**) Ribbon representations of the kinesin-1 motor domain (PDB 4HNA) associated with tubulin in the ATP-bound state and (**C,F,I**) enlarged views of PL, S1, S2, and α0 interactions. Secondary structure elements are indicated by color, P-loop (PL, yellow), Switch 1 (S1, purple), and Switch 2 (S2, green), α0 (orange). (**E,F**) For the CNB+Latch mutant motor, enhanced interactions between S2-PL, S1-S2, α0-PL, and α0-S1 suggest enhanced nucleotide coordination and closure of the catalytic site. (**H,I**) For the Latch mutant motor, enhanced interactions between S1-PL, S2-PL, and S1-S2 suggest enhanced catalytic site closure.

states (Figure 2.10C, blue topographic lines). Starting from the same 2KIN structure, the CNB+Latch mutant sampled an additional conformational space closer to that defined by the ATP-bound, microtubule bound kinesin structures (Figure 2.10C, red topographic lines). Overall, this suggests that the CNB +Latch mutant has a higher degree of structural flexibility in its microtubule-binding regions as compared to the WT motor domain. This structural flexibility would enable the motor to more readily adopt a conformation compatible with strong microtubule binding in response to ATP in the nucleotide pocket and could account for the enhanced microtubule-landing rate and processivity observed in single-molecule assays.

2.3.5 CNB and N-latch mutations do not affect the ability of teams of kinesin1 motors to transport low-load cargo (peroxisomes) in cells

Having defined the force generating properties of individual CNB, Latch, and CNB+Latch mutant motors, we sought to test whether the integrity of CNB formation followed by NL latching is a critical determinant for kinesin motors working in teams to drive cargo transport in cells. To do this, we used an inducible recruitment strategy (Kapitein et al., 2010) to link teams of motors to the surface of membrane-bound organelles and monitored transport to the cell periphery after 30 min (Figure 2.11A). Previous studies utilized single-particle tracking of peroxisomes in COS-7 cells and found that they exhibit sub-diffusive motion in the perinuclear region and that 2–15 pN of force, depending on peroxisome size, is required to move a peroxisome away from this region (Efremov et al., 2014). Therefore, the peroxisome can be considered a low-load cargo [Figure 6B, (Schimert et al., 2019)] requiring teams of kinesin-1 motors to collectively transport against loads < 3 times greater than the force required to stall a single motor.

COS-7 cells were cotransfected with a plasmid for expression of *Rn*KIF5C(1-560) motors tagged with monomeric NeonGreen (mNG) and FRB domain and a plasmid for expression of a peroxisome targeted PEX-mRFP-FKBP fusion protein. In the absence of rapamycin, the PEX-RFP-FKBP fusion proteins localized to the peroxisome surface and the WT KIF5C-mNG-FRB proteins were diffusely localized throughout the cell (Figure 2.12A). Addition of rapamycin resulted in recruitment of motors to the peroxisome surface via dimerization of the FRB and FKBP domains and motor activity

drove dispersion of the peroxisomes to the cell periphery (Figure 2.12A). Cargo dispersion before and after motor recruitment was quantified using two different methods. First, cargo dispersion in each cell was qualitatively scored as clustered, partially dispersed, diffusely dispersed, or peripherally dispersed (Figure 2.13A) with the data for the population of cells summarized as a stacked bar plot. Second, peroxisome dispersion was quantified by generating a radial profile of cargo intensity for each cell and converting this profile into a normalized distance distribution; the distance distribution across multiple cells was then averaged across all cells for each motor construct (Figure 2.13B).

In the absence of rapamycin, peroxisomes were largely clustered in middle of cell (Figure 2.12A,E; Figure 2.11C, qualitatively 67% of cells have clustered peroxisomes; Figure 2.11D, quantitatively 95% of the peroxisome intensity adjacent to the nucleus). Thirty minutes after addition of rapamycin and recruitment of teams of WT kinesin-1 motors, peroxisomes were transported to the periphery of the cell (Figure 2.12A,E; Figure 2.11C, qualitatively 94% of cells have dispersed peroxisomes; Figure 2.11D, quantitatively 81% of the peroxisome intensity at the cell periphery). Notably, although mutant motors are crippled in their ability to transport against load as single motors in an optical trap (Figure 2.6), as teams these motors are able to cooperate to transport peroxisomes to the cell periphery to a similar extent as teams of WT motors. Specifically, thirty minutes after addition of rapamycin and motor recruitment, teams of CNB, Latch, or CNB+Latch mutant motors were able to disperse peroxisomes to the periphery of the cell (Figure 2.12 B–E; Figure 2.11C, qualitatively 97%, 92%, and 97% of cells have dispersed peroxisomes, respectively; Figure 2.11D–F, quantitatively 84%, 81%, and 79% of the peroxisome intensity at the cell periphery, respectively). Statistical analysis indicates that peroxisome dispersion by the mutant motors was not significantly different than that of the WT motor (Figure 2.11D–F). These results suggest that impaired force generation by weakening CNB and/or N-latch formation can be overcome by teams of motors for efficient transport of a low-load, membrane-bound cargo in cells.

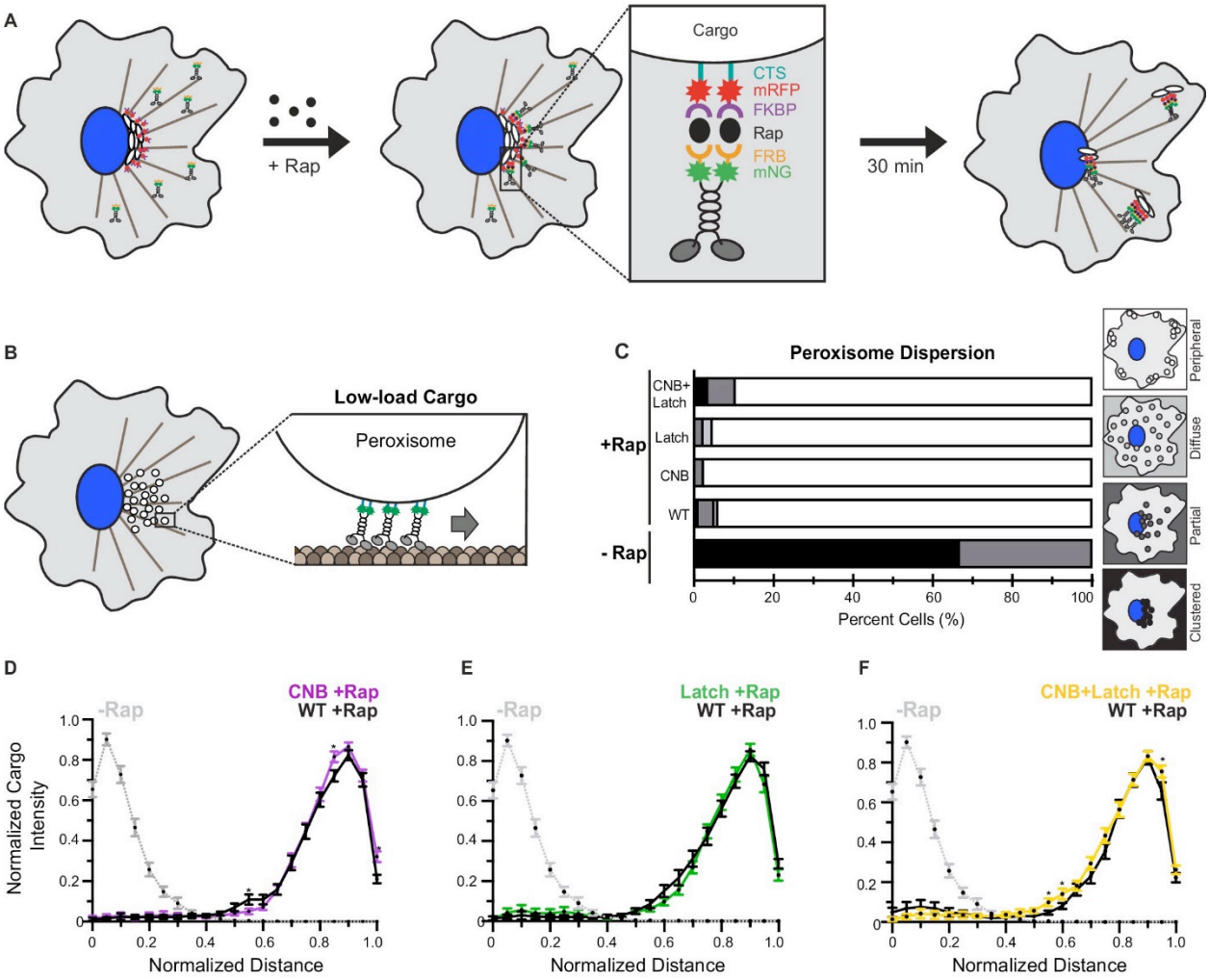

Figure 2.11 CNB and Latch mutations do not affect transport of peroxisomes (low-load cargo) by teams of kinesin-1 motors in cells.

(**A**) Schematic of the inducible motor recruitment assay. A kinesin motor tagged with monomeric NeonGreen (mNG) and an FRB domain (KIF5C-mNG-FRB) is coexpressed with a cargo targeting sequence (CTS) tagged with monomeric red fluorescent protein (mRFP) and FKBP domain (CTS-mRFP-FKBP) in COS-7 cells. Addition of rapamycin (+Rap) causes heterodimerization of the FRB and FKBP domains and recruitment of motors to the cargo membrane. Recruitment of active motors drives cargo dispersion to the cell periphery. (**B**) Schematic of the inducible peroxisome dispersion assay. Peroxisomes are loosely clustered in the perinuclear region of COS-7 cells and are largely immotile, thus providing a low-load cargo for transport by teams of recruited motors. (**C**) Qualitative analysis of peroxisome dispersion. Peroxisome localization in individual cells was scored as clustered (black), partially dispersed (dark grey), diffusely dispersed (light grey), or peripherally dispersed (white) 30 min after recruitment of teams of WT, CNB, Latch, or CNB+Latch motors. The data for each construct is summarized as a stacked bar plot. For each construct, N ≥ 50 cells were analyzed across three separate experiments. (**D–F**) Quantitative analysis of peroxisome dispersion. A radial profile of peroxisome intensity was generated for each cell and the data for each condition was converted to an averaged and normalized distance distribution across all cells. Each data point indicates the mean normalized cargo intensity ± SEM for N ≥ 50 cells across three separate trials. Gray dotted line: WT -Rap; Black line: WT +Rap; Purple line: CNB +Rap; Green line: Latch +Rap; Yellow line: CNB+Latch +Rap. Statistically significant differences in peroxisome localization comparing the mean normalized cargo intensity of the mutant motors to the wild type at any binned distance was determined; *, $p<0.05$.

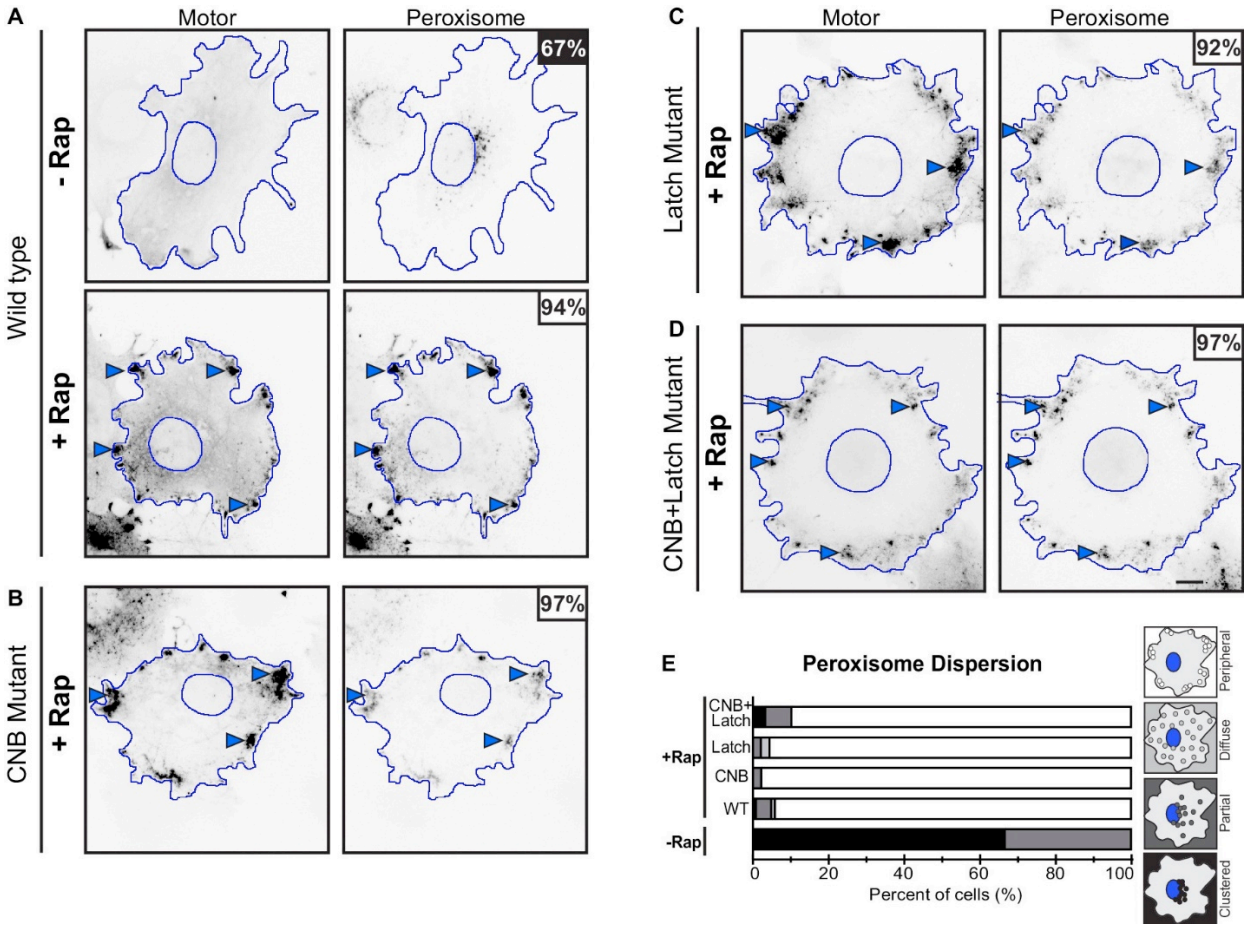

Figure 2.12 Peroxisome dispersion (low-load cargo) by teams of WT or CNB and/or NL docking mutant motors.

(**A–D**) Representative images of peroxisome dispersion before (-Rap) and after (+Rap) motor recruitment to the peroxisome surface. Blue lines indicate the nucleus and periphery of each cell. Blue arrowheads indicate redistribution of peroxisomes after addition of rapamycin (+Rap), bar 10 μm. Percentages in the upper corner indicate the percent of cells with the indicated dispersion phenotype: black: clustered peroxisomes; dark gray: partially dispersed peroxisomes; light gray: diffusely dispersed peroxisomes; white: peripherally dispersed peroxisomes. (**E**) Qualitative analysis of peroxisome dispersion. Cells were scored as clustered (black), partially dispersed (dark grey), diffusely dispersed (light grey), or peripherally dispersed (white) for N ≥ 50 cells for each construct across at least three trials. The data for each construct are summarized as a stacked bar plot.

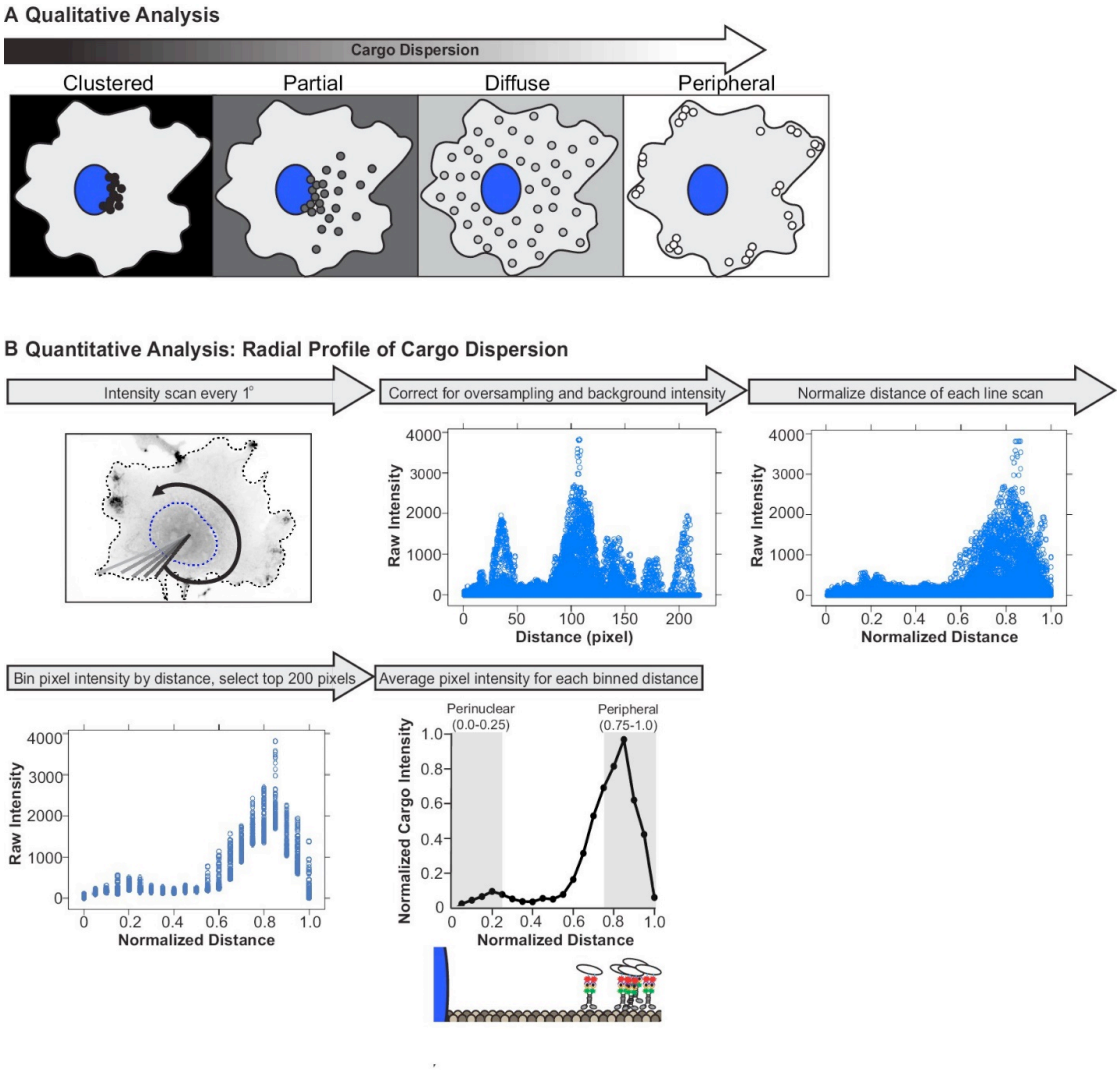

Figure 2.13 Analysis of cargo dispersion in cells.

(**A**) Qualitative analysis of cargo dispersion. Cargo localization was scored as: black: clustered (cargo is tightly clustered near the nucleus of the cell); dark gray: partially dispersed (cargo is loosely clustered, majority of the cargo remains near nucleus, but some cargo has been redistributed closer to the cell periphery); light gray: diffusely dispersed (cargo is dispersed diffusely throughout the cell with minimal cargo remaining in the perinuclear region); or white: peripherally dispersed (cargo is no longer clustered in the perinuclear region of the cell but instead accumulated at the cell periphery). (**B**) Quantitative analysis of cargo dispersion. To quantify cargo localization in a cell, (1) a custom ImageJ plugin generates a line scan from the centroid of the nucleus to the periphery of the cell; this is repeated every one degree for a total of 360 line scans around the cell. The fluorescence intensity along each line scan is determined. (2) For background subtraction, a line scan starting from the centroid of the nucleus to the cell periphery is generated in a region of the cell that lacks cargo and is subtracted from each line scan (scaled background subtraction). Distances that correspond to regions inside the nucleus are removed from each line scan, such that point 0 corresponds to the edge of the nuclear membrane. Oversampling of pixels in the center of the cell was corrected, following the assumption that the cell is a perfect circle. (3) The total distance of each line scan was normalized to itself, such that the distance of each line scan was between 0 (nuclear membrane) and 1 (cell periphery). (4) Pixel intensities were grouped in bins by distance (width, 0.05) and only the top 200 pixels within each bin were included in further analysis. (5) Pixel intensity was averaged for each binned distance to generate a dispersion profile for the cell. Dispersion profiles of all cells were averaged and plotted as mean ± SEM for each normalized distance bin. Cargo intensity in 0.0–0.25 normalized distance bins is in the perinuclear region of the cell while cargo intensity in 0.75–1.0 normalized distance bins is at the periphery of the cell.

2.3.6 CNB and N-latch mutations impair the ability of teams of kinesin-1 motors to transport high-load cargo (Golgi elements) in cells

Although CNB formation and NL latching were not required for teams of kinesin motors to transport peroxisomes to the cell periphery, we considered the possibility that NL docking may be critical under conditions where motors must generate high forces and work against high loads. To address how motors cooperate in teams to transport high-load cargo in cells, we used the inducible recruitment strategy (Figure 2.11A) to link teams of motors to the Golgi membrane using a GMAP210 Golgi localization sequence (Engelke et al., 2016; Schimert et al., 2019) and monitored cargo transport to the cell periphery after 30 min. The Golgi is a compact organelle and its localization near the nucleus is maintained by a variety of mechanisms including microtubule minus-end directed activity of cytoplasmic dynein motors (Brownhill, Wood, & Allan, 2009). Using an optical trap, Guet et al. determined that over 150 pN of force is required to deform the Golgi network in cells (Guet et al., 2014). Therefore, the Golgi can be considered a high-load cargo [Figure 2.14, (Schimert et al., 2019)] as teams of motors driving Golgi dispersion are required to cooperate to transport against forces ~ 30 times greater than the force required to stall one kinesin-1 motor.

To validate that peroxisome and Golgi dispersion represent low- and high-load cargoes in cells, respectively, we assessed whether teams of kinesin-8 KIF18A motors, previously characterized to stall at 1 pN of force (Jannasch et al., 2013), can cooperate to transport peroxisomes and Golgi elements. Before addition of rapamycin, both peroxisomes and Golgi were clustered in middle of cell (Figure 2.15A,B). Thirty minutes after addition of rapamycin and recruitment of teams of KIF18A motors, peroxisomes were dispersed to the periphery of the cell (Figure 2.15A–C, qualitatively 91% of cells have dispersed peroxisomes, quantitatively 80% of peroxisome intensity at the cell periphery). However, thirty minutes after addition of rapamycin and recruitment of teams of KIF18A motors to Golgi membranes, a majority of Golgi elements remained localized in the perinuclear region of the cell with minimal accumulation at the cell periphery (Figure 2.15 1D–F, qualitatively 86% of cells have clustered Golgi; quantitatively 66% of Golgi intensity adjacent to the nucleus). Overall these findings suggest that teams of

KIF18A motors are able to generate sufficient force to transport peroxisomes but not Golgi elements to the cell periphery.

We thus examined the ability of teams of WT or mutant kinesin-1 motors to transport Golgi elements to the cell periphery. Before addition of rapamycin, the Golgi was clustered near the nucleus of the cell (Figure 2.16A,E; Figure 2.14B, qualitatively 85% of cells have clustered Golgi; Figure 2.14C, quantitatively 83% of Golgi intensity near the nucleus). 30 min after addition of rapamycin and recruitment of teams of WT kinesin-1 motors to the Golgi surface, Golgi elements were efficiently dispersed to the cell periphery (Figure 2.14 A,E; Figure 2.14B, qualitatively 82% of cells have dispersed Golgi; Figure 2.14C, 50% of Golgi intensity at the cell periphery). However, hindering either CNB or N-latch formation resulted in motors that were crippled in their ability to cooperate in teams to transport Golgi elements to the cell periphery. Thirty minutes after addition of rapamycin and recruitment of teams of CNB or Latch mutants, a significant fraction of Golgi elements remained clustered in the perinuclear region rather than accumulated at the cell periphery (Figure 2.16B,C,E; Figure 2.14B, qualitatively only 64% of cells have dispersed Golgi for CNB and 42% for Latch mutant; Figure 2.14C, quantitatively only 34% of Golgi intensity at the cell periphery for CNB and Figure 2.14D, only 35% for Latch mutant). In this cellular assay, the effects of the CNB and N-latch mutations were additive as teams of CNB +Latch mutants were even more crippled in their capacity to cooperate and transport Golgi elements than the CNB and Latch mutant motors. Upon recruitment of CNB+Latch mutant motors, the majority of the Golgi elements remained clustered in the perinuclear region of the cell (Figure 2.16,E; Figure 2.14B, qualitatively only 13% of cells have dispersed Golgi; Figure 2.14E, quantitatively only 22% of Golgi intensity at the cell periphery). Statistical analysis indicates that there is significant impairment of Golgi dispersion to the cell periphery after recruitment of mutant motors compared to WT motors (Figure 2.14C–E).

To verify that the inability of the CNB, Latch, and CNB+Latch mutant motors to drive Golgi dispersion was due to the increased load imposed by this cargo, we repeated the assay in cells where the contribution of cytoplasmic dynein to Golgi clustering was reduced. To do this, we overexpressed a truncated dynein intermediate

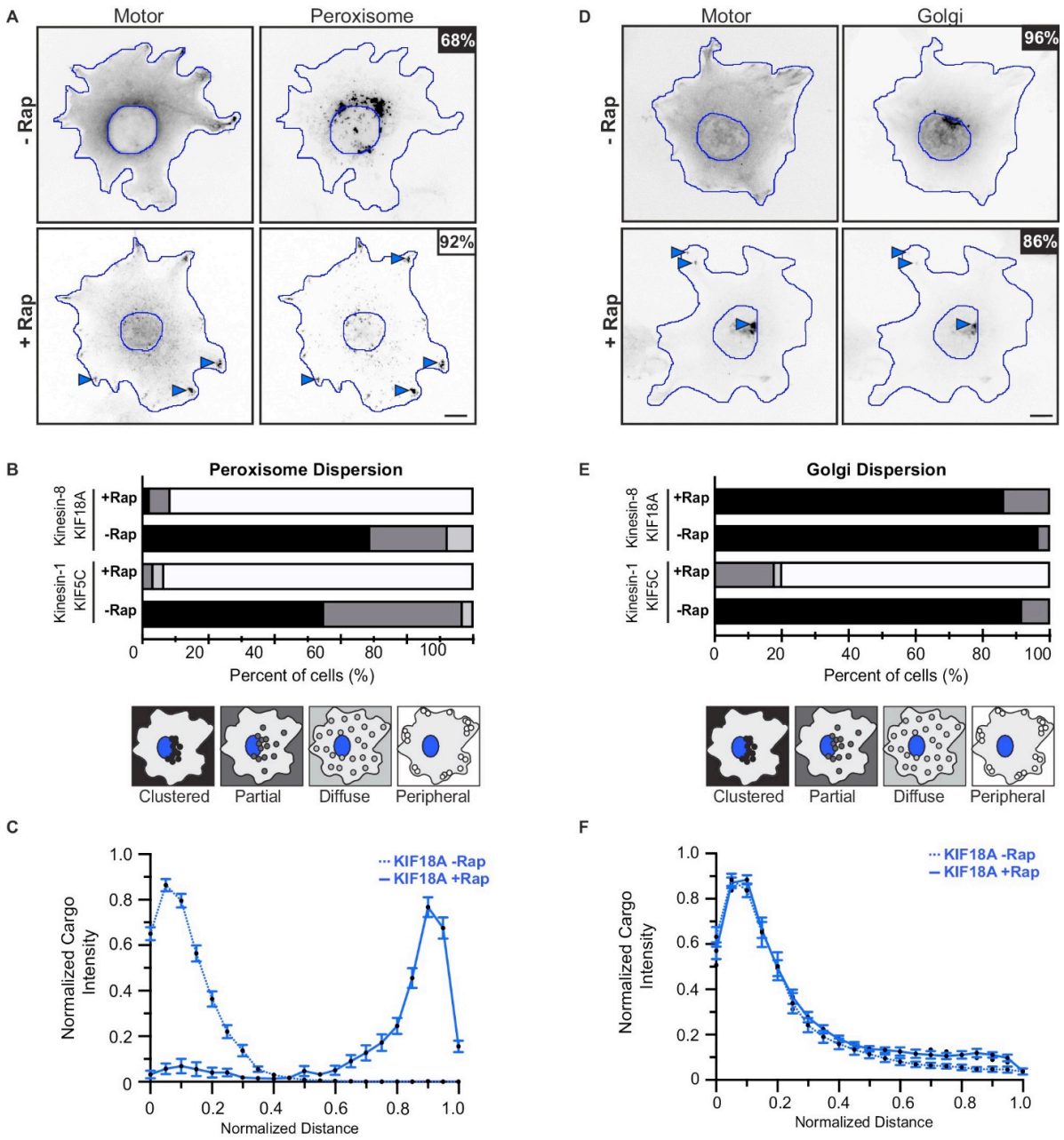

2.15 Validation of peroxisome and Golgi as low- and high-load cargoes, respectively.

(**A,D**) Representative images of (**A**) peroxisome dispersion or (**D**) Golgi dispersion before (-Rap) and after (+Rap) recruitment of teams of KIF18A motors. (**A**) COS-7 cells were cotransfected with plasmids encoding for the expression of KIF18A-mNG-FRB and peroxisome targeting PEX3-mFRP-FKBP fusion proteins. (**D**) COS-7 cells were cotransfected with plasmids encoding for the expression of KIF18A-mNG-FRB and the Golgi-targeting GMAP201p-mRFP-FKBP fusion proteins. Blue lines indicate the nucleus and periphery of each cell. Blue arrowheads indicate peroxisomes dispersed after addition of rapamycin (+Rap), bar 10 µm. Percentages in the upper corner indicate the percent of cells with the indicated dispersion phenotype: Black: clustered; Dark gray: partially dispersed; Light gray: diffusely dispersed; White: peripherally dispersed. (**B,E**) Qualitative analysis of (**B**) peroxisome or (**E**) Golgi dispersion. Cells were scored as clustered (black), partially dispersed (dark grey), diffusely dispersed (light grey), or peripherally dispersed (white) for N ≥ 40 cells for each construct across two experimental trials and results are summarized as a stacked bar plot. (**C,F**) Quantitative analysis of (**C**) peroxisome or (**F**) Golgi dispersion. A radial profile of peroxisome or Golgi intensity was generated for each cell and the data for each condition was converted to an averaged and normalized distance distribution across all cells. Each data point indicates the mean normalized cargo intensity ± SEM for N ≥ 40 cells across three separate trials. KIF18A, -Rap (dotted blue); KIF18A, +Rap (solid blue).

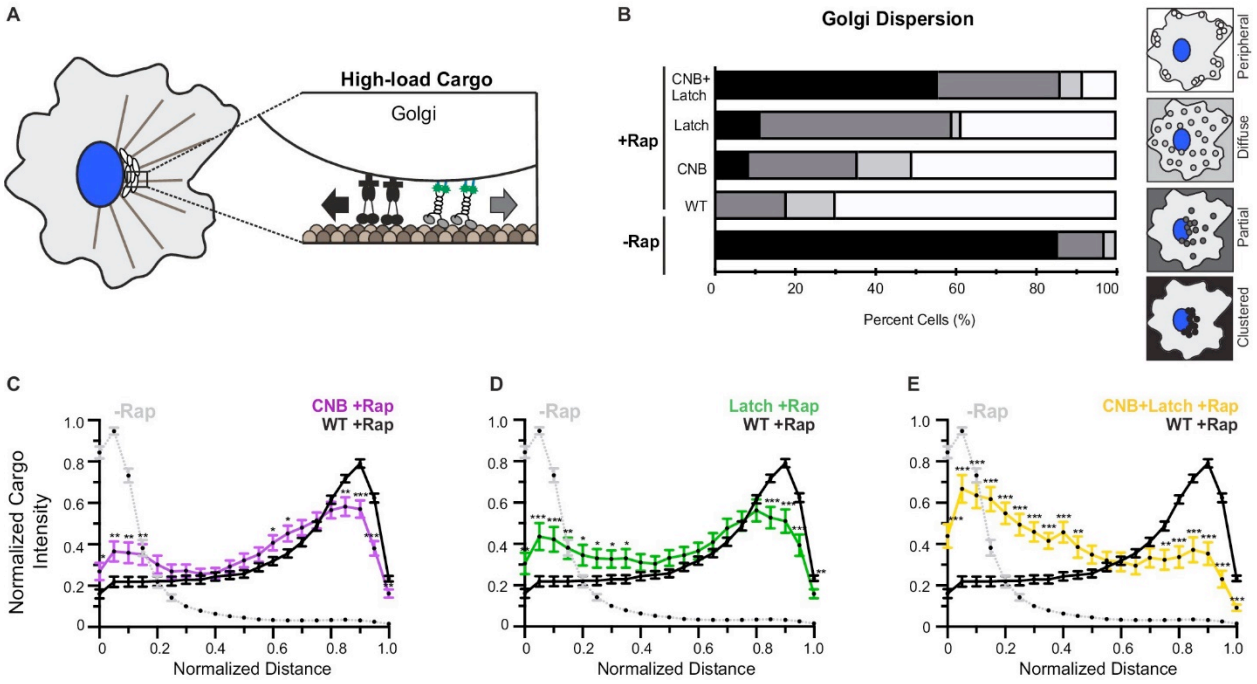

Figure 2.14 CNB and NL docking mutations impair transport of Golgi elements (high-load cargo) by teams of kinesin-1 motors in cells.

(**A**) Schematic of inducible Golgi dispersion assay. A variety of mechanisms, including the action of cytoplasmic dynein motors (black), maintain the Golgi in a compact cluster near the nucleus. Thus, the Golgi is a high-load cargo for transport by teams of recruited kinesin motors. (**B**) Qualitative analysis of Golgi dispersion. COS-7 cells were cotransfected with plasmids encoding for the expression of WT or mutant KIF5C-mNG-FRB motors together with the Golgi-targeting GMAP210p-mFRP-FKBP fusion protein. Motor recruitment was induced by addition of rapamycin (+Rap) and cells were fixed after 30 min and stained with an antibody to the Golgi marker giantin. Golgi localization in individual cells was scored as clustered (black), partially dispersed (dark grey), diffusely dispersed (light grey), or peripherally dispersed (white) after recruitment of teams of WT, CNB, Latch, or CNB+Latch motors. For each construct, N ≥ 30 cells were analyzed across three separate experiments. The results for each construct are summarized as a stacked bar plot. (**C–E**) Quantitative analysis of Golgi dispersion. A radial profile of Golgi intensity was generated for each cell and the data for each condition were converted to an averaged and normalized distance distribution across all cells. Each data point indicates the mean normalized cargo intensity ± SEM for N ≥ 30 cells across three separate experiments. Gray line: WT -Rap; Black line: WT +Rap; Purple line: CNB +Rap; Green line: Latch +Rap; Yellow line: CNB+Latch + Rap. Significant differences in mean normalized cargo intensity after recruitment of mutant motors as compared to WT motors are indicated for each distance; *, p<0.05; **, p<0.01; ***, p<0.001.

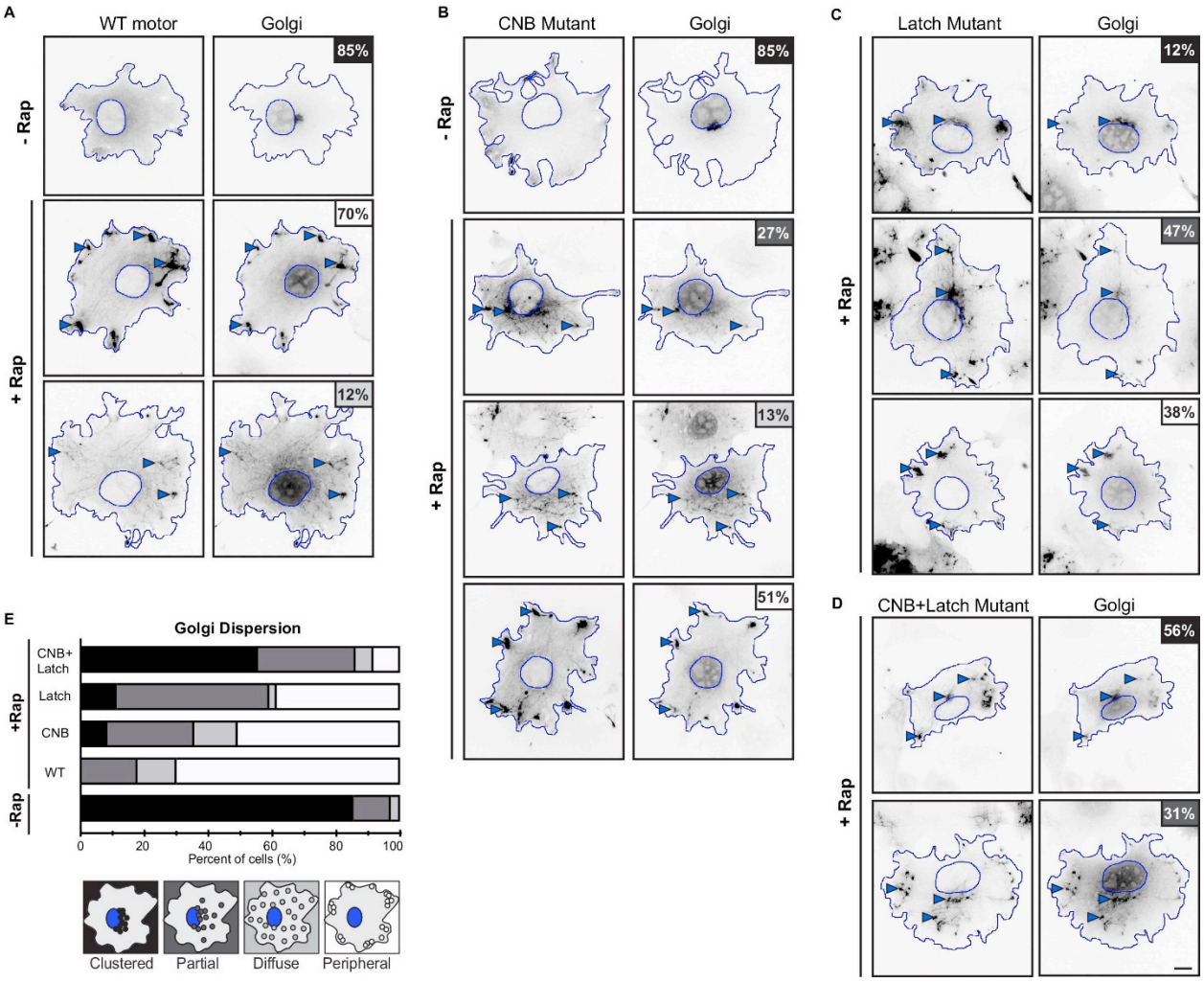

2.16 Golgi dispersion (high-load cargo) by teams of WT or NL docking mutant motors.

(**A–D**) Representative images of Golgi dispersion before (-Rap) and after (+Rap) recruitment of teams of motors to the Golgi surface. COS-7 cells were cotransfected with plasmids encoding for the expression of (**A**) WT, (**B**) CNB, (**C**) Latch, or (**D**) CNB+Latch KIF5C-mNG-FRB motors and Golgi-targeting GMAP210p-mFRP-FKBP fusion proteins. Blue lines indicate the nucleus and periphery of each cell. Blue arrowheads indicate Golgi elements dispersed after addition of rapamycin (+Rap), bar 10 μm. Percentages in the upper corner indicate the percent of cells with the indicated dispersion phenotype: Black: clustered Golgi; Dark gray: partially dispersed Golgi; Light gray: diffusely dispersed Golgi; White: peripherally dispersed Golgi. (**E**) Qualitative analysis of Golgi dispersion. Cells were scored as clustered (black), partially dispersed (dark grey), diffusely dispersed (light grey), or peripherally dispersed (white) for N ≥ 30 cells for each construct across multiple trials. The data for each construct is summarized as a stacked bar plot.

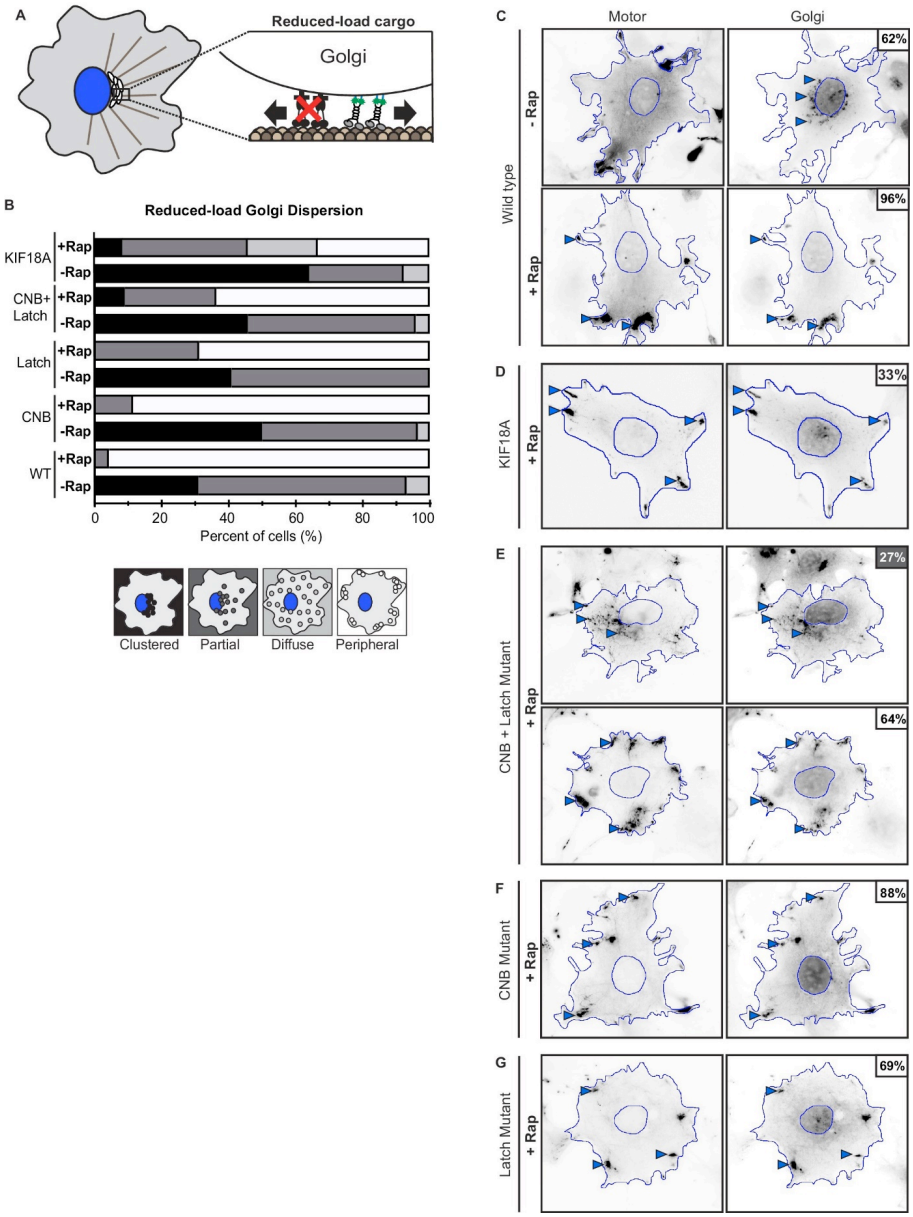

Figure 2.17 Kinesin-1 CNB and/or Latch mutants can drive transport of reduced-load Golgi elements.

(**A**) Schematic of Golgi dispersion assay with reduced-load. A truncated dynein intermediate chain (IC2), which acts as a dominant negative (DN) for dynein function, was expressed to interfere with dynein association with Golgi elements. In cells expressing the dynein DN, Golgi elements are a reduced-load for recruited kinesin-1 motors. (**B–F**) Representative images of reduced-load Golgi dispersion (in cells expressing dynein DN) before (-Rap) or after (+Rap) recruitment of teams of kinesin motors to the Golgi surface. COS-7 cells were cotransfected with plasmids encoding for the expression of mNG-FRB tagged motors, Golgi targeting GMAP201p-mRFP-FKBP, and dynein DN IC2 (IC2-N237-BFP) fusion proteins. Cells were selected and Golgi dispersion scored in cells expressing high levels of dynein DN IC2. Blue lines indicate the nucleus and periphery of each cell. Blue arrowheads indicate Golgi elements dispersed after addition of rapamycin (+Rap), bar 10 µm. Percentages in the upper corner indicate the percent of cells with the indicated dispersion phenotype: Black: clustered Golgi; Dark gray: partially dispersed Golgi; Light gray: diffusely dispersed Golgi; White: peripherally dispersed Golgi. (**G**) Qualitative analysis of Golgi dispersion. Cells were scored as clustered (black), partially dispersed (dark grey), diffusely dispersed (light grey), or peripherally dispersed (white) before (- Rap) or after (+Rap) recruitment of teams of kinesin motors. N ≥ 16 cells for each construct across two trials. The results for each construct are summarized as a stacked bar plot.

chain 2 (IC2-N237) that acts in a dominant negative (DN) manner to block endogenous dynein function and causes partial dispersion of the Golgi complex [Figure 2.17A, (Blasius et al., 2013; King, 2003)]. In cells overexpressing the dynein DN, transport of Golgi elements by teams of KIF18A motors was enhanced (Figure 2.17B,D; qualitatively 54% of cells have dispersed Golgi; quantitatively 37% of Golgi intensity at the cell periphery). These results indicate that cytoplasmic dynein contributes to the forces that teams of recruited kinesin motors must overcome to transport Golgi elements to the cell periphery. In cells overexpressing the dynein DN, the ability of the CNB Latch, and CNB+Latch mutant motors to drive Golgi dispersion was also enhanced (2.17B,E–G, qualitatively 96% of cells have dispersed Golgi for WT, 88% for CNB mutant, 69% for Latch mutant, and 64% for CNB+Latch mutant). Taken together, these results suggest that while weak kinesin motors can cooperate for transport of a low-load membrane-bound cargo, they are unable to work in teams when faced with a high-load cargo in cells.

2.4 Discussion

Studies at the single motor level have led to the hypothesis that CNB formation is the force-generating element for kinesin motors. Here we use molecular dynamics simulations, optical trapping, and single-molecule assays to show that both CNB and N-latch formation are critical for single kinesin-1 motors to transport against force. Weakening of either CNB or N-latch formation results in motors that do not stall under load and detach at low forces. Under unloaded conditions, mutant motors display improved motility properties due to allosteric effects of NL docking on the microtubule and nucleotide binding regions of the motor. We also use cellular assays to examine the contribution of CNB and N-Latch formation to the ability of motors to work in teams for transport of membrane-bound organelles. We find that both CNB formation and NL latching are critical for kinesin-1 motors to transport a high-load cargo in cells, even when the motors are working in teams.

2.4.1 Impact of CNB and N-latch formation on kinesin-1 force generation

We used MD simulations to prioritize contacts whose mutation would weaken CNB formation (interaction of β9 with CS) and/or NL latching (interaction of N-latch and β10 with β7). Importantly, the ability of the CNB and/or Latch mutant motors to undergo processive motility was not impaired (Figure 2.7), indicating that the mutations are tolerated by the motor when stepping under no load. Measurements of individual motors in an optical trap demonstrate that disruption of either CNB or N-latch formation resulted in motors unable to stall under load and more likely to detach when subjected to low forces (average detachment force ~1 pN, Figure 2.6). The effects of the CNB and N-latch mutations were not additive as weakening of both elements in the CNB+Latch mutant resulted in motors with similar behavior under load and similar detachment forces as the CNB and Latch mutant motors.

These results support the model that the CS plays a critical mechanical role in the force generation of kinesin-1 motors (Hesse et al., 2013; Hwang et al., 2008; Khalil et al., 2008; Rice et al., 1999). It is interesting that mutation of the two CS residues (A5 and S8) in our rat kinesin-1 motor resulted in an average detachment force of ~1 pN whereas previous work demonstrated that mutation of the same CS residues in the fly kinesin-1 motor resulted in an average detachment force of ~3 pN (Khalil et al., 2008). An intriguing possibility is that the additional residues at the N-terminus of the fly kinesin-1 motor (Figure 2.1C) can engage in additional interactions with the core motor domain and thereby partially compensate for the mutations during CNB formation.

Our results provide the first experimental demonstration of the contribution of N-latch formation to kinesin-1 force generation. A role for N-latch formation was previously implicated in MD simulations where forced breakage of the N-latch resulted in complete undocking of the NL (Hwang et al., 2008). Experimentally, a previous study mutated the N-latch of human kinesin-1 KIF5B (N332A) and found that force generation was crippled (Rice et al., 2003), however, the contribution of the N-latch in this study was examined in the context of i) mutation of the proceeding residue (V331A) predicted to be important for CNB formation, and ii) a cysteine-light kinesin-1 motor domain whose force dependence is dampened compared to WT kinesin-1 (Andreasson et al., 2015). Our results indicate that without N-latch formation, single kinesin-1 motors can generate a

power stroke via CNB formation but cannot sustain force generation (Figure 2.6). At present, it is unclear whether an impaired N-latch disrupts force production due to dissociation of the CNB, as predicted in the simulations (Hwang et al., 2008) and/or due to an inability to coordinate processive stepping and the out-of-phase mechanochemical cycles of a dimeric kinesin-1 motor.

2.4.2 Allosteric effects of CNB and N-latch mutations on unloaded motility

Although mutant motors with weakened NL docking underwent premature detachment under loaded conditions, they exhibited enhanced motility properties under unloaded conditions. Specifically, the CNB, Latch, and CNB+Latch mutant motors displayed enhanced velocity in single-molecule motility assays (Figure 2.7), similar to previous results with the CS mutant version of fly kinesin-1 (Khalil et al., 2008). The enhanced velocity is likely due to allosteric effects of NL docking on core motor regions that coordinate and bind nucleotide (α0, S1, S2, PL; Figure 2.9) and could result in enhanced catalytic site closure that would favor ATP hydrolysis in the mutant motors. Our findings are consistent with previous structural and enzymatic studies suggesting that NL docking allosterically gates ATPase activity (Cao et al., 2014; Hahlen et al., 2006). Our findings are also consistent with previous time-resolved $(TR)^2$ FRET studies of kinesin-1 and kinesin-5 motors demonstrating that NL docking is allosterically coupled to active site closure (Muretta et al., 2015; Muretta et al., 2018). Collectively, these results highlight how subtle changes in NL docking elements (CS, β9, N-latch/β10) can act as a molecular gearshift, where speed and processivity comes at the cost of robust force production.

The CNB, Latch, and CNB+Latch mutant motors also displayed longer runs and an increased landing rate (Figure 2.7). These results indicate that NL docking also has allosteric effects on the microtubule-binding surface of kinesin-1. PCA analysis demonstrated that the major structural difference between motors in the ADP-bound and microtubule-free state and motors in the ATP-bound and microtubule-bound state is the positioning of α4 (Figure 2.9). MD simulations of CNB+Latch mutant motors indicated an increased ability of this motor's microtubule-binding surface to sample a conformation compatible with strong microtubule binding (Figure 2.9, α4 up). We

suggest that these allosteric changes can account for the mutant motors' enhanced run lengths and ability to enter or re-enter a processive run.

That weakening of CNB and N-latch formation resulted in increased detachment under loaded conditions but reduced detachment under unloaded conditions is intriguing and further work is required to understand the mechanistic basis. These results highlight the benefits of a simulation-guided approach to weaken single contact points between the NL and the core motor domain in a manner that can reveal mechanical features of the motor under load yet can be tolerated by the motor when stepping under no load. In the future, this approach can be utilized to examine how sequence changes in CS and NL elements across the kinesin superfamily impact the force generation and motility properties of these motors.

2.4.3 Physiological relevance of NL docking and implications for multi-motor transport in cells

Our results suggest that both CNB formation and NL latching are essential for teams of kinesin-1 motors to collectively transport high-load, but not low-load, membrane-bound cargoes in cells. Teams of CNB and/or N-latch mutant motors were impaired in their ability to transport Golgi elements to the cell periphery as compared to WT kinesin-1 motors (Figure 2.14) but were able to transport peroxisomes to the cell periphery in a manner indistinguishable from the WT motor (Figure 2.11). Notably, this is the first evidence that a power stroke mechanism and force generation are critical for multi-motor driven transport under physiological conditions. Further support for the conclusion that force generation by individual kinesin-1 motors within a team is required for transport of high-load cargoes in cells comes from two additional findings. First, the kinesin-8 motor KIF18A, which generates only 1 pN of force individually (Jannasch et al., 2013), is able to cooperate to drive peroxisome motility but is unable to drive Golgi dispersion (Figure 2.15). Second, single-headed kinesin motors that weakly engage with the microtubule track as individual motors can cooperate to drive peroxisome motility but are largely unable to drive Golgi dispersion (Schimert et al., 2019). Taken together, these results suggest that motility properties other than a power stroke-like mechanism can contribute to collective motility and cargo transport but only under low-load conditions.

Interestingly, the CNB, Latch, and CNB+Latch mutant motors differ in their ability to work collectively to drive dispersion of a high-load cargo. Teams of CNB+Latch mutant motors were more impaired in their ability to drive Golgi dispersion as compared to the CNB and N-Latch mutants (Figure 2.14). This result was surprising as we observed similar properties under load for the CNB, Latch, and CNB+Latch mutants as single motors in optical trap assays (Figure 2.6). These results highlight the limitations of extrapolating single-molecule properties to understand motor behavior in teams and/or in a cellular environment. The most likely explanation for why the CNB+Latch mutant is more impaired in Golgi dispersion relates to differences in the assays themselves. The optical trap assay measures the behavior of single motors whereas the cargo dispersion assays report on the cooperative activity of teams of motors. In addition, in the optical trap assay, motors are statically attached to a bead whereas in the cellular assays, motors can freely diffuse in the lipid environment of the membrane-bound organelle.

In multi-motor assays, the motility of individual motors can be facilitated or hindered by other motors in the complex. For example, motors at the leading edge of a membrane-bound vesicle are predicted to shoulder most of the load during transport, and can generate assisting forces that promote the stepping of motors at the trailing edge (Leduc et al., 2010; Nelson et al., 2014). For kinesin-1, assisting loads as small as 1.5 pN could restore forward stepping and processive motion of a severely crippled kinesin-1 motor (Khalil et al., 2008). It may be that the CNB and Latch mutants are more amenable to assisting forces in the Golgi dispersion assay than the CNB+Latch mutant motors. Other parameters that have been noted to influence the ability of motors to work in teams are the load-dependent detachment of the motor from the microtubule track (Arpăg et al., 2014; Norris et al., 2014) and the ability to rebind to the microtubule after detachment (Feng et al., 2018). These parameters seem less likely to explain the differences between the CNB, Latch, and CNB+Latch mutant motors in Golgi dispersion as all of the mutant motors readily detached from the microtubule as single motors under load (Figure 2.6) and displayed an enhanced microtubule landing rates under unloaded conditions (Figure 2.7).

Although our findings provide strong support for the hypothesis that CNB formation, as the mechanical element for kinesin force production, is required for high-load cargo transport in cells, it is possible that the differences observed between the peroxisome and Golgi dispersion assays are due to experimental conditions rather than motor force generation. While experimental conditions such as kinesin expression level and the effectiveness of motor recruitment have minimal influence on peroxisome dispersion in these assays (Efremov et al., 2014; Kapitein et al., 2010; Schimert et al., 2019), it is possible that differences in size and/or local microenvironment fluidity result in cargo-specific steric effects and/or drag forces that impact transport driven by the exogenous motors. Further work with reconstitution systems are required to examine these possibilities.

2.4.4 Implications for CNB formation and NL docking in other kinesins

The motor domain is highly conserved in both sequence and structure across the kinesin superfamily and many chemical and mechanical features are likely to be shared across all members. Formation of a CNB has also been observed structurally for members of the kinesin-3, kinesin-5 and kinesin-6 families (Atherton et al., 2017; Hesse et al., 2013; Ren et al., 2018) although a mechanical role in force generation has only been tested for kinesin-1 motors. Whether N-latch formation and docking of β10 along the core motor domain play important roles beyond kinesin-1 remain to be investigated. The asparagine residue involved in N-latch formation is highly conserved across processive kinesins with the exception of kinesin-6 family members (Figure 2.3) and recent work failed to resolve a docked NL conformation for the kinesin-6 motor MKLP2 (human KIF20A) even in the ATP- and microtubule-bound state (Atherton et al., 2017).

In the absence of ATP, formation of the CNB is prevented by occupancy of the docking pocket by the hydrophobic CTR [I9 in kinesin-1 KIF5C (Cao et al., 2014; Nitta et al., 2008; Shang et al., 2014; Sindelar & Downing, 2010)]. Structural changes induced by ATP binding open up this pocket to occupancy by the NIS [I327 in kinesin-1 KIF5C (Cao et al., 2014; Nitta et al., 2008; Shang et al., 2014; Sindelar & Downing, 2010)]. As an isoleucine or valine residue is found in the CTR and NIS positions across a large number of kinesin sequences (Figure 2.3), mutually exclusive access of the CTR and the NIS to the docking cleft may be a shared feature for N-kinesins that generate force

and processive motility. In support of this possibility, structural studies have demonstrated that the docking pocket is occluded by CS residues in the absence of ATP for kinesin-3 and kinesin-6 motors (Arora et al., 2014; Atherton et al., 2017)

How variations in the length and sequence of the CS influence family-specific force and motility properties is not understood. We note that kinesin-3 motors have the shortest CS (Figure 2.3) and a recent study found that the kinesin-3 motor KIF13B forms a short CNB with weaker CS-NL interactions than kinesin-1 (Ren, et al., 2018). Given our results, a short CS and weak CNB could contribute to the fast and superprocessive motility and high landing rate observed for motors in the kinesin-3 family (Soppina & Verhey, 2014) as well as their tendency to detach from the microtubule under load (Arpağ et al., 2014; Norris et al., 2014). Interestingly, a short CS and weak CNB formation do not appear to negatively impact force output as single kinesin-3 motors are capable of withstanding forces equivalent to that of single kinesin-1 motors [~6 pN, (Huckaba et al., 2011; Tomishige et al., 2002)]. Further work on the force generation of kinesin-3 and other family members will provide important information about mechanical and structural features shared across the kinesin superfamily.

2.5 References

Andreasson, J. O., Shastry, S., Hancock, W. O., & Block, S. M. (2015). The Mechanochemical Cycle of Mammalian Kinesin-2 KIF3A/B under Load. *Curr Biol, 25*(9), 1166-1175. doi:10.1016/j.cub.2015.03.013

Arora, K., Talje, L., Asenjo, A. B., Andersen, P., Atchia, K., Joshi, M., Sosa, H., Allingham, J. S., Kwok, B. H. (2014). KIF14 binds tightly to microtubules and adopts a rigor-like conformation. *J Mol Biol, 426*(17), 2997-3015. doi:10.1016/j.jmb.2014.05.030

Arpağ, G., Shastry, S., Hancock, W. O., & Tuzel, E. (2014). Transport by populations of fast and slow kinesins uncovers novel family-dependent motor characteristics important for in vivo function. *Biophys J, 107*(8), 1896-1904. doi:10.1016/j.bpj.2014.09.009

Asenjo, A. B., Weinberg, Y., & Sosa, H. (2006). Nucleotide binding and hydrolysis induces a disorder-order transition in the kinesin neck-linker region. *Nat Struct Mol Biol, 13*(7), 648-654. doi:10.1038/nsmb1109

Atherton, J., Farabella, I., Yu, I. M., Rosenfeld, S. S., Houdusse, A., Topf, M., & Moores, C. A. (2014). Conserved mechanisms of microtubule-stimulated ADP release, ATP binding, and force generation in transport kinesins. *Elife, 3*, e03680. doi:10.7554/eLife.03680

Atherton, J., Yu, I. M., Cook, A., Muretta, J. M., Joseph, A., Major, J., Sourigues, Y., Clause, J., Topf, M., Rosenfeld, S. S., Houdusse, A., Moores, C. A. (2017). The divergent mitotic kinesin MKLP2 exhibits atypical structure and mechanochemistry. *Elife, 6*. doi:10.7554/eLife.27793

Bas, D. C., Rogers, D. M., & Jensen, J. H. (2008). Very fast prediction and rationalization of pKa values for protein-ligand complexes. *Proteins, 73*(3), 765-783. doi:10.1002/prot.22102

Blasius, T. L., Reed, N., Slepchenko, B. M., & Verhey, K. J. (2013). Recycling of kinesin-1 motors by diffusion after transport. *PLoS One, 8*(9), e76081. doi:10.1371/journal.pone.0076081

Block, S. M. (2007). Kinesin motor mechanics: binding, stepping, tracking, gating, and limping. *Biophys J, 92*(9), 2986-2995. doi:10.1529/biophysj.106.100677

Brownhill, K., Wood, L., & Allan, V. (2009). Molecular motors and the Golgi complex: staying put and moving through. *Semin Cell Dev Biol, 20*(7), 784-792. doi:10.1016/j.semcdb.2009.03.019

Cai, D., Hoppe, A. D., Swanson, J. A., & Verhey, K. J. (2007). Kinesin-1 structural organization and conformational changes revealed by FRET stoichiometry in live cells. *J Cell Biol, 176*(1), 51-63. doi:10.1083/jcb.200605097

Cao, L., Wang, W., Jiang, Q., Wang, C., Knossow, M., & Gigant, B. (2014). The structure of apo-kinesin bound to tubulin links the nucleotide cycle to movement. *Nat Commun, 5*, 5364. doi:10.1038/ncomms6364

Case, D. A., Cheatham, T. E., 3rd, Darden, T., Gohlke, H., Luo, R., Merz, K. M., Jr., Onufriev, A., Simmerling, C., Wang, B., Woods, R. J. (2005). The Amber

biomolecular simulation programs. *J Comput Chem, 26*(16), 1668-1688. doi:10.1002/jcc.20290

Case, R. B., Rice, S., Hart, C. L., Ly, B., & Vale, R. D. (2000). Role of the kinesin neck linker and catalytic core in microtubule-based motility. *Curr Biol, 10*(3), 157-160. doi:10.1016/s0960-9822(00)00316-x

Clancy, B. E., Behnke-Parks, W. M., Andreasson, J. O., Rosenfeld, S. S., & Block, S. M. (2011). A universal pathway for kinesin stepping. *Nat Struct Mol Biol, 18*(9), 1020-1027. doi:10.1038/nsmb.2104

Dogan, M. Y., Can, S., Cleary, F. B., Purde, V., & Yildiz, A. (2015). Kinesin's front head is gated by the backward orientation of its neck linker. *Cell Rep, 10*(12), 1967-1973. doi:10.1016/j.celrep.2015.02.061

Efremov, A. K., Radhakrishnan, A., Tsao, D. S., Bookwalter, C. S., Trybus, K. M., & Diehl, M. R. (2014). Delineating cooperative responses of processive motors in living cells. *Proc Natl Acad Sci U S A, 111*(3), E334-343. doi:10.1073/pnas.1313569111

Engelke, M. F., Winding, M., Yue, Y., Shastry, S., Teloni, F., Reddy, S., Blasius, T. L., Soppina, P., Hancock, W. O., Gelfand, V. I., Verhey, K. J. (2016). Engineered kinesin motor proteins amenable to small-molecule inhibition. *Nat Commun, 7*, 11159. doi:10.1038/ncomms11159

Feng, Q., Mickolajczyk, K. J., Chen, G. Y., & Hancock, W. O. (2018). Motor Reattachment Kinetics Play a Dominant Role in Multimotor-Driven Cargo Transport. *Biophys J, 114*(2), 400-409. doi:10.1016/j.bpj.2017.11.016

Gigant, B., Wang, W., Dreier, B., Jiang, Q., Pecqueur, L., Pluckthun, A., Wang, C. Knossow, M. (2013). Structure of a kinesin-tubulin complex and implications for kinesin motility. *Nat Struct Mol Biol, 20*(8), 1001-1007. doi:10.1038/nsmb.2624

Guet, D., Mandal, K., Pinot, M., Hoffmann, J., Abidine, Y., Sigaut, W., Bardin, S., Schauer, K., Goud, B., Manneville, J. B. (2014). Mechanical role of actin dynamics in the rheology of the Golgi complex and in Golgi-associated trafficking events. *Curr Biol, 24*(15), 1700-1711. doi:10.1016/j.cub.2014.06.048

Hahlen, K., Ebbing, B., Reinders, J., Mergler, J., Sickmann, A., & Woehlke, G. (2006). Feedback of the kinesin-1 neck-linker position on the catalytic site. *J Biol Chem, 281*(27), 18868-18877. doi:10.1074/jbc.M508019200

Hariharan, V., & Hancock, W. O. (2009). Insights into the Mechanical Properties of the Kinesin Neck Linker Domain from Sequence Analysis and Molecular Dynamics Simulations. *Cell Mol Bioeng, 2*(2), 177-189. doi:10.1007/s12195-009-0059-5

Hesse, W. R., Steiner, M., Wohlever, M. L., Kamm, R. D., Hwang, W., & Lang, M. J. (2013). Modular aspects of kinesin force generation machinery. *Biophys J, 104*(9), 1969-1978. doi:10.1016/j.bpj.2013.03.051

Hirokawa, N., Noda, Y., Tanaka, Y., & Niwa, S. (2009). Kinesin superfamily motor proteins and intracellular transport. *Nat Rev Mol Cell Biol, 10*(10), 682-696. doi:10.1038/nrm2774

Hornak, V., Abel, R., Okur, A., Strockbine, B., Roitberg, A., & Simmerling, C. (2006). Comparison of multiple Amber force fields and development of improved protein backbone parameters. *Proteins, 65*(3), 712-725. doi:10.1002/prot.21123

Huckaba, T. M., Gennerich, A., Wilhelm, J. E., Chishti, A. H., & Vale, R. D. (2011). Kinesin-73 is a processive motor that localizes to Rab5-containing organelles. *J Biol Chem, 286*(9), 7457-7467. doi:10.1074/jbc.M110.167023

Hwang, W., Lang, M. J., & Karplus, M. (2008). Force generation in kinesin hinges on cover-neck bundle formation. *Structure, 16*(1), 62-71. doi:10.1016/j.str.2007.11.008

Hwang, W., Lang, M. J., & Karplus, M. (2017). Kinesin motility is driven by subdomain dynamics. *Elife, 6*. doi:10.7554/eLife.28948

Isojima, H., Iino, R., Niitani, Y., Noji, H., & Tomishige, M. (2016). Direct observation of intermediate states during the stepping motion of kinesin-1. *Nat Chem Biol, 12*(4), 290-297. doi:10.1038/nchembio.2028

Jannasch, A., Bormuth, V., Storch, M., Howard, J., & Schaffer, E. (2013). Kinesin-8 is a low-force motor protein with a weakly bound slip state. *Biophys J, 104*(11), 2456-2464. doi:10.1016/j.bpj.2013.02.040

Kapitein, L. C., Schlager, M. A., van der Zwan, W. A., Wulf, P. S., Keijzer, N., & Hoogenraad, C. C. (2010). Probing intracellular motor protein activity using an

inducible cargo trafficking assay. *Biophys J, 99*(7), 2143-2152. doi:10.1016/j.bpj.2010.07.055

Khalil, A. S., Appleyard, D. C., Labno, A. K., Georges, A., Karplus, M., Belcher, A. M., . . . Lang, M. J. (2008). Kinesin's cover-neck bundle folds forward to generate force. *Proc Natl Acad Sci U S A, 105*(49), 19247-19252. doi:10.1073/pnas.0805147105

King, S. M. (2003). Organization and regulation of the dynein microtubule motor. *Cell Biol Int, 27*(3), 213-215. doi:10.1016/s1065-6995(02)00337-2

Kozielski, F., Sack, S., Marx, A., Thormahlen, M., Schonbrunn, E., Biou, V., Thompson, A., Mandelkow, E. M., Mandelkow, E. (1997). The crystal structure of dimeric kinesin and implications for microtubule-dependent motility. *Cell, 91*(7), 985-994. doi:10.1016/s0092-8674(00)80489-4

Lang, M. J., & Hwang, W. (2010). Motor proteins: kinesin drives with an underhead cam. *Curr Biol, 20*(9), R408-410. doi:10.1016/j.cub.2010.03.015

Leduc, C., Pavin, N., Julicher, F., & Diez, S. (2010). Collective behavior of antagonistically acting kinesin-1 motors. *Phys Rev Lett, 105*(12), 128103. doi:10.1103/PhysRevLett.105.128103

Liu, D., Liu, X., Shang, Z., & Sindelar, C. V. (2017). Structural basis of cooperativity in kinesin revealed by 3D reconstruction of a two-head-bound state on microtubules. *Elife, 6*. doi:10.7554/eLife.24490

Meagher, K. L., Redman, L. T., & Carlson, H. A. (2003). Development of polyphosphate parameters for use with the AMBER force field. *J Comput Chem, 24*(9), 1016-1025. doi:10.1002/jcc.10262

Muretta, J. M., Jun, Y., Gross, S. P., Major, J., Thomas, D. D., & Rosenfeld, S. S. (2015). The structural kinetics of switch-1 and the neck linker explain the functions of kinesin-1 and Eg5. *Proc Natl Acad Sci U S A, 112*(48), E6606-6613. doi:10.1073/pnas.1512305112

Muretta, J. M., Reddy, B. J. N., Scarabelli, G., Thompson, A. F., Jariwala, S., Major, J., Rich, J. N., Willard, B., Thomas, D. D., Stumpff, J., Grant, B. J., Gross, S. P., Rosenfeld, S. S. (2018). A posttranslational modification of the mitotic kinesin Eg5 that enhances its mechanochemical coupling and alters its mitotic function. *Proc Natl Acad Sci U S A, 115*(8), E1779-E1788. doi:10.1073/pnas.1718290115

Muthukrishnan, G., Zhang, Y., Shastry, S., & Hancock, W. O. (2009). The processivity of kinesin-2 motors suggests diminished front-head gating. *Curr Biol, 19*(5), 442-447. doi:10.1016/j.cub.2009.01.058

Nelson, S. R., Trybus, K. M., & Warshaw, D. M. (2014). Motor coupling through lipid membranes enhances transport velocities for ensembles of myosin Va. *Proc Natl Acad Sci U S A, 111*(38), E3986-3995. doi:10.1073/pnas.1406535111

Nitta, R., Okada, Y., & Hirokawa, N. (2008). Structural model for strain-dependent microtubule activation of Mg-ADP release from kinesin. *Nat Struct Mol Biol, 15*(10), 1067-1075. doi:10.1038/nsmb.1487

Nitta, T., Tanahashi, A., Obara, Y., Hirano, M., Razumova, M., Regnier, M., & Hess, H. (2008). Comparing guiding track requirements for myosin- and kinesin-powered molecular shuttles. *Nano Lett, 8*(8), 2305-2309. doi:10.1021/nl8010885

Norris, S. R., Soppina, V., Dizaji, A. S., Schimert, K. I., Sept, D., Cai, D., Sivaramakrishnan, S., Verhey, K. J. (2014). A method for multiprotein assembly in cells reveals independent action of kinesins in complex. *J Cell Biol, 207*(3), 393-406. doi:10.1083/jcb.201407086

Parke, C. L., Wojcik, E. J., Kim, S., & Worthylake, D. K. (2010). ATP hydrolysis in Eg5 kinesin involves a catalytic two-water mechanism. *J Biol Chem, 285*(8), 5859-5867. doi:10.1074/jbc.M109.071233

Reinemann, D. N., Norris, S. R., Ohi, R., & Lang, M. J. (2018). Processive Kinesin-14 HSET Exhibits Directional Flexibility Depending on Motor Traffic. *Curr Biol, 28*(14), 2356-2362 e2355. doi:10.1016/j.cub.2018.06.055

Reinemann, D. N., Sturgill, E. G., Das, D. K., Degen, M. S., Voros, Z., Hwang, W., Ohi, R., Lang, M. J. (2017). Collective Force Regulation in Anti-parallel Microtubule Gliding by Dimeric Kif15 Kinesin Motors. *Curr Biol, 27*(18), 2810-2820 e2816. doi:10.1016/j.cub.2017.08.018

Ren, J., Zhang, Y., Wang, S., Huo, L., Lou, J., & Feng, W. (2018). Structural Delineation of the Neck Linker of Kinesin-3 for Processive Movement. *J Mol Biol, 430*(14), 2030-2041. doi:10.1016/j.jmb.2018.05.010

Rice, S., Cui, Y., Sindelar, C., Naber, N., Matuska, M., Vale, R., & Cooke, R. (2003). Thermodynamic properties of the kinesin neck-region docking to the catalytic core. *Biophys J, 84*(3), 1844-1854. doi:10.1016/S0006-3495(03)74992-3

Rice, S., Lin, A. W., Safer, D., Hart, C. L., Naber, N., Carragher, B. O., Cain, S. M., Pechatnikova, E., Wildon-Kubalek, E. M., Whittaker, M., Pate, E., Cooke, R., Taylor, E. W., Milligan, R. A., Vale, R. D. (1999). A structural change in the kinesin motor protein that drives motility. *Nature, 402*(6763), 778-784. doi:10.1038/45483

Rosenfeld, S. S., Jefferson, G. M., & King, P. H. (2001). ATP reorients the neck linker of kinesin in two sequential steps. *J Biol Chem, 276*(43), 40167-40174. doi:10.1074/jbc.M103899200

Sack, S., Muller, J., Marx, A., Thormahlen, M., Mandelkow, E. M., Brady, S. T., & Mandelkow, E. (1997). X-ray structure of motor and neck domains from rat brain kinesin. *Biochemistry, 36*(51), 16155-16165. doi:10.1021/bi9722498

Scarabelli, G., & Grant, B. J. (2013). Mapping the structural and dynamical features of kinesin motor domains. *PLoS Comput Biol, 9*(11), e1003329. doi:10.1371/journal.pcbi.1003329

Schimert, K. I., Budaitis, B. G., Reinemann, D. N., Lang, M. J., & Verhey, K. J. (2019). Intracellular cargo transport by single-headed kinesin motors. *Proc Natl Acad Sci U S A, 116*(13), 6152-6161. doi:10.1073/pnas.1817924116

Shang, Z., Zhou, K., Xu, C., Csencsits, R., Cochran, J. C., & Sindelar, C. V. (2014). High-resolution structures of kinesin on microtubules provide a basis for nucleotide-gated force-generation. *Elife, 3*, e04686. doi:10.7554/eLife.04686

Shastry, S., & Hancock, W. O. (2010). Neck linker length determines the degree of processivity in kinesin-1 and kinesin-2 motors. *Curr Biol, 20*(10), 939-943. doi:10.1016/j.cub.2010.03.065

Shastry, S., & Hancock, W. O. (2011). Interhead tension determines processivity across diverse N-terminal kinesins. *Proc Natl Acad Sci U S A, 108*(39), 16253-16258. doi:10.1073/pnas.1102628108

Sindelar, C. V., Budny, M. J., Rice, S., Naber, N., Fletterick, R., & Cooke, R. (2002). Two conformations in the human kinesin power stroke defined by X-ray

crystallography and EPR spectroscopy. *Nat Struct Biol, 9*(11), 844-848. doi:10.1038/nsb852

Sindelar, C. V., & Downing, K. H. (2010). An atomic-level mechanism for activation of the kinesin molecular motors. *Proc Natl Acad Sci U S A, 107*(9), 4111-4116. doi:10.1073/pnas.0911208107

Skiniotis, G., Surrey, T., Altmann, S., Gross, H., Song, Y. H., Mandelkow, E., & Hoenger, A. (2003). Nucleotide-induced conformations in the neck region of dimeric kinesin. *EMBO J, 22*(7), 1518-1528. doi:10.1093/emboj/cdg164

Skjaerven, L., Yao, X. Q., Scarabelli, G., & Grant, B. J. (2014). Integrating protein structural dynamics and evolutionary analysis with Bio3D. *BMC Bioinformatics, 15*, 399. doi:10.1186/s12859-014-0399-6

Soppina, V., & Verhey, K. J. (2014). The family-specific K-loop influences the microtubule on-rate but not the superprocessivity of kinesin-3 motors. *Mol Biol Cell, 25*(14), 2161-2170. doi:10.1091/mbc.E14-01-0696

Svoboda, K., & Block, S. M. (1994). Force and velocity measured for single kinesin molecules. *Cell, 77*(5), 773-784. doi:10.1016/0092-8674(94)90060-4

Tomishige, M., Klopfenstein, D. R., & Vale, R. D. (2002). Conversion of Unc104/KIF1A kinesin into a processive motor after dimerization. *Science, 297*(5590), 2263-2267. doi:10.1126/science.1073386

Tomishige, M., & Vale, R. D. (2000). Controlling kinesin by reversible disulfide cross-linking. Identifying the motility-producing conformational change. *J Cell Biol, 151*(5), 1081-1092. doi:10.1083/jcb.151.5.1081

Turner, J., Anderson, R., Guo, J., Beraud, C., Fletterick, R., & Sakowicz, R. (2001). Crystal structure of the mitotic spindle kinesin Eg5 reveals a novel conformation of the neck-linker. *J Biol Chem, 276*(27), 25496-25502. doi:10.1074/jbc.M100395200

Verhey, K. J., & Hammond, J. W. (2009). Traffic control: regulation of kinesin motors. *Nat Rev Mol Cell Biol, 10*(11), 765-777. doi:10.1038/nrm2782

Yildiz, A., Tomishige, M., Gennerich, A., & Vale, R. D. (2008). Intramolecular strain coordinates kinesin stepping behavior along microtubules. *Cell, 134*(6), 1030-1041. doi:10.1016/j.cell.2008.07.018

Chapter 3: Conservation of the Functional Role of the Coverstrand Across the Kinesin Superfamily

Author contributions:

B.G.B performed all assays except optical trapping assays and molecular dynamics simulations; D.N.R preformed optical trapping assays, G.S performed molecular dynamics simulations, B.G.B, D.N.R, and G.S analyzed data. B.G.B and K.J.V wrote the text and composed figures.

3.1 Introduction

Kinesin motor proteins are responsible for orchestrating fundamental microtubule-based processes including cell division, intracellular trafficking, cytoskeletal organization, and cilia function (Hirokawa et al., 2009; Verhey & Hammond, 2009). Here we investigate the motility of motors from the kinesin-1, -2, and -3 families. All three motor families serve critical roles in intracellular transport in many cells types, including neurons (Hirokawa et al., 2010; Verhey & Hammond, 2009). Under unloaded, single-molecule conditions, kinesin-1, -2, and -3 motors are fast, processive motors with some degree of difference in their velocities and run lengths [velocity - KIF5C: 600 nm/s, KIF3AB: 400 nm/s, KIF1A: 2000 nm/s; runlength - KIF5C: 1.0 μm, KIF3AB: 1.0 μm; KIF1A: >20.0 μm; (Budaitis et al., 2019; Guzik-Lendrum et al., 2015; Scarabelli et al., 2015; Soppina & Verhey, 2014)].

However, their ability to drive transport under load is strikingly different. Specifically, kinesin-1 motors drive robust transport under load, eventually slowing and stalling along the microtubule track at high loads (Budaitis et al., 2019; Khalil et al., 2008; Svoboda & Block, 1994). However, heterodimeric kinesin-2 motor KIF3AB and kinesin-3 motor KIF1A are sensitive to detaching from the microtubule track when subjected to small loads (Andreasson et al., 2015; Arpăg et al., 2014; Milic et al., 2017; Tomishige et al., 2002). Recent computational and biophysical studies predict that a

motor's sensitivity to detaching under load is an important parameter that dictates the ability for motors to cooperate to drive transport, and therefore can lead to novel transport behaviors by teams of motors in cells (Arpăg et al., 2014; Norris et al., 2014; Ohashi et al., 2019). However, the molecular elements of the kinesin motor domain that modulate the force output of a motor are not well understood.

For kinesin-1, the founding member of the kinesin superfamily, zippering of the first half of the NL (β9) with β0 of the coverstrand (CS) at the N-terminus of the motor domain, forms a 2-stranded β-sheet termed the cover-neck bundle (CNB, Figure 3.1). CNB formation drives the NL forward into the docking pocket along the motor domain, providing the power stroke for force generation (Budaitis et al., 2019; Hwang et al., 2008; Khalil et al., 2008). After CNB formation, the second half of the NL (β10) latches along the surface of the core motor domain by interactions between a highly conserved asparagine residue (N334) in the NL and β7 of the docking pocket. NL latching is important for processive stepping under load [Figure 3.1; (Budaitis et al., 2019; Hwang et al., 2008)].

Structural observations of CNB formation and NL latching by other kinesins suggest a conserved mechanism for force generation (Atherton et al., 2014; Atherton et al., 2017; Hesse et al., 2013; Nitta et al., 2008; Ren et al., 2018), however their mechanical role in force generation has only been tested for kinesin-1 (Budaitis et al., 2019; Hesse et al., 2013; Khalil et al., 2008). Previous work found that chimeric kinesin-1 motors that have the CS, NL, and/or Loop13 sequences of the kinesin-5 motor Eg5 have a reduced force output in optical trap assays, providing the first hint that differences in CNB formation across the kinesin superfamily may be a strategy to tune the force output of a motor (Hesse et al., 2013). Moreover, sequence alignment reveals striking differences in the length and sequence of the coverstrand across the kinesin superfamily (Figure 3.1).

To qualitatively understand whether differences in the sequence and length of the coverstrand tune the functional output of kinesin motors, we used molecular dynamics (MD) simulations to predict CNB formation in kinesin-1, -2, and -3 motors. To understand how differences in CNB formation may modulate the function output of motors, we generated mutations in the CS of kinesin-1 and -2 motors and tasked

motors to drive transport of membrane-bound cargo in cells. Specifically, we find that truncation of the CS in kinesin-1 and kinesin-2 motors cripples their ability to drive transport of high-lad cargo in cells, supporting the proposed mechanical role of the CS for generating a power stroke. Notably, this is the first evidence that the CS serves an important role for high-load transport in a motor other than kinesin-1. Furthermore, work presented in this chapter provides a framework of how sequence diversity of the CS, NL, and docking pocket may influence a motor's force output across the kinesin superfamily.

3.2 Materials and Methods

Detailed in the materials and methods of Chapter 2.

3.3 Results

3.3.1. High-load transport by teams of kinesin motors in cells

To better understand the functional differences between kinesin families under physiological conditions, we tasked members from the kinesin-1, -2, -3 and -8 families to drive the transport of low- or high-load cargoes in cells. We used a non-inducible recruitment strategy to link teams of motors to the surface of peroxisomes [low-load, 2-15 pN, (Efremov et al., 2014)] or Golgi elements [high-load, +150 pN, (Budaitis et al., 2019)] and monitored transport to the cell periphery after 8 hours using fluorescence microscopy. Cargo dispersion in individual cells were qualitatively scored before and after motor recruitment as clustered (black), partially dispersed (dark grey), diffusely dispersed (light grey), and peripherally dispersed (white) (Figure 3.1) and summarized as a stacked bar plot.

Specifically, COS-7 cells were transfected with a plasmid for expression of a constitutively-active kinesin motor tagged with monomeric citrine and fused to PEX26 or GMAP210p sequence to target motors to the surface of peroxisomes or Golgi elements, respectively (Figure 3.1A). We screened a number of kinesin motors in this assay: the kinesin-1 motors KIF5A, KIF5B, KIF5C, the kinesin-2 motors KIF3AB, KIF17, the kinesin-3 motors KIF1A, KIF13A, KIF16B, and the kinesin-8 motor KIF18A.

In untransfected cells, peroxisomes and Golgi elements are typically clustered near the nucleus of the cell (82% cells have clustered peroxisomes, 84% cells have

clustered Golgi, Figure 3.1B,C). We find that as teams, all kinesin motors we screened can drive the transport of low-load cargo to the cell periphery (Figure 3.1B), however there are striking differences in their abilities to drive the transport of high-load cargo (Figure 3.1C). We find that members of the kinesin-1 family are robust transporters of high-load cargo, with KIF5A, 5B, and 5C driving peripheral dispersion of Golgi elements in 83%, 49%, and 76% of cells, respectively. We also find that kinesin-3 motors are also able to drive the transport of high-load cargo, with KIF1A, 13B, 16B motors driving peripheral dispersion of Golgi elements in 62%, 58%, and 77% of cells, respectively. However, members of the kinesin-2 family had striking differences in their ability to drive high-load transport. Specifically, we find that heterodimeric motor KIF3AB drives peripheral dispersion of Golgi elements in 78% cells compared to 6% of cells by homodimeric kinesin-2 KIF17. Finally, we find that teams of KIF18A motors, with a single molecule force output of 1 pN (Jannasch et al., 2013), cannot collectively

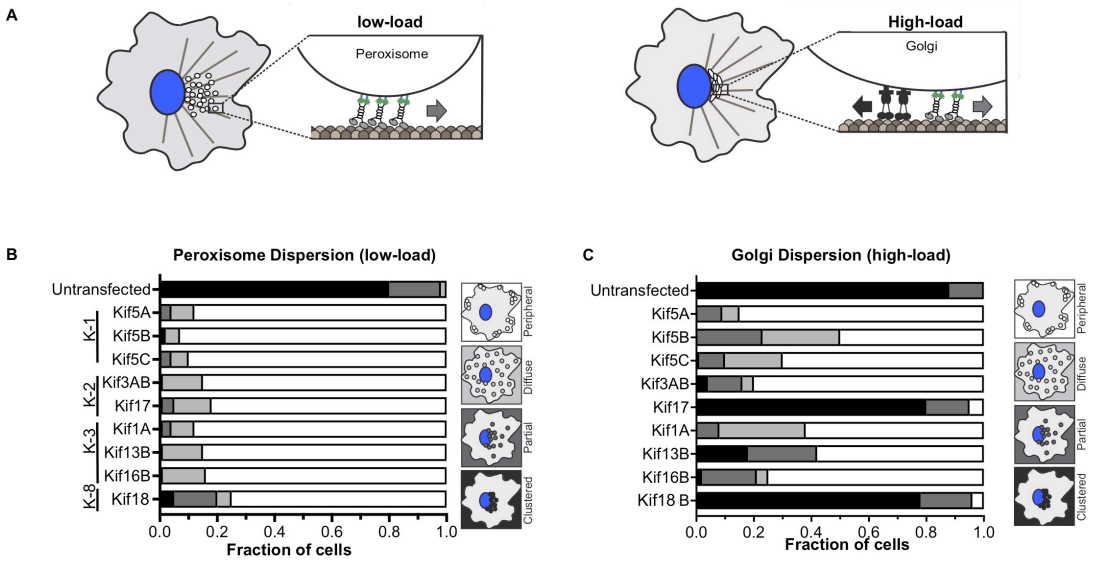

Figure 3.1 Diversity in the ability of teams of kinesin motors to drive transport of high-load in cells

(**A**) Schematic of the peroxisome dispersion assay (left) and Golgi dispersion assay (right). Peroxisomes are loosely clustered in the perinuclear region of COS-7 cells and are largely immotile, thus providing a low-load cargo for transport by teams of recruited motors. However, a variety of mechanisms, including the action of cytoplasmic dynein motors (black), maintain the Golgi in a compact cluster near the nucleus. Thus, the Golgi is a high-load cargo for transport by teams of recruited team of kinesin motors. (**B-C**) Qualitative analysis of (**B**) peroxisome dispersion and (**C**) Golgi dispersion. Cargo localization in individual cells was scored as clustered (black), partially dispersed (dark grey), diffusely dispersed (light grey), or peripherally dispersed (white) 8 hours after recruitment of teams. The data for each construct is summarized as a stacked bar plot.

generate sufficient forces to drive transport of Golgi elements (4% of cells have Golgi dispersed to the periphery; Figure 3.1C). Thus, most kinesin motors as a team can drive transport of low-load cargo, however they show striking differences in their ability to drive the transport of high-load cargo.

3.3.2 MD simulations predict sequence divergence in the CS and NL alters CNB formation

One possible reason for differences in the ability of kinesins to drive transport of high-load cargo is sequence changes in the mechanical elements of the motor domain responsible for generation a robust power stroke [i.e. the cover-neck bundle (CNB), dashed box, Figure 3.2A]. Sequence alignment of the coverstrand across the kinesin superfamily indicates an isoleucine or valine residue is found as the C-terminal residue (CTR) of the coverstrand. The CTR is important for initiating CNB formation (Hwang et al., 2008), suggesting that CNB formation may be a shared strategy for kinesins to generate force. However, there is substantial variation in the length and sequence of the remainder of the coverstrand (Figure 3.2B).

We used molecular dynamics (MD) simulations to investigate whether sequence differences in the coverstrand (CS) and neck linker (β9 of the NL) of transport kinesins from the kinesin-1 (KIF5C), -2 (KIF17 and KIF3AB) and -3 families (KIF1A) affect CNB formation. Residues that contribute to CNB formation for each of these motors are highlighted in Figure 3.2C. The residues in the CS or β9 of the NL are each represented by a row of boxes, and the y-axis of each box corresponds to the time of the simulation. In each box, a thin horizontal yellow line indicates each time during the simulation that the residue made an interaction important for CNB formation and the percent of time the residue contributes to CNB during the simulation is denoted. Kinesin-1 motor KIF5C has stable interactions between residues in the coverstrand and residues in β9 of the NL to form a long CNB [Figure 3.2C; (Budaitis et al., 2019; Hwang et al., 2008)].

There were notable differences in the length of CNB formation for kinesin-2 and kinesin-3 motors. Specifically, kinesin-2 motor KIF3A forms a long CNB, like kinesin-1 KIF5C (Figure 3.2C). However, kinesin-2 motor KIF3B has a proline residue in the middle of β9 of the NL that is predicted to shorten CNB formation (Figure 3.2C). Thus, as a heterodimer, KIF3AB motors have one motor head that forms a long CNB (KIF3A)

and one motor head that forms a short CNB (KIF3B), providing a unique opportunity to study the mechanism of force generation. Conversely, the homodimeric kinesin-2 motor KIF17 has a short coverstrand and a proline residue in the middle of β9 of the NL that collectively lead to a short CNB (Figure 3.2C). Finally, the kinesin-3 motor KIF1A has a short coverstrand composed of mainly alanine and glycine residues (Figure 3.2B), which have low propensities to form a beta sheet (Kim & Berg, 1993). Our MD simulations suggest that residues of the CS and β9 of the NL transiently interact to form the CNB, suggesting weak/dynamic CNB formation (Figure 3.2C). This is consistent with MD simulations of another kinesin-3 motor KIF13B (Ren et al., 2018). Overall, our MD simulations suggest that sequence divergence in the CS and β9 of the NL lead to differences in CNB formation for kinesin motors within and between kinesin families.

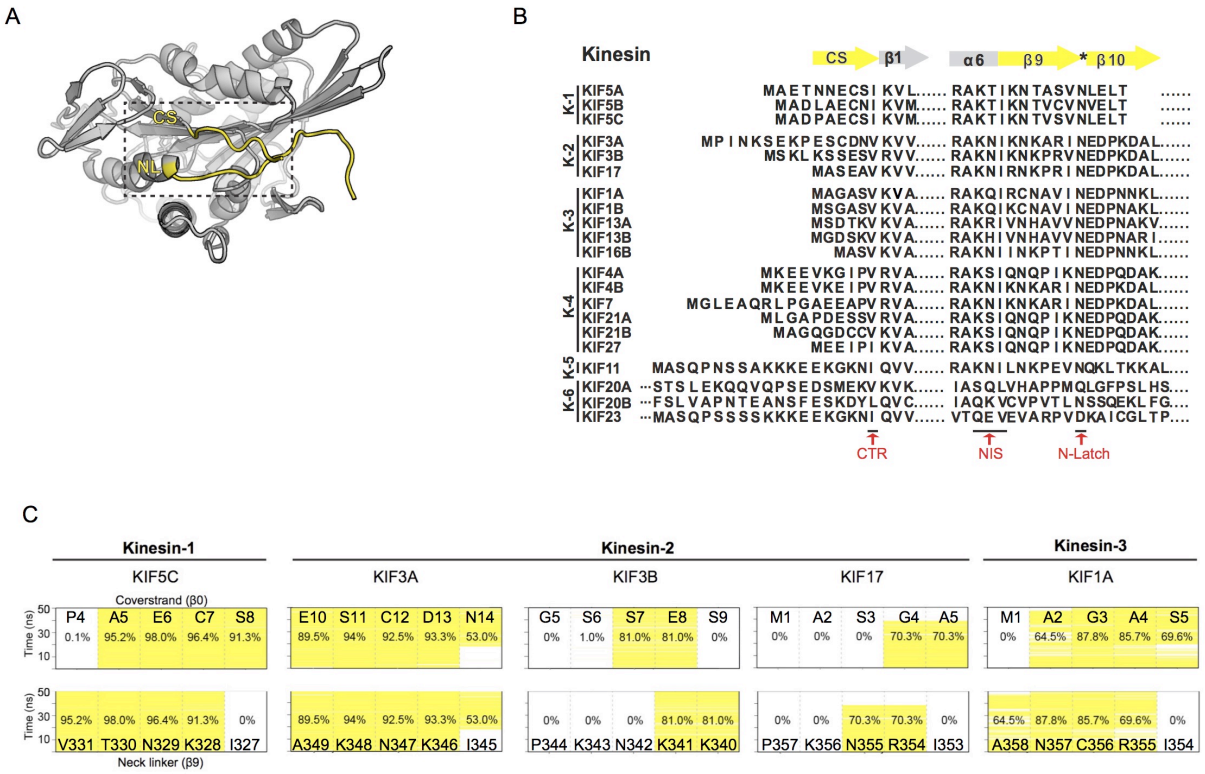

Figure 3.2 Sequence changes in the CS and NL of kinesin-1, -2, and -3 families are predicted to affect CNB formation

(**A**) Cartoon representation of the kinesin-1 motor domain in the ATP-bound, post-power stroke state (PDB 4HNA). Elements important for CNB formation are colored in yellow. Coverstrand (CS); Neck linker (NL). (**B**) Comparison of the sequence of the coverstrand (CS) and neck linker (NL) across kinesin-1, -2, -3, -4, -5, and -6 families. (**C**) MD simulations of CNB formation of motors in the kinesin-1, -2, and -3 families. The residues in the CS or β9 of the NL are each represented by a row of boxes, and the y-axis of each box corresponds to the time of the simulation. In each box, a thin horizontal yellow line indicates each time during the simulation that the residue made an interaction important for CNB formation; the percent of time that the residue contributes to CNB during the simulation is denoted within each box.

3.3.3 Truncation of the kinesin-1 CS enhances motility of single motors under no-load but severely cripples motility under load.

Notably, the length of the CS is highly variable across the kinesin superfamily. Deletion of the entire coverstrand was previously reported to impair force generation for single *Drosophila melanogaster* kinesin-1 motors in an optical trap (Khalil et al., 2008). However, whether shortening the CS and consequently the number of residues that contribute to CNB formation can tune rather than cripple the force output of a motor is not clear. To delineate the importance of the length of the CS for kinesin-1 motility, we generated mutations that shorten the CS by three (Δ3), six (Δ6), or nine residues (Δ9, Figure 3.3A) and used single-molecule motility assays to examine the behavior of the CS truncation mutants under unloaded and loaded conditions.

Cell lysates containing kinesin-1 *Rn*KIF5C(1-560) motors tagged with three tandem monomeric citrine (mCit) fluorescent proteins were added to flow chambers containing polymerized microtubules and their single-molecule, unloaded motility was examined using total internal reflection fluorescence (TIRF) microscopy. The velocity, run length, and microtubule-landing rate were determined from kymograph analysis and kymographs are displayed with time displayed horizontally and distance vertically (Figure 3.3B). Motility events were quantified for each motor and summarized as a histogram or dot plot (Figure 3.3C-D). Remarkably, motors with a coverstrand lacking three or six residues were faster (Δ3: 936± 6 nm/s and Δ6: 1033±5 nm/s) and more processive (Δ3: 3.0±0.2 μm and Δ6: 8.6±0.2 μm) compared to the WT motor (733±8 nm/s, 1.2±0.07 μm, Figure 3.3C,D). Motors with the entire coverstrand removed were similar speeds (Δ9: 747±14 nm/s) but were more processive (Δ9: 4.8±0.3 μm) than the WT motors (Figure 3.3C,D). Examination of the kymographs indicated an increase in the number of motility events for coverstrand truncation motors compared to WT motors. We therefore quantified how often Δ3, Δ6, and Δ9 motors landed on a microtubule to start a processive run (landing rate) and measured landing rates of 1.06±0.01, 1.62±0.03, 0.69±0.07 events•$\mu m^{-1} nM^{-1} s^{-1}$, respectively, compared with WT motor rate of 0.172±0.04 events•$\mu m^{-1} nM^{-1} s^{-1}$. Thus, as the CS is shortened, kinesin-1 motors become faster and more processive. This is consistent with previous studies that

find kinesin-1 motors with weakened CNB formation have enhanced unloaded motility properties (Budaitis et al., 2019; Khalil et al., 2008).

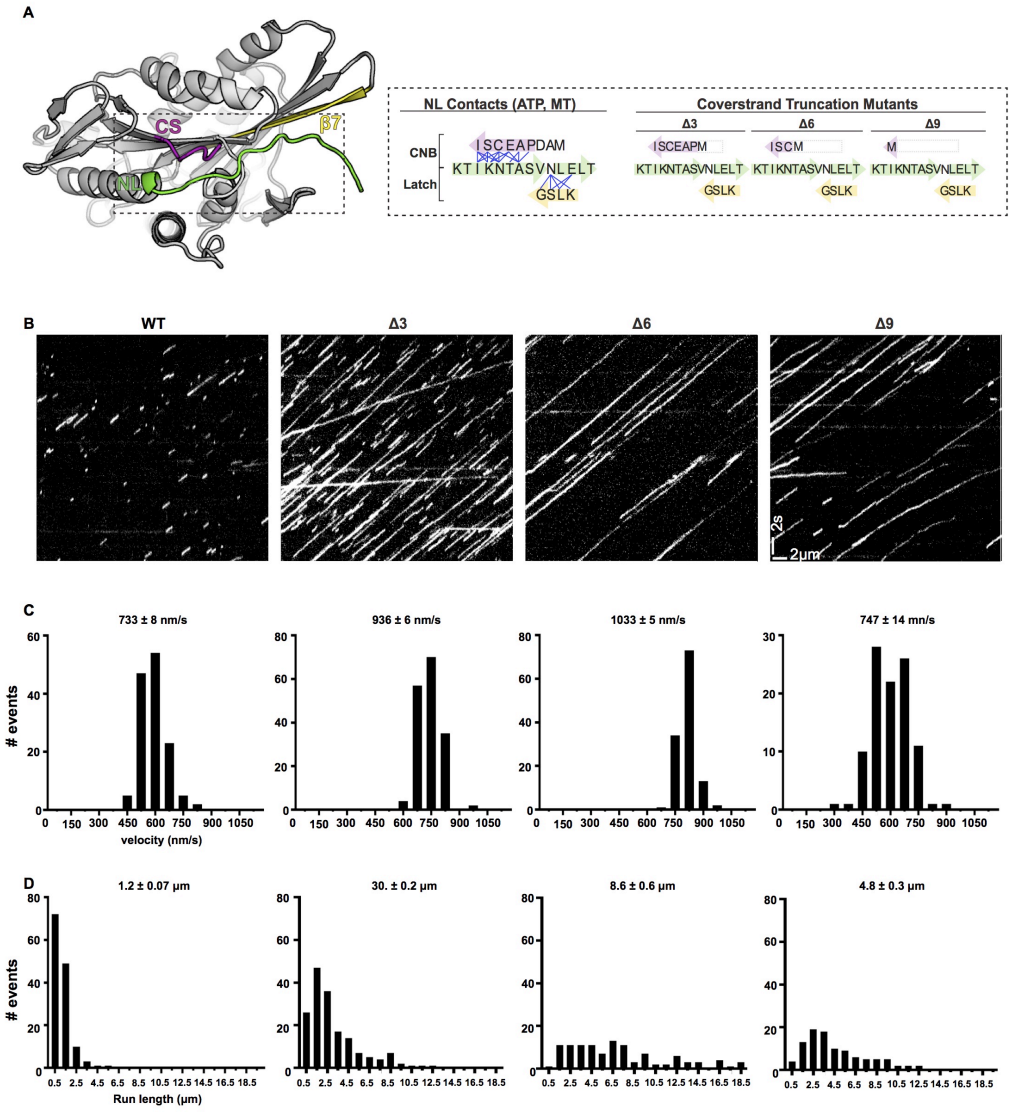

Figure 3.3 CNB truncation mutants display enhanced motility properties under single-molecule, unloaded conditions

(**A**) Cartoon ribbon representation of the kinesin-1 motor domain in the ATP-bound, post-power stroke state (PDB 4HNA). Elements important for force generation are colored as: coverstrand (CS, purple), β7 (yellow), neck linker (NL, green). (**B**) Motility properties of WT or mutant motors tagged with three tandem monomeric citrines (3xmCit) at their C-termini were analyzed in standard single-molecule motility assays using TIRF microscopy. Representative kymographs are shown with time displayed on the x-axis (bar, 2 s) and distance displayed on the y-axis (bar, 2 μm). (**C–D**) Quantification of motility properties. From the kymographs, single-motor (**C**) velocities and (**D**) run lengths were determined and the data for each population is plotted as a histogram.

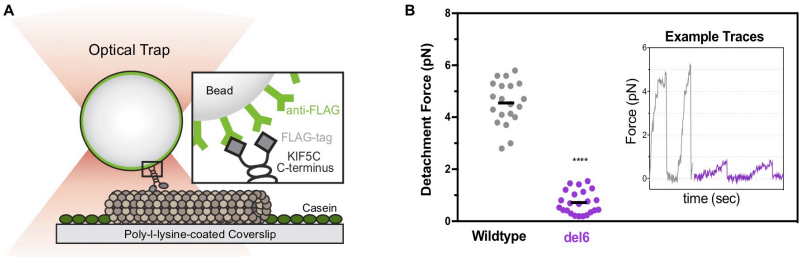

Figure 3.4 Single molecule properties of kinesin-1 CS truncation mutant under load

(**A**) Schematic of single-molecule optical trap assay. Cell lysates containing FLAG-tagged motors were incubated with beads functionalized with anti-FLAG antibodies and subjected to standard optical trapping assays. (**B**) Force generation of WT (grey) or Δ6 mutant motors (purple) under single-molecule conditions. Detachment forces are plotted as a dot plot where each dot indicates the maximum detachment force of an event and the mean for each construct is indicated by a black horizontal line. Maximum detachment forces include motility events where single motors reached a plateau stall before detachment and events where the motor abruptly detached from the microtubule. N ≥ 20 events for each construct; ***, p<0.001, compared to the WT motor. Inset includes representative traces.

We used a custom-built optical trap apparatus with nanometer-level spatial resolution to assess the effect of truncating half the coverstrand (6 residues) in kinesin-1's force output. COS-7 cell lysates containing FLAG-tagged, constitutively-active versions of WT [*Rn*KIF5C(1-560)] or the mutant version with six residues of the coverstrand removed (Δ6) were subjected to standard singe-molecule trapping assays [Figure 3.4A; (Reinemann et al., 2018; Reinemann et al., 2017; Svoboda & Block, 1994)]. Individual WT motors were motile in the absence of load, stalled on the microtubule when approaching the detachment force, and detached from the microtubule at an average force of 4.6 ± 0.8 pN (Figure 3.4B,C), consistent with previous studies (Khalil et al., 2008; Svoboda and Block, 1994). In contrast, the Δ6 mutant motors detached from the microtubule before stalling (Figure 3.4C) and at much lower loads than WT motors (mean detachment force 0.78 ± 0.47 pN, Figure 3.4B). Notably, the severity of removing 6 residues of the CS versus the entire CS on the force output of single kinesin-1 motors is comparable (Khalil et al., 2008) and suggests small changes in the length of the CS may have a dramatic impact on the force output of a motor. Collectively, our single-molecule motility data highlights an important mechanical role for the CS, where shortening the CS increases speed and processivity but at a cost to force production.

3.3.4 Truncation of the coverstrand does not affect the ability of teams of kinesin-1 motors to transport low-load cargo

Having defined the motility properties of individual kinesin-1 coverstrand truncation mutants, we sought to test whether CNB formation is critical under conditions where motors must drive the transport of membrane-bound cargo under physiological conditions. To do this, we used an inducible recruitment strategy (Kapitein et al., 2010) to link teams of motors to the surface of low-load [peroxisomes, 2-15 pN, (Efremov et al., 2014)] or high-load cargo [Golgi elements, +150 pN, (Budaitis et al., 2019; Schimert et al., 2019)] and monitored transport to the cell periphery after 30 minutes (Figure 3.5A). Dispersion was quantified by generating a radial profile of cargo intensity for each cell and converting this profile into a normalized distance distribution (Chapter 2, methods); the distance distribution was then averaged across all cells for each motor construct.

We first tested whether the integrity of CNB formation is a critical determinant for kinesin motors working in teams to drive transport of low-load cargo (peroxisomes) in cells. Specifically, COS-7 cells were cotransfected with a plasmid for expression of *Rn*KIF5C(1-560) WT or CS mutant motor tagged with monomeric NeonGreen (mNG) and FRB domain and a plasmid for expression of peroxisome-targeted PEX3-mRFP-FKBP fusion protein. In the absence of rapamycin, the PEX3-mRFP-FKBP fusion proteins localized to the peroxisome surface and peroxisomes clustered near the nucleus of the cell (Figure 3.5B, grey dashed line). The WT KIF5C-mNG-FRB proteins were diffusely localized throughout the cell. Thirty minutes after addition of rapamycin and recruitment of teams of WT kinesin-1 motors to the peroxisome surface, peroxisomes were efficiently dispersed to the cell periphery (Figure 3.5B, black line). As a team, CS truncation mutant motors are able to cooperate to transport peroxisomes to the cell periphery to a similar extent as teams of WT motors (Figure 3.5B, Δ3: magenta line, Δ9: dark purple line). These results suggest that impaired force generation by weakening CNB formation can be overcome by teams of motors for efficient transport of a low-load, membrane-bound cargo in cells, consistent with previous results (Budaitis et al., 2019; Schimert et al., 2019).

Surprisingly, peroxisomes are no longer clustered near the nucleus of the cell upon expression of the Δ6 mutant motors (-rap) and the motors are observed to decorate “filaments” throughout the cell (data not shown). Previous work demonstrates that loss of the microtubule network leads to dispersion of peroxisomes in COS-7 cells (Efremov et al., 2014). We therefore hypothesized that Δ6 truncation mutant may alter the microtubule network in cells. Current efforts are focused on understanding how binding of the motor impacts the microtubule network in cells.

3.3.5 Coverstrand truncation mutations impair the ability of teams of kinesin-1 motors to transport high-load cargo (Golgi elements) in cells

Although CNB formation was not required for teams of motors to transport peroxisomes to the cell periphery, we considered the possibility that it may be critical under conditions where motors must generate high forces and work against high loads. To address how motors cooperate in teams to transport high-load cargo in cells, we used the inducible recruitment strategy (Figure 3.5A) to link teams of motors to the Golgi membrane using a GMAP210p Golgi-localization sequence (Budaitis et al., 2019; Schimert et al., 2019) and monitored cargo transport to the cell periphery after 30 min.

Before addition of rapamycin, the Golgi was clustered near the nucleus of the cell (Figure 3.5C, grey dashed line). Thirty minutes after addition of rapamycin and recruitment of teams of WT kinesin-1 motors to the Golgi surface, Golgi elements were dispersed to the cell periphery (Figure 3.5C, black line). Shortening the CS crippled the ability of motors to transport Golgi elements to the cell periphery as a majority of the Golgi remained clustered near the nucleus of the cell (Figure 3.5B, Δ3: magenta line, Δ9: dark purple line). Collectively, this suggests that impaired force generation by shortening the CS (Figure 3.4) can be overcome by grouping motors as a team for efficient transport of low-load but not high-load membrane bound cargos. Given the striking effects of shortening CNB formation on the functional output of single kinesin-1 motors and teams of kinesin-1 motors in cells, we thus hypothesized that differences in CNB formation predicted by our MD simulations may be responsible for differences in the ability kinesin-2 motors KIF17 and KIF3AB motors to drive high-load transport in cells (Figure 3.1).

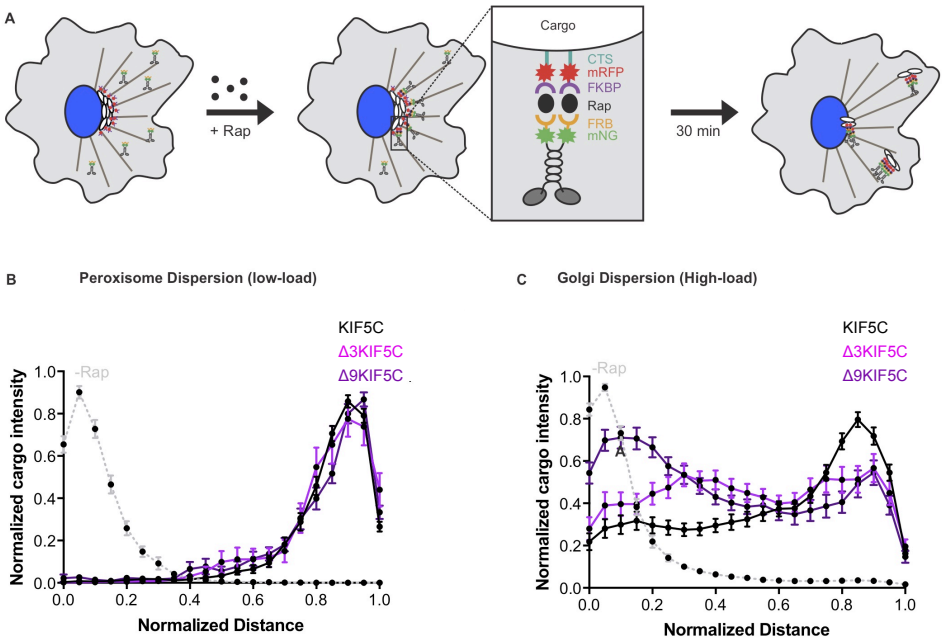

Figure 3.5 Truncation of the CS in kinesin-1 cripples the ability for teams of motors to drive high-load cargo in cells

(**A**) Schematic of the inducible motor recruitment assay. A kinesin motor tagged with monomeric NeonGreen (mNG) and an FRB domain (motor-mNG-FRB) is coexpressed with a cargo targeting sequence (CTS) tagged with monomeric red fluorescent protein (mRFP) and FKBP domain (CTS-mRFP-FKBP) in COS-7 cells. Addition of rapamycin (+Rap) causes heterodimerization of the FRB and FKBP domains and recruitment of motors to the cargo membrane. Recruitment of active motors drives cargo dispersion to the cell periphery. (**B-C**) Quantitative analysis of cargo dispersion. (**B**) Peroxisome dispersions (low-load) and (**C**) Golgi-dispersion (high-load). A radial profile of cargo intensity was generated for each cell and the data for each condition were converted to an averaged and normalized distance distribution across all cells. Each data point indicates the mean normalized cargo intensity ± SEM. Gray dotted line: WT -Rap; black line: WT +Rap; magenta line: Δ3 +Rap; dark purple line: Δ9 +Rap.

3.3.6 The ability of heterodimeric KIF3AB motors to drive high-load transport in cells is sensitive to changes in the length of the CS of KIF3A but not KIF3B

Given the high sequence identity between the KIF3A and 3B motor domains (80% sequence identity), it is unclear how each motor domain is functionally distinct from one another and how pairing their activities are advantageous in cells. Notably, our MD simulations predict that heterodimeric KIF3AB motors have one long CNB (KIF3A) and one short CNB (KIF3B) and thus offer a unique opportunity to study transport under load (Figure 3.2). We found that teams of KIF3AB motors were robust transporters of high-load cargo (Figure 3.1), and therefore predicted that long CNB formation by the KIF3A motor imparts the ability for the heterodimeric motors to drive high-load transport. To test this possibility, we truncated the sequences of KIF3A and/or KIF3B motors N-

terminal to the CS and tasked teams of mutant motors to drive transport of high-load cargo (Golgi) in cells. KIF3AB CS truncations are equivalent to Δ3 truncation for kinesin-1 (Figure 3.3).

Before addition of rapamycin, the Golgi was clustered near the nucleus of the cell (92% of cells have clustered Golgi, Figure 3.6B). Ten minutes after addition of rapamycin and recruitment of teams of WT KIF3AB motors to the Golgi surface, Golgi elements were efficiently dispersed to the cell periphery (80% of cells have peripherally dispersed Golgi, Figure 3.6B). As anticipated, truncation of the KIF3B CS did not impact the ability of KIF3AB motors to drive transport of high-load cargo to the cell periphery (86% and 80% of cells have Golgi dispersed to the cell periphery, 10 and 30 minutes after recruitment, respectively). However, truncation of the KIF3A CS moderately crippled teams of KIF3AB motors to transport high-load cargo. Specifically, it takes motors more time to drive peripheral dispersion of high-load cargo (56% and 86% of cells have peripherally dispersed Golgi 10 and 30 minutes after recruitment, Figure 3.6B). Strikingly teams of KIF3AB motors with CS truncations in both motor domains are strongly crippled in their ability to drive high-load transport (24% of cells had peripherally dispersed peroxisomes after 10 minutes) compared to heterodimeric motor where just the CS of KIF3A is truncated (56% of cells had peripherally dispersed peroxisomes after 10 minutes). These results suggest a conserved role for the CS as an important mechanical element for transport of high-load cargo and suggest that the KIF3A motor domain is critical for high-load transport. Additional studies are required to delineate whether truncating the sequence N-terminal to the CS impairs the stability of CNB formation or whether theses residues contribute to CNB formation.

Interestingly, despite the high sequence identity between the KIF3A and KIF3B motor domains (>80% sequence identity), the CSs of the two motor domains differ in their length, sequence, and charge (Figure 3.2B). Therefore, we also swapped the CS of KIF3A and KIF3B and tasked chimeric motors to drive transport of high-load cargo (Figure 3.6C). Chimeric motors where both motor domains have a KIF3A CS were able to drive high-load transport comparable to WT motors (80% of cells have peripherally dispersed Golgi compared to 80% for WT motors 10 minutes after recruitment, Figure 3.6D). However, chimeric motors where both motor domains have a KIF3B CS were

crippled in their ability to drive high-load transport (0% of cells have peripherally dispersed Golgi compared to 80% for WT motors 10 minutes after recruitment, Figure 3.6D). This effect is worsened when the CSs are swapped in both motor domains (0% of cells have peripherally dispersed Golgi compared to 80% for WT motors 10 minutes after recruitment; Figure 3.6D). Thus, swapping the CS even between closely related motors indicates that the CSs are not functionally equivalent. It is possible that the CS and β9 of the NL of a motor have co-evolved to tune the mechanical output of that motor and therefore it may be more insightful to generate point mutations rather than large sequence swaps to study the functional impact of CNB formation across the kinesin superfamily.

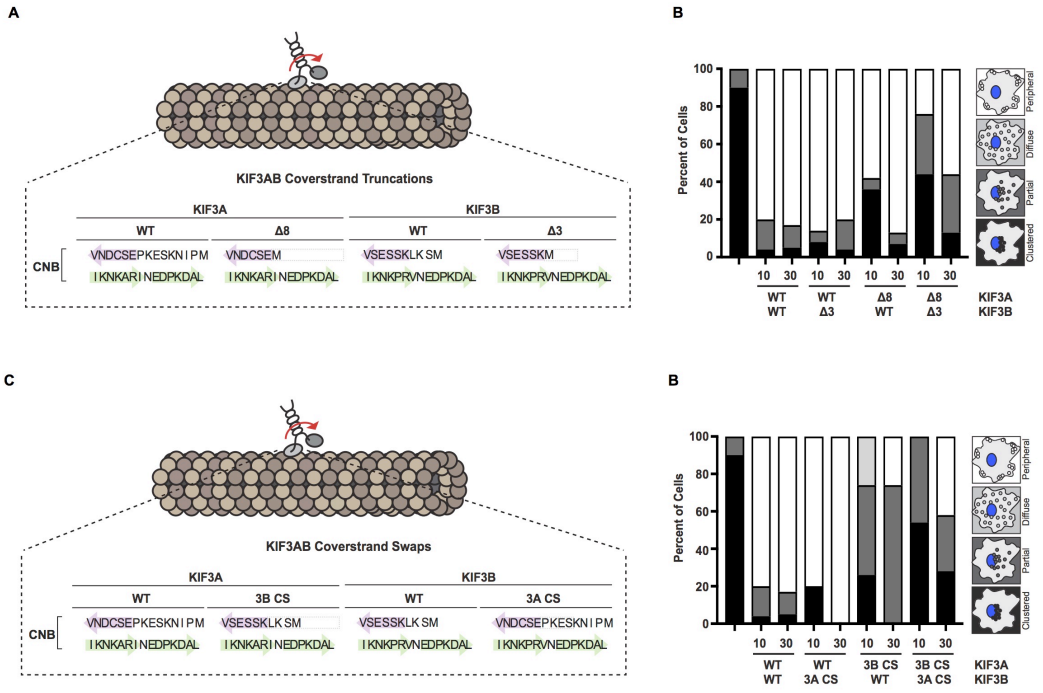

Figure 3.6 The ability for heterodimeric KIF3AB motors to drive high-load transport is sensitive to changes in the length and sequence of the CS of KIF3A but not KIF3B

(**A**, **D**) Schematic of CNB formation for WT, (**A**) CS truncation, and (**C**) CS swap mutant KIF3A and KIF3B motors. (**B, D**) Qualitative analysis of Golgi dispersion by (**B**) KIF3AB CS truncation mutants and (**D**) KIF3AB CS swap mutants. Cargo localization in individual cells was scored as clustered (black), partially dispersed (dark grey), diffusely dispersed (light grey), or peripherally dispersed (white) 10 and 30 minutes after recruitment of teams to the surface of the Golgi. The data for each construct are summarized as a stacked bar plot.

3.3.7 Strengthening CNB formation does not enhance the ability for teams of KIF17 motors to drive high-load transport in cells

Homodimeric kinesin-2 KIF17 motors have a short coverstrand as well as a proline residue in β9 that are collectively predicted to shorten the number of residues that contribute to CNB formation (Figure 3.2). Therefore, we generated sequence changes in the CS of KIF5C to make CNB formation similar to KIF17. Specifically, we (1) shortened the KIF5C CS to the same length as the CS of KIF17 motors (Δ4), (2) mutated residue V331 to a proline in β9 (V331P), and (3) combined the CS truncation and β9 mutation (Δ4+V331P) and tasked motors to collectively drive transport of high-load cargo in cells (Figure 3.7A). Strikingly, either strategy cripples the ability of teams of kinesin-1 motors to drive transport of high-load cargo after eight hours compared to WT kinesin-1 (Figure 3.7B; 2%, 43%, and 81% of cells have diffusely dispersed Golgi, for Δ4, V331P, and WT, respectively). Combining the Δ4 CS truncation and V331P point mutations did not further cripple the ability for teams of motors to drive high-load transport (Figure 3.7B; 57% cells has dispersed Golgi). Collectively, this suggests that the sequence changes in KIF17 may have the potential to cripple its ability to drive the transport of high-load cargo in cells (Figure 3.1).

We also generated the converse sequence changes in the CS and NL of KIF17 to lengthen CNB formation. Specifically, we (1) swapped the KIF17 CS with the longer KIF5C coverstrand, (2) mutated the proline residue in β9 of the NL to a valine residue (P339V), or (3) combined the CS swap and β9 mutation (5C CS+P339V) and tasked mutant motors to drive transport of high-load cargo in cells (Figure 3.7A). Strikingly, elongation of the CS and removal of the proline residue in β9 of the NL of KIF17 did not enhance the ability of teams of motors to drive the transport of high-load cargo in cells (98% of cells have clustered Golgi for P339V; 97% of cells have clustered Golgi for 5C CS; 96% of cells have clustered Golgi for 5C CS+P339V; and 89% of cells have clustered Golgi for WT; Figure 3.7B). Swapping the KIF17 CS with the CS from kinesin-2 KIF3A also had no effect (data not shown).

To assess whether the inability of teams of KIF17 motors to drive Golgi dispersion was due to the increased load imposed by this cargo, we repeated the assay where the contribution of cytoplasmic dynein to Golgi clustering was reduced. To do

this, we overexpressed a truncated dynein intermediate chain 2 (IC2-N237) that acts in a dominant negative (DN) manner to block endogenous dynein function and causes partial dispersion of the Golgi complex [Figure 3.8A,B, (Blasius et al., 2013; King, 2003)]. In cells overexpressing the dynein DN, transport of Golgi elements by teams of KIF17 motors was moderately enhanced compared to KIF17 motors targeted to Golgi elements with associated dynein motors (48% of cells have clustered Golgi, 82% of cells have clustered Golgi, respectively, Figure 3.8B). These results indicate that opposing forces generated by Golgi-associated dynein motors may partially contribute to the inability of teams of KIF17 motors to disperse the Golgi. However, this also suggests that there are effects other than the force output of KIF17 that may affect this motor's ability to drive dispersion of the Golgi.

3.4 Discussion

Recent optical trap studies find that kinesin motors have differences in their force output as single motors. Moreover, we find that most kinesins motors are able to drive the transport of low-load cargo in cells but note differences in their abilities to drive high-load transport (Figure 3.1). Although the molecular elements important for kinesin-1 motors to generate force are better understood (cover-neck bundle formation and NL latching), whether these elements are responsible for differences in high-load transport by other kinesin family members is not clear. Our MD simulations suggest that sequence difference in the CS and NL change the length and stability of the CNB for other transport kinesins (kinesin-1, -2, and -3 families). We find that truncating the CS in kinesin-1 and kinesin-2 motor cripples their ability to drive high-load transport in cells, consistent with the proposed role of the CS for generation of a power stroke. Notably, this is the first evidence that CNB formation is critical for high-load transport by an N-terminal kinesin motor other than kinesin-1 and suggests that modulation of CNB formation may serve an important role to tune the functional output of a motor.

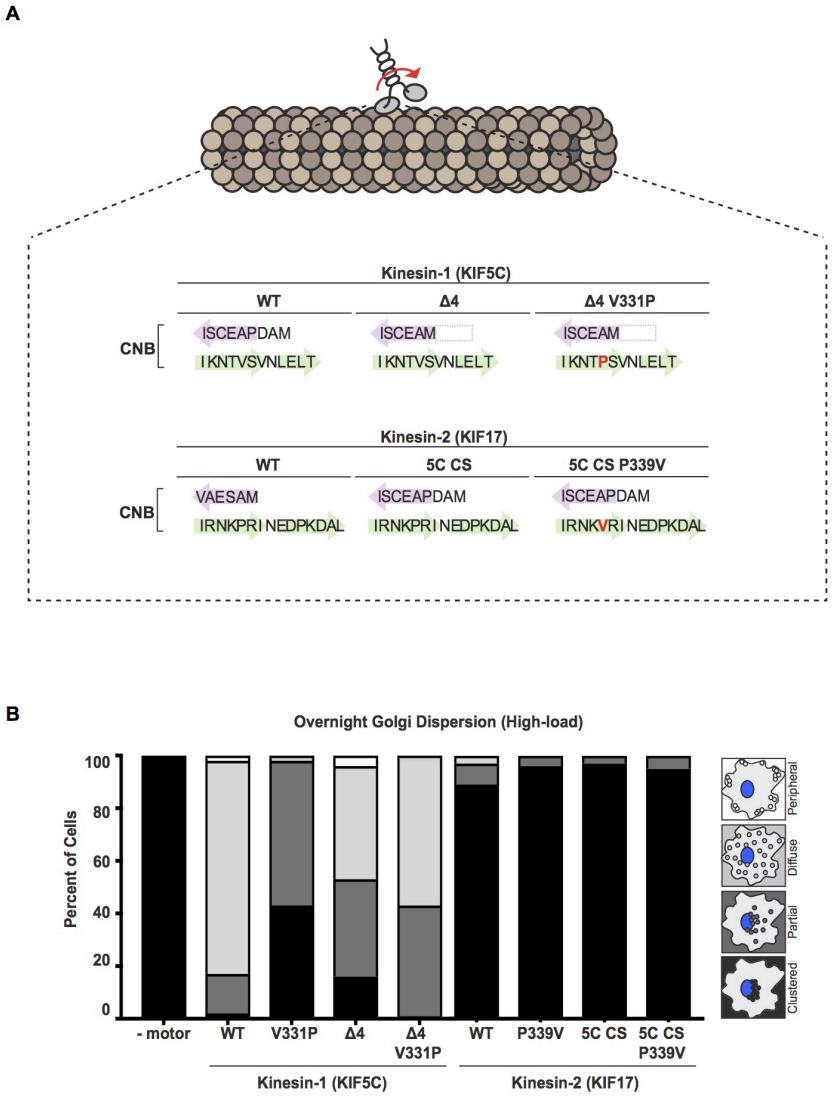

Figure 3.7 Strengthening CNB formation and NL docking does not modulate the ability for KIF17 motors to drive high-load transport in cells

(**A**) Schematic of CNB mutations in kinesin-1 KIF5C and kinesin-2 KIF17. (**B**) Qualitative analysis of Golgi dispersion by KIF5C and KIF17 CNB mutants. Cargo localization in individual cells was scored as clustered (black), partially dispersed (dark grey), diffusely dispersed (light grey), or peripherally dispersed (white) 8 hours after recruitment of teams. The data for each construct are summarized as a stacked bar plot.

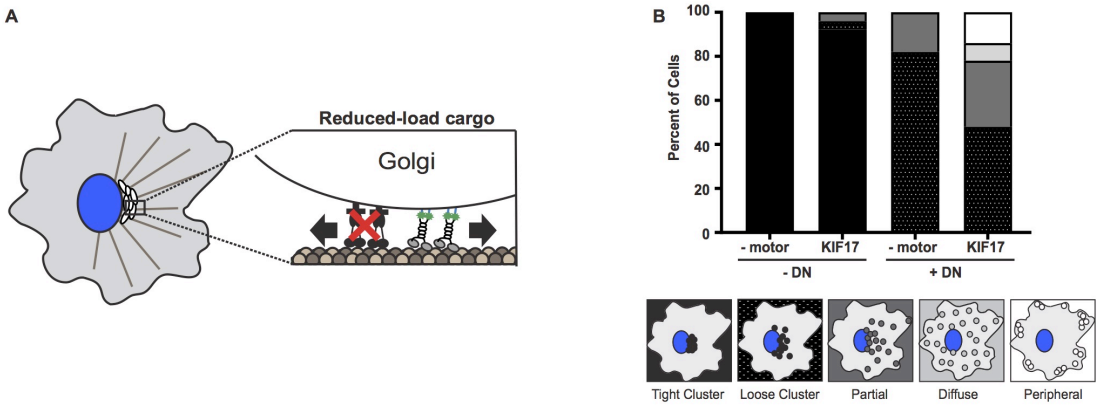

Figure 3.8 Teams of KIF17 motors are moderate transporters of reduced-load Golgi

(**A**) Schematic of Golgi dispersion assay with reduced-load. A truncated dynein intermediate chain (IC2), which acts as a dominant negative (DN) for dynein function, was expressed to interfere with dynein association with Golgi elements. In cells expressing the dynein DN, Golgi elements are a reduced-load for recruited kinesin-1 motors. (**B**) Qualitative analysis of Golgi dispersion by teams of KIF17. Cargo localization in individual cells was scored as tightly clustered (black), loosely clustered (black with white dots), partially dispersed (dark grey), diffusely dispersed (light grey), or peripherally dispersed (white) 8 hours after recruitment of teams. The data for each construct is summarized as a stacked bar plot.

3.4.1 CNB formation across the kinesin superfamily

Our results combined with previous studies of CNB formation in kinesin-1 motors (Budaitis et al., 2019; Hesse et al., 2013; Hwang et al., 2008; Khalil et al., 2008), provide a model for how differences in CNB formation may tune the force output of a motor. Specifically, the (1) sequence of the CS, (2) length of the CS, and (3) interactions of the NL with the docking pocket are predicted to be important for generation of a power stroke and transport against load. Furthermore, this may serve as a guide to assess the contribution of CNB formation to the motility of other kinesins across the kinesin superfamily.

3.4.1.1 Sequence of the CS

Previous molecular dynamics simulations of CNB formation in kinesin-1 suggest that backbone-backbone interactions between the CS and β9 of the NL drives formation of a β-sheet called the cover-neck bundle (CNB). The C-terminal residue of the CS and N-terminal residue of the NL in kinesins are hydrophobic residues with high propensities to form a β-sheet [CTR, isoleucine or valine; NTR isoleucine; Figure 2.2; (Kim & Berg, 1993)]. Interactions between the CTR and NTR are predicted to be important for

initiating formation of the CNB. The remaining residues of the CS and β9 form backbone-backbone interactions to lengthen the CNB. Therefore, the specific amino acid residues of the CS are not predicted to affect CNB formation. Indeed, the sequence of the CS across the kinesin superfamily is highly variable [Figure 3.2 ,(Hwang et al., 2008)].

Although most amino acid residues can contribute to backbone-backbone interactions with β9 of the NL to form the CNB, the CS of some kinesins have a number of residues that have poor propensities to form a β-sheet. For instance, motors in the kinesin-4 family have a proline residue following the CTR of the CS (Figure 3.2B) that and may kink β9 to break or shorten the CNB. The force output of motors in the kinesin-4 family is not well understood, therefore whether the proline residue impacts the motility properties of kinesin-4 motors remains to be tested. In addition, the CS of kinesin-3 motors have a number of residues with low propensities to form a β-sheet [alanine or glycine; (Kim & Berg, 1993)]. Mutating two residues of the coverstrand of kinesin-1 to glycine residues dramatically compromises the force output of single motors in an optical trap and teams driving the transport of high-load cargo in cells (Budaitis et al., 2019; Khalil et al., 2008). Therefore, it is possible that alanine and glycine residues contribute to the reduced stability of CNB formation predicted by MD simulations [Figure, 3.2; (Ren et al., 2018)].

3.4.1.2 Length of the CS

Previous molecular dynamics simulations suggest that the CTR and the next 5 residues of the CS form interactions with β9 of the NL to form the CNB (Hwang et al., 2008). We find that removing the N-terminal half of the residues that contribute to CNB formation (Δ6KIF5C; Figure 3.1A) severely compromises the force output of single motors in an optical trap (Figure 3.4). The severity of this truncation is comparable to the force output of a kinesin-1 motor where the entire CS was deleted (Khalil et al., 2008). Therefore, even small changes to compromise CNB formation can have dramatic effects on the force output of kinesin-1. Whether this holds true for other kinesins is not clear.

In addition, most kinesin motors have additional residues at the N-terminal end of the CS (Figure 3.2) and their contribution to the force output of a motor is not clear. We find that deleting the N-terminal portion of the CS that is not predicted to contribute to CNB formation in kinesin-1 (Δ3KIF5C, Figure 3.1A) compromises the ability of teams to transport high-load cargo in cells (Figure 3.5). Therefore, although residues N-terminal to the CS may not form important interactions that directly contribute to CNB, it is possible that this added length is important for the overall stability of the β-sheet. Comparable CS truncations in KIF3AB motors also cripple the ability of teams of motors to drive high-load transport in cells (Figure 3.6B). Although the force output of teams of KIF3AB motors is reduced, additional work is needed to determine whether these residues form important interactions with the NL to directly contribute to CNB formation.

Strikingly, in addition to having a number of residues with low propensities to form a β-sheet, motors in the kinesin-3 family lack the N-terminal sequence of the CS (Figure 3.2B). Our MD simulations suggest that CNB formation is shorter and less stable in KIF1A, consistent with previous MD simulations of the kinesin-3 motor KIF13B (Ren et al., 2018). Additional work is need to assess how the CS in kinesin-3 motors impacts their motility and whether a short, dynamic CS is responsible for the sensitivity of KIF1A to detach from the microtubule track under low loads (Arpăg et al., 2014; Norris et al., 2014).

3.4.1.3 Interactions between β9 of the NL and the docking pocket

ATP-dependent CNB formation causes generation of a power stroke and positions the NL into the docking pocket (α1-β3, β7, Loop13-β8) of the motor domain. After CNB formation, the asparagine residue between β9 and β10 of the NL begins the process of NL latching in kinesin-1(Hwang et al., 2008). NL latching is important for kinesin-1 motors to transport continuously under load (Budaitis et al., 2019). However, in kinesin-5 motors, Loop13 of the docking pocket is predicted to interact with β9 of the NL so that as the CNB forms to generate a power stroke, interactions between β9 and the docking pocket latch the NL down to the core motor domain. This is predicted to reduce the likelihood of NL undocking in response to force and compensate for poor CNB formation, thereby enabling kinesin-5 motor to transport under moderate forces

(Hesse et al., 2013; Valentine et al., 2006). Conversely, previous work has implicated that sequences changes to Loop13 can change the conformation of the NL docking pocket in kinesin-1 to sterically block CNB formation and NL docking (Case et al., 2000; Hwang et al., 2008). It is possible that bulky residues from Loop13 or other elements that make up the docking pocket, may decouple CNB formation with positioning of the NL into the docking pocket, and therefore decouple force production and stepping. Although, Loop13 is highly conserved across the kinesin superfamily, there are sequence changes that introduce bulky residues in Loop13 of kinesin-2 and -6 motors. Whether this is a strategy that modulates the force output of other kinesins is not clear.

3.4.2 Allosteric implications for CNB formation

Surprisingly we find that kinesin-1 motors with a short CS exhibit enhanced motility properties under unloaded conditions. Specifically, Δ3 and Δ6KIF5C motors displayed enhanced velocity (Figure 3.3). This is consistent with previous studies of kinesin-1 with glycine mutations to weaken CNB formation (Budaitis et al., 2019; Khalil et al., 2008). In CS truncation mutants, the enhanced velocity is likely due to allosteric effects of CNB formation and NL docking on core motor regions that coordinate and bind nucleotide and could result in enhanced catalytic closure that would favor ATP hydrolysis. Collectively, these results highlight how subtle changes in NL docking elements (CS, β9, N-latch/β10) can act as a molecular gearshift, where speed and processivity comes at the cost of robust force production. Whether this tradeoff is true for other kinesins family members is not clear.

3.4.3 Other factors that may affect high-load transport

Our molecular dynamics simulations suggest that the short length of the coverstrand and a proline residue in β9 of the NL reduces the number of residues that can contribute to cover-neck bundle formation for kinesin-2 motors KIF17 and KIF3B. Consistent with this prediction, teams of KIF17 motors were able to drive the transport of low- but not high-load cargo to the cell periphery. However, mutations predicted to lengthen CNB formation in KIF17 did not enhance the ability for teams of motors to drive high load-transport. Strikingly, recent optical trap studies demonstrate that KIF17

is able to continuously transport against high forces under single molecule conditions [6 pN stall force; (Milic et al., 2017)].

The disparity between KIF17's single molecule motility properties and its inability to drive high-load transport in cells is puzzling. KIF17 is best known for its function in driving intraflagellar transport in primary cilia and vesicle transport in neurons (Hirokawa et al., 2010; Verhey, Dishinger, & Kee, 2011), situations that both have specialized compartments with tight regulation of transport. Therefore, it is possible that high- and low-load artificial cargo assays are not a good method to probe the functional output of KIF17. One possibility is that the activity of KIF17 is regulated in an unanticipated manner in the cytoplasm of cells. For instance, the functional output of KIF17 may be regulated by post-translational modifications or by proteins that directly bind to KIF17. Indeed, kinesin binding protein (KBP) was recently identified to bind to the motor domain of KIF1A, preventing its association with microtubules in neurons (Kevenaar et al., 2016).

Another possibility is that KIF17 requires a specific subset of microtubules drive transport. However, increasing polyglutamylation, acetylation, or detyrosination of microtubules in COS-7 cells did not enhance the ability for teams of KIF17 motors to drive high-load transport (data not shown). Therefore, recruitment of KIF17 motors to cargo it's native cellular context may be a better strategy to understand its transport properties in cells (Engelke et al., 2019; Franker et al., 2016).

Finally, it is also possible that the as a single motor, KIF17 is robust at transporting high-load but as a team the motors are unexpectedly unable to cooperate. To address this possibility, it will be important to characterize the motility properties of defined numbers of KIF17 motors (Derr et al., 2012; Furuta et al., 2013; Grover et al., 2016; Norris et al., 2014) and compare this to their behavior as single motors.

3.5 References

Andreasson, J. O., Shastry, S., Hancock, W. O., & Block, S. M. (2015). The Mechanochemical Cycle of Mammalian Kinesin-2 KIF3A/B under Load. *Curr Biol, 25*(9), 1166-1175. doi:10.1016/j.cub.2015.03.013

Arpağ, G., Shastry, S., Hancock, W. O., & Tuzel, E. (2014). Transport by populations of fast and slow kinesins uncovers novel family-dependent motor characteristics

important for in vivo function. *Biophys J, 107*(8), 1896-1904. doi:10.1016/j.bpj.2014.09.009

Asenjo, A. B., Weinberg, Y., & Sosa, H. (2006). Nucleotide binding and hydrolysis induces a disorder-order transition in the kinesin neck-linker region. *Nat Struct Mol Biol, 13*(7), 648-654. doi:10.1038/nsmb1109

Atherton, J., Farabella, I., Yu, I. M., Rosenfeld, S. S., Houdusse, A., Topf, M., & Moores, C. A. (2014). Conserved mechanisms of microtubule-stimulated ADP release, ATP binding, and force generation in transport kinesins. *Elife, 3*, e03680. doi:10.7554/eLife.03680

Atherton, J., Yu, I. M., Cook, A., Muretta, J. M., Joseph, A., Major, J., . . . Moores, C. A. (2017). The divergent mitotic kinesin MKLP2 exhibits atypical structure and mechanochemistry. *Elife, 6*. doi:10.7554/eLife.27793

Blasius, T. L., Reed, N., Slepchenko, B. M., & Verhey, K. J. (2013). Recycling of kinesin-1 motors by diffusion after transport. *PLoS One, 8*(9), e76081. doi:10.1371/journal.pone.0076081

Brownhill, K., Wood, L., & Allan, V. (2009). Molecular motors and the Golgi complex: staying put and moving through. *Semin Cell Dev Biol, 20*(7), 784-792. doi:10.1016/j.semcdb.2009.03.019

Budaitis, B. G., Jariwala, S., Reinemann, D. N., Schimert, K. I., Scarabelli, G., Grant, B. J., . . . Verhey, K. J. (2019). Neck linker docking is critical for Kinesin-1 force generation in cells but at a cost to motor speed and processivity. *Elife, 8*. doi:10.7554/eLife.44146

Cao, L., Cantos-Fernandes, S., & Gigant, B. (2017). The structural switch of nucleotide-free kinesin. *Sci Rep, 7*, 42558. doi:10.1038/srep42558

Case, R. B., Rice, S., Hart, C. L., Ly, B., & Vale, R. D. (2000). Role of the kinesin neck linker and catalytic core in microtubule-based motility. *Curr Biol, 10*(3), 157-160. doi:10.1016/s0960-9822(00)00316-x

Clancy, B. E., Behnke-Parks, W. M., Andreasson, J. O., Rosenfeld, S. S., & Block, S. M. (2011). A universal pathway for kinesin stepping. *Nat Struct Mol Biol, 18*(9), 1020-1027. doi:10.1038/nsmb.2104

Dogan, M. Y., Can, S., Cleary, F. B., Purde, V., & Yildiz, A. (2015). Kinesin's front head is gated by the backward orientation of its neck linker. *Cell Rep, 10*(12), 1967-1973. doi:10.1016/j.celrep.2015.02.061

Efremov, A. K., Radhakrishnan, A., Tsao, D. S., Bookwalter, C. S., Trybus, K. M., & Diehl, M. R. (2014). Delineating cooperative responses of processive motors in living cells. *Proc Natl Acad Sci U S A, 111*(3), E334-343. doi:10.1073/pnas.1313569111

Engelke, M. F., Waas, B., Kearns, S. E., Suber, A., Boss, A., Allen, B. L., & Verhey, K. J. (2019). Acute Inhibition of Heterotrimeric Kinesin-2 Function Reveals Mechanisms of Intraflagellar Transport in Mammalian Cilia. *Curr Biol, 29*(7), 1137-1148 e1134. doi:10.1016/j.cub.2019.02.043

Franker, M. A., Esteves da Silva, M., Tas, R. P., Tortosa, E., Cao, Y., Frias, C. P., . . . Hoogenraad, C. C. (2016). Three-Step Model for Polarized Sorting of KIF17 into Dendrites. *Curr Biol, 26*(13), 1705-1712. doi:10.1016/j.cub.2016.04.057

Gigant, B., Wang, W., Dreier, B., Jiang, Q., Pecqueur, L., Pluckthun, A., . . . Knossow, M. (2013). Structure of a kinesin-tubulin complex and implications for kinesin motility. *Nat Struct Mol Biol, 20*(8), 1001-1007. doi:10.1038/nsmb.2624

Guzik-Lendrum, S., Rank, K. C., Bensel, B. M., Taylor, K. C., Rayment, I., & Gilbert, S. P. (2015). Kinesin-2 KIF3AC and KIF3AB Can Drive Long-Range Transport along Microtubules. *Biophys J, 109*(7), 1472-1482. doi:10.1016/j.bpj.2015.08.004

Hahlen, K., Ebbing, B., Reinders, J., Mergler, J., Sickmann, A., & Woehlke, G. (2006). Feedback of the kinesin-1 neck-linker position on the catalytic site. *J Biol Chem, 281*(27), 18868-18877. doi:10.1074/jbc.M508019200

Hariharan, V., & Hancock, W. O. (2009). Insights into the Mechanical Properties of the Kinesin Neck Linker Domain from Sequence Analysis and Molecular Dynamics Simulations. *Cell Mol Bioeng, 2*(2), 177-189. doi:10.1007/s12195-009-0059-5

Hesse, W. R., Steiner, M., Wohlever, M. L., Kamm, R. D., Hwang, W., & Lang, M. J. (2013). Modular aspects of kinesin force generation machinery. *Biophys J, 104*(9), 1969-1978. doi:10.1016/j.bpj.2013.03.051

Hirokawa, N., Niwa, S., & Tanaka, Y. (2010). Molecular motors in neurons: transport mechanisms and roles in brain function, development, and disease. *Neuron, 68*(4), 610-638. doi:10.1016/j.neuron.2010.09.039

Hirokawa, N., Noda, Y., Tanaka, Y., & Niwa, S. (2009). Kinesin superfamily motor proteins and intracellular transport. *Nat Rev Mol Cell Biol, 10*(10), 682-696. doi:10.1038/nrm2774

Huang, C. F., & Banker, G. (2012). The translocation selectivity of the kinesins that mediate neuronal organelle transport. *Traffic, 13*(4), 549-564. doi:10.1111/j.1600-0854.2011.01325.x

Hwang, W., Lang, M. J., & Karplus, M. (2008). Force generation in kinesin hinges on cover-neck bundle formation. *Structure, 16*(1), 62-71. doi:10.1016/j.str.2007.11.008

Isojima, H., Iino, R., Niitani, Y., Noji, H., & Tomishige, M. (2016). Direct observation of intermediate states during the stepping motion of kinesin-1. *Nat Chem Biol, 12*(4), 290-297. doi:10.1038/nchembio.2028

Kapitein, L. C., Schlager, M. A., van der Zwan, W. A., Wulf, P. S., Keijzer, N., & Hoogenraad, C. C. (2010). Probing intracellular motor protein activity using an inducible cargo trafficking assay. *Biophys J, 99*(7), 2143-2152. doi:10.1016/j.bpj.2010.07.055

Khalil, A. S., Appleyard, D. C., Labno, A. K., Georges, A., Karplus, M., Belcher, A. M., . . . Lang, M. J. (2008). Kinesin's cover-neck bundle folds forward to generate force. *Proc Natl Acad Sci U S A, 105*(49), 19247-19252. doi:10.1073/pnas.0805147105

Kim, C. A., & Berg, J. M. (1993). Thermodynamic beta-sheet propensities measured using a zinc-finger host peptide. *Nature, 362*(6417), 267-270. doi:10.1038/362267a0

King, S. M. (2003). Organization and regulation of the dynein microtubule motor. *Cell Biol Int, 27*(3), 213-215. doi:10.1016/s1065-6995(02)00337-2

Kozielski, F., Sack, S., Marx, A., Thormahlen, M., Schonbrunn, E., Biou, V., . . . Mandelkow, E. (1997). The crystal structure of dimeric kinesin and implications for microtubule-dependent motility. *Cell, 91*(7), 985-994. doi:10.1016/s0092-8674(00)80489-4

Liu, D., Liu, X., Shang, Z., & Sindelar, C. V. (2017). Structural basis of cooperativity in kinesin revealed by 3D reconstruction of a two-head-bound state on microtubules. *Elife, 6*. doi:10.7554/eLife.24490

Milic, B., Andreasson, J. O. L., Hogan, D. W., & Block, S. M. (2017). Intraflagellar transport velocity is governed by the number of active KIF17 and KIF3AB motors and their motility properties under load. *Proc Natl Acad Sci U S A, 114*(33), E6830-E6838. doi:10.1073/pnas.1708157114

Nitta, R., Okada, Y., & Hirokawa, N. (2008). Structural model for strain-dependent microtubule activation of Mg-ADP release from kinesin. *Nat Struct Mol Biol, 15*(10), 1067-1075. doi:10.1038/nsmb.1487

Norris, S. R., Soppina, V., Dizaji, A. S., Schimert, K. I., Sept, D., Cai, D., . . . Verhey, K. J. (2014). A method for multiprotein assembly in cells reveals independent action of kinesins in complex. *J Cell Biol, 207*(3), 393-406. doi:10.1083/jcb.201407086

Ohashi, K. G., Han, L., Mentley, B., Wang, J., Fricks, J., & Hancock, W. O. (2019). Load-dependent detachment kinetics plays a key role in bidirectional cargo transport by kinesin and dynein. *Traffic, 20*(4), 284-294. doi:10.1111/tra.12639

Reinemann, D. N., Norris, S. R., Ohi, R., & Lang, M. J. (2018). Processive Kinesin-14 HSET Exhibits Directional Flexibility Depending on Motor Traffic. *Curr Biol, 28*(14), 2356-2362 e2355. doi:10.1016/j.cub.2018.06.055

Reinemann, D. N., Sturgill, E. G., Das, D. K., Degen, M. S., Voros, Z., Hwang, W., . . . Lang, M. J. (2017). Collective Force Regulation in Anti-parallel Microtubule Gliding by Dimeric Kif15 Kinesin Motors. *Curr Biol, 27*(18), 2810-2820 e2816. doi:10.1016/j.cub.2017.08.018

Ren, J., Zhang, Y., Wang, S., Huo, L., Lou, J., & Feng, W. (2018). Structural Delineation of the Neck Linker of Kinesin-3 for Processive Movement. *J Mol Biol, 430*(14), 2030-2041. doi:10.1016/j.jmb.2018.05.010

Rice, S., Lin, A. W., Safer, D., Hart, C. L., Naber, N., Carragher, B. O., . . . Vale, R. D. (1999). A structural change in the kinesin motor protein that drives motility. *Nature, 402*(6763), 778-784. doi:10.1038/45483

Rosenfeld, S. S., Jefferson, G. M., & King, P. H. (2001). ATP reorients the neck linker of kinesin in two sequential steps. *J Biol Chem, 276*(43), 40167-40174. doi:10.1074/jbc.M103899200

Scarabelli, G., Soppina, V., Yao, X. Q., Atherton, J., Moores, C. A., Verhey, K. J., & Grant, B. J. (2015). Mapping the Processivity Determinants of the Kinesin-3 Motor Domain. *Biophys J, 109*(8), 1537-1540. doi:10.1016/j.bpj.2015.08.027

Schimert, K. I., Budaitis, B. G., Reinemann, D. N., Lang, M. J., & Verhey, K. J. (2019). Intracellular cargo transport by single-headed kinesin motors. *Proc Natl Acad Sci U S A, 116*(13), 6152-6161. doi:10.1073/pnas.1817924116

Shang, Z., Zhou, K., Xu, C., Csencsits, R., Cochran, J. C., & Sindelar, C. V. (2014). High-resolution structures of kinesin on microtubules provide a basis for nucleotide-gated force-generation. *Elife, 3*, e04686. doi:10.7554/eLife.04686

Sindelar, C. V., & Downing, K. H. (2010). An atomic-level mechanism for activation of the kinesin molecular motors. *Proc Natl Acad Sci U S A, 107*(9), 4111-4116. doi:10.1073/pnas.0911208107

Skiniotis, G., Surrey, T., Altmann, S., Gross, H., Song, Y. H., Mandelkow, E., & Hoenger, A. (2003). Nucleotide-induced conformations in the neck region of dimeric kinesin. *EMBO J, 22*(7), 1518-1528. doi:10.1093/emboj/cdg164

Soppina, V., & Verhey, K. J. (2014). The family-specific K-loop influences the microtubule on-rate but not the superprocessivity of kinesin-3 motors. *Mol Biol Cell, 25*(14), 2161-2170. doi:10.1091/mbc.E14-01-0696

Svoboda, K., & Block, S. M. (1994). Force and velocity measured for single kinesin molecules. *Cell, 77*(5), 773-784. doi:10.1016/0092-8674(94)90060-4

Tomishige, M., Klopfenstein, D. R., & Vale, R. D. (2002). Conversion of Unc104/KIF1A kinesin into a processive motor after dimerization. *Science, 297*(5590), 2263-2267. doi:10.1126/science.1073386

Tomishige, M., & Vale, R. D. (2000). Controlling kinesin by reversible disulfide cross-linking. Identifying the motility-producing conformational change. *J Cell Biol, 151*(5), 1081-1092. doi:10.1083/jcb.151.5.1081

Valentine, M. T., Fordyce, P. M., Krzysiak, T. C., Gilbert, S. P., & Block, S. M. (2006). Individual dimers of the mitotic kinesin motor Eg5 step processively and support substantial loads in vitro. *Nat Cell Biol, 8*(5), 470-476. doi:10.1038/ncb1394

Verhey, K. J., & Hammond, J. W. (2009). Traffic control: regulation of kinesin motors. *Nat Rev Mol Cell Biol, 10*(11), 765-777. doi:10.1038/nrm2782

Yildiz, A., Tomishige, M., Gennerich, A., & Vale, R. D. (2008). Intramolecular strain coordinates kinesin stepping behavior along microtubules. *Cell, 134*(6), 1030-1041. doi:10.1016/j.cell.2008.07.018

Chapter 4: KIF1A Mutations Associated with Neurodevelopmental Disorders have Allosteric Effects on Motor Output

This chapter is modified from the following manuscript:

Budaitis B.G., Jariwala S.J*, Rao L.*, Sept, D., Verhey K.J., Gennerich A. (in preparation). KIF1A mutations associated with neurodevelopmental disorders have allosteric effects on motor output.*

**equal contribution, authors listed alphabetically*

Author contributions:

B.G.B performed unloaded single-molecule TIRF assays, cellular cargo transport assays, and prepared protein for optical trapping assays; S.J. performed molecular dynamics simulations; L.R. performed optical trapping assays. B.G.B, S.J. and L.R. analyzed data and composed figures. B.G.B and K.J.V wrote the text with input from authors.

4.1 Introduction

The cytoskeleton of eukaryotic cells forms the structural framework for fundamental cellular processes including cell division, cell motility, intracellular trafficking, and cilia function. In most if not all processes, the functional output of the microtubule cytoskeleton depends on a family of molecular motor proteins called kinesins. Kinesins are defined by the presence of a kinesin motor domain that is highly conserved in both sequence and structure across the kinesin superfamily. The kinesin-3 family is one of the largest among the kinesin superfamily and its members are largely involved in the anterograde transport of cargoes toward the plus ends of the microtubules in the periphery of the cell (Hirokawa et al., 2009). Studies have shown that kinesin-3 proteins have strikingly different motility properties than other kinesins as they are fast and superprocessive and have a dramatically higher

landing rate (ability to productively engage with the microtubule) than other kinesin motors (Hammond et al., 2009; Scarabelli et al., 2015; Soppina & Verhey, 2014).

Genetic and microscopy studies have implicated mammalian KIF1A and its *C. elegans* homolog UNC-104 in the transport of synaptic vesicle precursors (SVPs) and dense core vesicles (DCVs) to the axon terminal (Barkus et al., 2008; Hall & Hedgecock, 1991; Okada et al., 1995; Yonekawa et al., 1998). Recently, a number of disease-associated genetic variants and de novo mutations have been identified in human *KIF1A* from clinical studies. These mutations have been linked to neurodevelopmental disorders, collectively termed KIF1A Associated Neurological Disorder (KAND), with a spectrum of phenotypic presentations including hereditary spastic paraplegias, intellectual disability, autism, microcephaly, peripheral neuropathy, cerebral and cerebellar atrophy, and seizures (Cheon et al., 2017; Citterio et al., 2015; Esmaeeli Nieh et al., 2015; Hasegawa et al., 2017; Hotchkiss et al., 2016; Iqbal et al., 2017; Klebe et al., 2012; Lee et al., 2015; Megahed et al., 2016; Ohba et al., 2015; Okamoto et al., 2014; Raffa et al., 2017; Roda, Schindler, & Blackstone, 2017; Samanta & Gokden, 2019; Tomaselli et al., 2017; Travaglini et al., 2018; Ylikallio et al., 2015; Yoshikawa et al., 2019). KAND mutations span the entirety of the KIF1A protein sequence; the majority are located within the kinesin motor domain (aa 1-369; Figure 4.1A) and are thus predicted to affect the motor's motility properties whereas mutations located outside the motor domain are likely involved in mediating cargo binding, dimerization, and/or autoinhibition (Hammond et al., 2009; Ren et al., 2018; Soppina et al., 2014; Tomishige et al., 2002).

Here we delineate the impact of two KAND mutations, V8M and Y89D that lie in regions of the KIF1A motor domain predicted to participate in force generation. Our understanding of how kinesin motors generate force is largely based on studies of kinesin-1, the founding member of the kinesin superfamily. Force generation requires the neck linker (NL), a flexible structural element that immediately follows the motor domain, to dock along the surface of the motor domain in response to ATP binding. NL docking occurs in two steps: "zippering" where the first half of the NL (β9) forms a short beta strand with β0 [the cover strand (CS)] to generate a cover-neck bundle (CNB) followed by "latching" where the second half of the NL (β10) interacts with surface

residues of α1-β3 and β7 of the docking pocket (Budaitis et al., 2019; Gigant et al., 2013; Hwang et al., 2008; Khalil et al., 2008). In the absence of ATP, the NL's initial docking site (the docking pocket) is occluded by the CS (Budaitis et al., 2019; Cao et al., 2014; Gigant et al., 2013; Lang & Hwang, 2010; Nitta et al., 2008; Shang et al., 2014; Sindelar & Downing, 2010). For KIF1A, the V8M mutation is located in β1, immediately following the CS (Figure 4.1B) and may therefore prevent CNB formation. Notably, a valine in this position is highly conserved across the kinesin superfamily [Figure 4.2B; (Richard et al., 2016)]. The Y89D mutation is located at the α1-β3 intersection (Figure 4.1B) and an aromatic residue (tyrosine or phenylalanine) is highly conserved at this position across the kinesin superfamily [Figure 4.2B; (Atherton et al., 2017; Budaitis et al., 2019)]. These two mutations are thus likely to impact not only the motility properties of KIF1A but also its force output.

We used molecular dynamics (MD) simulations to probe the impact of V8M and Y89D directly on NL docking as well as allosteric effects on nucleotide binding and/or hydrolysis. We used single-molecule assays to probe motor properties under no-load conditions and find that both mutations result in a decrease in speed, processivity, and landing rate on microtubules. In addition, motors containing the Y89D mutation display an increase in diffusive events. Using an optical trap assay to determine the force output of the motors, we find that KIF1A motors do not reach a stall force but readily detach from the microtubule track at 2-3 pN resisting force. The motors then quickly reattach to the microtubule and resume transport, leading to a characteristic saw tooth force pattern that is distinct from other kinesin motors to date. Both KAND mutations result in a decrease in motor force output but have no effect on the motor's ability to rapidly re-engage with the microtubule track. We then used a peroxisome-targeting assay to probe the ability of wild-type and mutant motors to work in teams to drive organelle transport in cells. We find that mutant motors show a significant delay in organelle transport. Collectively our results support the proposed role for the NL as a mechanical element important for kinesin motors to transport against load and provide insight into how KAND mutations affect KIF1A transport in cells.

4.2 Materials and Methods

Structural model preparation of KIF1A motor complex

Initial coordinates of KIF1A kinesin motor domain in the ATP-bound state (ATP analogue, AMPPNP), in complex with the tubulin heterodimer were taken from PDB 4UXP (Atherton et al., 2014). The kinesin motor domain sequence was *Hs*KIF1A (Uniprot ID Q12756). Missing coordinates, where applicable, were modeled using MODELLER v9.18 (Sali & Blundell, 1993). A total of 100 models were generated with the following options in MODELLER: variable target function method (VTFM) was set to slow with associated conjugate gradient set to 150 iterations, MD with simulated annealing option was set to slow, and the entire optimization process was repeated twice. The top-scoring model was selected for MD simulations with discrete optimized protein energy (DOPE) score (Shen & Sali, 2006) for loop refinement.

Molecular dynamics simulations of KIF1A motor complex

Energy minimization and molecular dynamics (MD) simulations were performed with AMBER 18 (Case et al., 2018) and the ff99SB AMBER force field (Hornak et al., 2006). Nucleotide parameters were obtained from (Meagher, Redman, & Carlson, 2003). Histidine protonation states were assigned based on the their pKa values calculated by PROPKA (Li, Robertson, & Jensen, 2005). The simulation setup and procedures were adopted as described (Budaitis et al., 2019; Muretta et al., 2018). MD simulations were started from equilibrated structures with at least four independent runs of at least 200 ns each. All simulations were performed in-house on NVIDIA GPU cards with the GPU version of PMEMD (pmemd.cuda). We thank NVIDIA for their gift of GPU card through their Academic GPU seed grant. Trajectory analyses were carried out in R using the Bio3D v2.3-3 package (Skjaerven et al., 2014).

Residue-residue distance differences

Statistically significant residue-residue distance differences between wild-type (WT) and mutant ATP-bound kinesin motor domains in complex with tubulin heterodimer were identified with ensemble difference distance matrix (eDDM) analysis routine (Muretta et al., 2018). For this analysis, a total of 400 conformations were

obtained for each state under comparison by extracting 100 equally time-spaced conformations from the last 20 ns of each simulation replicate. The details of obtaining the distance matrices from simulation trajectories, their processing, and the method of selecting significantly different residue-residue distances are descried previously (Budaitis et al., 2019; Muretta et al., 2018). Briefly, the eDDM routine reduces the difference between long distances while the difference between short distances are kept intact. The significance of residue distance variation between ATP-bound WT and mutant states were evaluated with the Wilcoxon test. Residue pairs showing a p-value< 10^{-5} and an average masked distance difference > 1Å were considered statistically significant residue-residue distance differences for further analysis.

Plasmids

A truncated, constitutively active kinesin-3 [rat KIF1A(1-393)] followed by a leucine zipper was used (Soppina & Verhey, 2014). Point mutations were generated using QuickChange site-directed mutagenesis and all plasmids were verified by DNA sequencing. Motors were tagged with a monomeric NeonGreen-FLAGtag, or Halo-FLAGtag for single molecule imaging assays and a monomeric NeonGreen (mNG)-FRB for inducible cargo dispersion assays in cells (Kapitein et al., 2010). The peroxisome-targeting PEX3-mRFP-FKBP construct was a gift from Casper Hoogenraad [Utrecht University, (Kapitein et al., 2010)]. Constructs coding for FRB (DmrA) and FKBP (DmrC) sequences were obtained from ARIAD Pharmaceuticals and are now available from Takara Bio Inc. Plasmids encoding monomeric NeonGreen were obtained from Allele Biotechnology.

Cell culture, transfection, and lysate preparation

COS-7 (African green monkey kidney fibroblasts, American Type Culture Collection) were grown at 37˚C with 5% (vol/vol) CO_2 in Dulbecco's Modified Eagle Medium (Gibco) supplemented with 10% (vol/vol) Fetal Clone III (HyClone) and 2 mM GlutaMAX (L-alanyl-L-glutamine dipeptide in 0.85% NaCl, Gibco). Cells are checked annually for mycoplasma contamination and were authenticated through mass spectrometry (the protein sequences exactly match those in the African green monkey

genome). 4 hr after seeding, the cells were transfected with plasmids encoding for the expression of motor tagged with Halo-FLAG or mNeonGreen-FLAG, TransIT-LT1 transfection reagent (Mirus), and Opti-MEM Reduced Serum Medium (Gibco). Cells were trypsinized and harvested 24 hr after transfection by low-speed centrifugation at 3000 x g at 4˚C for 3 min. The pellet was resuspended in cold 1X PBS, centrifuged at 3000 x g at 4˚C for 3 min, and the pellet was resuspended in 50 µL of cold lysis buffer [25 mM HEPES/KOH, 115 mM potassium acetate, 5 mM sodium acetate, 5 mM $MgCl_2$, 0.5 mM EGTA, and 1% (vol/vol) Triton X-100, pH 7.4] with 1 mM ATP, 1 mM phenylmethylsulfonyl fluoride, and 1% (vol/vol) protease inhibitor cocktail (P8340, SigmaAldrich). Lysates were clarified by centrifugation at 20,000 x g at 4˚C for 10 min and lysates were snap frozen in 5 µL aliquots in liquid nitrogen and stored at 80˚C.

TIRF single-molecule motility assays

Microtubules were polymerized (purified tubulin unlabeled and HiLyte-647-labeled tubulin, Cytoskeleton Inc) in BRB80 buffer (80 mM Pipes/KOH pH 6.8, 1 mM $MgCl_2$, 1 mM EGTA) supplemented with GTP and $MgCl_2$ and incubated for 60 min at 37°C. 2 µM taxol in prewarmed BRB80 was added and incubated for 60 min to stabilize microtubules. Microtubules were stored in the dark at room temperature for up to 2 weeks. Flow cells were prepared by attaching a #1.5 mm coverslip (Thermo Fisher Scientific) to a glass slide (Thermo Fisher Scientific) using double-sided tape. Microtubules were diluted in fresh BRB80 buffer supplemented with 10 µM taxol, infused into flow cells, and incubated for four minutes to allow for nonspecific absorption to the glass. Flow cells were then incubated with blocking buffer [30 mg/mL casein in P12 buffer (12 mM Pipes/KOH pH 6.8, 1 mM $MgCl_2$, 1 mM EGTA) supplemented with 10 µM taxol] for four minutes. Flow cells were then infused with motility mixture (0.5–1.0 µL of COS-7 cell lysate, 25 µL P12 buffer, 15 µL blocking buffer, 1 mM ATP, 0.5 µL 100 mM DTT, 0.5 µL, 0.5 µL 20 mg/mL glucose oxidase, 0.5 µL 8 mg/mL catalase, and 0.5 µL 1 M glucose), sealed with molten paraffin wax, and imaged on an inverted Nikon Ti-E/B total internal reflection fluorescence (TIRF) microscope with a perfect focus system, a 100x/1.49 NA oil immersion TIRF objective, three 20 mW diode lasers (488 nm, 561 nm, and 640 nm) and EMCCD camera (iXon+ DU879; Andor). Image acquisition was

controlled using Nikon Elements software and all assays were performed at room temperature.

Motility data were analyzed by first generating maximum intensity projections to identify microtubule tracks (width = 3 pixels) and then generating kymographs in ImageJ (National Institutes of Health). Only motility events that lasted for at least three frames were analyzed. Events that ended as a result of a motor reaching the end of a microtubule were included; therefore, the reported run lengths for highly processive motors are likely to be an underestimation. For each motor construct, the velocities and run lengths were binned and a histogram was generated by plotting the number of motility events for each bin. Motor velocities were fit to a Gaussian cumulative distribution as previously described (Arpăg et al., 2014; Norris et al., 2014) and a one-way analysis of variance test was used to assess whether velocity distributions were significantly different between motors. A Kruskal-Wallis one-way analysis of variance was used to assess whether run length distributions were significantly different between motors.

Optical trapping assay

The polystyrene trapping beads, microtubules and slides were prepared as described previously (Rao et al., 2019). Briefly, polystyrene beads with an average diameter of 500 nm (Bangs Laboratories Inc. #PC02002) were coated with streptavidin and α-casein, or with an anti-GFP antibody and α-casein. Coverslips (Zeiss #474030-9000-000) were cleaned with 25% HNO_3 and 2 M NaOH, washed with ddH_2O, air dried, and stored at 4°C. The flow chamber was assembled with a glass slide, parafilm stripes, and a cleaned coverslip as described (Rao, et al., 2019). Microtubules with incorporated biotinylated tubulin were attached to the cover glass surface via α-casein-biotin and streptavidin.

Control cell lysate without KIF1A expression was tested to ensure there are no non-specific interactions between other endogenous motors in the lysate with the beads. 100 beads were tested and no force generation was observed under the same experimental conditions used for cell lysates containing tagged KIF1A constructs. Cell lysate with KIF1A was pre-diluted 50-200x. 1 µl of the predilution was incubated with 0.4

µl beads on ice for 15 min. The lysate was pre-diluted so that less than 10% of the beads showed force generation. The protein-bead mixture was diluted in 40 µL assay buffer (60 mM HEPES, 50 mM KAc, 2 mM $MgCl_2$, 1 mM EGTA, 1 mM DTT, 10 µM taxol, 2 mM ATP, 50 mM glucose oxidase, 1.25 mg/ml α-casein, 10% glycerol) and flowed into the slide chamber. All optical trapping experiments were performed with LUMICKS C-trap®, which combines optical tweezers with 3-color total internal reflection fluorescence (TIRF) microscopy and interference reflection microscopy (to visualize unlabeled MTs).

4.3 Results

4.3.1 KIF1A disease variants cluster within functionally distinct regions of the motor domain

To provide insight into how KAND mutations may affect KIF1A motility, mutations (red) were mapped onto the protein sequence (Figure 4.1A) or structure [Figure 4.1B, PDB 4UY0, (Atherton et al., 2014)] of the KIF1A motor domain. Amino acid residues within the KIF1A motor domain were colored according to their role in **(1) microtubule binding** (Loop2, Loop7, Loop8, α4, Loop12, α5; α6; dark blue), **(2) nucleotide binding and hydrolysis** [α0, Loop9/Switch1, Loop11/Switch2, PLoop (PL); cyan], **(3) or stepping and force generation** [coverstrand (CS), α1-β3, Loop13, neck linker (NL, β9-β10); blue]. A majority of KAND mutations cluster within these functional elements (21/31 mutations; Figure 4.1A,B, red). This is consistent with clustering of mutations found in other neuronal kinesins (KIF5A, KIF5C, KIF1C) linked to neurodevelopmental and/or neurodegenerative disorders [(Jennings et al., 2017), Figure 4.2A-C, red text indicates disease-associated mutations].

KIF1A motors have a unique set of positively-charged residues within Loop8, Loop11, Loop12, and α6 that make important interactions with negatively-charged residues in α- and β-tubulin throughout the ATPase cycle [Figure 4.2C, (Atherton et al., 2014; Nitta et al., 2004; Okada & Hirokawa, 1999)]. Indeed, many KAND mutations that mapped to elements important for microtubule binding [α4 (L278P); Loop12 (P305L, R307Q); α5 (R316W); α6 (R350G)] were loss-of-charge mutations (Figure 4.1A, B). Previous mutational studies have attributed these residues to be important for endowing

KIF1A motors with the enhanced microtubule-landing rate and/or super processivity, characteristics that are unique to the kinesin-3 family (Nitta et al., 2004; Scarabelli et al., 2015; Soppina & Verhey, 2014; Uchimura et al., 2010).

Additionally, a number of mutations mapped to elements important for binding and hydrolyzing nucleotide [PLoop (T99M, 102S/D); Loop9 (Switch1; A202P, S215R/H, R216C, S217Y); Loop11 (Switch 2; L249Q, E253K, R254P/W/Q, A255V), Figure 4.1A, B] that are highly conserved across the kinesin superfamily (Figure 4.2A), myosin motors, and other G-proteins (Kull, Vale, & Fletterick, 1998). Biochemical and biophysical studies assessing the function of these residues have established their conserved role in the ATPase activity of the motor domain (i.e. single-molecule velocity). In addition, motors that harbor mutations in these elements often have a reduced microtubule affinity, emphasizing an important role of allosteric communication between the nucleotide-binding pocket with elements important for microtubule binding (Auerbach & Johnson, 2005; Brendza et al., 1999; Cao et al., 2014; Jennings et al., 2017; Song & Endow, 1998; Yun et al., 2001).

Last, there are two mutations, V8M and Y89D, located in elements important for kinesin-1 motors to step against force (Figure 4.1A, B). For kinesin-1, NL docking starts with zippering of the first half (β9) of the NL with the CS (β0) to form the cover-neck bundle (CNB) (Budaitis et al., 2019; Gigant et al., 2013; Hwang et al., 2008; Khalil et al., 2008). The V8M mutation is located in β1, immediately following the CS (Figure 4.1B), and may therefore impact CNB formation and the force output of the motor. Notably a valine in this position is highly conserved across the kinesin superfamily with exception of the kinesin-10 family [Figure 4.2B; (Richard et al., 2016)]. Although formation of the CNB has been observed structurally for members of the kinesin-3, kinesin-5, and kinesin-6 families (Atherton et al., 2017; Hesse et al., 2013; Ren et al., 2018), its mechanical role in force generation has only been tested in kinesin-1 motors (Budaitis et al., 2019; Khalil et al., 2008).

Following CNB formation in kinesin-1 motors, the second half of the NL (β10) docks along the core motor domain through interactions with α1-β3 and β7 (NL docking) and uses a conserved asparagine residue to “latch” these interactions [the N-latch, (Budaitis et al., 2019; Hwang et al., 2008)]. The KAND mutation Y89D is located at the

intersection between α1 and β3 (Figure 4.1B) and may therefore impact NL docking and the force output of the motor. In support of this possibility, recent structural studies of a motor domain-NL-coiled-coil construct of the kinesin-3 motor KIF13B support the idea that α1-β3 plays a role in NL docking and thus a conserved role in kinesin force generation (Ren et al., 2018).

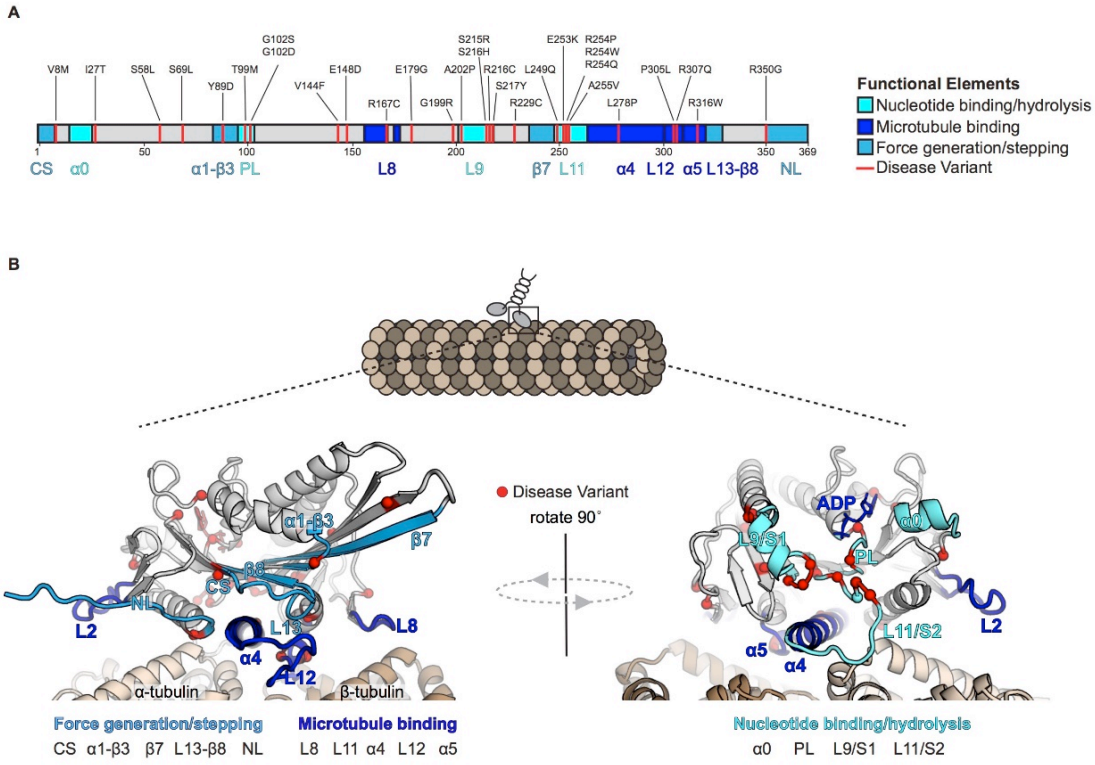

Figure 4.1 KIF1A disease variants are clustered within regions of the motor domain critical for microtubule binding, nucleotide binding/hydrolysis, and stepping/force generation

(**A**) Cartoon representation of KIF1A disease variants (red) mapped onto the peptide sequence of the motor domain. Amino acid residues of the motor domain are colored in light grey and residues that compose functional elements are indicated as: microtubule binding (Loop2, Loop8, α4, Loop12, α5; dark blue), nucleotide binding/hydrolysis (Loop9/Switch1, Loop11/Switch2, P-Loop, α0; cyan), and stepping/force generation (coverstrand CS, α1-β3, β8, Loop13, neck linker NL; blue)**.** (**B**) Ribbon representation of the KIF1A motor domain in the ADP-bound, tubulin-bound state (PDB 4UYO). In the pre-power stroke state, the neck linker (NL, blue) is represented as flexible and undocked from the motor domain. Secondary structural elements are colored as in (A) and KIF1A disease variants are indicated as red circles.

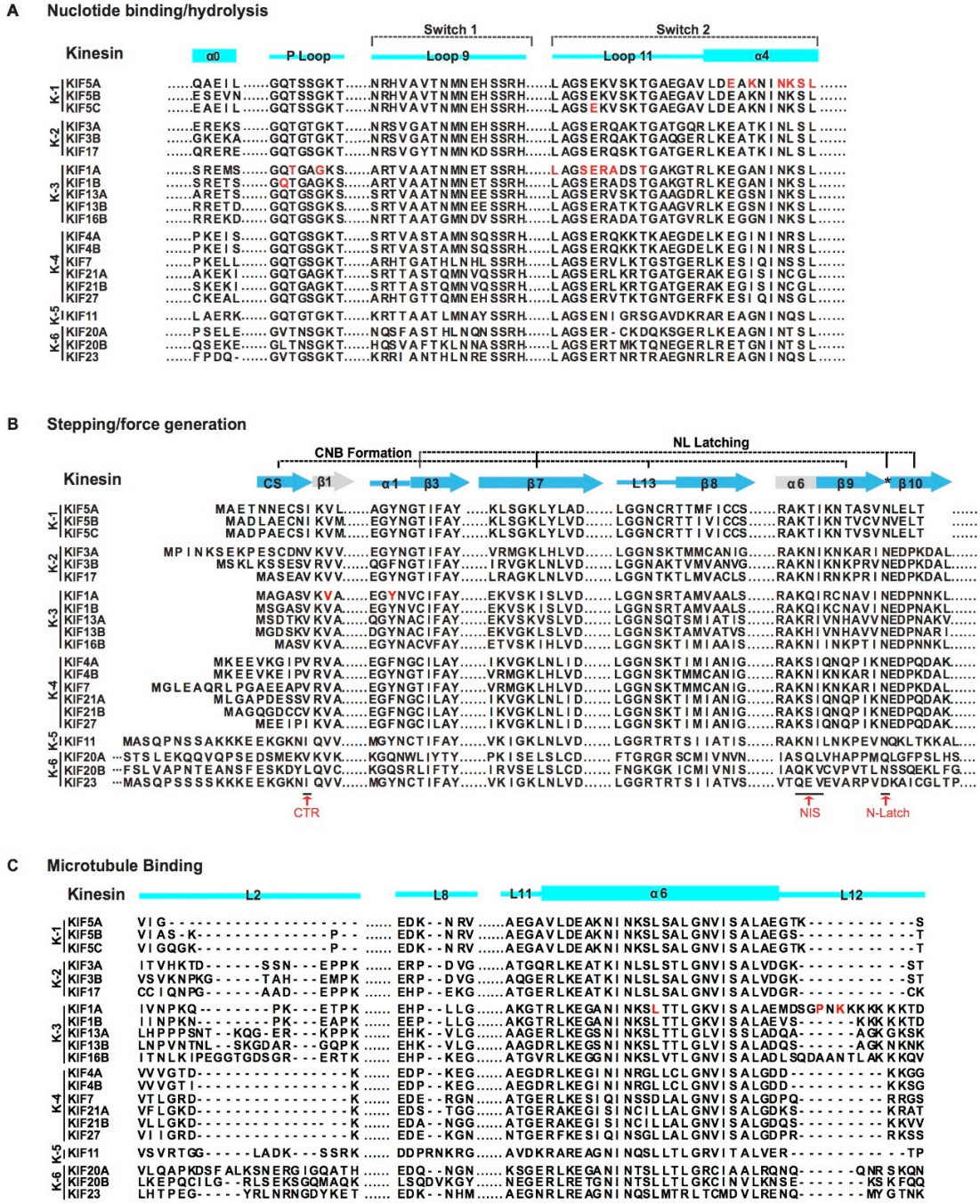

Figure 4.2 Sequence alignment of functional elements of the kinesin motor domain across the kinesin superfamily

(**A-C**)**.** Sequence alignment of the human kinesin motor domains from kinesin-1, -2, -3, -4, -5, and -6 families. Secondary structural elements important for (**A**) nucleotide binding/hydrolysis, (**B**) force generation/stepping, and (**C**) microtubule binding are illustrated and colored according to Figure 4.1A. Red text denotes residues identified to be mutated in neurodevelopmental and/or neurodegenerative disorders.

4.3.2 Molecular dynamics simulations predict that V8M and Y89D mutations impact neck linker docking and closure of the nucleotide-binding pocket

To delineate the local and global effects of the V8M and Y89D KAND mutations on the KIF1A motor domain, we used molecular dynamics (MD) simulations. We performed 100 ns all-atom MD simulations of the wild-type (WT) or KAND mutant (V8M or Y89D) motor domains bound to the microtubule in the ATP-bound state [post-power stroke, PDB 4UXP, (Atherton et al., 2014)]. Four replicate simulations were carried out and analysis across replicate simulations was used to predict statistically significant differences in residue-residue distances between the WT and KAND mutant motors ($p<10^{-5}$, V8M Figure 4.3, Y89D Figure 4.4).

For the V8M mutation, the MD simulations predict local changes in residue-residue interactions important for NL-dependent motor stepping and force generation (Figure 4.3A, B, E). Enhanced interactions are observed between the initial residues of β9 of the NL and the second residue (S6) of the CS (Figure 4.3A-B, red lines; Figure 4.3E, red box marked CS-NL). This is predicted to contribute to CNB formation and force output, however, reduced interactions are observed for the remainder of β9 and elements that position it for NL docking. In particular, reduced interactions are observed between β9 and residues of α4 that line the docking pocket (Figure 4.3A-B, blue lines, Figure 4.3E blue box marked α4-NL). Thus, the V8M mutation may position the CS such that it sterically alters the NL's access to the docking pocket. The MD simulations also predict reduced interactions between elements important for coordinating and hydrolyzing nucleotide (Figure 4.3C-D blue lines; Figure 4.3E boxes marked S1-PL and S2-S1). As closure of the switch regions is necessary for ATP hydrolysis (Cao et al., 2014; Hahlen et al., 2006), these results suggest that the V8M mutant motor may have problems coordinating and/or hydrolyzing ATP and therefore have a reduced velocity compared to WT motors.

For the Y89D mutation, the MD simulations predict more severe restrictions on NL docking and thus a greater impact on motor stepping and force generation. Specifically, the MD simulations reveal reduced interactions important for positing β9 of the NL in the docking pocket (Figure 4.4A-B blue lines; Figure 4.4E blue box marked α4-NL) and for subsequent docking of β10 along the core motor domain (Figure 4.4A-B

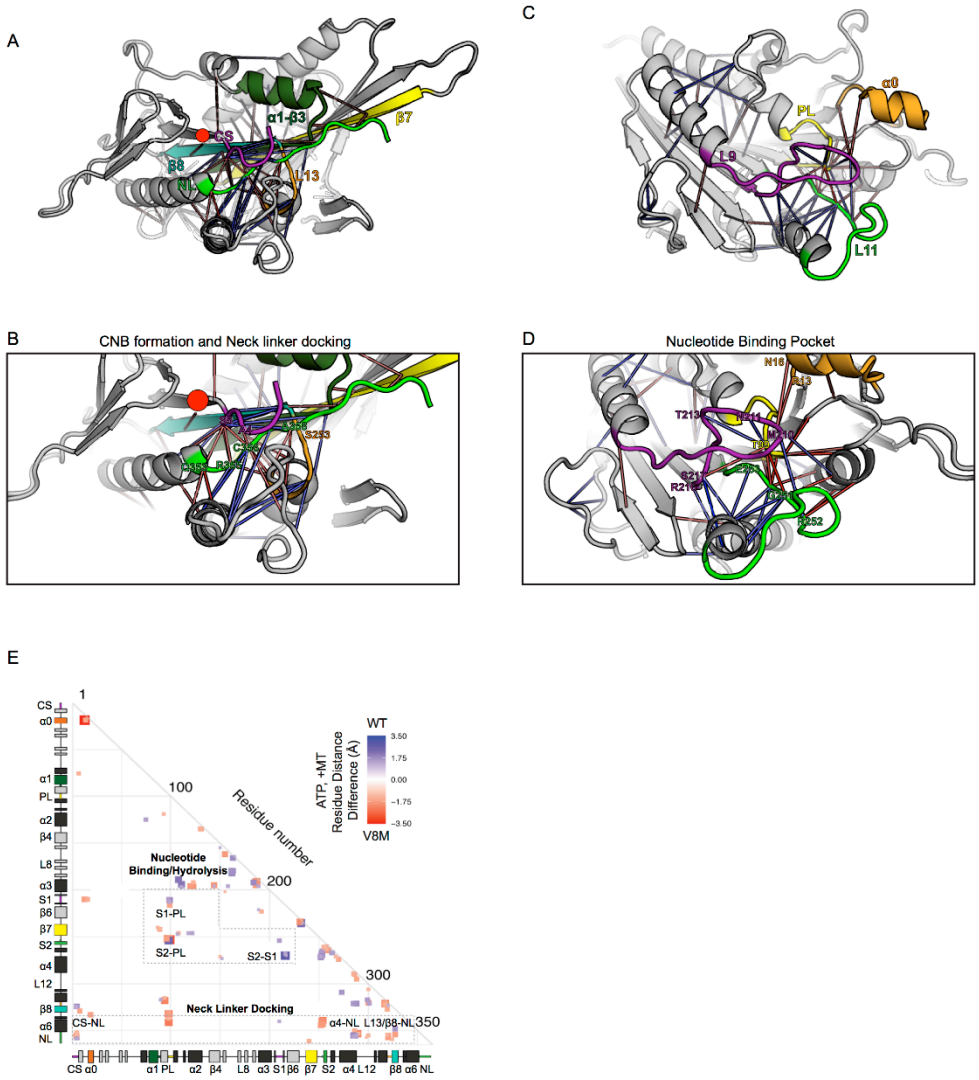

Figure 4.3 Molecular dynamics simulations predict that the V8M mutation alters neck linker docking and catalytic site closure

(**A-D**) Ribbon representation of the KIF1A motor domain in the ATP-bound, tubulin-bound state (PDB 4UXP). In the post-power stroke state, the neck linker (NL, green) is represented as flexible and docked along the motor domain. The motor domain is colored in light grey, secondary elements are indicated as: coverstrand (CS, purple), α1-β3 (dark green), β7 (yellow), β8 (teal), Loop13 (L13, orange), Loop9/Switch1 (L9/S1, purple), Loop11/Switch2 (L11/S2, green), P-Loop (PL, yellow), and α0 (orange). KAND mutant V8M (β1) is denoted as a red circle. (**A,C**) View of the (**A**) NL-docking pocket or (**C**) nucleotide-binding pocket. Red lines depict residue-residue distances that are shorter in the V8M mutant motor versus WT motor; blue lines depict residue-residue distances that are shorter in the WT motor versus V8M mutant motor. The magnitude of the distance change is indicated by line color intensity. (**B,D**). Enlarged view of interactions important for (**B**) NL docking (**D**) closure of the nucleotide-binding pocket. (**E**) Differences in residue-residue distances between WT KIF1A and V8M mutant motor in the ATP-bound, tubulin-bound state in molecular dynamics simulations. The secondary structure elements are laid out along the x- and y-axes with α- helices in black, β-strands in grey, or colored according to (A). Residue interactions that are significantly shorter ($p<10^{-5}$) in V8M mutant (red) or WT (blue) motor are displayed. The magnitude of the distance changes is indicated by color intensity; interactions between structural elements are labeled.

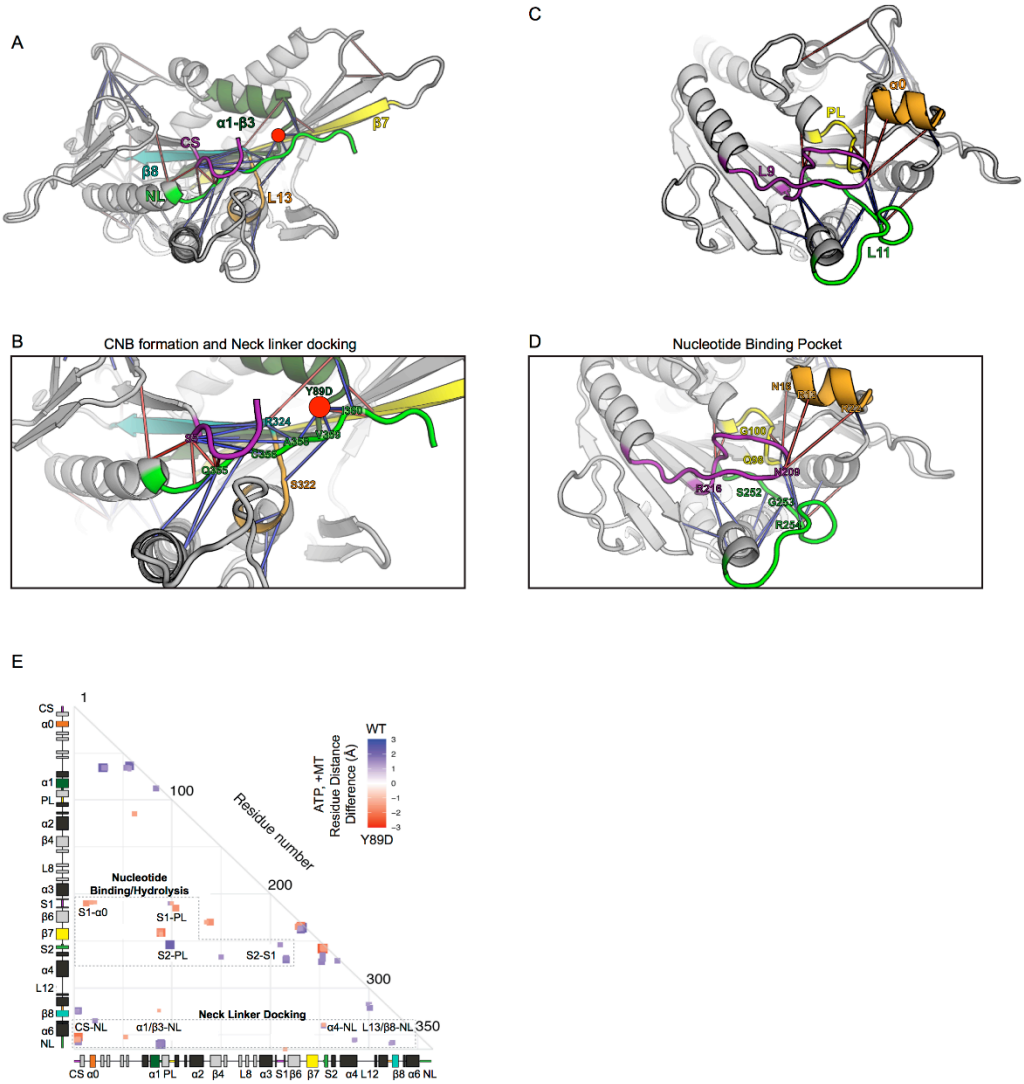

Figure 4.4 Molecular dynamics simulations predict that the Y89D mutation alters neck linker docking and catalytic site closure

(**A-D**) Ribbon representation of the KIF1A motor domain in the ATP-bound, tubulin-bound state (PDB 4UXP). In the post-power stroke state, the neck linker (NL, green) is represented as flexible and docked along the motor domain. The motor domain is colored in light grey, secondary elements are indicated as: coverstrand (CS, purple), α1-β3 (dark green), β7 (yellow), β8 (teal), Loop13 (L13, orange), Loop9/Switch1 (L9/S1, purple), Loop11/Switch2 (L11/S2, green), P-Loop (PL, yellow), and α0 (orange). KAND mutant Y89D (α1-β3) is denoted as a red circle. (**A,C**) View of the (**A**) NL-docking pocket or (**C**) nucleotide-binding pocket. Red lines depict residue-residue distances that are shorter in the Y89D mutant motor versus WT motor; blue lines depict residue-residue distances that are shorter in the WT motor versus Y89D mutant motor. The magnitude of the distance change is indicated by line color intensity. (**B,D**) Enlarged view of interaction important for (**B**) NL docking (**D**) closure of the nucleotide-binding pocket. (**E**) Differences in residue-residue distances between WT KIF1A or Y89D mutant motor in the ATP-bound, tubulin-bound state in molecular dynamics simulations. The secondary structure elements are laid out along the x- and y-axes with α- helices in black, β-strands in grey, or colored according to (A). Residue interactions that are significantly shorter ($p<10^{-5}$) in Y89D mutant (red) or WT (blue) motor are displayed. The magnitude of the distance changes is indicated by color intensity; interactions between structural elements are labeled.

blue lines; Figure 4.4E blue boxes marked α1/β3-NL, L13/β8-NL). In addition, the MD simulations revealed mixed effects of the Y89D mutation on interactions between elements in the nucleotide-binding pocket. There are enhanced interactions between elements important for gating and capture of nucleotide [Figure 4.4C-D red lines; Figure 4.4E red boxes marked S1-α0, (Hwang, Lang, & Karplus, 2017)], however, there are reduced interactions between elements important for nucleotide hydrolysis and exchange [Figure 4.4C-D blue lines, Figure 4.4E blue boxes marked S2-PL, S2-S1, (Cao et al., 2014; Clancy et al., 2011; Parke et al., 2010; Turner et al., 2001)]. Therefore, these results suggest that although the mutant motor may have no restrictions on binding ATP, it may display a reduced ability to hydrolyze ATP and undergo processive motility.

4.3.3 Impact of V8M and Y89D mutations on motility properties of homodimeric motors under force

To examine the effects of the V8M and Y89D mutations on the force output of the motors, we used an optical trap with nanometer-level spatial resolution. As the force generation of mammalian KIF1A has not yet been analyzed by optical trap methods, we first characterized the force generation of human KIF1A as compared to that of the widely-studied kinesin-1 KIF5C as a control. For this work, we used a truncated version of KIF1A that is constitutively active [KIF1A(1-393)] followed by a leucine zipper (LZ) to ensure the motor is in a dimeric state (Hammond et al., 2009). Lysates of COS-7 cells expressing biotinylated KIF5C(1-560)-Avitag or KIF1A(1-393)-LZ-Avitag motors were bound to beads and were subjected to standard single-molecule optical trap assays (Rao et al., 2019). Individual KIF5C motors were motile in the absence of load, stalled on the microtubule when approaching the detachment force, and detached from the microtubule at an average force of 4.2 pN (Figure 4.5 A, E), consistent with previous studies (Budaitis et al., 2019; Khalil et al., 2008; Svoboda & Block, 1994). Individual KIF1A motors underwent fast motility in the absence of load but in contrast to KIF5C, KIF1A motors did not stall but rather rapidly detached from the microtubule when subjected to force (Figure 4.5 B), with an average detachment force of 2.7 pN (Figure 4.5 E). Interestingly, KIF1A shows a high on-rate towards microtubules such that after

detaching from the microtubule, it quickly rebinds and moves forward again. This rapid detachment under force and reattachment once the force has dissipated results in the "clustering" behavior shown in Figures 4.5 B. The number of rebinding events within a cluster of force-generating events is on the magnitude of 10 – 10^2 for KIF1A. In contrast, the number of rebinding events of KIF5C is 0 – 5.

We next examined the force generation of WT and KAND mutant KIF1A(393)-LZ motors. Both the V8M and Y89D KAND mutant motors were sensitive to small opposing forces exerted by the trap. Similar to the WT motor, the V8M and Y89D motors did not stall under load but rather detached from the microtubule (Figure 4.5 C, D). Both mutant motors displayed a reduced force output as their average detachment forces (1.9 and 1.0 pN, respectively) were significantly reduced compared to the WT motor (Figure 4.5 E). The reduced force output of the mutant motors is consistent with our MD simulations that predicted that the KAND mutations would impair docking of β9 and/or β10 of the NL to the core motor domain (Figures 4.3 and 4.4).

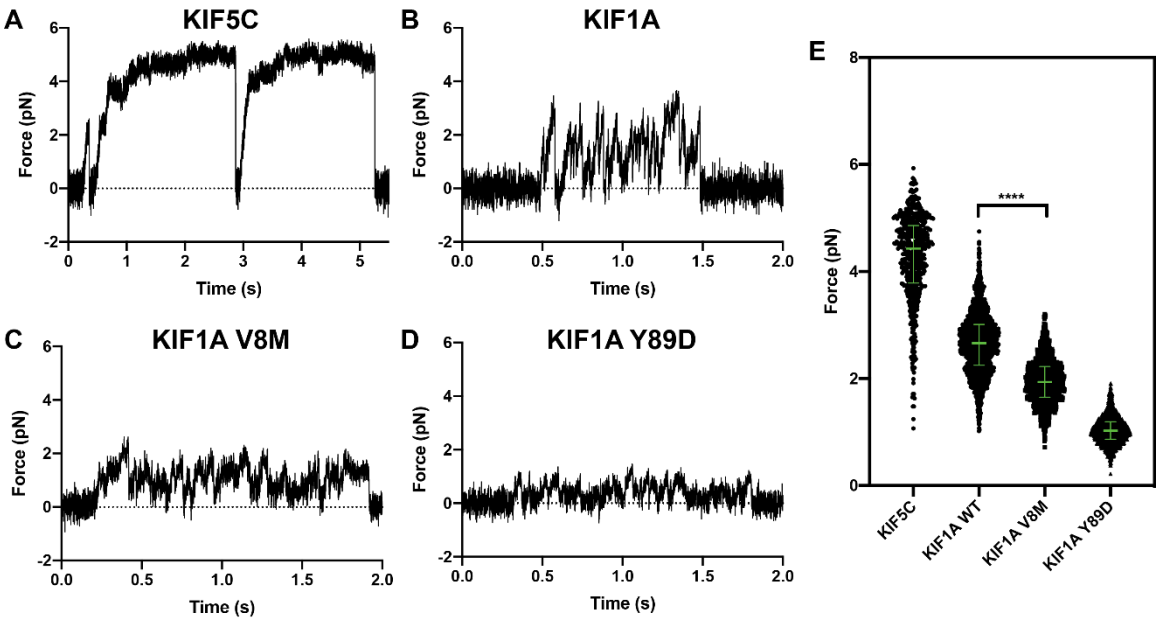

Figure 4.5 Force generation of KIF1A

(**A-D**) Examples of force generation of (**A**) KIF5C, (**B**) KIF1A, (**C**) V8M mutant, and (**D**) Y89D mutant motors. (**E**) Detachment forces of KIF5C, KIF1A, V8M mutant, and Y89D mutant. Green bar indicates the median value with quartiles. KIF5C: 4.43 [3.79, 4.86] pN (n = 557 events for 9 beads); KIF1A: 2.66 [2.24, 3.01] pN (n = 1912 events for 10 beads); V8M: 1.94 [1.65, 2.22] pN (n = 1343 events for 8 beads); Y89D: 1.02 [0.87, 1.19] pN (n = 1468 events for 7 beads). Unpaired t-test between KIF1A and V8M has p-value < 0.0001.

4.3.4 Strategy for Designing Homodimeric and Heterodimeric motors

We used single-molecule motility assays to examine the behavior of either WT or KAND mutant KIF1A motors under unloaded conditions using total internal reflection florescence (TIRF) microscopy. For this work, we used a truncated version of KIF1A that is dimeric and constitutively active [KIF1A(1-393)-LZ]. Since only copy of the V8M and Y89D mutant gene can manifest in disease, we also wanted to examine the behavior of heterodimeric KIF1A motors, where one motor domain is WT and the second motor domain harbors a KAND mutation. We tried two strategies to generate heterodimeric KIF1A motors (Figure 4.6).

First, a synthetic heterodimerization domain sequence (SHD) was designed similar to previous work (Albracht et al., 2014; Guzik-Lendrum et al., 2015; Lindhout et al., 2004; Rank et al., 2012) and fused to the native KIF1A coiled-coil. Coiled-coil prediction software was used to ensure the SHD sequences were placed in register with the native KIF1A coiled-coil (Marcoils). One SHD sequence was tagged with three tandem monomeric citrine florescent proteins [KIF1A(393)-SHD1-3xmCit] and the other tagged with three tandem monomeric cherry proteins [KIF1A(393)-SHD2-3xmCH, Figure 4.6]. COS-7 lysates from cells cotransfected with plasmids coding for the expression of KIF1A(393)-SHD1-3xmCit and KIF1A(393)-SHD2-3xmCH motors were subjected to single-molecule imaging using TIRF microscopy to assess whether SHD sequences drive stable dimerization of KIF1A motors. Unfortunately, a majority of motility events were not heterodimeric (magenta/green). The few heterodimeric events observed were short and non-processive (Figure 4.6B), unlike the fast, super-processive motility of stable dimeric KIF1A motors (Figure 4.6D). These results suggest that swapping coiled-coiled sequences from one motor to the next may not be as straightforward as anticipated.

Second, we utilized the leucine zipper sequence (LZ) of GCN4 fused to the native KIF1A coiled-coil to drive formation of dimeric motors (Huckaba et al., 2011; Schimert et al., 2019; Soppina et al., 2014; Tomishige & Vale, 2000) and differential fluorescence tagging to distinguish heterodimeric motors. COS-7 cells were cotransfected with plasmids that code for the expression of KIF1A(393)-LZ tagged with either a red or a green flourophore, resulting in three populations of motors observed in

single molecule assays: green/green, green/magenta, and magenta/magenta (Figure 4.6C) where green/magenta motility events report on the behavior of heterodimeric motors.

The motility characteristics of homodimeric motors tagged with either 3xmCit and 3xmCH behave similar under single molecule conditions, however, these fluorophores are dim and sensitive to photobleaching (Norris et al., 2015). For better tracking in single-molecule assays, mCit and mCH fluorophores were replaced with brighter, more photostable fluorophores, NeonGreen and Halo-tag/JF549 Halo ligand, respectively (Figure 4.6C).

We examined the behavior of KIF1A(393)-LZ motors tagged with monomeric NeonGreen (mNG) or with Halo-tag covalently linked to its fluorescent ligand (JF552) by single-molecule imaging using TIRF microscopy. In general, KIF1A motors appear to be sticky in our experiments and decorated the imaging surface (Figure 4.7A, horizontal lines). To improve visualization of motor movement along microtubules, regions of interest were photobleached before imaging. The velocity, run length, and microtubule landing rate in P12 imaging buffer were determined from kymograph analysis with time displayed horizontally and distance vertically. The average velocity and run length of processive motility events of KIF1A motors tagged with mNG (2.0 ± 0.01 μm/s; 20.6 ± 1.4 μm) was comparable to motors tagged with Halo-tag (2.1 ± 0.01 μm/s; 26.7 ± 1.4 μm, Figure 4.7D, E). However, 67.9% of microtubule-binding events (dwell time > 400 ms) by NG-tagged motors were diffusive (Figure 4.7A,C; P12, white arrows) compared to 21.2% by Halo-tagged motors (Figure 4.7A,C; P12 buffer), leading to an aberrantly high microtubule on-rate for motors tagged with NG (Figure 4.7B; P12 buffer).

We therefore examined the behavior of NG- and Halo-tagged motors in different imaging buffers (BRB80, BRB40, PERM). Consistent with previous studies, differences in buffer conditions had little effect on velocity [Figure 4.7A, D, (Norris et al., 2015)]. The percentage of diffusive events by NG-tagged motors was drastically reduced in higher salt buffer compared to Halo-tagged motors (Figure 4.7A, C) and the microtubule on-rate was comparable between NG- and Halo-tagged motors (Figure 4.7B). However, there were dramatic changes in the average run length of Halo-tagged motors compared to NG-tagged motors in BRB80 and PERM buffers (Figure 4.7A, E).

Collectively, these results highlight the importance of examining the behavior of a motor tagged with different fluorophores to ensure the motility characteristics measured are specific to the motor and not an effect of the fluorescent tag. Furthermore, these effects can be different depending on the kinesin motor under study. To ensure the fluorescent-tag is not altering the motility properties of KIF1A, motors were imaged in BRB40 buffer.

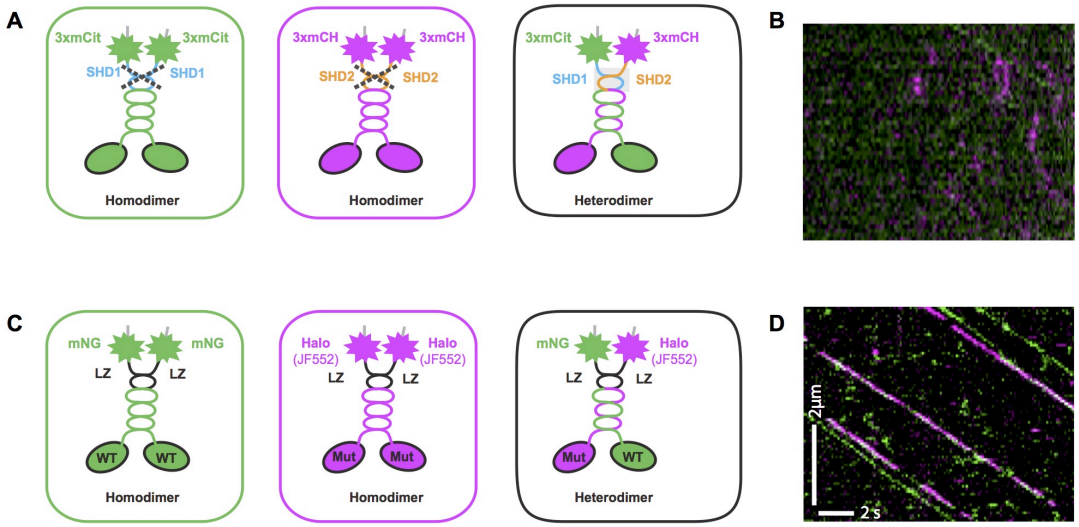

Figure 4.6 Strategies for designing heterodimeric motors

(**A**) Schematic for the generation of heterodimeric KIF1A motors by synthetic heterodimerization (SHD) sequence. To generate heterodimeric motors, the KIF1A motor domain (aa. 1-369) followed by the native coiled-coil sequence (aa. 367-393) is fused to synthetic heterodimerization sequences (SHD1, blue or SHD2, orange). Unlike the leucine zipper sequence of GCN4, the SHD1 and SHD2 sequences are not expected to homodimerize (left and middle) and instead are expected to form a heterodimer (right). SHD1 and SHD2 sequences were tagged with three-tandem monomeric citrines (3xmCit) or three-tandem monomeric mCherry (3xmCH), respectively, to visualize motor dimerization states in TIRF single-molecule assays. (**B**) Representative kymographs of TIRF single-molecule assays of lysates from COS-7 cells cotransfected with KIF1A-SHD1-3xmCit and KIF1A-SHD2-3xmCH. Time is displayed on the x-axis (bar, 2 s) and distance displayed on the y-axis (bar, 2 µm). (**C**) Schematic for KIF1A dimerization by leucine zipper (LZ) sequence. Constructs encode for the KIF1A motor domain (aa. 1-369), followed by native coiled-coil sequence (aa. 367-393) fused to the LZ sequence of GCN4. Motors were tagged with either monomeric NeonGreen (mNG) or Halo-FLAGtag covalently linked to fluorescent Halotag (JF552), respectively, and cotransfected into COS-7 cells. Three populations of motors are expected in TIRF single-molecule assays: homodimeric Halo-FLAG tagged motors, homodimeric mNG tagged motors, and heterodimeric Halo-FLAG/mNG tagged motors. (**D**) Representative kymograph of single-molecule assays of lysates from COS-7 cells cotransfected with plasmids encoding for the expression of KIF1A-LZ-mNG and KIF1A-LZ-Halo-FLAG. Time is displayed on the x-axis (bar, 2 s) and distance displayed on the y-axis (bar, 2 µm).

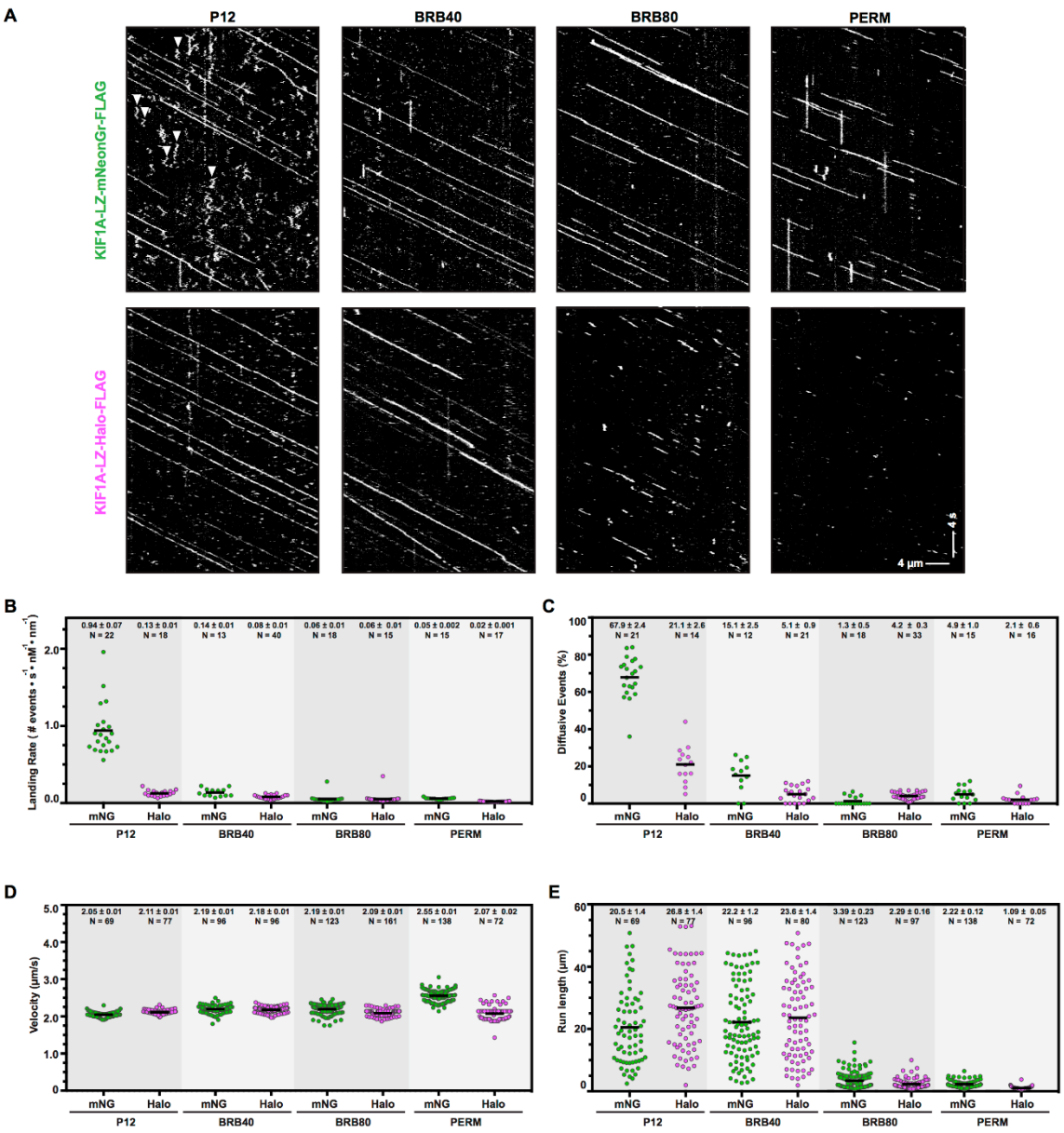

Figure 4.7 Influence of fluorescent-tag on KIF1A motility

(**A**) Motility properties of KIF1A motors dimerized by a leucine zipper sequence (LZ) and tagged at their C-termini with monomeric NeonGreen (mNeonGreen) or Halo-FLAGtag covalently linked to fluorescent Halotag (JF552) were analyzed in standard single-molecule motility assays using TIRF microscopy. Representative kymographs are shown with time displayed on the y-axis (bar, 4 s) and distance displayed on the x-axis (bar, 4 µm). White arrowheads indicate motility events scored as a diffusive. (**B-E**) Quantification of motility properties. From the kymographs, single-motor (**B**) landing rate, (**C**) percent diffusive events, (**D**) velocity, and (**E**) run length were determined and the data for each population is plotted as a dot plot. The mean is indicated by a horizontal black line and the mean ± SEM is indicated above. (**B**) Each dot represents the landing rate along a single microtubule. Quantification of landing rate accounts for motility events (diffusive and processive) with dwell times longer than 400 ms. (**C**) Each dot represents the percent of events along a single microtubule that were diffusive (rapid plus- and minus-end movement with a net displacement is less than 300 nm, dwell time longer than 400ms).

4.3.5 Impact of V8M and Y89D mutations on unloaded motility properties of homodimeric motors

We used single-molecule motility assays to examine the behavior of either WT or KAND mutant KIF1A motors under unloaded conditions. For this work, we used a truncated version of KIF1A [KIF1A(1-393)] followed by a leucine zipper (LZ), a HaloTag for fluorescent labeling with JF552 ligand, and FLAG tag. Cell lysates containing KIF1A(393)-LZ-Halo-FLAG motors were added to flow chambers containing polymerized microtubules and their single-molecule motility properties were examined using total internal reflection florescence (TIRF) microscopy. The velocity, run length, and landing rate on the microtubule were determined from kymographs with time displayed vertically and distance horizontally (Figure 4.8A-B). At least 250 motility events were quantified for each motor across three independent trials and summarized as a histogram or dot plot (Figure 4.8C-G).

As expected, the WT motor displayed fast (2.1 ± 0.009 μm/s) and superprocessive (19.0 ± 0.7 μm) motility with a high landing rate of 0.23 ± 0.008 events•$nm^{-1}nM^{-1}s^{-1}$ (Figure 4.8 A-E), consistent with previous work (Soppina, et al., 2014). The V8M mutant motors displayed a significant decrease in overall velocity (1.3 ± 0.009 μm/s, Figure 4.8C) and processivity (5.2± 0.2 μm, Figure 4.8D, Table 4.1). The reduced velocity of the V8M mutant motors is consistent with the MD simulations that predict allosteric effects on elements of the nucleotide-binding pocket that result in reduced catalytic site closure and reduced ATP hydrolysis (Figure 4.3 C-E). The V8M motors also displayed a significant decrease in landing rate of 0.06 ± 0.001 events•$nm^{-1}nM^{-1}s^{-1}$ (Figure 4.8E, Table 4.1).

The Y89D mutant motors also displayed a decrease in velocity (1.7± 0.01 μm/s, Figure 4.8C), processivity (2.9± 0.2 μm, Figure 4.8D), and landing rate (0.12 ± 0.04 events/$nm^{-1}nM^{-1}s^{-1}$, Figure 4.8E, Table 4.1) as compared to the WT motor. Further examination of the kymographs indicated two additional differences in the motility behavior of Y89D mutant motors. First, the tracks of Y89D motility were not smooth but rather the motor appeared to “wobble” or move sideways as it walked along the microtubule track (Figure 4.8B). Second, a large number of non-productive, diffusive events (net displacement along microtubule < 300 nm) were observed (Figure 4.8A,

white arrowheads). We quantified the percentage of diffusive events with a dwell time great than 400 ms for each motor (Figure 4.8F). The Y89D mutant motors displayed a greater percentage of diffusive events (17.6 ± 0.8% of binding events) than the WT or V8M motors (4.0 ± 0.6% and 5.5 ± 0.4 %, respectively) (Figure 4.8F, Table 4.1) and the duration of the diffuse events was longer for the Y89D mutant motors (1.34 ± 0.2 s) than for the WT or V8M mutant motors (0.81 ± 0.01 s and 0.69 ± 0.02 s for WT and V8M, respectively, Figure 4.8G). The increase in diffusive events for the Y89D mutant motors is consistent with the MD simulations that predict allosteric effects of the Y89D mutation on the motor's ability to hydrolyze ATP (Figure 4.4C-E).

Overall we conclude that as homodimeric motors, the V8M motor shows more significant impairment in velocity and landing rate than the Y89D motor whereas the Y89D motor shows more significant impairment in processivity and ability to engage in processive rather than diffusive motility.

Table 4.1 Single Molecule Properties of KIF1A disease variants V8M and Y89D

Kinesin	Landing Rate (# events • s^{-1} • nM^{-1} • nm^{-1})	% Diffusive Events (diffusive / total events)	Velocity (μm/s)	Runlength (μm)
WT / WT	0.23 ± 0.008	4.0 ± 0.6	2.1 ± 0.09	19.0 ± 0.7
V8M / V8M	0.06 ± 0.001	5.5 ± 0.4	1.3 ± 0.01	5.2 ± 0.2
Y89D / Y89D	0.12 ± 0.004	17.6 ± 0.8	1.7 ± 0.01	2.9 ± 0.1
WT / V8M	ND	ND	1.3 ± 0.01	11.2 ± 0.4
WT / Y89D	ND	ND	1.9 ± 0.01	11.4 ± 0.4

Value, Mean ± SEM
ND, not determined

4.3.6 Impact of V8M and Y89D mutations on unloaded motility properties of heterodimeric motors

We next examined the behavior of heterodimeric KIF1A motors, where one motor domain is WT and the second motor domain harbors the KAND mutation. COS-7 cells were cotransfected with plasmids for expression of WT KIF1A(393)-LZ-mNG motors and KAND mutant KIF1A(393)-LZ-Halo(JF552) motors. Lysates were added to flow chambers containing polymerized microtubules and single-molecule motility was examined using TIRF microscopy.

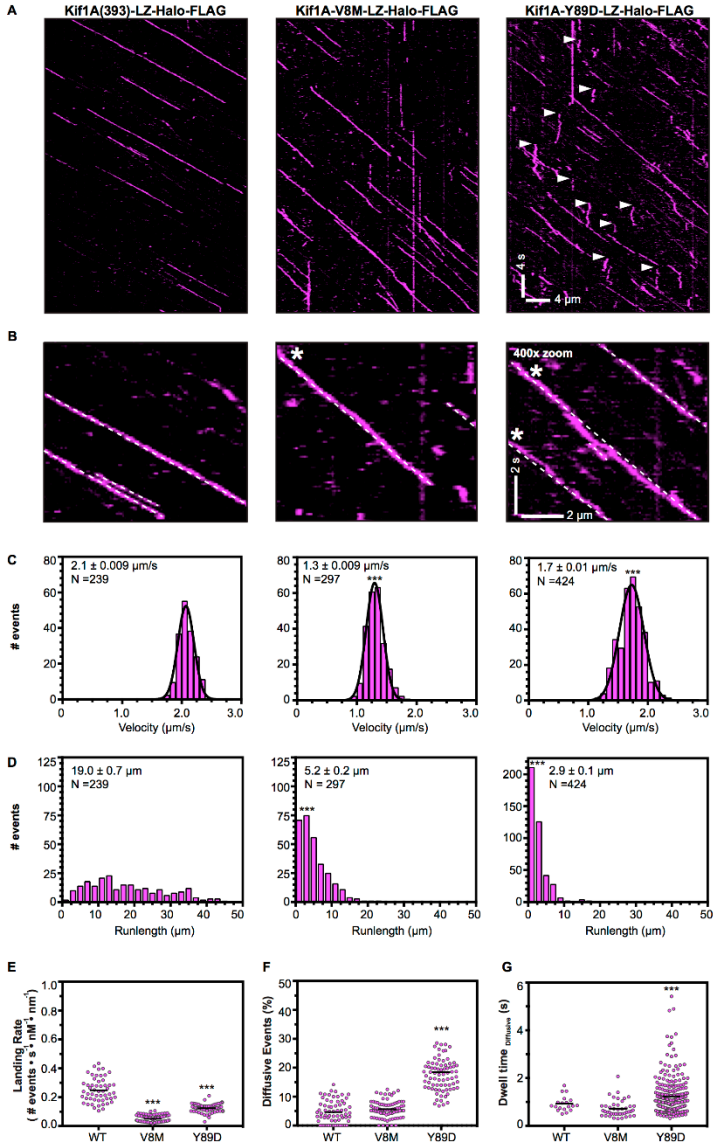

Figure 4.8 Unloaded motility properties of homodimeric V8M or Y89D mutant motors

(**A**) Motility properties of WT or mutant motors tagged at the C-terminus with Halo-FLAGtag covalently linked to fluorescent Halotag (JF552) were analyzed in standard single-molecule motility assays using TIRF microscopy. Representative kymographs are shown with time displayed on the y-axis (bar, 4 s) and distance displayed on the x-axis (bar, 4 µm). White arrowheads indicate motility events scored as diffusive events. (**B**) Magnified view of the representative kymographs in (A) with x-axis bar, 2 µm and y-axis bar, 2 s. Straight dotted white lines were overlaid on top of motility events to visualize deviation from smooth motility; white asterisks indicate "wobbly" motility events. (**C-E**) Quantification of motility properties. From the kymographs, singe-motor (**C**) velocities, (**D**) run lengths, and (**E**) landing rates were determined and the data for each population is plotted as a histogram or dot plot. **C,D.** The mean ± SEM are above each graph; N ≥ 230 events across three independent experiments for each construct; ***, p<0.001 as compared to the WT motor. (**E**) Each dot indicates motor landing rate along a single microtubule with the mean for the population indicated by a horizontal black line across three independent experiments for each construct; ***, p>0.001 as compared to the WT motor. (**F,G**) Quantification of diffusive motility events. From the kymographs, (**F**) the percent of diffusive events (dwell time longer than 400 ms, net displacement less than 300 um) and the (**G**) dwell time of diffusive events were determined and the data is plotted as a dot plot. Black horizontal lines indicate the mean; ***, p<0.001 as compared to WT motor.

The velocity (2.1± 0.009 μm/s) and run length (20.0 ± 0.7 μm) of WT/WT motors tagged with both mNG and Halo(JF552) fluorophores (Figure 4.9B,C,D) are comparable to those of KIF1A(393)-LZ-Halo-Flag motors (Figure 4.8). The presence of the V8M motor domain resulted in a significant reduction in velocity (1.3± 0.01 μm/s Figure 4.9E,F) such that the heterodimeric WT/V8M motor's velocity is comparable to that of homodimeric V8M/V8M mutant motors (1.3± 0.01 μm/s Figure 4.9F, Table 4.1). In addition, the processivity of WT/V8M motors (11.2 ± 0.7 μm, Figure 4.9E,G) was significantly reduced compared to WT/WT motors but was not as severely hindered as in the V8M/V8M motors (5.2 ± 0.2 μm Figure 4.9G, Table 4.1).

The presence of the Y89D motor domain had minimal effects on the velocity of the WT/Y89D motor (1.9±0.01 μm/s, Figure 4.9H,I) as compared to the WT/WT motor but resulted in a significant reduction in the processivity of the motor (11.4 ± 0.6 μm Figure 4.9H,J) although the effects on processivity were not as severe as the Y89D/Y89D motors (2.9±0.1 um, Figure 4.8, Table 4.1). In addition, the WT/Y89D heterodimeric motors did not exhibit the diffusive behavior of the Y89D/Y89D homodimeric motors (Figure 4.9H). Collectively, these results suggest that when paired with a WT motor domain in a heterodimeric motor, both the V8M and Y89D mutations cripple the overall motility with greater effects on motor processivity than motor speed.

4.3.7 Impact of V8M and Y89D mutations on the transport of membrane-bound organelles in cells

We next sought to test whether these mutations impacted the ability of motors to work as a team to drive cargo transport in cells. To do this we used an inducible recruitment strategy (Khalil et al., 2008) to link teams of motors to the surface of membrane-bound organelles and monitored their ability to drive organelle transport to the cell periphery (Figure 4.10A). To assess how teams of WT or KAND mutant KIF1A motors drive the transport of a low-load, membrane-bound organelle (Budaitis et al., 2019; Efremov et al., 2014; Schimert et al., 2019), motors were inducibly recruited to the surface of peroxisomes, and transport of peroxisomes to the cell periphery was monitored 5, 10, and 30 minutes later. Cargo dispersion before and after motor recruitment was qualitatively scored as clustered (black), partially dispersed

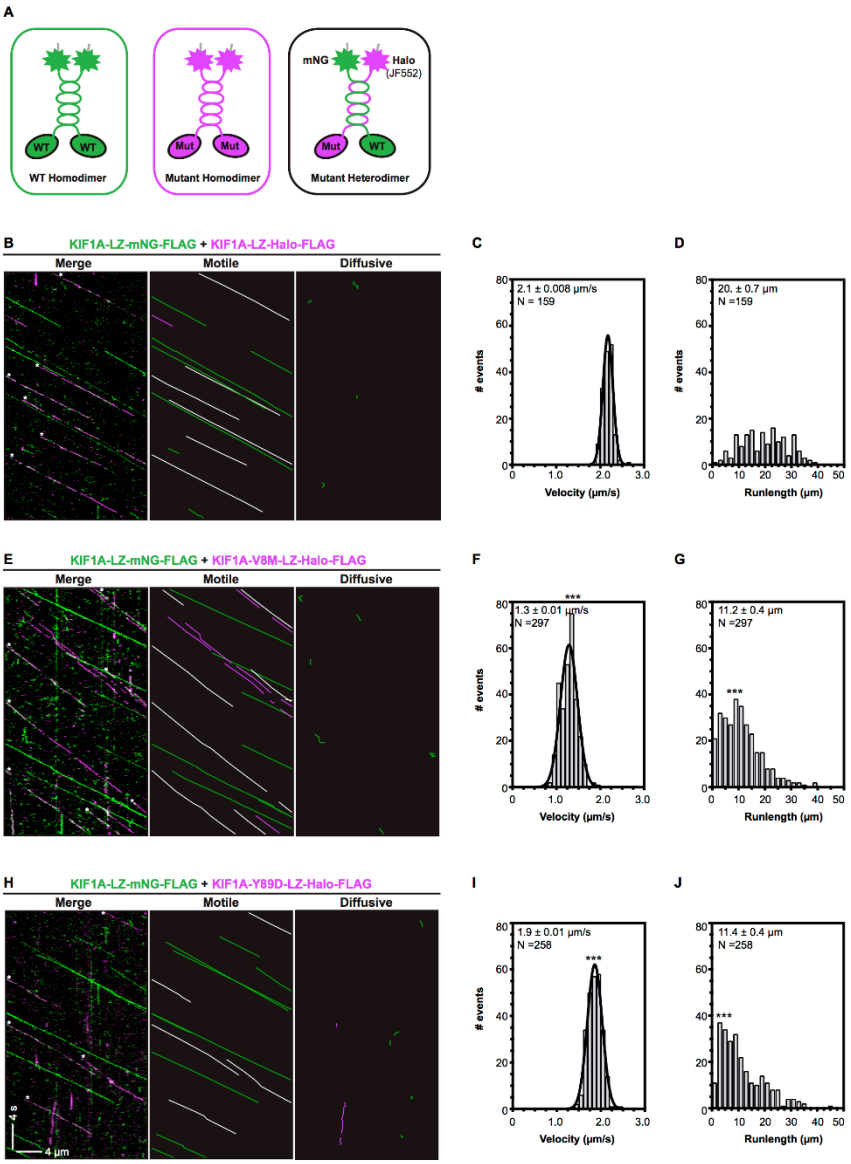

Figure 4.9 Unloaded motility properties of heterodimeric V8M or Y89D mutant motors

(**A**) Schematic for the generation of mutant heterodimeric KIF1A motors. Constructs encode for the KIF1A motor domain (aa. 1-369), followed by native coiled-coil sequence (aa. 367-393) fused to the leucine zipper (LZ) sequence of GCN4. WT and KAND mutant motors were tagged with monomeric NeonGreen (mNG) and Halo-FLAGtag covalently linked to fluorescent Halotag (JF552), respectively, and cotransfected into COS-7 cells. Three populations of motors are expected in TIRF single-molecule assays of cell lysates: homodimeric WT motors tagged with mNG, homodimeric mutant motors tagged with Halo/JF552, and heterodimeric mutant motors tagged with mNG and Halo/JF552. (**B-J**) Motility properties of mutant heterodimeric KIF1A motors were analyzed in standard single-molecule motility assays using TIRF microscopy. (**B,E,H**) Representative kymographs are shown with time displayed on the y-axis (bar, 4 s) and distance displayed on the x-axis (bar, 4 µm). Cartoon kymographs were generated from merged kymographs to more clearly illustrate motile (middle) and diffusive events (right). From the kymographs, single-motor (**C,F,I**) velocities and (**D,G,J**) run lengths were determined and the data for each population is plotted as a histogram. The mean ± SEM are indicated above each graph; N ≥ 150 events across three independent experiments for each construct; ***, p<0.001 as compared to the WT motor.

(dark grey), diffusively dispersed (light grey), or peripherally dispersed (white; Figure 4.10B).

COS-7 cells were cotransfected with a plasmid for the expression of WT or KAND mutant KIF1A(393)-LZ motors tagged with monomeric Neongreen (mNG) and FRB domain and a plasmid for the expression of a peroxisome-targeted PEX-mRFP-FKBP fusion protein. In the absence of rapamycin, the PEX-RFP-FKBP fusion proteins localized to the peroxisome surface and the KIF1A(393)-LZ-mNG-FRB motors accumulated at the periphery of the cell (93% of cells had peroxisomes clustered near the nucleus of the cell; Figure 4.10B). Addition of rapamycin resulted in recruitment of motors to the peroxisome surface via dimerization of the FRB and FKBP domains and motor activity drove dispersion of peroxisomes to the cell periphery after 5 minutes (100% of cells have peripherally dispersed peroxisomes, Figure 4.10B). Notably, 5 minutes after recruitment of teams of V8M or Y89D mutant motors to the surface of peroxisomes, peroxisomes remained clustered near the nucleus of the cell (9% of cells have peripherally dispersed peroxisomes for V8M and Y89D, Figure 4.10B). However, after 10 minutes, teams of V8M or Y89D mutant motors drove peroxisome transport to the cell periphery, almost similar to peroxisomes dispersion by teams of WT motors (68% and 93% of cells have peripherally dispersed peroxisomes, respectively; Figure 4.10B). These results suggest that despite their reduced processivity and velocity under single-molecule conditions, the mutant motors can drive low-load transport although they show a significant delay in completing the transport event.

4.4 Discussion

Despite the identification of an increasing number of disease-associated mutations in the KIF1A motor domain, how the mutations alter the mechanical output of the motor and manifest in disease is not clear. Here, we used a combination of computational and biophysical methods to characterize the effects of two KIF1A disease-associated variants located within elements predicted to be important for motor stepping and force generation. We find that, unlike conventional kinesin-1, WT mammalian KIF1A motors do not stall and instead have a tendency to detach from the microtubule track under low forces. Furthermore, the WT KIF1A motors rapidly reattach

to the microtubule and continue forward motion, a strategy that may enable the fast transport of presynaptic vesicles over long distances. We find that disease-associated V8M and Y89D mutations compromise the force output of single motors and result in decreased velocity, processivity, and landing rate via allosteric effects on regions of the core motor domain that coordinate and bind nucleotide. These results highlight the benefits of combining single-molecule assays with simulations to investigate how subtle sequence changes can impact the mechanical output of a motor.

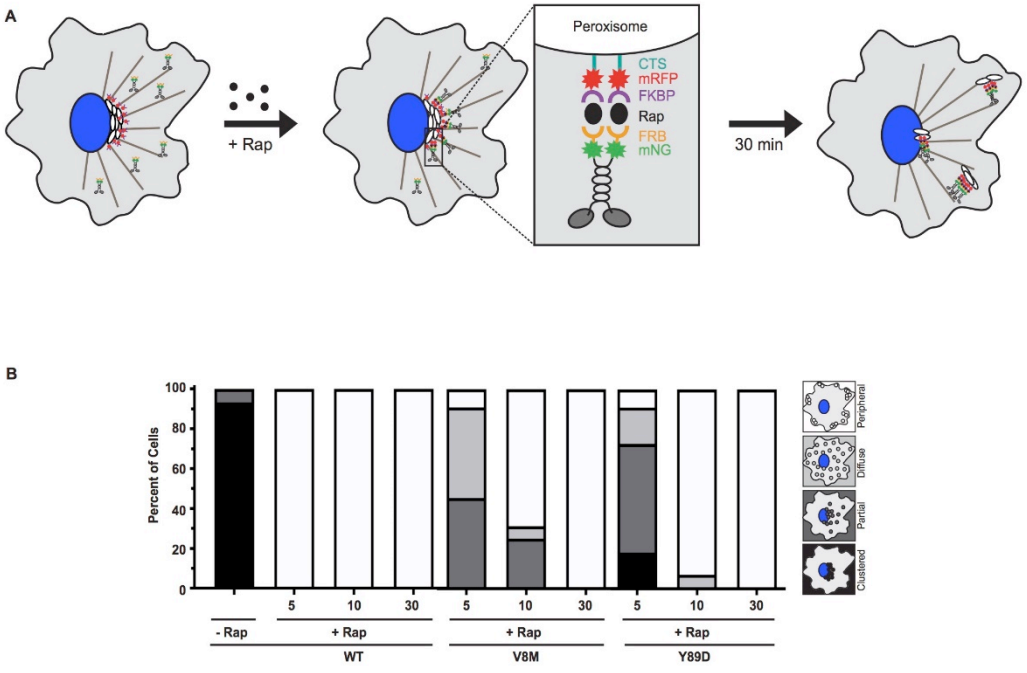

Figure 4.10 Impact of V8M and Y89D mutations on transport of membrane-bound organelles in cells

(**A**) Schematic of the inducible motor recruitment assay. A kinesin motor tagged with monomeric NeonGreen (mNG) and an FRB domain (KIF1A-LZ-mNG-FRB) is coexpressed with a cargo targeting sequence (CTS) tagged with monomeric red fluorescent protein (mRFP) and FKBP domain (CTS-mRFP-FKBP) in COS-7 cells. Addition of rapamycin (+Rap) causes heterodimerization of the FRB and FKBP domains and recruitment of motors to the cargo membrane. Recruitment of active motors drives cargo dispersion to the cell periphery. (**B**) Qualitative analysis of peroxisome dispersion. Cells were scored as clustered (black), partially dispersed (dark grey), diffusely dispersed (light grey), or peripherally dispersed (white). The data for each construct are summarized as a stacked bar plot.

4.4.1 KAND Mutations Provide Insight into a Conserved Mechanism of Kinesin Force Generation

Recent structural and biochemical assays with dimeric kinesin-1 motors have provided strong support for the model that nucleotide-dependent conformational changes in the NL provide the power stroke for force generation. NL docking is initiated by an ATP-dependent conformational change in α6 that drives a two-step NL docking: zipping together of the NL's β9 with the CS (β0) to form the CNB and then latching of the NL's β10 along the surface of the core motor domain (Budaitis et al., 2019; Hwang et al., 2008; Khalil et al., 2008). Structural studies have determined that similar ATP-induced changes occur to α6 and the NL in members of the kinesin-3 and kinesin-5 families (Atherton et al., 2014; Goulet et al., 2012; Nitta et al., 2008; Ren, et al., 2018), supporting the hypothesis that NL docking is a force-generating mechanism utilized by all superfamily members. Here we directly test this model for the kinesin-3 motor KIF1A.

We focused on two recently identified *de novo KIF1A* disease variants, V8M and Y89D mutations, based on their a) location in structural elements of the motor domain predicted to have roles in CNB formation and NL docking and b) occurrence in residues that are highly conserved across the kinesin superfamily (Figure 4.2). Our MD simulations predicted that the V8M and Y89D mutations would impair docking of the N-terminal (β9) or C-terminal (β10) portions of the NL to the KIF1A motor domain, respectively (Figure 4.3 and Figure 4.4). Indeed, using an optical trap assay, we found that mutation of V8M and Y89D resulted in the detachment of mutant motors when subjected to low forces (Figure 4.5). Thus, our results extend the model that nucleotide-dependent conformational changes in the NL are an important mechanical element for force generation by kinesin motors.

Previous work on KIF1A by Nitta et al. examined the effects of mutations in β0, β9 and β10 on the output of monomeric KIF1A motors and found that while the mutations had minimal effects on ATPase activity, mutation of β9 resulted in a decreased output in microtubule gliding assays (Nitta et al., 2008). While these results support the idea that NL docking is critical for the power stroke, these mutations were examined in the context of a chimeric motor consisting of the catalytic core of KIF1A

fused to the NL of the kinesin-1 motor KIF5C. Thus, our work provides the first evidence that NL docking is critical for force generation and cargo transport by KIF1A motors.

4.4.2 KIF1A is a weak motor but its high on-rate to the microtubule enables persistent transport under low-load conditions

Previous work examining kinesin-3 motors has demonstrated that under no-load conditions, KIF1A motors readily engage with the microtubule and quickly move long distances before dissociating (Soppina & Verhey, 2014). These motor properties were suggested to be tuned for the long-distance axonal transport functions of this motor. However, a motor's response to load is a key parameter that underlies emergent mechanisms of microtubule-based transport in cells (Arpăg et al., 2014; Norris et al., 2014). Here we provide the first analysis of mammalian kinesin-3 motors under load and note several interesting aspects of KIF1A force generation that are likely to impact its cellular functions.

First, KIF1A motors do not stall when subjected to resisting forces but rather rapidly detach from the microtubule track; this is in stark contrast to the ability of single kineisn-1 motors to resist detachment under load (Budaitis et al., 2019; Khalil et al., 2008; Schnitzer & Block, 1997; Svoboda & Block, 1994; Yildiz et al., 2004). A high load-dependent detachment rate is consistent with previous work showing that kinesin-3 motors give up easily when attached to the same cargo as kinesin-1 motors (Arpăg et al., 2014; Norris et al., 2014). Interestingly, kinesin-2 (KIF3A/KIF3B) and kinesin-5 (Eg5) motors also have a tendency to detach under low to moderate forces in optical trap assays (Andreasson et al., 2015; Milic et al., 2017; Valentine et al., 2006) and give up easily in competition assays with kinesin-1 (Arpăg et al., 2014).

Second, KIF1A motors can only sustain an average 2.7 pN of force before detachment from the microtubule track. The detachment of KIF1A at low forces seems unlikely to be related to the binding strength of the KIF1A motor domain to the microtubule as KIF1A has a higher microtubule affinity than kinesin-1 (Atherton et al., 2014; Soppina & Verhey, 2014). It seems more likely that the detachment of KIF1A at low forces can be attributed to a mechanical feature of the motor. An intriguing possibility is that the length of the N-terminal extension that proceeds the CS impacts the strength of the CNB and thus the force output of the motor. Kinesin-3 motors lack an

N-terminal extension and recent structural studies and MD simulations of KIF13B showed that this kinesin-3 motor forms a short CNB with weaker CS-NL interactions than kinesin-1 (Ren et al., 2018). However, KIF1A's *C. elegans* homolog, UNC-104, also lacks an N-terminal extension yet displays larger detachment forces [~6 pN, (Tomishige et al., 2002)]. This may be a species-specific adaptation as differences in force outputs have also been noted for across kineisn-5 orthologs and may reflect adaption to different functional requirements in each organism.

Third, after detachment, KIF1A motors rapidly reattached to the microtubule and again moved forward out of the trap. This behavior is consistent with the role of the kinesin-3-specific K-loop (Loop12), whose positively-charged residues enhance the affinity of the motor domain for negatively-charged tubulin subunits of the microtubule (Soppina & Verhey, 2014). The rapid detachment and reattachment of single KIF1A motors resulted in a characteristic "sawtooth" pattern for the force versus time plot.

Taken together, these properties are likely matched to the cellular functions of KIF1A and are optimized for transport under physiological conditions. Teams of KIF1A motors drive fast, long-range transport of SVPs and DCVs in neurons (Barkus et al., 2008; Hall & Hedgecock, 1991; Okada et al., 1995; Yonekawa et al., 1998). It may be that large forces are not required for the transport of these small membrane-bound organelles [diameter ~ 50 nm; (Efremov et al., 2014)]. Specifically, KIF1A motors at the leading edge of the cargo experience higher forces and rather than reduce their speed or stall, they can detach and be replaced by other motors without a cost to overall speed of cargo movement. Additionally, axons are crowded and a rapid detachment and reattachment of motors may be advantageous in the context of a crowded axon. Indeed, we note that while team-based transport driven by V8M and Y89D motors in cells is delayed (Figure 4.10), they do catch up to the WT motors given enough time.

4.4.3 Allostery between force generation and motility properties

KIF1A motors containing V8M or Y89D mutations also exhibited changes in unloaded motility, consistent with the deficiencies in coordinating and/or hydrolyzing nucleotide predicted in the MD simulations. The mutant motors moved with reduced speeds, likely due to allosteric effects of NL docking on core motor regions that coordinate and bind nucleotide (S1-PL, S1-S2, Figure 4.3 and 4.4). These findings are

consistent with previous structural and enzymatic studies that suggest that docking of the NL gates ATPase activity in both kinesin-1 and kinesin-3 motors (Cao et al., 2014; Hahlen et al., 2006; Muretta et al., 2015; Muretta et al., 2018; Nitta et al., 2008).

The mutant motors also exhibited defects in motor-microtubule interactions as they were less able to engage productively with the microtubules (lower on-rate) and moved with reduced processivity. In addition, a significant fraction of Y89D mutants engaged in non-productive, diffusive microtubule-binding events and those motors that did undergo processive motility appeared to "wobble" as they walked (Figure 4.7). This is consistent with allosteric effects of NL docking on core moor regions that coordinate and bind nucleotide (S1-PL, S1-S2, Figure 4.4). These results highlight the benefits of combining single molecule assays with simulations to explain how subtle sequence changes can have unexpected effects on the mechanical output of a motor. In the future, this approach can be utilized to examine the local and global impact of other disease-associated mutations or family-specific sequence changes on the kinesin motor domain.

4.4.4 Insight into disease

Our computational and experimental analyses suggest that the V8M and Y89D disease-associated variants affect the speed, processivity, landing-rate, and force output of single KIF1A motors. Under physiological conditions, these altered motility characteristics can impact transport driven by teams of mutant motors as the mutant motors took a longer time to drive transport to the cell periphery than teams of WT motors (Figure 4.10). This effect may be even more pronounced in neurons, where the distances required of KIF1A-mediated transport are significantly longer. Recent work by Chiba et al. found that two different KAND mutations (V8M and R360) caused mislocalization of presynaptic vesicles in neurons and defects in neuronal function in *C. elegans* (Chiba et al., 2019).

In KAND mutants, only one copy of the V8M or Y89D mutant gene can manifest in disease and the patient's cells likely have a mixed population of homodimeric WT, homodimeric mutant, and heterodimeric WT/mutant motors. Our unloaded single-molecule motility results suggest that the presence of a mutant motor domain is sufficient to impair the motility properties of heterodimeric WT/mutant motors (Figure

4.10). Studies assessing the effects of mixed populations of mutant motors or heterdimeric motors on a shared cargo in a physiological, disease context are lacking. A previous study characterized the localization of mixed populations of WT or mutant KIF1A motors in neuron as a readout for defects in transport, however the study was done with monomeric KIF1A, making it difficult to interpret to a mechanism where transport is drive by the foot-over-foot stepping (Cheon et al., 2017). A more careful dissection of multi-motor transport in neuronal like cells using fast, live cell imaging to quantify transport speeds, pausing events, or frequency of directional switches may help tease apart effects on intracellular transport.

In addition to mutations in the core motor domain, other mutations have been identified in the coiled-coil or tail domain of KIF1A (Gabrych et al., 2019). These mutations may alter the ability for stable dimerization of motor domains or prevent motor recruitment to cargo rather than affect the functional output of the motor domain. Another intriguing possibility is that mutations in the coiled-coil domain or tail-domain relieve autoinhibition, resulting in population of constitutively active motors rather than a loss of function effect. Indeed, KAND mutations V8M and R360 relieve KIF1A autoinhibition in worms and causes misaccumulation of presynaptic vesicles in neurons (Chiba et al., 2019). Collectively, this highlights the diverse nature of KIF1A-disease associated mutations that can lead to dramatic changes in the functional output of the motor.

4.5 References

Albracht, C. D., Rank, K. C., Obrzut, S., Rayment, I., & Gilbert, S. P. (2014). Kinesin-2 KIF3AB exhibits novel ATPase characteristics. *J Biol Chem, 289*(40), 27836-27848. doi:10.1074/jbc.M114.583914

Andreasson, J. O., Shastry, S., Hancock, W. O., & Block, S. M. (2015). The Mechanochemical Cycle of Mammalian Kinesin-2 KIF3A/B under Load. *Curr Biol, 25*(9), 1166-1175. doi:10.1016/j.cub.2015.03.013

Arpağ, G., Shastry, S., Hancock, W. O., & Tuzel, E. (2014). Transport by populations of fast and slow kinesins uncovers novel family-dependent motor characteristics important for in vivo function. *Biophys J, 107*(8), 1896-1904. doi:10.1016/j.bpj.2014.09.009

Atherton, J., Farabella, I., Yu, I. M., Rosenfeld, S. S., Houdusse, A., Topf, M., & Moores, C. A. (2014). Conserved mechanisms of microtubule-stimulated ADP release, ATP binding, and force generation in transport kinesins. *Elife, 3*, e03680. doi:10.7554/eLife.03680

Atherton, J., Yu, I. M., Cook, A., Muretta, J. M., Joseph, A., Major, J., . . . Moores, C. A. (2017). The divergent mitotic kinesin MKLP2 exhibits atypical structure and mechanochemistry. *Elife, 6*. doi:10.7554/eLife.27793

Auerbach, S. D., & Johnson, K. A. (2005). Kinetic effects of kinesin switch I and switch II mutations. *J Biol Chem, 280*(44), 37061-37068. doi:10.1074/jbc.M502985200

Barkus, R. V., Klyachko, O., Horiuchi, D., Dickson, B. J., & Saxton, W. M. (2008). Identification of an axonal kinesin-3 motor for fast anterograde vesicle transport that facilitates retrograde transport of neuropeptides. *Mol Biol Cell, 19*(1), 274-283. doi:10.1091/mbc.e07-03-0261

Brendza, K. M., Rose, D. J., Gilbert, S. P., & Saxton, W. M. (1999). Lethal kinesin mutations reveal amino acids important for ATPase activation and structural coupling. *J Biol Chem, 274*(44), 31506-31514. doi:10.1074/jbc.274.44.31506

Budaitis, B. G., Jariwala, S., Reinemann, D. N., Schimert, K. I., Scarabelli, G., Grant, B. J., . . . Verhey, K. J. (2019). Neck linker docking is critical for Kinesin-1 force generation in cells but at a cost to motor speed and processivity. *Elife, 8*. doi:10.7554/eLife.44146

Cao, L., Wang, W., Jiang, Q., Wang, C., Knossow, M., & Gigant, B. (2014). The structure of apo-kinesin bound to tubulin links the nucleotide cycle to movement. *Nat Commun, 5*, 5364. doi:10.1038/ncomms6364

Cheon, C. K., Lim, S. H., Kim, Y. M., Kim, D., Lee, N. Y., Yoon, T. S., . . . Lee, J. R. (2017). Autosomal dominant transmission of complicated hereditary spastic paraplegia due to a dominant negative mutation of KIF1A, SPG30 gene. *Sci Rep, 7*(1), 12527. doi:10.1038/s41598-017-12999-9

Chiba, K., Takahashi, H., Chen, M., Obinata, H., Arai, S., Hashimoto, K., . . . Niwa, S. (2019). Disease-associated mutations hyperactivate KIF1A motility and anterograde axonal transport of synaptic vesicle precursors. *Proc Natl Acad Sci U S A, 116*(37), 18429-18434. doi:10.1073/pnas.1905690116

Citterio, A., Arnoldi, A., Panzeri, E., Merlini, L., D'Angelo, M. G., Musumeci, O., . . . Bassi, M. T. (2015). Variants in KIF1A gene in dominant and sporadic forms of hereditary spastic paraparesis. *J Neurol, 262*(12), 2684-2690. doi:10.1007/s00415-015-7899-9

Clancy, B. E., Behnke-Parks, W. M., Andreasson, J. O., Rosenfeld, S. S., & Block, S. M. (2011). A universal pathway for kinesin stepping. *Nat Struct Mol Biol, 18*(9), 1020-1027. doi:10.1038/nsmb.2104

Efremov, A. K., Radhakrishnan, A., Tsao, D. S., Bookwalter, C. S., Trybus, K. M., & Diehl, M. R. (2014). Delineating cooperative responses of processive motors in living cells. *Proc Natl Acad Sci U S A, 111*(3), E334-343. doi:10.1073/pnas.1313569111

Esmaeeli Nieh, S., Madou, M. R., Sirajuddin, M., Fregeau, B., McKnight, D., Lexa, K., . . . Sherr, E. H. (2015). De novo mutations in KIF1A cause progressive encephalopathy and brain atrophy. *Ann Clin Transl Neurol, 2*(6), 623-635. doi:10.1002/acn3.198

Gigant, B., Wang, W., Dreier, B., Jiang, Q., Pecqueur, L., Pluckthun, A., . . . Knossow, M. (2013). Structure of a kinesin-tubulin complex and implications for kinesin motility. *Nat Struct Mol Biol, 20*(8), 1001-1007. doi:10.1038/nsmb.2624

Goulet, A., Behnke-Parks, W. M., Sindelar, C. V., Major, J., Rosenfeld, S. S., & Moores, C. A. (2012). The structural basis of force generation by the mitotic motor kinesin-5. *J Biol Chem, 287*(53), 44654-44666. doi:10.1074/jbc.M112.404228

Guzik-Lendrum, S., Rank, K. C., Bensel, B. M., Taylor, K. C., Rayment, I., & Gilbert, S. P. (2015). Kinesin-2 KIF3AC and KIF3AB Can Drive Long-Range Transport along Microtubules. *Biophys J, 109*(7), 1472-1482. doi:10.1016/j.bpj.2015.08.004

Hahlen, K., Ebbing, B., Reinders, J., Mergler, J., Sickmann, A., & Woehlke, G. (2006). Feedback of the kinesin-1 neck-linker position on the catalytic site. *J Biol Chem, 281*(27), 18868-18877. doi:10.1074/jbc.M508019200

Hall, D. H., & Hedgecock, E. M. (1991). Kinesin-related gene unc-104 is required for axonal transport of synaptic vesicles in C. elegans. *Cell, 65*(5), 837-847. doi:10.1016/0092-8674(91)90391-b

Hammond, J. W., Cai, D., Blasius, T. L., Li, Z., Jiang, Y., Jih, G. T., . . . Verhey, K. J. (2009). Mammalian Kinesin-3 motors are dimeric in vivo and move by processive motility upon release of autoinhibition. *PLoS Biol,* *7*(3), e72. doi:10.1371/journal.pbio.1000072

Hasegawa, A., Koike, R., Koh, K., Kawakami, A., Hara, N., Takiyama, Y., & Ikeuchi, T. (2017). Co-existence of spastic paraplegia-30 with novel KIF1A mutation and spinocerebellar ataxia 31 with intronic expansion of BEAN and TK2 in a family. *J Neurol Sci, 372*, 128-130. doi:10.1016/j.jns.2016.11.032

Hesse, W. R., Steiner, M., Wohlever, M. L., Kamm, R. D., Hwang, W., & Lang, M. J. (2013). Modular aspects of kinesin force generation machinery. *Biophys J, 104*(9), 1969-1978. doi:10.1016/j.bpj.2013.03.051

Hirokawa, N., Noda, Y., Tanaka, Y., & Niwa, S. (2009). Kinesin superfamily motor proteins and intracellular transport. *Nat Rev Mol Cell Biol, 10*(10), 682-696. doi:10.1038/nrm2774

Hornak, V., Abel, R., Okur, A., Strockbine, B., Roitberg, A., & Simmerling, C. (2006). Comparison of multiple Amber force fields and development of improved protein backbone parameters. *Proteins, 65*(3), 712-725. doi:10.1002/prot.21123

Hotchkiss, L., Donkervoort, S., Leach, M. E., Mohassel, P., Bharucha-Goebel, D. X., Bradley, N., . . . Bonnemann, C. G. (2016). Novel De Novo Mutations in KIF1A as a Cause of Hereditary Spastic Paraplegia With Progressive Central Nervous System Involvement. *J Child Neurol,* *31*(9), 1114-1119. doi:10.1177/0883073816639718

Huckaba, T. M., Gennerich, A., Wilhelm, J. E., Chishti, A. H., & Vale, R. D. (2011). Kinesin-73 is a processive motor that localizes to Rab5-containing organelles. *J Biol Chem, 286*(9), 7457-7467. doi:10.1074/jbc.M110.167023

Hwang, W., Lang, M. J., & Karplus, M. (2008). Force generation in kinesin hinges on cover-neck bundle formation. *Structure,* *16*(1), 62-71. doi:10.1016/j.str.2007.11.008

Hwang, W., Lang, M. J., & Karplus, M. (2017). Kinesin motility is driven by subdomain dynamics. *Elife, 6*. doi:10.7554/eLife.28948

Iqbal, Z., Rydning, S. L., Wedding, I. M., Koht, J., Pihlstrom, L., Rengmark, A. H., . . . Toft, M. (2017). Correction: Targeted high throughput sequencing in hereditary ataxia and spastic paraplegia. *PLoS One, 12*(10), e0186571. doi:10.1371/journal.pone.0186571

Jennings, S., Chenevert, M., Liu, L., Mottamal, M., Wojcik, E. J., & Huckaba, T. M. (2017). Characterization of kinesin switch I mutations that cause hereditary spastic paraplegia. *PLoS One, 12*(7), e0180353. doi:10.1371/journal.pone.0180353

Kapitein, L. C., Schlager, M. A., van der Zwan, W. A., Wulf, P. S., Keijzer, N., & Hoogenraad, C. C. (2010). Probing intracellular motor protein activity using an inducible cargo trafficking assay. *Biophys J, 99*(7), 2143-2152. doi:10.1016/j.bpj.2010.07.055

Khalil, A. S., Appleyard, D. C., Labno, A. K., Georges, A., Karplus, M., Belcher, A. M., . . . Lang, M. J. (2008). Kinesin's cover-neck bundle folds forward to generate force. *Proc Natl Acad Sci U S A, 105*(49), 19247-19252. doi:10.1073/pnas.0805147105

Klebe, S., Lossos, A., Azzedine, H., Mundwiller, E., Sheffer, R., Gaussen, M., . . . Stevanin, G. (2012). KIF1A missense mutations in SPG30, an autosomal recessive spastic paraplegia: distinct phenotypes according to the nature of the mutations. *Eur J Hum Genet, 20*(6), 645-649. doi:10.1038/ejhg.2011.261

Kull, F. J., Vale, R. D., & Fletterick, R. J. (1998). The case for a common ancestor: kinesin and myosin motor proteins and G proteins. *J Muscle Res Cell Motil, 19*(8), 877-886. doi:10.1023/a:1005489907021

Lang, M. J., & Hwang, W. (2010). Motor proteins: kinesin drives with an underhead cam. *Curr Biol, 20*(9), R408-410. doi:10.1016/j.cub.2010.03.015

Lee, J. R., Srour, M., Kim, D., Hamdan, F. F., Lim, S. H., Brunel-Guitton, C., . . . Michaud, J. L. (2015). De novo mutations in the motor domain of KIF1A cause cognitive impairment, spastic paraparesis, axonal neuropathy, and cerebellar atrophy. *Hum Mutat, 36*(1), 69-78. doi:10.1002/humu.22709

Li, H., Robertson, A. D., & Jensen, J. H. (2005). Very fast empirical prediction and rationalization of protein pKa values. *Proteins, 61*(4), 704-721. doi:10.1002/prot.20660

Lindhout, D. A., Litowski, J. R., Mercier, P., Hodges, R. S., & Sykes, B. D. (2004). NMR solution structure of a highly stable de novo heterodimeric coiled-coil. *Biopolymers, 75*(5), 367-375. doi:10.1002/bip.20150

Meagher, K. L., Redman, L. T., & Carlson, H. A. (2003). Development of polyphosphate parameters for use with the AMBER force field. *J Comput Chem, 24*(9), 1016-1025. doi:10.1002/jcc.10262

Megahed, H., Nicouleau, M., Barcia, G., Medina-Cano, D., Siquier-Pernet, K., Bole-Feysot, C., . . . Cantagrel, V. (2016). Utility of whole exome sequencing for the early diagnosis of pediatric-onset cerebellar atrophy associated with developmental delay in an inbred population. *Orphanet J Rare Dis, 11*(1), 57. doi:10.1186/s13023-016-0436-9

Milic, B., Andreasson, J. O. L., Hogan, D. W., & Block, S. M. (2017). Intraflagellar transport velocity is governed by the number of active KIF17 and KIF3AB motors and their motility properties under load. *Proc Natl Acad Sci U S A, 114*(33), E6830-E6838. doi:10.1073/pnas.1708157114

Muretta, J. M., Jun, Y., Gross, S. P., Major, J., Thomas, D. D., & Rosenfeld, S. S. (2015). The structural kinetics of switch-1 and the neck linker explain the functions of kinesin-1 and Eg5. *Proc Natl Acad Sci U S A, 112*(48), E6606-6613. doi:10.1073/pnas.1512305112

Muretta, J. M., Reddy, B. J. N., Scarabelli, G., Thompson, A. F., Jariwala, S., Major, J., . . . Rosenfeld, S. S. (2018). A posttranslational modification of the mitotic kinesin Eg5 that enhances its mechanochemical coupling and alters its mitotic function. *Proc Natl Acad Sci U S A, 115*(8), E1779-E1788. doi:10.1073/pnas.1718290115

Nitta, R., Kikkawa, M., Okada, Y., & Hirokawa, N. (2004). KIF1A alternately uses two loops to bind microtubules. *Science, 305*(5684), 678-683. doi:10.1126/science.1096621

Nitta, R., Okada, Y., & Hirokawa, N. (2008). Structural model for strain-dependent microtubule activation of Mg-ADP release from kinesin. *Nat Struct Mol Biol, 15*(10), 1067-1075. doi:10.1038/nsmb.1487

Nitta, T., Tanahashi, A., Obara, Y., Hirano, M., Razumova, M., Regnier, M., & Hess, H. (2008). Comparing guiding track requirements for myosin- and kinesin-powered molecular shuttles. *Nano Lett, 8*(8), 2305-2309. doi:10.1021/nl8010885

Norris, S. R., Nunez, M. F., & Verhey, K. J. (2015). Influence of fluorescent tag on the motility properties of kinesin-1 in single-molecule assays. *Biophys J, 108*(5), 1133-1143. doi:10.1016/j.bpj.2015.01.031

Norris, S. R., Soppina, V., Dizaji, A. S., Schimert, K. I., Sept, D., Cai, D., . . . Verhey, K. J. (2014). A method for multiprotein assembly in cells reveals independent action of kinesins in complex. *J Cell Biol, 207*(3), 393-406. doi:10.1083/jcb.201407086

Ohba, C., Haginoya, K., Osaka, H., Kubota, K., Ishiyama, A., Hiraide, T., . . . Matsumoto, N. (2015). De novo KIF1A mutations cause intellectual deficit, cerebellar atrophy, lower limb spasticity and visual disturbance. *J Hum Genet, 60*(12), 739-742. doi:10.1038/jhg.2015.108

Okada, Y., & Hirokawa, N. (1999). A processive single-headed motor: kinesin superfamily protein KIF1A. *Science, 283*(5405), 1152-1157. doi:10.1126/science.283.5405.1152

Okada, Y., Yamazaki, H., Sekine-Aizawa, Y., & Hirokawa, N. (1995). The neuron-specific kinesin superfamily protein KIF1A is a unique monomeric motor for anterograde axonal transport of synaptic vesicle precursors. *Cell, 81*(5), 769-780. doi:10.1016/0092-8674(95)90538-3

Okamoto, N., Miya, F., Tsunoda, T., Yanagihara, K., Kato, M., Saitoh, S., . . . Kosaki, K. (2014). KIF1A mutation in a patient with progressive neurodegeneration. *J Hum Genet, 59*(11), 639-641. doi:10.1038/jhg.2014.80

Parke, C. L., Wojcik, E. J., Kim, S., & Worthylake, D. K. (2010). ATP hydrolysis in Eg5 kinesin involves a catalytic two-water mechanism. *J Biol Chem, 285*(8), 5859-5867. doi:10.1074/jbc.M109.071233

Raffa, L., Matton, M. P., Michaud, J., Rossignol, E., Decarie, J. C., & Ospina, L. H. (2017). Optic nerve hypoplasia in a patient with a de novo KIF1A heterozygous mutation. *Can J Ophthalmol, 52*(5), e169-e171. doi:10.1016/j.jcjo.2017.02.021

Rank, K. C., Chen, C. J., Cope, J., Porche, K., Hoenger, A., Gilbert, S. P., & Rayment, I. (2012). Kar3Vik1, a member of the kinesin-14 superfamily, shows a novel kinesin

microtubule binding pattern. *J Cell Biol, 197*(7), 957-970. doi:10.1083/jcb.201201132

Rao, L., Berger, F., Nicholas, M. P., & Gennerich, A. (2019). Molecular mechanism of cytoplasmic dynein tension sensing. *Nat Commun, 10*(1), 3332. doi:10.1038/s41467-019-11231-8

Ren, J., Wang, S., Chen, H., Wang, W., Huo, L., & Feng, W. (2018). Coiled-coil 1-mediated fastening of the neck and motor domains for kinesin-3 autoinhibition. *Proc Natl Acad Sci U S A, 115*(51), E11933-E11942. doi:10.1073/pnas.1811209115

Ren, J., Zhang, Y., Wang, S., Huo, L., Lou, J., & Feng, W. (2018). Structural Delineation of the Neck Linker of Kinesin-3 for Processive Movement. *J Mol Biol, 430*(14), 2030-2041. doi:10.1016/j.jmb.2018.05.010

Richard, J., Kim, E. D., Nguyen, H., Kim, C. D., & Kim, S. (2016). Allostery Wiring Map for Kinesin Energy Transduction and Its Evolution. *J Biol Chem, 291*(40), 20932-20945. doi:10.1074/jbc.M116.733675

Roda, R. H., Schindler, A. B., & Blackstone, C. (2017). Multigeneration family with dominant SPG30 hereditary spastic paraplegia. *Ann Clin Transl Neurol, 4*(11), 821-824. doi:10.1002/acn3.452

Sali, A., & Blundell, T. L. (1993). Comparative protein modelling by satisfaction of spatial restraints. *J Mol Biol, 234*(3), 779-815. doi:10.1006/jmbi.1993.1626

Samanta, D., & Gokden, M. (2019). PEHO syndrome: KIF1A mutation and decreased activity of mitochondrial respiratory chain complex. *J Clin Neurosci, 61*, 298-301. doi:10.1016/j.jocn.2018.10.091

Scarabelli, G., Soppina, V., Yao, X. Q., Atherton, J., Moores, C. A., Verhey, K. J., & Grant, B. J. (2015). Mapping the Processivity Determinants of the Kinesin-3 Motor Domain. *Biophys J, 109*(8), 1537-1540. doi:10.1016/j.bpj.2015.08.027

Schimert, K. I., Budaitis, B. G., Reinemann, D. N., Lang, M. J., & Verhey, K. J. (2019). Intracellular cargo transport by single-headed kinesin motors. *Proc Natl Acad Sci U S A, 116*(13), 6152-6161. doi:10.1073/pnas.1817924116

Schnitzer, M. J., & Block, S. M. (1997). Kinesin hydrolyses one ATP per 8-nm step. *Nature, 388*(6640), 386-390. doi:10.1038/41111

Shang, Z., Zhou, K., Xu, C., Csencsits, R., Cochran, J. C., & Sindelar, C. V. (2014). High-resolution structures of kinesin on microtubules provide a basis for nucleotide-gated force-generation. *Elife, 3*, e04686. doi:10.7554/eLife.04686

Shen, M. Y., & Sali, A. (2006). Statistical potential for assessment and prediction of protein structures. *Protein Sci, 15*(11), 2507-2524. doi:10.1110/ps.062416606

Sindelar, C. V., & Downing, K. H. (2010). An atomic-level mechanism for activation of the kinesin molecular motors. *Proc Natl Acad Sci U S A, 107*(9), 4111-4116. doi:10.1073/pnas.0911208107

Skjaerven, L., Yao, X. Q., Scarabelli, G., & Grant, B. J. (2014). Integrating protein structural dynamics and evolutionary analysis with Bio3D. *BMC Bioinformatics, 15*, 399. doi:10.1186/s12859-014-0399-6

Song, H., & Endow, S. A. (1998). Decoupling of nucleotide- and microtubule-binding sites in a kinesin mutant. *Nature, 396*(6711), 587-590. doi:10.1038/25153

Soppina, V., Norris, S. R., Dizaji, A. S., Kortus, M., Veatch, S., Peckham, M., & Verhey, K. J. (2014). Dimerization of mammalian kinesin-3 motors results in superprocessive motion. *Proc Natl Acad Sci U S A, 111*(15), 5562-5567. doi:10.1073/pnas.1400759111

Soppina, V., & Verhey, K. J. (2014). The family-specific K-loop influences the microtubule on-rate but not the superprocessivity of kinesin-3 motors. *Mol Biol Cell, 25*(14), 2161-2170. doi:10.1091/mbc.E14-01-0696

Svoboda, K., & Block, S. M. (1994). Force and velocity measured for single kinesin molecules. *Cell, 77*(5), 773-784. doi:10.1016/0092-8674(94)90060-4

Tomaselli, P. J., Rossor, A. M., Horga, A., Laura, M., Blake, J. C., Houlden, H., & Reilly, M. M. (2017). A de novo dominant mutation in KIF1A associated with axonal neuropathy, spasticity and autism spectrum disorder. *J Peripher Nerv Syst, 22*(4), 460-463. doi:10.1111/jns.12235

Tomishige, M., Klopfenstein, D. R., & Vale, R. D. (2002). Conversion of Unc104/KIF1A kinesin into a processive motor after dimerization. *Science, 297*(5590), 2263-2267. doi:10.1126/science.1073386

Tomishige, M., & Vale, R. D. (2000). Controlling kinesin by reversible disulfide cross-linking. Identifying the motility-producing conformational change. *J Cell Biol, 151*(5), 1081-1092. doi:10.1083/jcb.151.5.1081

Travaglini, L., Aiello, C., Stregapede, F., D'Amico, A., Alesi, V., Ciolfi, A., . . . Nicita, F. (2018). The impact of next-generation sequencing on the diagnosis of pediatric-onset hereditary spastic paraplegias: new genotype-phenotype correlations for rare HSP-related genes. *Neurogenetics, 19*(2), 111-121. doi:10.1007/s10048-018-0545-9

Turner, J., Anderson, R., Guo, J., Beraud, C., Fletterick, R., & Sakowicz, R. (2001). Crystal structure of the mitotic spindle kinesin Eg5 reveals a novel conformation of the neck-linker. *J Biol Chem, 276*(27), 25496-25502. doi:10.1074/jbc.M100395200

Uchimura, S., Oguchi, Y., Hachikubo, Y., Ishiwata, S., & Muto, E. (2010). Key residues on microtubule responsible for activation of kinesin ATPase. *EMBO J, 29*(7), 1167-1175. doi:10.1038/emboj.2010.25

Valentine, M. T., Fordyce, P. M., Krzysiak, T. C., Gilbert, S. P., & Block, S. M. (2006). Individual dimers of the mitotic kinesin motor Eg5 step processively and support substantial loads in vitro. *Nat Cell Biol, 8*(5), 470-476. doi:10.1038/ncb1394

Yildiz, A., Tomishige, M., Vale, R. D., & Selvin, P. R. (2004). Kinesin walks hand-over-hand. *Science, 303*(5658), 676-678. doi:10.1126/science.1093753

Ylikallio, E., Kim, D., Isohanni, P., Auranen, M., Kim, E., Lonnqvist, T., & Tyynismaa, H. (2015). Dominant transmission of de novo KIF1A motor domain variant underlying pure spastic paraplegia. *Eur J Hum Genet, 23*(10), 1427-1430. doi:10.1038/ejhg.2014.297

Yonekawa, Y., Harada, A., Okada, Y., Funakoshi, T., Kanai, Y., Takei, Y., . . . Hirokawa, N. (1998). Defect in synaptic vesicle precursor transport and neuronal cell death in KIF1A motor protein-deficient mice. *J Cell Biol, 141*(2), 431-441. doi:10.1083/jcb.141.2.431

Yoshikawa, K., Kuwahara, M., Saigoh, K., Ishiura, H., Yamagishi, Y., Hamano, Y., . . . Kusunoki, S. (2019). The novel de novo mutation of KIF1A gene as the cause for

Spastic paraplegia 30 in a Japanese case. *eNeurologicalSci, 14*, 34-37. doi:10.1016/j.ensci.2018.11.026

Yun, M., Zhang, X., Park, C. G., Park, H. W., & Endow, S. A. (2001). A structural pathway for activation of the kinesin motor ATPase. *EMBO J, 20*(11), 2611-2618. doi:10.1093/emboj/20.11.2611

Chapter 5: Discussion and Future Outlook

5.1 Discussion

In this dissertation, I first presented work that addressed a gap in our understanding of the mechanism for how single kinesin-1 motors generate force. We find an unexpected trade-off in motility properties by modulating neck linker docking in kinesin-1 motors, providing insight into the design principles of the kinesin motor domain. We then used novel artificial cargo assays to assess the impact of how weakening kinesin-1's force output impacts its ability to collectively drive transport in cells. We provide the first evidence that a power stroke-based mechanism is required for teams of kinesin-1 motors to drive high-load transport under physiological conditions and that properties other than force generation can drive transport of low-load cargo [Chapter 2; (Budaitis et al., 2019)]. Our findings that weakening NL docking in kinesin-1 motors dramatically influences their single-molecule properties and ability to drive transport in cells, led us to test whether is true for other kinesin families (Chapter 3) or in kinesin motors that harbor disease-associated mutations (Chapter 4).

Collectively, this work provides insight into what molecular features of the kinesin motor domain are critical for teams of motors to drive transport in their native environment. Notably, this is one of the first studies where altering a motor's single molecule properties is directly correlated with its ability to drive transport in a physiological context, bridging the gap in understanding how a motor's single molecule properties dictates its function in biology. On a broader scale, this work addresses a common theme in biology of how subtle sequence changes can lead to large-scale changes in the functional output of a protein, providing insight into how sequence divergence in other large protein superfamilies lead to novel function.

5.1.1 The mechanism of force generation by kinesin motors

Although force generation is predicted to involve ATP-induced docking of the neck linker (NL) along the motor's core, the contribution of the proposed substeps [(1)

cover-neck bundle formation, (2) neck linker latching] is not clear. We show that CNB formation and NL latching are both required for single kinesin-1 motors to generate a power stroke and continuously transport under load. Specifically, weakening either substep decreases the force output of kinesin-1 motors under single molecule conditions (Chapter 2).

Recent trapping studies have revealed differences in the force output of motors across the kinesin superfamily [(Andreasson et al., 2015; Hesse et al., 2013; Milic et al., 2017; Muretta et al., 2018; Tomishige, Klopfenstein, & Vale, 2002), Chapter 4)]. However, the molecular features of the motor domain responsible for these differences are not clear. One possibility is that sequence divergence within the CS, NL, and docking pocket across the kinesin superfamily modulates their behavior under force. Indeed, CNB formation is structurally observed across the kinesin superfamily (Atherton et al., 2014; Atherton et al., 2017; Goulet et al., 2012; Hesse et al., 2013; Nitta et al., 2008), yet whether family-specific variations in the length and sequence of the CS contributes to the diversity of motility properties across the kinesin superfamily is not well understood.

Previous work suggests that kinesin-5 motor Eg5 has sequence changes in the NL docking pocket (Loop13) to help lock the NL along the core motor domain and compensate for its weak CNB, thereby enabling motors to step under moderate loads. To delineate the importance of these interactions, Hesse et al. generated chimeric kinesin-1 motors with CS, NL, and/or Loop13 sequences of Eg5 and then measured the force output of the chimeric motors in an optical trap. Swapping elements between kinesin motor domains is a common strategy in the motor field to describe a specific structural element's contribution to motility (Case et al., 2000; Endow & Waligora, 1998; Soppina & Verhey, 2014). Although the reduced force output of chimeric kinesin-1 motors support the prediction that changing interactions between the CS, NL and docking pocket (Loop13) can change the force output of a motor, the drastically different catalytic properties of kinesin-1 and -5 motors make it difficult to carefully extrapolate these findings to Eg5 (Hesse et al., 2013). An alternate approach is to use a similar strategy as presented in Chapter 2. Molecular dynamics simulations can be used to guide the design of mutations to either strengthen or weaken CNB formation and the

functional impact of the mutations can be characterized using a number of biophysical or cell-based assays. This approach can also be extended to delineate the contribution of other structural elements of the kinesin motor domain.

We noticed that the length of the CS across the kinesin superfamily is highly variable (Chapter 3) and sought to determine what the minimal CS length is required for high-load transport. We find that kinesin-1 motors with a truncated CS, and therefore shorter CNB, have a compromised force output as single motors in an optical trap and are also crippled in their ability to drive transport of high-load cargo in cells. Furthermore, we find that truncation the N-terminal portion of the CS, which is not contribute to CNB formation, cripples high-load transport of membrane-bound organelles in cells. In addition, we find that truncation of the N-terminal portion of the coverstrand of the kinesin-2 motor KIF3AB compromises its ability to drive high-load transport in cells (Chapter 3). This is the first experimental evidence that modulating CNB formation of an N-terminal motor from a different kinesin family compromises its ability to drive transport of high-load cargo in cells. This supports the model that the CS plays a conserved mechanical role in force generation (Budaitis et al., 2019; Hesse et al., 2013; Hwang et al., 2008; Khalil et al., 2008). Surprisingly we find that high-load transport by heterodimeric KIF3AB motors is crippled by weakening CNB formation of the KIF3A but not the KIF3B motor domain, suggesting that the KIF3A motor domain may be important to specify force. Further work is needed to address this functional difference.

Strikingly, molecular dynamics simulations predict that sequence changes in the CS and NL of homodimeric kinesin-2 motor KIF17 limit the number of residues that contribute to CNB formation and therefore this motor is predicted to have a reduced force output. Indeed, we find that teams of KIF17 motors are unable to transport high-load cargo (Golgi elements) in cells (Chapter 3). In contrast, recent optical trapping studies find that single KIF17 motors generate high-force and continuously drive transport under load (Milic et al., 2017). It is possible that there are additional sequences differences in the NL-docking pocket or elsewhere in the KIF17 motor domain that may compensate for poor CNB and enable motors to generate high force. Careful biophysical characterization of the behavior of single KIF17 motors and the

cooperative behavior of teams of KIF17 motors is needed to better understand this discrepancy (see future directions).

The N-latch is conserved in most kinesins, particularly in motors known to step processively along microtubules (Chapter 2) suggesting that NL latching may be a conserved feature for kinesin transport under load. Indeed, we find that the KIF1A KAND mutation in α1-β3 (Y89D) disrupts NL-latching and mutant motors are crippled in their force output (Chapter 4). Whether N-latch formation and docking of β10 along the core motor domain play important roles beyond kinesin-1 and -3 motors remains to be investigated.

5.1.2 Design principles of a kinesin motor domain: small changes have big effects

Despite high sequence and structural conservation of the kinesin motor domain, individual kinesins display amazing diversity in their motility properties. How sequence divergence can manifest in such dramatic changes in the functional output of a kinesin motor is puzzling. Sequence alignment of the motor domain across the kinesin superfamily has led to the identification and characterization of a number of family-specific sequence insertions [for example: kinesin-3 Loop12 (Soppina & Verhey, 2014); kinesin-5 Loop5 (Kapoor et al., 2000); kinesin-8 Loop2 (Kim et al., 2014); kinesin-13 Loop2 (Helenius et al., 2006; Hunter et al., 2003); kinesin-2 Loop11 (Guzik-Lendrum et al., 2015)]. However, often times there are no obvious sequence differences between motors and yet they have different motility properties. For example, the kinesin-4 family is composed of an immotile motor (KIF7), a slow but highly processive motor (KIF27), and a fast but moderately processive motor (KIF4) (Yue et al., 2018).

The work included in this dissertation is an example of how subtle mutations in the kinesin motor domain can have unanticipated effects on motility. Kinesin motors are allosteric enzymes where its functional output (stepping behavior) is dependent on tight coupling between microtubule binding, nucleotide hydrolysis, and force generation. Therefore, single amino acid changes that disrupt communication between these elements (allosteric hot spots) may be sources of sequence divergence responsible for distinct functional outputs of the kinesin motor domain. Indeed, a recent paper by Richards et al. not only identified networks of residue-residue interactions important for force generation, ATP hydrolysis, or microtubule binding, but also identified networks of

interactions critical for long-distance coupling between these functional elements. Notably many elements that form the NL docking pocket (α4, α1-β3, β7, and β8-L13) are linked to elements in the microtubule-binding interface or nucleotide-binding pocket (Richard et al., 2016). Therefore, mutations that disrupt NL docking are predicted to feedback to these elements to modulate microtubule binding and nucleotide binding/hydrolysis (and vice versa). How these networks of communication are disrupted or modified across the kinesin superfamily may be an important strategy to understand how sequence divergence underlies functional diversity.

Strikingly, we found that kinesin-1 motors with single residue changes to weaken CNB formation and NL latching displayed enhanced unloaded motility properties (landing rate, velocity, and run length; Chapter 2) due to allosteric effects on regions that coordinate nucleotide and bind microtubules. Collectively, these results highlight a striking feature of the kinesin motor domain, where subtle changes in force generating elements (CNB formation and NL latching) can act as a molecular gearshift, where speed and processivity come at the cost of robust force production. Whether this is a strategy used to tune motors to be fast and processive versus slower but stronger is not clear.

Moreover, a number of residues identified to form important allosteric networks for kinesin motility (Richard et al., 2016) are mutated in KIF1A associated neurological disorders (Chapter 4), including V8M and Y89D mutations characterized in Chapter 4. Thus, single residue changes that disrupt communication between the nucleotide-binding pocket, microtubule-binding elements, and force generating elements may be a common strategy to disrupt kinesin function and manifest in disease (Shen et al., 2017; Yang et al., 2012).

On a broader scale, this work highlights a common strategy in evolution for how small changes in sequence and/or biophysical properties (binding affinity, rates of catalysis, coupling between functional elements) can lead to novel behavior. Therefore, the use of interdisciplinary techniques to understand the functional output of sequence divergence within the kinesin superfamily can be applied across biology to other protein superfamilies, especially those whose properties are not easy to study under single-molecule conditions.

5.1.3 Insights into designing mutant kinesin motor proteins to probe cellular function

There are over 45 different kinesin motors in humans that display developmental- and tissue-specific expression patters. For example, a subset of kinesin motors is specifically expressed in neurons (Hirokawa et al., 2010; Hirokawa et al., 2009; Miki et al., 2003). It is unknown how kinesin motors are functionally distinct from one another. Gene knockout in model organisms have been used to better understand the biological significance of a specific kinesin. However, many times gene knockouts are embryonic lethal, have subtle effects as a result of functionally redundant motors, or the effects are secondary to the motor's function making it difficult to conclude the biological significance of a given motor (Nakajima et al., 2002; Yang et al., 2001). Furthermore, high sequence and structural conservation of the kinesin motor domain make development of inhibitors specific to a kinesin motor or family difficult [with exception of kinesin-5 Eg5 (Kapoor et al., 2000) and kinesin-15 KIF15 (Dumas et al., 2019)]. Thus, it has been challenging to specifically and dynamically probe kinesin function in a biological context. Work presented in this dissertation can be applied to design motors that are amenable to inhibition or motors that have altered functional outputs (force generation, velocity, and processivity) and can be used to probe kinesin function without genetically removing the protein.

5.1.3.1 Strategies to design inhibitable kinesin motors

Previous work has developed a chemical-genetic engineering approach to generate kinesin-1, -2, and -3 motors that are sensitive to cell permeable, small-molecule inhibitors. This method requires engineering a kinesin motor domain that has a sequence insertion to lock the motor domain into a conformation that is not amenable to microtubule-based stepping upon addition of an inhibitor (for example, prevents microtubule stimulated ATPase activity or generates a rigor kinesin that is locked on the microtubule track). One approach fuses a DmrB domain to the coverstrand and addition of rapalog links together the two DmrB domains of a dimeric kinesin and prevents stepping, reminiscent with someone trying to walk with their shoelaces tied together (Engelke et al., 2016). Given our findings in Chapter 2, DmrB dimerization is likely to prevent proper forming and/or breaking of the CNB and therefore motor stepping. This

is consistent with previous cross-linking studies that prevent dynamic forming and breaking of the CNB (Tomishige & Vale, 2000).

Strikingly, when designing inhibitable kinesin motors, fusing the DmrB domain to the coverstrand can render a motor (1) inactive in the presence and absence of inhibitor, (2) active in the absence of inhibitor and inactive in the presence of the inhibitor, or (3) active in the absence and presence of the inhibitor. This outcome is specific for each type of kinesin motor that is engineered (Engelke et al., 2019; Engelke et al., 2016) and most likely reflects differences in CNB formation across the kinesin superfamily. Therefore, work assessing the conservation of CNB formation across the kinesin superfamily (Chapter 2 and 3) can provide important insight into designing inhibitable motors. Due to the dynamic nature of CNB formation for kinesin motility and its predicted role in gating ATPase activity (Budaitis et al., 2019; Cao et al., 2014; Hahlen et al., 2006), the coverstrand may be an important mechanical element to modulate and selectively impair motility. Furthermore, as a small flexible element at the N-terminus, it is unlikely that sequence insertions before the coverstrand will cause instability or unfolding of the protein.

5.1.3.2 Strategies to design kinesin motors with altered motility properties

Although *in vitro,* single-molecule studies have provided considerable insight into how kinesins are functionally distinct from one another, how distinct motility properties specifies a motor's function in a physiological context is not clear. Adding to the complexity, most cargoes in cells contain multiple motors on their surface, including (1) motors of the same type, (2) different motors from the same superfamily, and/or (3) different classes of motors. The functional advantage for having mixed populations of motors associated with a cargo is unclear. One possibility is that motors serve functionally redundant roles. Another possibility is that the cooperative activity of these motors leads to emergent mechanisms of transport important for a specific biological task in the cell.

To more carefully dissect these possibilities, motors with altered motility properties (processivity, velocity, force generation, sensitivity to detachment under load), can be engineered to replace the WT motor in a model organism or cell culture system. Work from this dissertation can be used as a guide to design subtle mutations

in the kinesin motor domain to systematically modulate the force output of a motor [Chapters 2 - 4; (Budaitis et al., 2019)]. Furthermore, work from the Verhey lab has designed monomeric kinesins that are unable to step in a foot-over-foot manner (Schimert et al., 2019) and generated mutants with changes in their processivity or microtubule-landing rate (Soppina & Verhey, 2014; Scarabelli et al., 2015), collectively providing a tool box of strategies to alter the functional output of a kinesin motors.

5.2 Future Outlook

5.2.1 Strategies to study multi-motor transport in cells

We have used cell-based transport assays to screen for mutations in the kinesin motor domain that impact the ability for teams of motors to drive the transport of high- versus low-load cargo in cells, a property predicted to underlie functional distinctions between kinesin motors. This method provides an effective strategy to better understand how modulating a kinesin's single-molecule motility properties impact its ability to drive transport under native conditions. However, our conclusions about cargo transport are based on fixed samples. Thus, although we were able to collect higher sample sizes using fixed samples, we do not have information on the dynamics of transport. Future work can use live-cell imaging methods to provide additional insight into how mutations affect the ability of motors to cooperate to drive transport. For instance, transport speed and pause frequencies of individual cargoes may reveal functional underpinnings of emergent transport behaviors in cells (Efremov et al., 2014).

Unfortunately, it is still difficult to connect how the number and organization of motors on an endogenous cargo relates to transport in cells. However, modifications to this artificial cargo transport assay may help bridge this gap in knowledge. For instance, we use a strategy to coat the surface of membrane-bound cargo with kinesin motors, an exaggerated strategy to monitor kinesin-driven transport in cells. Instead, Efremov. et al. used a doxycycline-based method to regulate the number FKBP domains associated with a cargo, and therefore regulate the number of motors recruited to the surface of the cargo. Efremov. et al., found that varying the number of kinesin-1 motors on a low-load cargo did not impact the transport properties of the cargo (Efremov et al., 2014).

However, it would be interesting to see if this relationship changes with different kinesin families, mutants, or when motors are tasked to drive high-load transport.

Often times cargo transport is driven by mixed populations of motors [dynein or myosin, (Hendricks et al., 2010; Schuster et al., 2011; Shubeita et al., 2008; Soppina et al., 2009)]. Therefore, it may be advantageous to address this physiological requirement by inducibly recruiting different types of motors to the surface of cargoes and monitoring transport. Indeed, a variety of inducible recruitment strategies have been optimized to allow for rapid and specific recruitment of dynein, kinesin, or myosin motors [chemical recruitment strategies (Bentley & Banker, 2015; Duan et al., 2015; Efremov et al., 2014; Janssen et al., 2017; Kapitein et al., 2010) and optogenetic recruitment (van Bergeijk, Adrian, Hoogenraad, & Kapitein, 2015)].

Although peroxisome (low-load) and Golgi (high-load) dispersion assays in cells may be more reflective of true transport events than *in vitro* assays, this assay is still not a perfect representation of the functional requirements motors are tasked with in biology. Therefore, it may be beneficial to apply this strategy to study the behavior of motors driving microtubule-based tasks that are more representative of the motor's function in cells. For instance, kinesin-5 motor Eg5 is able to generate substantial forces to slide microtubules in cell division. However, we find that when these motors are coupled through a lipid membrane, they are unable to drive transport of low-load cargo (peroxisomes, data not shown). Therefore, although this may provide important information about how tight or loose coupling of motors can change transport behavior, this strategy would not be insightful to probe the mechanical properties of Eg5 motors. This also may be the reason for the conflicting behavior of the motility of KIF17 as single motors under purified conditions and as teams driving transport in cells.

5.2.2 Insight into disease

Loss of cellular organization or defects in cytoskeletal-based transport can lead to a number of diseases, including cancer (Yu & Feng, 2010), neurodevelopmental/neurodegenerative disorders (Gabrych et al., 2019; Salinas et al., 2008), and ciliopathies (Gerdes et al., 2009). The list of disease-associated mutations in kinesin motor proteins has grown substantially in the last 10 years. Notably, most

disease-associated mutations are located in the motor domain; however, how these mutations impact the functional output of a kinesin motor is not clear.

Often times, the functional impact of a disease-associated mutation is inferred from sequence alignment. However, a number of KIF1A associated mutations (Chapter 4) map to elements in the kinesin motor domain with no direct implication in microtubule binding, nucleotide binding/hydrolysis, or stepping/force generation. Therefore, it can be difficult to infer a mutations impact on kinesin function and careful characterization of how disease-associated mutations impact the functional output of a motor may be necessary. Recent work has identified a network of residues across the kinesin motor domain important for maintaining communication between functional elements and may serve as an important resource for understanding how mutations impact kinesin function (Richard et al., 2016).

Work from this dissertation suggests that disease-associated mutations may not only affect a motor's single-molecule motility properties but also its ability to cooperate to drive transport. Only a few previous studies assess the functional output of teams of mutant motors and this is typically done with microtubule-gliding assays (Arpăg et al, 2014; Nieh et al., 2017). Unfortunately, in microtubule gliding assays, motors are rigidly coupled to one another. Thus, although this assay may be informative for motors that drive microtubule sliding during cell division, it may not be the best way to assess the behavior of mutant motors driving transport of membrane-bound cargo, where motors are loosely coupled in a lipid membrane (Grover et al., 2016). Therefore, it may be important to compare the behavior of mutant motors under single-molecule conditions with their ability to drive microtubule-based tasks in cells using a functionally relevant assay to better understand of how changing their functional output manifests in disease.

Finally, some disease-associated mutations in kinesin motors have dominant effects (Gabrych et al., 2019). Therefore, it is important to understand the behavior of heterodimeric motors, where one motor domain harbors a mutation while the other motor domain is WT. We find that pairing a KIF1A KAND mutant motor domain with a WT KIF1A motor domain does not rescue motility. Methods to create heterodimeric motors will be important for future work. It is also possible that endogenous cargoes have mixed populations of (1) homodimer WT motors, (2) homodimeric mutant motors,

and (3) heterodimeric motors. Thus, it will also be important to understand how this impacts their ability to cooperatively drive transport in each scenario.

5.2.3 Conservation of CNB formation across the kinesin superfamily

Although there is structural evidence that the cover-neck bundle forms in a number of different kinesins (Atherton et al., 2014; Atherton et al., 2017; Goulet et al., 2012; Hesse et al., 2013; Nitta et al., 2008), biophysical evidence that the coverstrand is a conserved mechanical element important for kinesin motors to generate a power stroke is lacking. We used artificial transport assays in cells to screen how sequences changes in the CS or NL impacts the ability for different kinesin motors to drive transport of high-load versus low-load cargo in a physiological context. Although this work supports the model that CNB formation is a mechanical element important for high-load transport, how modulation of these elements impacts the functional output of single kinesins motors is not clear. Therefore, a more detailed characterization of CS and NL mutants across the kinesin superfamily will provide important insight into how differences in their force output contributes to their function in cells.

5.2.4 KIF17 and its functional output in cells

Our molecular dynamics simulations suggest that the short length of the coverstrand and a proline residue in β9 of the NL reduces the number of residues in the that can contribute to cover-neck bundle formation. Consistent with this prediction, teams of KIF17 motors were able to drive the transport of low- but not high-load cargo to the cell periphery. However, mutations predicted to lengthen CNB formation in KIF17 did not enhance the ability for teams of motors to drive high load-transport. Strikingly, recent optical trap studies suggest that KIF17 is able to continuously transport against high forces under single molecule conditions [6 pN stall force; (Milic et al., 2017)].

The disparity between KIF17's single-molecule motility properties and its inability to drive high-load transport in cells is puzzling. KIF17 is best known for its function in driving intraflagellar transport in primary cilia and vesicle transport in neurons (Hirokawa et al., 2010; Verhey, Dishinger, & Kee, 2011), both areas that have specialized compartments with tight regulation of transport (Hirokawa et al., 2010). Therefore, it is possible that our low- and high-load, artificial cargo assays are not appropriate methods

to probe the functional output of KIF17. One possibility is that the activity of KIF17 is regulated in an unanticipated manner in the cytoplasm of cells. For instance, the functional output of KIF17 may be regulated by posttranslational modifications or by proteins that directly bind to KIF17. Indeed, kinesin binding protein (KBP) was recently identified to bind to the motor domain of KIF1A, preventing its association with microtubules in neurons (Kevenaar et al., 2016). Another possibility is that KIF17 requires a specific subset of microtubules to drive transport along. However, increasing the polyglytamylation, acetylation, or detyrosination of microtubules in COS-7 cells had no effect on enhancing the ability for teams of KIF17 motors to drive high-load transport (data not shown). Therefore, recruitment of KIF17 motors to its native cargo in a cellular context may be a better strategy to understand its behavior in cells (Engelke et al., 2019; Franker et al., 2016).

Finally, it is also possible that as single motors, KIF17 is robust at transporting high-load but as a team they are unable to cooperate. To address this possibility, it will be important to characterize the motility properties of defined numbers of KIF17 motors (Derr et al., 2012; Furuta et al., 2013; Grover et al., 2016; Norris et al., 2014) and compare this to their behavior as single motors.

5.3 References

Andreasson, J. O., Shastry, S., Hancock, W. O., & Block, S. M. (2015). The Mechanochemical Cycle of Mammalian Kinesin-2 KIF3A/B under Load. *Curr Biol, 25*(9), 1166-1175. doi:10.1016/j.cub.2015.03.013

Atherton, J., Farabella, I., Yu, I. M., Rosenfeld, S. S., Houdusse, A., Topf, M., & Moores, C. A. (2014). Conserved mechanisms of microtubule-stimulated ADP release, ATP binding, and force generation in transport kinesins. *Elife, 3*, e03680. doi:10.7554/eLife.03680

Atherton, J., Yu, I. M., Cook, A., Muretta, J. M., Joseph, A., Major, J., . . . Moores, C. A. (2017). The divergent mitotic kinesin MKLP2 exhibits atypical structure and mechanochemistry. *Elife, 6*. doi:10.7554/eLife.27793

Bentley, M., & Banker, G. (2015). A Novel Assay to Identify the Trafficking Proteins that Bind to Specific Vesicle Populations. *Curr Protoc Cell Biol, 69*, 13 18 11-13 18 12. doi:10.1002/0471143030.cb1308s69

Budaitis, B. G., Jariwala, S., Reinemann, D. N., Schimert, K. I., Scarabelli, G., Grant, B. J., . . . Verhey, K. J. (2019). Neck linker docking is critical for Kinesin-1 force generation in cells but at a cost to motor speed and processivity. *Elife, 8*. doi:10.7554/eLife.44146

Cao, L., Cantos-Fernandes, S., & Gigant, B. (2017). The structural switch of nucleotide-free kinesin. *Sci Rep, 7*, 42558. doi:10.1038/srep42558

Case, R. B., Rice, S., Hart, C. L., Ly, B., & Vale, R. D. (2000). Role of the kinesin neck linker and catalytic core in microtubule-based motility. *Curr Biol, 10*(3), 157-160. doi:10.1016/s0960-9822(00)00316-x

Derr, N. D., Goodman, B. S., Jungmann, R., Leschziner, A. E., Shih, W. M., & Reck-Peterson, S. L. (2012). Tug-of-war in motor protein ensembles revealed with a programmable DNA origami scaffold. *Science, 338*(6107), 662-665. doi:10.1126/science.1226734

Duan, L., Che, D., Zhang, K., Ong, Q., Guo, S., & Cui, B. (2015). Optogenetic control of molecular motors and organelle distributions in cells. *Chem Biol, 22*(5), 671-682. doi:10.1016/j.chembiol.2015.04.014

Dumas, M. E., Chen, G. Y., Kendrick, N. D., Xu, G., Larsen, S. D., Jana, S., . . . Ohi, R. (2019). Dual inhibition of Kif15 by oxindole and quinazolinedione chemical probes. *Bioorg Med Chem Lett, 29*(2), 148-154. doi:10.1016/j.bmcl.2018.12.008

Efremov, A. K., Radhakrishnan, A., Tsao, D. S., Bookwalter, C. S., Trybus, K. M., & Diehl, M. R. (2014). Delineating cooperative responses of processive motors in living cells. *Proc Natl Acad Sci U S A, 111*(3), E334-343. doi:10.1073/pnas.1313569111

Endow, S. A., & Waligora, K. W. (1998). Determinants of kinesin motor polarity. *Science, 281*(5380), 1200-1202. doi:10.1126/science.281.5380.1200

Engelke, M. F., Waas, B., Kearns, S. E., Suber, A., Boss, A., Allen, B. L., & Verhey, K. J. (2019). Acute Inhibition of Heterotrimeric Kinesin-2 Function Reveals Mechanisms of Intraflagellar Transport in Mammalian Cilia. *Curr Biol, 29*(7), 1137-1148 e1134. doi:10.1016/j.cub.2019.02.043

Engelke, M. F., Winding, M., Yue, Y., Shastry, S., Teloni, F., Reddy, S., . . . Verhey, K. J. (2016). Engineered kinesin motor proteins amenable to small-molecule inhibition. *Nat Commun, 7*, 11159. doi:10.1038/ncomms11159

Franker, M. A., Esteves da Silva, M., Tas, R. P., Tortosa, E., Cao, Y., Frias, C. P., . . . Hoogenraad, C. C. (2016). Three-Step Model for Polarized Sorting of KIF17 into Dendrites. *Curr Biol, 26*(13), 1705-1712. doi:10.1016/j.cub.2016.04.057

Furuta, K., Furuta, A., Toyoshima, Y. Y., Amino, M., Oiwa, K., & Kojima, H. (2013). Measuring collective transport by defined numbers of processive and nonprocessive kinesin motors. *Proc Natl Acad Sci U S A, 110*(2), 501-506. doi:10.1073/pnas.1201390110

Gabrych, D. R., Lau, V. Z., Niwa, S., & Silverman, M. A. (2019). Going Too Far Is the Same as Falling Short(dagger): Kinesin-3 Family Members in Hereditary Spastic Paraplegia. *Front Cell Neurosci, 13*, 419. doi:10.3389/fncel.2019.00419

Gerdes, J. M., Davis, E. E., & Katsanis, N. (2009). The vertebrate primary cilium in development, homeostasis, and disease. *Cell, 137*(1), 32-45. doi:10.1016/j.cell.2009.03.023

Goulet, A., Behnke-Parks, W. M., Sindelar, C. V., Major, J., Rosenfeld, S. S., & Moores, C. A. (2012). The structural basis of force generation by the mitotic motor kinesin-5. *J Biol Chem, 287*(53), 44654-44666. doi:10.1074/jbc.M112.404228

Grover, R., Fischer, J., Schwarz, F. W., Walter, W. J., Schwille, P., & Diez, S. (2016). Transport efficiency of membrane-anchored kinesin-1 motors depends on motor density and diffusivity. *Proc Natl Acad Sci U S A, 113*(46), E7185-E7193. doi:10.1073/pnas.1611398113

Guzik-Lendrum, S., Rank, K. C., Bensel, B. M., Taylor, K. C., Rayment, I., & Gilbert, S. P. (2015). Kinesin-2 KIF3AC and KIF3AB Can Drive Long-Range Transport along Microtubules. *Biophys J, 109*(7), 1472-1482. doi:10.1016/j.bpj.2015.08.004

Hahlen, K., Ebbing, B., Reinders, J., Mergler, J., Sickmann, A., & Woehlke, G. (2006). Feedback of the kinesin-1 neck-linker position on the catalytic site. *J Biol Chem, 281*(27), 18868-18877. doi:10.1074/jbc.M508019200

Helenius, J., Brouhard, G., Kalaidzidis, Y., Diez, S., & Howard, J. (2006). The depolymerizing kinesin MCAK uses lattice diffusion to rapidly target microtubule ends. *Nature, 441*(7089), 115-119. doi:10.1038/nature04736

Hendricks, A. G., Perlson, E., Ross, J. L., Schroeder, H. W., 3rd, Tokito, M., & Holzbaur, E. L. (2010). Motor coordination via a tug-of-war mechanism drives bidirectional vesicle transport. *Curr Biol, 20*(8), 697-702. doi:10.1016/j.cub.2010.02.058

Hesse, W. R., Steiner, M., Wohlever, M. L., Kamm, R. D., Hwang, W., & Lang, M. J. (2013). Modular aspects of kinesin force generation machinery. *Biophys J, 104*(9), 1969-1978. doi:10.1016/j.bpj.2013.03.051

Hirokawa, N., Niwa, S., & Tanaka, Y. (2010). Molecular motors in neurons: transport mechanisms and roles in brain function, development, and disease. *Neuron, 68*(4), 610-638. doi:10.1016/j.neuron.2010.09.039

Hirokawa, N., Noda, Y., Tanaka, Y., & Niwa, S. (2009). Kinesin superfamily motor proteins and intracellular transport. *Nat Rev Mol Cell Biol, 10*(10), 682-696. doi:10.1038/nrm2774

Hunter, A. W., Caplow, M., Coy, D. L., Hancock, W. O., Diez, S., Wordeman, L., & Howard, J. (2003). The kinesin-related protein MCAK is a microtubule depolymerase that forms an ATP-hydrolyzing complex at microtubule ends. *Mol Cell, 11*(2), 445-457. doi:10.1016/s1097-2765(03)00049-2

Hwang, W., Lang, M. J., & Karplus, M. (2008). Force generation in kinesin hinges on cover-neck bundle formation. *Structure, 16*(1), 62-71. doi:10.1016/j.str.2007.11.008

Janssen, A. F. J., Tas, R. P., van Bergeijk, P., Oost, R., Hoogenraad, C. C., & Kapitein, L. C. (2017). Myosin-V Induces Cargo Immobilization and Clustering at the Axon Initial Segment. *Front Cell Neurosci, 11*, 260. doi:10.3389/fncel.2017.00260

Kapitein, L. C., Schlager, M. A., van der Zwan, W. A., Wulf, P. S., Keijzer, N., & Hoogenraad, C. C. (2010). Probing intracellular motor protein activity using an inducible cargo trafficking assay. *Biophys J, 99*(7), 2143-2152. doi:10.1016/j.bpj.2010.07.055

Kapoor, T. M., Mayer, T. U., Coughlin, M. L., & Mitchison, T. J. (2000). Probing spindle assembly mechanisms with monastrol, a small molecule inhibitor of the mitotic kinesin, Eg5. *J Cell Biol, 150*(5), 975-988. doi:10.1083/jcb.150.5.975

Kevenaar, J. T., Bianchi, S., van Spronsen, M., Olieric, N., Lipka, J., Frias, C. P., . . . Hoogenraad, C. C. (2016). Kinesin-Binding Protein Controls Microtubule Dynamics and Cargo Trafficking by Regulating Kinesin Motor Activity. *Curr Biol, 26*(7), 849-861. doi:10.1016/j.cub.2016.01.048

Khalil, A. S., Appleyard, D. C., Labno, A. K., Georges, A., Karplus, M., Belcher, A. M., . . . Lang, M. J. (2008). Kinesin's cover-neck bundle folds forward to generate force. *Proc Natl Acad Sci U S A, 105*(49), 19247-19252. doi:10.1073/pnas.0805147105

Kim, H., Fonseca, C., & Stumpff, J. (2014). A unique kinesin-8 surface loop provides specificity for chromosome alignment. *Mol Biol Cell, 25*(21), 3319-3329. doi:10.1091/mbc.E14-06-1132

Miki, H., Setou, M., Hirokawa, N., Group, R. G., & Members, G. S. L. (2003). Kinesin superfamily proteins (KIFs) in the mouse transcriptome. *Genome Res, 13*(6B), 1455-1465. doi:10.1101/gr.984503

Milic, B., Andreasson, J. O. L., Hogan, D. W., & Block, S. M. (2017). Intraflagellar transport velocity is governed by the number of active KIF17 and KIF3AB motors and their motility properties under load. *Proc Natl Acad Sci U S A, 114*(33), E6830-E6838. doi:10.1073/pnas.1708157114

Muretta, J. M., Reddy, B. J. N., Scarabelli, G., Thompson, A. F., Jariwala, S., Major, J., . . . Rosenfeld, S. S. (2018). A posttranslational modification of the mitotic kinesin Eg5 that enhances its mechanochemical coupling and alters its mitotic function. *Proc Natl Acad Sci U S A, 115*(8), E1779-E1788. doi:10.1073/pnas.1718290115

Nakajima, K., Takei, Y., Tanaka, Y., Nakagawa, T., Nakata, T., Noda, Y., . . . Hirokawa, N. (2002). Molecular motor KIF1C is not essential for mouse survival and motor-dependent retrograde Golgi apparatus-to-endoplasmic reticulum transport. *Mol Cell Biol, 22*(3), 866-873. doi:10.1128/mcb.22.3.866-873.2002

Nitta, R., Okada, Y., & Hirokawa, N. (2008). Structural model for strain-dependent microtubule activation of Mg-ADP release from kinesin. *Nat Struct Mol Biol, 15*(10), 1067-1075. doi:10.1038/nsmb.1487

Norris, S. R., Soppina, V., Dizaji, A. S., Schimert, K. I., Sept, D., Cai, D., . . . Verhey, K. J. (2014). A method for multiprotein assembly in cells reveals independent action of kinesins in complex. *J Cell Biol, 207*(3), 393-406. doi:10.1083/jcb.201407086

Richard, J., Kim, E. D., Nguyen, H., Kim, C. D., & Kim, S. (2016). Allostery Wiring Map for Kinesin Energy Transduction and Its Evolution. *J Biol Chem, 291*(40), 20932-20945. doi:10.1074/jbc.M116.733675

Salinas, S., Proukakis, C., Crosby, A., & Warner, T. T. (2008). Hereditary spastic paraplegia: clinical features and pathogenetic mechanisms. *Lancet Neurol, 7*(12), 1127-1138. doi:10.1016/S1474-4422(08)70258-8

Schimert, K. I., Budaitis, B. G., Reinemann, D. N., Lang, M. J., & Verhey, K. J. (2019). Intracellular cargo transport by single-headed kinesin motors. *Proc Natl Acad Sci U S A, 116*(13), 6152-6161. doi:10.1073/pnas.1817924116

Schuster, M., Kilaru, S., Fink, G., Collemare, J., Roger, Y., & Steinberg, G. (2011). Kinesin-3 and dynein cooperate in long-range retrograde endosome motility along a nonuniform microtubule array. *Mol Biol Cell, 22*(19), 3645-3657. doi:10.1091/mbc.E11-03-0217

Shen, Q., Cheng, F., Song, H., Lu, W., Zhao, J., An, X., . . . Zhang, J. (2017). Proteome-Scale Investigation of Protein Allosteric Regulation Perturbed by Somatic Mutations in 7,000 Cancer Genomes. *Am J Hum Genet, 100*(1), 5-20. doi:10.1016/j.ajhg.2016.09.020

Shubeita, G. T., Tran, S. L., Xu, J., Vershinin, M., Cermelli, S., Cotton, S. L., . . . Gross, S. P. (2008). Consequences of motor copy number on the intracellular transport of kinesin-1-driven lipid droplets. *Cell, 135*(6), 1098-1107. doi:10.1016/j.cell.2008.10.021

Soppina, V., Rai, A. K., Ramaiya, A. J., Barak, P., & Mallik, R. (2009). Tug-of-war between dissimilar teams of microtubule motors regulates transport and fission of endosomes. *Proc Natl Acad Sci U S A, 106*(46), 19381-19386. doi:10.1073/pnas.0906524106

Soppina, V., & Verhey, K. J. (2014). The family-specific K-loop influences the microtubule on-rate but not the superprocessivity of kinesin-3 motors. *Mol Biol Cell, 25*(14), 2161-2170. doi:10.1091/mbc.E14-01-0696

Tomishige, M., Klopfenstein, D. R., & Vale, R. D. (2002). Conversion of Unc104/KIF1A kinesin into a processive motor after dimerization. *Science, 297*(5590), 2263-2267. doi:10.1126/science.1073386

Tomishige, M., & Vale, R. D. (2000). Controlling kinesin by reversible disulfide cross-linking. Identifying the motility-producing conformational change. *J Cell Biol, 151*(5), 1081-1092. doi:10.1083/jcb.151.5.1081

van Bergeijk, P., Adrian, M., Hoogenraad, C. C., & Kapitein, L. C. (2015). Optogenetic control of organelle transport and positioning. *Nature, 518*(7537), 111-114. doi:10.1038/nature14128

Verhey, K. J., Dishinger, J., & Kee, H. L. (2011). Kinesin motors and primary cilia. *Biochem Soc Trans, 39*(5), 1120-1125. doi:10.1042/BST0391120

Yang, J. S., Seo, S. W., Jang, S., Jung, G. Y., & Kim, S. (2012). Rational engineering of enzyme allosteric regulation through sequence evolution analysis. *PLoS Comput Biol, 8*(7), e1002612. doi:10.1371/journal.pcbi.1002612

Yang, Z., Roberts, E. A., & Goldstein, L. S. (2001). Functional analysis of mouse C-terminal kinesin motor KifC2. *Mol Cell Biol, 21*(7), 2463-2466. doi:10.1128/MCB.21.7.2463-2466.2001

Yu, Y., & Feng, Y. M. (2010). The role of kinesin family proteins in tumorigenesis and progression: potential biomarkers and molecular targets for cancer therapy. *Cancer, 116*(22), 5150-5160. doi:10.1002/cncr.25461

Yue, Y., Blasius, T. L., Zhang, S., Jariwala, S., Walker, B., Grant, B. J., . . . Verhey, K. J. (2018). Altered chemomechanical coupling causes impaired motility of the kinesin-4 motors KIF27 and KIF7. *J Cell Biol, 217*(4), 1319-1334. doi:10.1083/jcb.201708179